

Departamento de Farmacia y Tecnología Farmacéutica
Facultad de Farmacia

UNIVERSIDAD DE NAVARRA



TESIS DOCTORAL

**“Metal-Organic Frameworks
for Drug Delivery Applications”**

Cristina Tamames Tabar

Pamplona, 2014

Departamento de Farmacia y Tecnología Farmacéutica
Facultad de Farmacia

UNIVERSIDAD DE NAVARRA



TESIS DOCTORAL

**“Metal-Organic Frameworks
for Drug Delivery Applications”**

Trabajo presentado por Cristina Tamames Tabar para obtener
el Grado de Doctor

Fdo. Cristina Tamames Tabar
Pamplona, 2014



Universidad de Navarra

FACULTAD DE FARMACIA

Departamento de Farmacia y Tecnología Farmacéutica

UNIVERSITÉ DE
VERSAILLES 
ST-QUENTIN-EN-YVELINES

INSTITUT LAVOISIER UMR CNRS 8180

Équipe de Solides Poreux

DÑA. MARÍA JOSÉ BLANCO PRIETO, Profesora Investigadora del Departamento de Farmacia y Tecnología Farmacéutica de la Facultad de Farmacia de la Universidad de Navarra y DÑA. PATRICIA HORCAJADA CORTÉS, Investigadora del Équipe de Solides Poreux del Institut Lavoisier UMR CNRS 8180 de la Université de Versailles-St-Quentin-en-Yvelines.

Certifican:

Que el presente trabajo, titulado “**Metal-Organic Frameworks for Drug Delivery Applications**”, presentado por DÑA. CRISTINA TAMAMES TABAR para optar al grado de Doctor en Farmacia, ha sido realizado bajo su dirección en el Departamento de Farmacia y Tecnología Farmacéutica de la Facultad de la Universidad de Navarra y en el Equipo de Sólidos Porosos del Institut Lavoisier UMR CNRS 8180 de la Université de Versailles-St-Quentin-en-Yvelines (Francia). Considerando finalizado el trabajo autorizan su presentación a fin de que pueda ser juzgado y calificado por el Tribunal correspondiente.

Y para que así conste, firman la presente:

Fdo.: Dra. María José Blanco Prieto

Fdo.: Dra. Patricia Horcajada Cortés

Pamplona, 2014

Las investigaciones realizadas en el presente trabajo se han desarrollado gracias a la financiación recibida a través de la **FEUN** (Fundación Empresa Universidad de Navarra), **CNRS** (Centre National de Recherche Scientifique, Francia), del proyecto francés **VIRMIL** (ANR-2010-RMNP-004-01) y de la **Unión Europea** (ERC-2007-209241-BioMOFs).

Cristina Tamames Tabar agradece asimismo la beca de Personal en Formación (PIF) de la Asociación de Amigos de la Universidad de Navarra (**ADA**).

A mis abuelos, *Federico y Ramona*

A *Luis*

A mi madre, *María*

*“Logic will get you from A to B.
Imagination will take you everywhere.”*

Albert Einstein

(1879-1955)

AGRADECIMIENTOS

Quizás la parte más difícil de esta tesis sea escribir los agradecimientos, ya que te enfrentas a la parte que, puede que sea más leída de esta Tesis y también porque es la más intangible, ya que te enfrentas a una página en blanco, sin ningún tipo de plantilla a seguir, y simplemente te basas en “ser tu mismo”. No es fácil dar las gracias, pero como dice el dicho “de bien nacido es ser agradecido”, es algo que intentaré hacer aquí. Hay mucha gente a la que tengo que dar las gracias, no solo a aquellas personas que al haber dado a su granito de arena “de aquí” y “de allí” que hacen que sea como soy hoy, sino que también a aquellas que me han ayudado en mi vertiente profesional. Pido disculpas con antemano si hay alguien al que no le nombre, ya que podría escribir un Tomo II de esta Tesis solo con agradecimientos.

Primero de todo, me gustaría agradecer a la Universidad de Navarra, al Departamento de Farmacia y Tecnología Farmacéutica y al *Équipe de Solides Poreux de l'Université de Versailles-St-Quentin-en-Yvelines* por haber confiado en mí y haberme dado la oportunidad de realizar este trabajo que presento hoy. Además, también me gustaría agradecer a toda la financiación que ha hecho posible el realizar esta investigación: a la Asociación de Amigos por la beca que he disfrutado, a la Fundación-Empresa Universidad de Navarra, al *Centre National de la Recherche Scientifique (CNRS)*, al Proyecto VIRMIL y a la financiación de la Unión Europea para el proyecto BioMOFs.

Muchas gracias a mis directoras, las Dras. María Blanco y Patricia Horcajada. María y Patricia: gracias una vez más por creer en mí y permitirme trabajar con vosotras todo este tiempo en proyectos de investigación tan punteros. Todavía me acuerdo el día que os conocí a cada una de vosotras. A ti María, allí por finales de Septiembre del 2003, justo recién llegada a la Universidad de Navarra, cuando ni sabía lo que era el “Transiberiano”, después de esto me guiaste durante mi Licenciatura hasta el día de hoy. A ti Patricia, a mediados de Marzo de 2010, después de un viaje con mil anécdotas (en 1 hora) hasta llegar al *Institut Lavoisier*. Entre las dos, me habéis enseñado lo que es una nanopartícula, como se sintetiza un MOF, para que sirva una liberación controlada de fármacos, como se redacta un *paper* y tener mucha imaginación y ganas para seguir el día a día, entre muchas otras cosas. Además, me habéis enseñado grandes valores que van más allá de una Tesis, como son la humanidad, las ganas de superación y la constancia.

Aunque haya tenido a mis directoras, también tengo que agradecer a todos los investigadores y profesores del Departamento de Farmacia y Tecnología Farmacéutica que siempre me han ayudado cuando lo he necesitado. Muchas gracias a: Dña. Carmen Dios, Dña Maribel Calvo, Dña. María Jesús Renedo, Dña. Pilar Ygartua, Dña. Conchita Tros,

Dña. María del Mar Goñi, Dña. María Jesús Garrido, Dña Socorro Espuelas, D. Iñaki Fdez. de Trocóniz, D. Juan Manuel Irache, D. Fernando Martínez, D. Félix Recarte, Dña. María Huici y D. Juan Luis Martín.

A mis compañeros de laboratorio.

A *Campi*, por haberme asesorado en todo lo que tiene que ver con el HPLC, así como cualquier duda que me ha surgido durante la tesis. ¡¡Muchas gracias por tu gran disponibilidad y todos esos buenos consejos!!

A Edurne, por haberme ayudado tanto, por estar allí en todo momento y por todo lo que me has enseñado, más allá de cómo hacer un MTT o una MIC. Eres un gran modelo a seguir tanto en el laboratorio como fuera de él. ¡¡Mil gracias por todo, un trozo (muy importante) de esta tesis es tuya!!

A Koldo, por ser un gran amigo, mucho más que un compañero de laboratorio, por estar disponible en cualquier momento y escuchar todo lo que me ocurría. Por esos *Jueves de Terapia* junto con Lara (“*los Himsters!*”) cuando teníamos días malos y por celebrar todos esos momentos buenos. Juntos empezamos en esta aventura y pronto terminaremos (bueno... itu antes!).

A Juana, por esos partidos de tenis (de día y también de noche), esas caminatas por el campus y por ser la mejor *compi* de piso que he tenido. Sigue así, siempre sonriente y que nadie te cambie. Mucha suerte con tu tesis.

A Paula, por siempre estar allí escuchando mi día a día y por todos esos buenos consejos. Me hubiese gustado que estuvieses por aquí hoy, pero sé que te estarás acordando mucho de mí. ¡Mucha suerte con tus ratitas y con lo que te queda, que sé que te irá genial!

A mis vecinas de sitio Rebeca y Patricia. Ha sido un placer estar con vosotras cada día... y también muchas gracias por ayudarme con tantas cosillas. He aprendido mucho de vosotras.

A Elisa, por todos los grandes consejos y el ejemplo que me has dado.

A Meli, por haber compartido tantas horas de trabajo y de consejos a lo largo de este camino. ¡Mucho ánimo que ya va quedando menos!

A Yolanda y a Simón, que aunque acabáis de empezar en esta aventura, he aprendido mucho de vosotros. ¡¡Mucho ánimo para vuestra continuación!!

A mis compañeros de equipo, que ya volaron del nido hace un *tiempecillo* y que están triunfando en sus trabajos en diferentes partes del mundo: a Ander, a Ángela, a Izas, a Fabio, a Esther, a Teresa y a Bea. Me ha encantado trabajar con vosotros.

A Sara por la paciencia que tienes, por ser cómo eres y compartir las cosas curiosas que te ocurren y sentir que no sólo a mí me pasa todo lo raro. ¡Ánimo en Holanda!

A Hugo, por haberme asesorado y ayudado en todo este tiempo y sobre todo, por tener tanta paciencia conmigo en el animalario.

A Luisa y a Judit por, entre muchas cosas, apoyarnos mutuamente cuando al HPLC se le cruzaban los cables. Os deseo lo mejor para vuestro futuro profesional.

A Maite, a Esther, a Eneko, a Marijo, a Nekane, a Laura, a Ana y a Inés. Aunque no haya trabajado directamente con vosotros, siempre me habéis echado un cable cuando lo he necesitado.

A todos los integrantes de Farmacocinética, a Ari, a Zinnia, a María, a Núria y a María que realmente os admiro por lo que hacéis. Mucha suerte en el futuro.

A Laura y a Ana Margarita, por siempre estar tan atentas conmigo y compartir esas tardes de risas en células.

A Elba y a Sheyla, que aunque no haya compartido mucho tiempo en el Departamento, he aprendido mucho de vosotras.

À Christian Serre, pour avoir m'accueilli à l'Équipe de Solides Poreux du premier moment que je suis arrivée et pour suivre mon travail même si à cause des horaires et à cause des voyages, on n'était pas dans le même endroit.

À tous les intégrants de l'Équipe de Solides Poreux, que m'ont aidé pendant tous ces années: Thomas, Stuart, Denise, Florence, Hubert, Valentina, Alfonso, Rasha, Elsa, Tarek, Florent, Paul, Vincent, Anh, Aude, Farid, Nathalie, Corinne, Elena, Nastya et Tania. Mes excuses si j'ai oublié à quelqu'un!

À Sana et Sofiane, pour m'avoir accueilli dans votre famille, pour partager des moments très importants avec moi (...) simplement pour être ma famille en France. Merci beaucoup pour tout!

A toda la gente que me ha acompañado desde que llegué a Pamplona allí por Septiembre de 2003, ya que para mi no sólo es terminar un trabajo de mis últimos 4 años, sino que una parte muy importante de mi vida.

A mis amigos César y Paula. Que aunque no coincidimos todo el tiempo que nos hubiese gustado en Pamplona, lo pasamos genial y estemos donde estemos siempre estamos al día de cada uno.

A mis compañeras de piso (que después de estar más de 10 años por aquí he tenido unas cuantas), que han sido mi familia por aquí. En especial, a Ana (la ya Dra. Ana Gómez-Úriz!!) por todo lo que he aprendido de ti, además de todos esos ratos de *bicho-bola* en el sofá y a Bea, por haber sido la persona que quizás ha estado más tiempo conmigo durante la carrera.

A mis compañeros del Máster Javi y Manuel, el otro 50%. Hicimos un buen equipo. Gracias por esos momentos.

A mis amigas de la carrera, en especial a Nerea, que siempre desde Corella ha seguido los pasos en mi vida profesional (aún me acuerdo cuando ese verano de 2004 te dije que dejaría la carrera...).

A la Montse i a l'Esther, per sempre estar al costat durant la carrera fins ara, ja que sabem que estar fora de casa no és d'allò més fàcil. Moltes gràcies noies!

A Olatz, mi amiga, mi médico y mi cardiólogo particular. ¿Quién nos hubiese dicho que hubiésemos llegado hasta aquí (bueno.... en realidad... iyo ya pensé que tu llegarías bien lejos!)?

A Dani, por estar allí siempre, aunque sea al otro lado del Atlántico. Nos conocimos en 1994 y desde entonces siempre te has interesado por todo lo que he hecho. ¡Muchas gracias por todo!

A todas mis amigas del "cole", en especial a Ale y a Carlota. Aunque no nos hemos podido ver todo lo que nos hubiese gustado durante todos estos años, siempre me habéis apoyado desde la distancia. Muchas gracias por siempre estar allí y Ale... por compartir uno de tus días más felices conmigo (¡ia estas fechas ya estarás casada!!).

A toda mi familia, que aunque sea pequeñita, siempre han creído en mí.

A Montse, mi *súper*-madrina. Por siempre estar allí dejando el pabellón bien alto... y por acompañarme en días tan importantes como éste.

A mi padre, que la gente que me conoce, sabe que no suelo hablar de él. Aunque casi no coincidí contigo y apenas te conocí, espero que estés orgulloso de mí desde allí arriba.

A mis abuelos, Federico y Ramona, dos de las personas más importantes de mi vida y los mejores abuelos del mundo. Gracias por todo lo que me habéis dado y por todo lo que me habéis enseñado siempre. No tengo manera de agradecer todo lo que habéis hecho por mí. Por ello, a vosotros os dedico mi tesis. ¡Abuelo, sé que desde allí arriba me ayudarás para que este día sea genial!

A Luis. Que aunque me dijese que no tenía que dedicarte nada, tengo que agradecerte mucho más de lo que crees. Gracias por siempre estar allí (en especial estos últimos tiempos que no han sido fáciles), por acompañarme en este camino y por ser como eres. Por ello, a ti también te dedico este trabajo.

Y por último a mi madre, María, que sin ella, si que todo esto hubiese sido imposible de ser realidad. Gracias *Mami* por todo, por ser la mejor, por dejarme vivir mi sueño, por estar allí donde siempre te he necesitado y por hacer que entendías cuando te hablaba de la validación HPLC, de lo que era un MOF o sobre la encapsulación de la genistéina (entre muchas cosas). Cuando me di cuenta que no te había agradecido en mi manuscrito del máster (aparte de pensar en el error que había cometido), supe que a la última persona y

el gracias más grande tenía que dar, tenía ser para ti, además de dedicarte todo esto. Por esto, y por todo lo demás...¡¡MUCHAS GRACIAS!!

TABLE OF CONTENTS

ABBREVIATIONS · ABREVIATURAS · ABRÉVIATIONS	1
SYNOPSIS · SINÓPSIS · SYNOPSIS	13
INTRODUCTION: MOFs In Pharmaceutical Technology.....	19
General Objectives And Author Contributions	21
Synopsis	25
1. Introduction	27
2. Metal-Organic Frameworks	28
2.1 Description	28
2.2 Synthesis, Formulation And Functionalization/Shaping	29
2.3 Stability And Toxicity	32
3. MOFs For Therapeutics	35
3.1 BioMOFs.....	35
3.2 Active Ingredient Adsorption And Release From MOFs	37
3.3 Understanding	42
3.4 Theranostics.....	45
3.5 Efficacy	46
4. Conclusions	47
References	47
HYPOTHESIS AND OBJECTIVES · HIPÓTESIS Y OBJETIVOS	59
CHAPTER 1: Cytotoxicity Of Nanoscaled Metal-Organic Frameworks	63
General Objectives And Author Contributions	65
Abstract.....	69
1. Introduction	71
2. Experimental Section	72
2.1 Material Synthesis.....	72
2.2 Material Characterisation.....	73
2.3 Cell Culture and Cytotoxicity Assays.....	74
2.4 Cellular Penetration Assays: Confocal Microscopy.....	74
3. Results And Discussion	75
3.1 Synthesis and Characterisation of MOFs	75
3.2 Cytotoxicity Evaluation.....	79
3.3 Cell Penetration Studies	83
4. Conclusions	87
Acknowledgements	87
Notes And References	87
References	88
SUPPLEMENTARY INFORMATION: Cytotoxicity Of Nanoscaled Metal-Organic Frameworks.....	91

1. Reactants	93
2. Synthesis Of The Organic Linkers	94
3. Material Synthesis	94
3.1. MIL-127_nano or $(\text{Fe}_3\text{O}(\text{OH})(\text{H}_2\text{O})_3[(\text{C}_{16}\text{N}_2\text{O}_8\text{H}_6)_3 n \cdot \text{H}_2\text{O}])$	94
3.2. MIL-100_nano or $(\text{Fe}_3\text{O}(\text{OH})(\text{H}_2\text{O})_2[(\text{CO}_2)_3\text{C}_6\text{H}_3]_2 n \cdot \text{H}_2\text{O})$	94
3.3. MIL-100_micro or $(\text{Fe}_3\text{O}(\text{H}_2\text{O})_2\text{OH}[\text{C}_6\text{H}_3(\text{CO}_2)_3]_2 n \cdot \text{H}_2\text{O})$	95
3.4. MIL-101_2CH ₃ _nano or $(\text{Fe}_3\text{O}(\text{OH})(\text{H}_2\text{O})_2[(\text{CO}_2)_2\text{C}_6\text{H}_2(\text{CH}_3)_2]_3 n \cdot \text{H}_2\text{O})$	95
3.5. MIL-101_NH ₂ _nano or $(\text{Fe}_3\text{O}(\text{OH})(\text{H}_2\text{O})_2[(\text{CO}_2)_2\text{C}_6\text{H}_3\text{NH}_2]_3 n \cdot \text{H}_2\text{O})$	95
3.6. MIL-88A_nano or $(\text{Fe}_3\text{O}(\text{OH})(\text{H}_2\text{O})_2[(\text{CO}_2)_2\text{C}_2\text{H}_2]_3 n \cdot \text{H}_2\text{O})$	95
3.7. MIL-88B_nano or $(\text{Fe}_3\text{O}(\text{OH})(\text{H}_2\text{O})_2[(\text{CO}_2)_2\text{C}_6\text{H}_4]_3 n \cdot \text{H}_2\text{O})$	96
3.8. MIL-88B_CH ₃ _nano or $(\text{Fe}_3\text{O}(\text{OH})(\text{H}_2\text{O})_2[(\text{CO}_2)_2\text{C}_6\text{H}_3(\text{CH}_3)]_3 n \cdot \text{H}_2\text{O})$	96
3.9. MIL-88B_2CH ₃ _nano or $(\text{Fe}_3\text{O}(\text{OH})(\text{H}_2\text{O})_2[(\text{CO}_2)_2\text{C}_6\text{H}_2(\text{CH}_3)_2]_3 n \cdot \text{H}_2\text{O})$	96
3.10. MIL-88B_4CH ₃ _nano or $(\text{Fe}_3\text{O}(\text{OH})(\text{H}_2\text{O})_2[(\text{CO}_2)_2\text{C}_6(\text{CH}_3)_4]_3 n \cdot \text{H}_2\text{O})$	96
3.11. MIL-88B_2CF ₃ _nano or $(\text{Fe}_3\text{O}(\text{OH})(\text{H}_2\text{O})_2[(\text{CO}_2)_2\text{C}_6\text{H}_2(\text{CF}_3)_2]_3 n \cdot \text{H}_2\text{O})$	97
3.12. MIL-88B_NH ₂ _nano or $(\text{Fe}_3\text{O}(\text{OH})(\text{H}_2\text{O})_2[(\text{CO}_2)_2\text{C}_6\text{H}_3(\text{NH}_2)]_3 n \cdot \text{H}_2\text{O})$	97
3.13. MIL-88B_NO ₂ _nano or $(\text{Fe}_3\text{O}(\text{OH})(\text{H}_2\text{O})_2[(\text{CO}_2)_2\text{C}_6\text{H}_3(\text{NO}_2)]_3 n \cdot \text{H}_2\text{O})$	97
3.14. UiO-66_nano or $(\text{Zr}_6\text{O}_4(\text{OH})_4(\text{H}_2\text{O})_2[(\text{CO}_2)_2\text{C}_6\text{H}_4]_6 n \cdot \text{H}_2\text{O})$	97
3.15. ZIF-8_nano or $[\text{Zn}(\text{C}_4\text{H}_6\text{N}_2)_2 n \cdot \text{H}_2\text{O}]$	98
4. Material Characterisation	98
4.1. X-Ray Powder Diffraction (XRPD).....	98
4.2. Infrared Spectroscopy (FTIR)	99
4.3. Thermogravimetric Analysis (TGA)	99
4.4. Nitrogen Sorption Porosimetry	100
4.5. pH Variations.....	100
4.6. Zeta Potential.....	101
4.7. Degradation Tests	101
5. References	102

CHAPTER 2: Metal-Organic Frameworks: New Delivery Systems For

Genistein Administration	103
General Objectives And Author Contributions	105
Abstract.....	109
1. Introduction	111
2. Experimental Section	113
2.1 Genistein Encapsulation And <i>In Vitro</i> Release	113
2.2. Pharmacokinetic And Bioavailability Profile Of GEN And GEN-Loaded MIL-100(Fe)_NPs.....	115
3. Results And Discussion	116
3.1 GEN Encapsulation And <i>In Vitro</i> Release.....	116
3.2 Pharmacokinetic And Bioavailability Profile Of GEN And GEN-Loaded MIL-100(Fe) NPs	123
4. Conclusion	126
Acknowledgements	126
References	126

SUPPLEMENTARY INFORMATION: Metal-Organic Frameworks: New Delivery Systems For Genistein Administration	135
1. Chemicals and Reagents	137
2. MOF Synthesis.....	138
2.1 Iron(III) Trimesate Nanoparticles	
MIL-100(Fe)_NPs	138
2.2 Iron(III) 2,6-Naphthalenedicarboxylate Nanoparticles	
MIL-88C(Fe)_NPs.....	138
2.3 Zirconium(IV) Aminoterephthalate Microparticles	
UiO-66_NH ₂ (Zr)_MPs	138
2.4 Zirconium(IV) 2,5-Diperfluoromethylterephthalate Microparticles	
UiO-66_2CF ₃ (Zr)_MPs	138
2.5 Zirconium(IV) 2,6-Naphthalenedicarboxylate Microparticles	
UiO-66_NDC(Zr)_MPs	139
2.6 Zirconium(IV) 4,4'-Biphenyldicarboxylate Microparticles	
UiO-66_BPDC(Zr)_MPs	139
2.7 Zirconium(IV) 4,4'-Biphenyldicarboxylate Microparticles	
MIL-140C(Zr)_MPs.....	139
3. Genistein Encapsulation.....	139
3.1 XRPD	141
3.2 Particle Size And ζ -Potential	143
3.3 Genistein Quantification.....	144
3.4 N ₂ Adsorption	145
3.5 FTIR	147
3.6 Solid Stated ¹³ C-NMR	148
4. Computing Simulation	149
5. Genistein Release	150
6. In Vivo Experiments.....	155
6.1 Animal Diet	155
6.2 Treatment Resuspension	155
References	156

CHAPTER 3: A Zinc Azelate MOF: Combining Antibacterial Effect	159
General Objectives And Author Contributions	161
Abstract.....	165
1. Introduction	167
2. Experimental Section	168
2.1. Chemicals And Reagents.....	168
2.2. BioMIL-5 Synthesis And Characterization	168
2.3. BioMIL-5 Degradation And Release Of AzA And Zn	169
2.4. Antibacterial Activity Studies	170
3. RESULTS AND DISCUSSION	172
3.1. BioMIL-5 Synthesis And Characterisation	172
3.2. BioMIL-5 Degradation And Release Of AzA And Zn	174
3.3. Antibacterial Activity Studies	177
4. Conclusion	179

Associated Content	179
Author Information	179
Acknowledgments	180
References	180
SUPPLEMENTARY INFORMATION: A Zinc Azelate MOF: Combining	
Antibacterial Effect	183
1. Crystallographic Data	187
2. Thermogravimetric Analysis (TGA)	188
3. Thermal Stability	188
4. Stability In Solution	189
GENERAL DISCUSSION	191
GENERAL CONCLUSIONS · CONCLUSIONES GENERALES · CONCLUSIONS	
GÉNÉRALES	211
ANNEX I: Résumé Générale	219
ANNEX II: A Simple And Robust High-Performance Liquid Chromatography	
Coupled To A Diode-Array Detector Method For The Analysis Of Genistein In	
Mouse Tissues	239

ABBREVIATIONS

ABREVIATURAS

ABRÉVIATIONS

5-FU	5-Fluorouracil 5-Fluorouracilo 5-Fluorouracile
aa	Aminoacid Aminoácido Aminoacide
AAS	Atomic Absorption Spectroscopy Espectroscopía de Absorción Atómica Spectroscopie d'Absorption Atomique
AcN	Acetonitrile Acetonitrilo Acetonitrile
AUC	Area Under the Curve Área Bajo la Curva Aire Sous la Courbe
AzA	Azelaic Acid Ácido Azelaico Acide Azélaïque
AZT-Tp	Azidothymidine Triphosphate Azidotimidina Trifosfato Azidothymidine Triphosphate
BET	Brunauer Emmett Teller (N ₂ Porosimetry) Brunauer Emmett Teller (Porosimetría de N ₂) Brunauer Emmett Teller (Porosimétrie de N ₂)
BA/F	Bioavailability Biodisponibilidad Biodisponibilité
BD	Biodistribution Biodistribución Biodistribution
BDC	Terephthalic Acid or 1,4-Benzenedicarboxylic Acid Ácido Tereftálico o Ácido 1,4-Benzenodicarboxílico Acide Térépthalique ou 1,4-Benzenedicarboxylique
BDC_2CF₃	2,5-Diperfluoromethylterephthalic Acid Ácido 2,5-Diperfluorometiltereftálico Acide 2,5-Diperfluorométhyltérépthalique
BDC_CH₃	2-Methylterephthalic Acid Ácido 2-Metiltereftálico Acide 2-Méthyltérépthalique
BDC_2CH₃	2,5-Dimethylterephthalic Acid

	Ácido 2,5-Dimetiltereftálico
	Acide 2,5-Diméthyltéréphthalique
BDC_4CH₃	2,3,5,6-Tetramethylterephthalic Acid
	Ácido 2,3,5,6-Tetrametiltereftálico
	Acide 2,3,5,6-Tetraméthyltéréphthalique
BDC_NH₂	2-Aminoterephthalic Acid
	Ácido 2-Aminotereftálico
	Acide 2-Aminotéréphthalique
BDC_NO₂	2-Nitroterephthalic Acid
	Ácido 2-Nitrotereftálico
	Acide 2-Nitrotéréphthalique
BioMIL	Biologically Active Materials of Institut Lavoisier
	Materials del Institut Lavoisier Biológicamente Activos
	Matériaux de l'Institut Lavoisier Biologiquement Actifs
BioMIL-5	Zinc Azelate
	Azelato de Zinc
	Azélate de Zinc
BioMOF	Bioactive Metal-Organic Frameworks
	Materials Híbridos Bioactivos
	Matériau Hybrides Bioactifs
b.p.	Boiling Point
	Punto de Ebullición
	Point d'Ébullition
BPDC	4,4'-Biphenyldicarboxylic Acid
	Ácido 4,4'-Bifenildicarboxílico
	Acide 4,4'-Biphényldicarboxilique
BPs	Bisphosphonates
	Bifosfonatos
	Bisphosphonates
Br-BODIPY	1,3,5,7-tetramethyl-4,4-difluoro-8-bromomethyl-4-bora-3a,4a-diaza-s-indacene
	1,3,5,7-tetrametil-4,4-difluoro-8-bromometil-4-bora-3a,4a-diaza-s-indaceno
	1,3,5,7-tetramethyl-4,4-difluoro-8-bromomethyl-4-bora-3a,4a-diaza-s-indacene
BTC	1,3,5-Benzenetricarboxylic Acid or Trimesic acid
	Ácido 1,3,5-Benceno Tricarboxílico o Ácido Trimésico
	Acide Benzène 1,3,5-Benzenetricarboxylique ou Acide Trimésique
Bu	Busulfan
	Busufan

	Busulfan
Caf	Caffeine Cafeína Caféine
CCRF-CEM	Human Leukaemia Cell Line Línea Celular de Leucemia Humana Lignée Cellulaire de Leucémie Humaine
CDV	Cidofovir Cidofovir Cidofovir
CLSM	Confocal Laser Scanning Microscopy Microscopía Confocal Láser de Barrido Microscopie Confocale Laser à Balayage
C_{max}	Maximum Concentration Peak Pico de Máxima Concentration Pic de Concentration Maximale
C-NMR	Carbon Nuclear Magnetic Resonance Resonancia Magnética Nuclear de Carbono Résonance Magnétique Nucléaire de Carbone
CNTs	Carbon Nanotubes Nanotubos de Carbono Nanotubes de Carbone
CORMs	Carbon Monoxide Releasing Molecules Moléculas Liberadoras de Monóxido de Carbono Molécules Libératrices de Monoxyde de Carbone
CPO	Coordination Polymer of Oslo Polímeros de Coordinación de Oslo Polymères de Coordination d'Oslo
CUS	Coordinatively Unsaturated Metal Sites Centros Metálicos de Coordinación Insaturados Centres Métalliques de Coordination Insaturés
DAD	Diode-Array Detector Detector de Diodos en Serie Détecteur de Diodes en Série
DCM	Dichloromethane Diclorometano Dichlorométhane
DDS	Drug Delivery System Sistema de Liberación Controlada Système de Libération Contrôlée

DEF	Diethylformamide Dietilformamida Diethylformamide
DFT	Density Functional Theory Teoría del Funcional de la Densidad Théorie de la Fonctionnelle de la Densité
DHPMA	2,3-Dihydroxypropyl Methacrylate 2,3-Dihidroxipropil Metacrilato 2,3-Dihydroxypropyl Methacrylate
DLS	Dynamic Light Scattering Dispersión Dinámica de Luz Diffusion Dynamique de la Lumière
DMF	<i>N,N</i> -dimethylformamide <i>N,N</i> -dimetilformamida <i>N,N</i> -diméthylformamide
DNA	Deoxyribonucleic Acid Ácido Deoxiribonucleico Acide Désoxyribonucléique
DOPE	Dioleoyl L- α -phosphatidylethalamine Dioleil L- α -fosfatidiletanolamina Dioleoyl L- α -phosphatidylethalamine
DOTAP	Dioleoyl Trimethylammonium Propane Dioleil Trimetilamonio Propane Dioleoyl Trimethylammonium Propane
Doxo/DOX	Doxorubicin Doxorrubicina Doxorubicine
DSCP	Disuccinatocisplatin Disuccinato de Cisplatino Disuccinate de Cisplatine
EGDMA	Ethylene Glycol Dimethacrylate Etilén Glicol Dimetacrilato Ethylène Glycol Dimethacrylate
EtOH	Ethanol Etanol Éthanol
ESCP	Ethoxysuccinatocisplatin Etoxisuccinato de Cisplatino Ethoxysuccinate de Cisplatine
FBS	Foetal Bovine Serum

	Suero Bovino Fetal
	Sérum de Beau Fœtal
FTIR	Fourier Transformed Infrared Spectroscopy Espectroscopia Infrarrojo por Transformada de Fourier Spectroscopie Infrarouge à Transformée de Fourier
FUM	Fumaric Acid Ácido Fumárico Acide Fumarique
GCa	Genistein Calcium Salt Sal de Genistéina Cálcica Sel de Génistéine Calcique
GEN	Genistein Genistéina Génistéine
GNPs	Glyconanoparticles Gliconanopartículas Glyconanoparticules
H460	Human Non-Small Cell Lung Cancer Cell Line Línea Celular de Cáncer de Grandes Células de Pulmón Humana Lignée Cellulaire de Cancer Poumon Humaines du Type à Grandes Cellules
hAEC	Human Amniotic Epithelial Cell Line Línea Celular Epitelial Amniótica Humana Lignée Cellulaire Épithéliale Amniotique Humaine
HeLa	Cervical Cancer Cell Line Línea Celular de Cáncer de Cérvix Lignée Cellulaire de Cancer de Cervix
HEMA	2-Hydroxyethyl Methacrylate 2-Hidroxietil Metacrilato 2-Hydroxyéthyl Méthacrylate
HKUST	Hong Kong University of Science and Technology Universidad de Ciencia y Tecnología de Hong Kong Université de Science et Technologie de Hong Kong
HL-60	Human Promyelocytic Leukaemia Cell Line Línea Celular de Leucemia Promielocítica Humana Lignée Cellulaire de Leucémie Promyélocyte Humaine
HPLC	High Performance Liquid Chromatography Cromatografía Líquida de Alta Resolución Chromatographie Liquide à Haute Performance
Ibu	Ibuprofen Ibuprofeno

	Ibuprofène
IC₅₀	Half Maximal Inhibitory Concentration Concentración Mínima Inhibitoria Media Concentration Minimale Inhibitoire Moyenne
i.p.	Intraperitoneal Route Vía Intraperitoneal Voie Intrapéritonéale
IS	Internal Standard Patrón Interno Étalon Interne
i.v.	Intravenous Route Vía Intravenosa Voie Intraveineuse
IRMOF	Isorecticular Metal-Organic Framework Material Organo-Metálico Isorecticular Matériau Organo-Metallique Isoréctulaire
J774	Mouse Macrophage Cell Line Línea Celular de Macrófagos Murinos Lignée Cellulaire de Macrophages Murins
LLOQ	Lower Limit of Quantification Límite de Cuantificación Limite de Quantification
Ln	Lanthanide Lantánido Lanthanide
MBC	Minimal Bactericidal Concentration Concentración Mínima Bactericida Concentration Minimale Bactéricide
MCF-7	Breast Cancer Cell Line Línea Celular de Cáncer de Mama Lignée Cellulaire de Cancer du Sein
MI	2-Methylimidazole 2-Metilimidazolato 2-Méthylimidazole
MIC	Minimal Inhibitory Concentration Concentración Mínima Inhibitoria Concentration Minimale Inhibitrice
MIL	Materials of Institut Lavoisier Materiales del Institut Lavoisier Matériaux de l'Institut Lavoisier

MIL-88A(Fe)	Iron(III) Fumarate Fumarato de Hierro(III) Fumarate de Fer(III)
MIL-88B(Fe)	Iron(III) Terephthalate Tereftalato de Hierro(III) Téréphthalate de Fer(III)
MIL-88C(Fe)	Iron(III) 2,6-Naphthalenedicarboxylate 2,6-Naftalendicarboxilato de Hierro(III) 2,6-Naphthalèndicarboxylate de Fer(III)
MIL-100(Fe)	Iron(III) Trimesate Trimesato de Hierro(III) Trimesate de Fer(III)
MIL-101(Fe)	Iron(III) Terephthalate Tereftalato de Hierro(III) Téréphthalate de Fer(III)
MIL-127(Fe)/ soc-MOF(Fe)	Iron(III) 3,3',5,5'-Azobenzenetetracarboxylate 3,3',5,5'-Azobenzenotetracarboxilato de Hierro(III) 3,3',5,5'-Azobenzènetetracarboxylate de Fer(III)
MIL-140C(Zr)	Zirconium(IV) 4,4'-Biphenyldicarboxylate 4,4'-Bifenildicarboxilato de Zirconio(IV) 4,4'-Biphényldicarboxylate de Zirconium(IV)
M'MOF	Mixed Metal Organic Framework Materiales Organo-Metálicos Mixtos Matériaux Organo-Metalliques Mixtes
MOF	Metal-Organic Framework Materiales Organometálicos Matériaux Organométalliques
MPs	Microparticles Micropartículas Microparticules
MRI	Magnetic Resonance Imaging Imagen de Resonancia Magnética Imagerie de Résonance Magnétique
MRT	Mean Residence Time Tiempo Medio de Residencia Temps Moyen de Résidence
MTT	3-(4,5-dimethylthiazol-2-yl)-2,5-diphenyltetrazolium Bromide Bromuro de 3-(4,5-dimetiltiazol-2-il)-2,5-difenil Tetrazolio Bromure de 3-(4,5-dimethylthiazol-2-yl)-2,5-dyphenyltetrazolium
MTX	Methotrexate

	Metotrexato
	Méthotrexate
NanoMOF	MOF Nanoparticles Nanopartículas de MOF Nanoparticules de MOF
NCI-H446	Human Lung Carcinoma Cell Line Línea Celular de Carcinoma Pulmonar Humana Lignée Cellulaire de Carcinome Pulmonaire Humaine
NDC	2,6-Naphthalenedicarboxylic Acid Ácido 2,6-Naftelenodicarboxílico Acide 2,6-Naphthalènedicarboxylique
NIR	Near Infrared Spectroscopy Espectroscopía Infrarrojo Cercano Spectroscopie Proche Infrarouge
NPs	Nanoparticles Nanopartículas Nanoparticules
O/W	Oil in Water Aceite en Agua Huile dans l'Eau
PAN	Polyacrylonitrile Poliacrilonitrilo Polyacrylonitrile
PBMC	Peripheral Blood Mononuclear Cells Células Mononucleares de Sangre Periférica Cellules Mononucléaire du Sang Périphérique
PBS	Phosphate Buffered Saline Tampón Fosfato Salino Tampon Phosphate Salin
PCPs	Porous Coordination Polymers Polímeros de Coordinación Porosos Polymères de Coordination Poreux
PEG	Poly(ethylene Glycol) Poli(etilén Glicol) Poly(éthylène Glycol)
PHCl	Procainamide Hydrochloride Procainamida Clorhidrato Procainamide Chlorhydrate
PK	Pharmacokinetics Farmacocinética

PLA	Pharmacocinétique Poly(lactic Acid) Ácido Poliláctico Acide Polylactique
PLGA	Poly(lactic-co-glycolic Acid) Ácido Poli(láctico-co-glicólico) Acide Poly(lactique-co-glycolique)
p.o.	Oral Route Vía Oral Voie Orale
PS	Polystyrene Poliestireno Polystyrène
PVP	Poly(vinylpyrrolidone) Polivinil Pirrolidona Poly(vinylpyrrolidone)
QDs	Quantum Dots Punto Cuántico Boîte Quantique
RES	Reticuloendothelial System Sistema Retículoendotelial Système Réticuloendothéliale
RPMI-8226	Human Multiple Myeloma Cell Line Línea Celular de Mieloma Múltiple Humano Lignée Cellulaire Myéloïde Multiple Humaine
SEM	Scanning Electron Microscopy Microscopía Electrónica de Barrido Microscopie Électronique à Balayage
STAM	Saint Andrews MOF MOF de Saint Andrews MOF de Saint Andrews
t_{1/2}	Biological Half Life Tiempo de Vida Media Temps de Demi-Vie Biologique
Tabz	3,3',5,5'-Azobenzene tetracarboxylic Acid Ácido 3,3',5,5'-Azobenzotetracarboxílico Acide 3,3',5,5'-Azobenzètetracarboxylique
TEM	Transmission Electron Microscopy Microscopio Electrónico de Transmisión Microscopie Électronique à Transmission

TGA	Thermogravimetric Analysis Análisis Termogravimétrico Analyse Thermogravimétrique
T_{max}	Time to Reach C _{max} Tiempo para Alcanzar C _{max} Temps pour Arriver à C _{max}
UCNPs	Upconversion Nanoparticles Nanopartículas de Upconversión Nanoparticules d'Upconversion
UiO	University of Oslo Universidad de Oslo Université d'Oslo
UiO-66(Zr)	Zirconium(IV) Terephthalate Tereftalato de Zirconio(IV) Téréphthalate de Zirconium(IV)
UMCM	University of Michigan Crystalline Material Materiales Cristalinos de la Universidad de Michigan Matériaux Cristallins de l'Université de Michigan
UV	Ultraviolet Ultravioleta Ultraviolet
VP	N-vinyl-2-pyrrolidone N-vinil-2-pirrolidona N-vinyl-2-pyrrolidone
W/O	Water in Oil Agua en Aceite Eau dans l'Huile
wt.	Weight Peso Poids
XRPD	X-Ray Powder Diffraction Difracción de Rayos X Diffraction de Rayons X
ZIF	Zeolitic Imidazolate Framework Redes Zeolíticas a Base de Imidazolatos Réseaux Zeolitiques à Base d'Imidazolates
ζ-pot	Zeta Potential Potencial Zeta Potential Zêta

SYNOPSIS

SINÓPSIS

SYNOPSIS

SYNOPSIS

In this work, a new type of particles denoted as MOFs or Metal-Organic Frameworks, have been studied as a new drug carriers.

First, they were synthesised at the nanoscale (NPs) using, when possible, biofriendly methods. Their cytotoxicity, as well as that from their constitutive linkers, was evaluated by the MTT test in murine macrophage (J774) and in cervix carcinoma (HeLa) cell lines, observing: (i) a low cytotoxicity of MOFs, comparable with other described particulated systems, (ii) a strong influence of the composition (toxicity order: Fe<Zr<Zn; hydrophilic<hydrophobic linkers), (iii) a higher cytotoxicity in J774 than HeLa, due to their higher phagocytosis activity and (iv) MIL-100(Fe)_NPs was an excellent candidate for bioapplications ($IC_{50}=0.7 \text{ mg}\cdot\text{mL}^{-1}$). MIL-100(Fe)_NPs are rapidly cell-uptaken, being immediately internalised in J774 cells.

Next, the non-toxic bioflavonoid genistein (GEN) with antitumoral properties was successfully encapsulated in porous Fe or Zr carboxylate MOFs, achieving GEN payloads ($160\text{-}340 \text{ }\mu\text{g GEN}\cdot\text{mg formulation}^{-1}$), higher than other existing formulations and dependent on their composition and topology. Furthermore, GEN was progressively released under simulated physiological conditions from 2 days to several weeks, being appropriate as long release drug delivery systems (DDS). Finally, the pharmacokinetics and bioavailability evaluation of MIL-100(Fe)_NPs' formulation was carried out in comparison with the free drug after its oral unique administration ($30 \text{ mg}\cdot\text{Kg}^{-1}$) to mice, depicting (i) higher and longer plasmatic levels, (ii) an increase in the relative and (iii) a better oral bioavailability and a mean residence time. Furthermore, higher and more prolonged drug levels were detected in organs, suggesting that the MOF worked as a drug shelter, protecting GEN from metabolisation.

Finally, a new biologically active MOF (denoted BioMIL-5), based on the antibacterial and dermatologically active azelaic acid (AzA) and Zn, was successfully synthesised by a totally biofriendly route. Both active components BioMIL-5 were slowly released to the media, either pure water or bacteria medium, upon its structural degradation. Its antibacterial activity was evidenced in *S. aureus* and in *S. epidermidis*, observing an interesting additive effect with however high minimal inhibitory (MIC) and minimal bactericidal concentrations (MBC), in agreement with the isolated components. Finally, BioMIL-5 exhibited a lengthened bactericidal ($4.3 \text{ mg}\cdot\text{mL}^{-1}$) and bacteriostatic (0.9 and $1.7 \text{ mg}\cdot\text{mL}^{-1}$) in contact with *S. epidermidis* for one week.

SINÓPSIS

En este trabajo, se han estudiado un nuevo tipo de partículas denominadas MOFs o *Metal-Organic Frameworks* como transportadores de fármacos.

Primero, se sintetizaron en escala nanométrica (NP) sustituyendo los disolventes tóxicos cuando fuese posible. Se evaluó su citotoxicidad, así como la de sus ligandos, mediante el test de MTT en las líneas celulares J774 (macrófagos murinos) y en HeLa (carcinoma de cérvix), observando: (i) una baja citotoxicidad de los MOFs, comparable a otros sistemas particulados, (ii) una fuerte influencia de su composición (orden de toxicidad: Fe<Zr<Zn; ligandos hidrofílicos<hidrofóbicos), (iii) una toxicidad mayor en J774 que en HeLa, debido a una actividad fagocítica mayor y (iv) MIL-100(Fe)_NPs resultó ser un candidato excelente para bioaplicaciones ($IC_{50}=0,7 \text{ mg}\cdot\text{mL}^{-1}$). Asimismo, éstas partículas se internalizaron inmediatamente en J774.

A continuación, se encapsuló satisfactoriamente un bioflavonoide no tóxico denominado genisteína (GEN), con actividad antitumoral en unos carboxilatos porosos de Fe o Zr, alcanzando unas cargas ($160\text{-}340 \mu\text{g GEN}\cdot\text{mg formulación}^{-1}$) mayores que cualquier otra formulación y que dependían de su composición y topología. Además, GEN se liberó progresivamente bajo condiciones fisiológicas simuladas desde 2 días a varias semanas, siendo un tipo de DDS (sistema de liberación controlada) adecuado. Finalmente, la evaluación farmacocinética y de biodisponibilidad de la formulación de MIL-100(Fe)_NPs, se realizó tras su comparación con GEN libre tras su administración única ($30 \text{ mg}\cdot\text{Kg}^{-1}$) por vía oral a ratones, mostrando (i) unos niveles de GEN más elevados durante más tiempo, (ii) un aumento en la biodisponibilidad relativa y (iii) en la biodisponibilidad oral, así como del tiempo medio de resistencia. Además, se observaron niveles de fármaco más elevados y durante más tiempo en órganos, sugiriendo que el MOF servía como una protección al fármaco, protegiéndolo de su metabolización.

Por último, se sintetizó satisfactoriamente y en condiciones biológicamente favorables, un nuevo MOF biológicamente activo (denominado BioMIL-5), basado en dos componentes con propiedades antibacterianas y para el cuidado de la piel, que son el ácido azelaico (AzA) y el Zn. Ambos componentes se liberaron de forma sostenida en solución (agua o medio de cultivo bacteriano), como consecuencia de la degradación del BioMOF. Su actividad antibacteriana se evidenció en *S. aureus* y en *S. epidermidis*, observando asimismo un efecto sumatorio interesante con unas concentraciones mínimas inhibitorias (MIC) y mínimas bactericidas (MBC) altas, en concordancia con los componentes aislados del BioMOF. Finalmente, BioMIL-5 mostró una actividad bactericida ($4.3 \text{ mg}\cdot\text{mL}^{-1}$) y bacteriostática (0.9 y a $1.7 \text{ mg}\cdot\text{mL}^{-1}$) prolongada durante una semana en *S.epidermidis*.

SYNOPSIS

Ce travail de thèse est centré sur l'étude d'un nouveau type de matériau, les solides hybrides cristallins MOFs (ou *Metal-Organic Frameworks*) comme systèmes de vectorisation de médicaments.

Tout d'abord, les MOFs ont été synthétisés à l'échelle nanométrique (NP), en utilisant des méthodes biocompatibles, quand possible. Leur cytotoxicité, ainsi que celle de leurs ligands constitutifs, a été évaluée par le test MTT sur des macrophages murins (J774) et du carcinome cervical (HeLa). Nous avons pu constater: (i) une faible cytotoxicité des MOFs, comparable à celle d'autres particules commercialisées, (ii) une influence importante de la composition du MOF (ordre de toxicité: Fe<Zr<Zn; ligands hydrophiles<hydrophobes), (iii) une toxicité plus élevée sur la lignée J774 que sur la HeLa, associée à sa plus grande activité phagocytaire et (iv) le MIL-100(Fe)_NPs est un candidat prometteur pour des bioapplications, montrant une très faible cytotoxicité ($IC_{50}=0,7 \text{ mg}\cdot\text{mL}^{-1}$) et une internalisation cellulaire rapide, voir immédiate dans les J774.

Ensuite, le bioflavonoïde non-toxique génistéine (GEN), avec une activité antitumorale remarquable, a été encapsulé avec succès dans des carboxylates de Fe ou de Zr poreux, obtenant des capacités très élevées ($160\text{-}340 \mu\text{g GEN}\cdot\text{mg formulation}^{-1}$) en fonction de la structure et composition du MOF. Ces capacités sont bien en dessus de celles reportées par d'autres formulations. En outre, la GEN est libérée progressivement (de 2 jours à quelques semaines) sous des conditions physiologiques simulées, ce qui semble approprié pour son utilisation comme système de libération contrôlée (DDS). L'évaluation de la pharmacocinétique et de la biodisponibilité de la formulation à base du MIL-100(Fe)_NPs, a été réalisée et comparée à celle de la GEN libre après une administration unique ($30 \text{ mg}\cdot\text{Kg}^{-1}$) par voie orale aux souris. Nous avons conclu que cette formulation permet d'y obtenir (i) des niveaux de GEN plus élevés et prolongés, (ii) une biodisponibilité relative supérieure et (iii) une meilleure biodisponibilité orale et un temps moyen de résidence. Les niveaux de GEN dans les organes ont été davantage plus élevés et prolongés, suggérant que le MOF puisse protéger la GEN de la métabolisation.

Finalement, un nouveau MOF biologiquement actif (BioMIL-5), a été synthétisé par une voie totalement biocompatible à base de deux composants antibactériens et dermatologiques, l'acide azélaïque (Aza) et le Zn. La libération progressive des deux au milieu (l'eau ou le milieu bactérien) à travers de la dégradation du BioMIL-5, conduit à un effet antibactérien sur *S. aureus* et *S. epidermidis*. En prime, un effet antibactérien additif a été mis en évidence, avec cependant des concentrations minimales inhibitoires (MIC) et minimales bactéricides (MBC) assez élevées et en accord avec celles des composants

isolés. Enfin, le BioMIL-5 a montré une activité bactéricide ($4.3 \text{ mg}\cdot\text{mL}^{-1}$) et bactériostatique (0.9 et $1.7 \text{ mg}\cdot\text{mL}^{-1}$) prolongée (7 jours) sur *S. epidermidis*.

INTRODUCTION

MOFs IN PHARMACEUTICAL TECHNOLOGY

GENERAL OBJECTIVES AND AUTHOR CONTRIBUTIONS

C. Tamames-Tabar, A. García-Márquez, M. J. Blanco-Prieto, C. Serre and P. Horcajada, “MOFs in Pharmaceutical Technology” in *Bio- and Bioinspired Nanomaterials*, Ed. E. Ruiz-Molina, Wiley-VCH Verlag GmbH & Co. KGaA (Germany), 2014, Accepted.

From Ancient times till today, pharmacy has evolved regarding the specific needs of the patient. Today, the inclusion of drugs in particulated systems with different natures (not only in size but also in composition), permits the formulation and design of tailored-made treatments for each individual. Among all the already existing drug delivery systems (DDS), Metal-Organic Frameworks (MOFs) are a very versatile new type of hybrid crystalline solids that have recently emerged in biomedicine. Despite the novelty of this last application, their usage in other industrial processes, such as, catalysis, gas storage and separation, has been widely studied.

Therefore, and with the aim of understanding the state of art of MOFs as DDS, we have investigated into detail all the important factors that take place in drug delivery and MOFs in the Introduction of this PhD Thesis, which has been reported as a Book Chapter. This work has been divided in 4 sections for an easier comprehension of the reader. The sections are: (i) introduction of MOFs in pharmaceutical technology, studying the evolution of pharmacy, as well as comparing several particulated DDS; (ii) a general description of MOFs regarding their synthesis, functionalisation, stability and toxicity profiles; (iii) a detailed study of MOFs for therapeutics in which two different strategies in drug delivery are discussed, including the inclusion of the drug inside the MOF porosity or as a constitutive part of the hybrid network, as well as the understanding of the encapsulation/release processes. In addition, the potential use of MOFs in theranostics and some efficacy studies regarding MOFs as DDS have been also discussed, and (iv) final conclusions and remarks of the work.

All the authors have actively contributed in the writing of this bibliographic work. In particular, C. Tamames-Tabar has participated in the introductory part (the description of MOFs, their stability and toxicity) and in the third part, MOFs for therapeutics. Dr. A. García-Márquez has been involved in the writing of the introduction part dealing with the synthesis, functionalisation and shaping of MOFs, as well as in the third part, specifically on the BioMOFs part. In addition, he has assessed in the rest of the manuscript. Dr. M. J. Blanco-Prieto has actively supervised the complete manuscript, especially all the topics regarding pharmaceutical technology and the *in vitro* and *in vivo* applications. Dr. C. Serre has actively supervised the whole manuscript, especially the second section dealing

with the MOF description. Finally, Dr. P. Horcajada has actively supervised the entire work, with a special emphasis in the second and third section.

MOFs IN PHARMACEUTICAL TECHNOLOGY

C. Tamames-Tabar^{a,b}, A. García-Márquez^a, M. J. Blanco-Prieto^b, C. Serre^{a*}, P. Horcajada^{a*}

^a. *Institut Lavoisier, UMR CNRS 8180, Université de Versailles Saint-Quentin-en-Yvelines, 45 Avenue des Etats-Unis, 78035 Versailles Cedex, France.*

^b. *Departamento de Farmacia y Tecnología Farmacéutica, Facultad de Farmacia, Universidad de Navarra, Irunlarrea 1, 31008 Pamplona, Spain.*

Emails: ctamames@alumni.unav.es, ponchacalongarma@gmail.com, mjblanco@unav.es, serre@chimie.uvsq.fr, horcajada@chimie.uvsq.fr

Bio-and Bioinspired Nanomaterials, Wiley-VCH Verlag GmbH & Co. KGaG (Germany)

2014

Edited by: Daniel Ruiz-Molina, Fernando Novio and Claudio Roscini

Accepted

Keywords: Controlled Release, Drug Carriers, Metal-Organic Frameworks (MOFs), Porosity, Biomedicine, Pharmacy.

SYNOPSIS

Nowadays, the main trend in pharmaceutical technology is the discovery of new dosage forms, which might improve the treatment and the lifestyle of the patient. Polymeric nanoparticles (NPs), lipid NPs, dendrimers, liposomes, nanocrystals and carbon nanotubes (CNTs), among others, have been proposed as drug delivery systems (DDS).

Metal-Organic Frameworks (MOFs) are a new alternative in this domain. These porous crystalline hybrids, built up from organic polycomplexant linkers and an inorganic core, are of interest due to: (i) their tunable hybrid composition (metals, linkers) and (ii) their important and regular porosity. Although these solids were first considered for other applications (*i.e.* catalysis, separation, gas storage, sensing), they have been recently introduced in biomedicine due to their excellent encapsulation and release properties. Furthermore, MOFs can be non-toxic (*i.e.* iron carboxylates) and might include within their framework biologically active moieties (BioMOFs), in which the therapeutic drug is released through the disruption of the framework.

We propose here an overview of (i) pharmaceutical technology, including drug administration routes and existing or new controlled drug carriers, (ii) the use of MOFs in biomedicine from their synthesis, formulation, toxicity, stability, as well as, other bioapplications (BioMOFs, etc.) and finally (iii) an analysis of their *in vitro* and *in vivo* efficacy.

1. INTRODUCTION

Since the early progress of medicine and pharmacy from the time of Hippocrates (460-370 B.C.) and Galen (130-200 A.D.), the perception of illness and its treatment have evolved over the years. Since the beginning of the 20th Century, the aim has been to achieve a more personalized treatment, a utopian idea that was first proposed in the 1980s, alongside the pioneering works that used microparticles (MPs) [1] and nanoparticles (NPs) [2]. This idea was based on the need to target a drug towards specific parts of the body, in order to decrease the toxicity of treatment, enhance the drug's properties, its effect and the patients' life quality together with the completion of the treatment [3].

The re-emergence of concepts that are already known like "drug controlled carriers" has gone hand-in-hand with this evolution in pharmaceutical technology. It is quite clear that when a drug is formulated in a pharmaceutical form, it is released to the media and depending on the dosage form, the release profile varies. One of the concepts that addresses such controlled targeted release is drug encapsulation, based on the association of two chemical species, the carrier and the selected drug, which are chosen according to the following criteria.

Encapsulating a drug into an inert or non-inert carrier can enhance several parameters, such as: the drug bio-distribution, the biological half-life ($t_{1/2}$) of the active species and its therapeutic effect. This overcomes problems like drug solubility, its colloidal stability and rapid decomposition. It also notably decreases its adverse effects [3]. In contrast, the type of carrier chosen for drug encapsulation must, above all, be safe and present compatibility with the drug's physicochemical characteristics by preserving its stability and activity. It should also respond to the treatment target, and permit the expected release profile for the chosen administration route. Nowadays, there are several commercial formulations using MPs and NPs, the majority for cancer chemotherapy [4].

Since the advent of nanotechnology and nanomedicine in the late 1990s [5], a large variety of NPs has been proposed as drug nanocarriers including lipids, polymers, metal clusters, carbon structures or hybrid coordination compounds [3; 5], among others. In addition to their different compositions, they can be dense, porous or hollow. Despite their complexity, a general classification independent of their organic, inorganic or hybrid nature consisting of three generations can be proposed: 1st generation or non-functionalized NPs, 2nd generation or those presenting a polymer coating and a 3rd generation exhibiting specific macromolecules such as antibodies, peptides or specific biomolecules for targeted release [5].

This field is in continuous development due to the discoveries made over the last few decades. One of the most recently proposed drug-carrier systems is based on NPs of Metal-Organic Frameworks (MOFs) or Porous Coordination Polymers (PCPs). Within the second part of this Book Chapter, MOFs will be reviewed. Due to their unique combination of porous architecture and physicochemical properties, one can nowadays consider these to be very promising drug carriers.

2. METAL-ORGANIC FRAMEWORKS

2.1 Description

MOFs are crystalline solids built up from the ionocovalent association of inorganic entities (polyhedra, clusters, layers, etc.) with polycomplexant ligands (*i.e.* phosphonates, carboxylates, imidazolates, etc.), giving rise to porous networks [6-8]. This new class of porous solids, which emerged in the late 1980s as a simple concept [9], became by the end of the 1990s a major field of research associated with a large number of potential applications.

The high versatility of MOFs, which is due to their large variety of compositions, crystalline structures or crystal shapes, brings other advantage over other types of materials. This is particularly the case for flexible MOFs, able to reversibly change their conformation or pore openings under external *stimuli* (*i.e.* molecule inclusion, temperature or pressure), thus behaving as dynamic frameworks [10; 11]. One can thus classify MOFs into two categories: flexible structures (see above) or rigid frameworks that possess a conformation remaining unchanged with respect to the application of external *stimuli*.

Moreover, MOFs encompass a wide variety of potential applications, such as fluid separation/storage, battery materials, catalysis, water purification, sensing and light harvesting devices [6; 7]. More recently, the biomedical field has emerged with promising features [12]. Since the pioneer concepts reported in 2006, many issues related to their potential limitations for practical use, such as their toxicity, degradability and formulation (including scale-up and shaping), have been tackled (Figure 1).

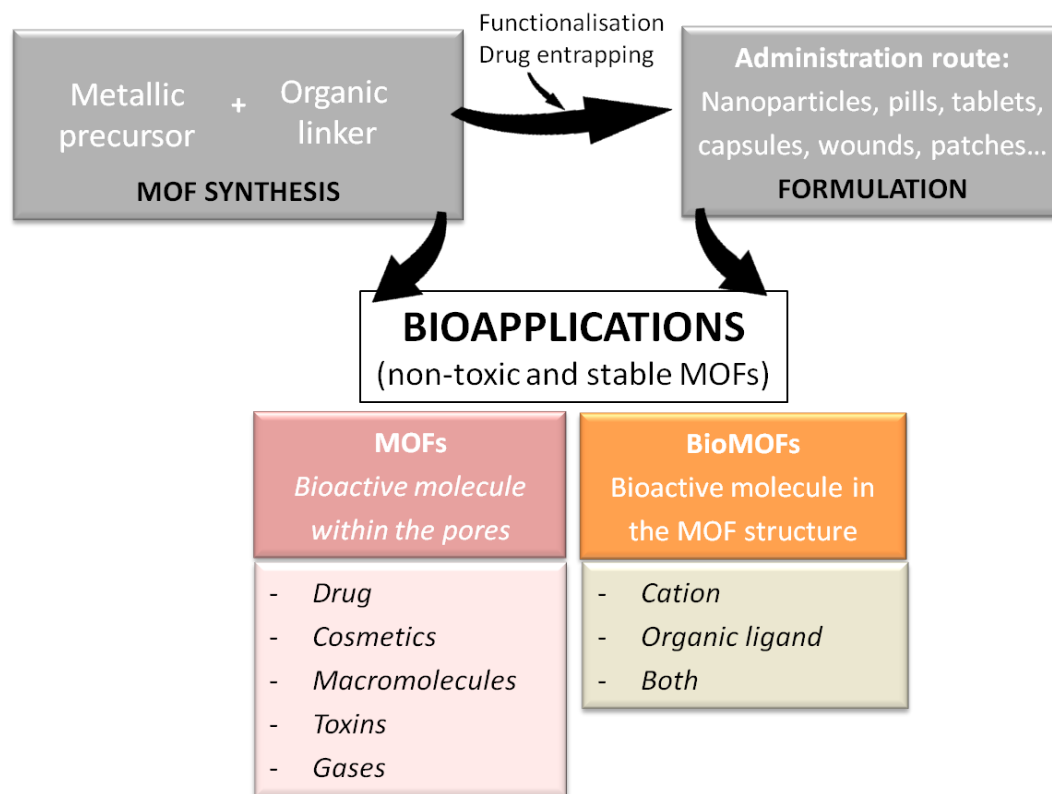


Figure 1. General scheme of the MOF manufacturing process for bioapplications, in which first the synthesis is done, continued by the activation and characterization processes together with further formulation/shaping, as well as MOFs in bioapplications, which are mainly divided into two groups: the incorporation of the bioactive molecule (*i.e.* drug, cosmetic, enzyme, toxin or gas) inside the pores of a MOF or the bioactive molecule being part of the MOF structure.

2.2 Synthesis, Formulation and Functionalization/Shaping

Synthesis and Formulation/Shaping

Prior to synthesizing a MOF for a given bio-application, it is necessary to consider the toxicity of all the reactants and additives used during the whole synthetic procedure, as well as the possible scale-up and sterilization treatments.

So far, it is clear that MOFs can be synthesized by different methods, including: hydro/solvo-thermal conventional heating route [13], microwave-assisted hydro/solvo-thermal synthesis [14; 15], mechano-chemistry [16], sono-chemistry [17], electrochemistry [18], ionic liquids [19] aerosol, inverse emulsion and microfluidics (Figure 1).

The microwave-assisted synthesis method has been widely used in organic chemistry and has been recently transferred to the synthesis of MOFs [14; 15]. It permits to shorten

reaction times from hours or days down to a few minutes, an important factor when considering the industrial scale-up. The fast crystal nucleation kinetics, associated with more homogeneous heating, often leads to high yields of monodispersed and smaller particle sizes in short times [20]. This method was successfully applied for the preparation of non-toxic submicron and nanometer sized iron (III) carboxylate MOFs [21-23].

One step further concerns the design of MOF dosage forms. However, one must first consider the administration route. NPs, pills, capsules, wounds and transdermal patches are possible examples of MOF-containing drug administration devices. We will describe here some of the current shaping techniques, coupled or not with the synthetic method, which would allow the elaboration of drug administration devices (Figure 1).

One of most recent advances in terms of MOF synthesis strategies is the continuous spray drying method (or aerosol casting) [24; 25]. Aerosol-based related techniques also present a very versatile alternative for shaping.

Microfluidic-assisted shaping of MOFs is also a nice way to obtain hierarchical solids in a continuous manner, and it can lead to monodisperse microcrystals [26] and nanofibers of coordination polymers [27].

Micro-emulsion techniques are suitable for particle shaping, allowing control over shape, size and polydispersity [28; 29].

In addition to the direct coupling of synthesis and shaping, other formulations have been proposed. For instance, one of the first reported MOF formulations consists of tablets, based on iron(III) carboxylates MIL-53 and MIL-100 containing ibuprofen (Ibu), obtained under low pressure without any binder [30]. Ananthoji *et al.*, have also developed a composite formulation containing an anionic iridium 4,5-imidazolecarboxylate MOF loaded with the anti-arrhythmic procainamide hydrochloride (PHCl) in a solution containing monomers and cross-linkers [31]. Other composite MOF formulations are based on hydrogels containing different polymers, such as poly(vinylpyrrolidone) (PVP), which are very resistant as well as water soluble when compared to other polymers, such as polyacrylonitrile (PAN) [32].

MOF thin films can also be considered as attractive porous supports for drug encapsulation [33], as well as micro and nanolithography techniques for diverse applications [34].

Morris *et al.*, have reported a topical patch, based on a mixture of nitric oxide (NO) entrapped within the pores of the nickel 2,5-dihydroxyterephthalate CPO-27(Ni) and hydrocolloids, which is able to release its NO content within 10 days [35].

Electrospinning has finally been already proposed as a possible MOF formulation, resulting in the preparation of porous MOF-polymer composite nanofibers [36], such as

ZIF-8 (zinc 2-methylimidazolate)/PVP nanofibers [37] and pearl necklace containing HKUST-1 and MIL-101(Fe) [38].

Functionalization

Modifying the surface of a porous solid can be achieved either directly on the framework itself (pores) or at the external surface of the particles. This is typically realized through the direct use of functionalized linkers or more commonly, *via* a post-synthetic approach [39]. In accordance with the second and third NP generation defined in Section 1, these NPs present a functionalization of the outer surface of the particle with specific entities that confer hydrophilicity, stealth character or targeted drug delivery through specific recognition biomolecules. Following this strategy, it is possible to cross the first immunologic barrier, modulate the hydro/lipophilic balance of the drug delivery material, specifically target an active site or increase its stability towards physiological conditions.

One of the first functionalizations of the outer surface was performed by grafting different poly(ethylenglycol) (PEG) polymers to confer stealth properties by increasing the blood circulation times of MOF NPs [22]. The authors have also observed that such a functionalization occurs both within the pores and at the external surface. This nevertheless settles the way to perform selective functionalization of the particle external surface with a large variety of biosourced or biocompatible polymers/molecules, leading to more stable nanosized drug loaded MOF dispersions [40].

Coordination polymers with lipidic shell coatings have led to a targeted delivery of antifolate cancer drugs with superior *in vitro* activity [41]. Liu *et al.*, worked on the design of a new coordination polymer containing bisphosphonates (BPs) [42] and Huxford *et al.* studied a new BioMOF containing methotrexate (MTX) in the MOF structure [41]. In both cases, particles were covered with a lipid bilayer containing several lipids. More sophisticated lipidic shells can bear specific groups, thus yielding a third generation of drug nanocarrier. The functionalization of a calcium palmidronate coordination polymer with a dioleoyl trimethylammonium propane, allowed the internalization of the drug nanocarrier [42]. The surface functionalization *via* sol-gel chemistry can also confer additional properties or an increased stability. Thus, Lin and co-workers have reported MOF-templated silica core-shell rod-like nanostructures as sensitive luminescence probes [43].

2.3 Stability and Toxicity

A key factor for the practical use of MOFs in biomedicine is their stability in body fluids. It is vital to assess this, since the drug loaded MOF NPs will reach the active site and deliver the cargo, and then later degrade, avoiding the toxicity effects derived from accumulation phenomena. In some cases, when the drug is incorporated as a constitutive part of the MOF skeleton, the release of the active compound will inherently rely on the kinetics of MOF degradation [44].

Prior to select a MOF for a given administration route, one needs to determine its stability in water and in several simulated body fluids.

One of the first studies described the poor stability of a microporous metal 2,5-dihydroxyterephthalate M-CPO-27 (M=Ni, Co, Mg, Zn and Mn) [45]. Further reports showed that iron(III) carboxylate MIL-100 [46; 47], zirconium(IV) terephthalate UiO-66 [48; 49] and zinc adeninate [50] exhibited higher stabilities in pure water. Additional degradation tests in more complex media showed that iron(III) carboxylates are biodegradable in presence of phosphate buffer saline (PBS) solutions, due to the formation of iron oxides or phosphates out of the slightly acidic or neutral conditions [22; 51].

However, as mentioned in Section 2.2, the stability of the MOF can be modulated *via* functionalization (*i.e.* silica coatings) and an adequate selection of the structure and composition.

MOFs toxicity must be evaluated prior to any biomedical application [52]. Due to their high versatility, there might be no general rule regarding their toxicity profile. Rationally, each cation used for MOF synthesis has its own toxicity, the values for chronic oral dose ranging from daily doses of $\mu\text{g}\cdot\text{Kg}^{-1}$ (*i.e.* Cd) up to more than $1\text{ g}\cdot\text{Kg}^{-1}$ (*i.e.* Ca) [53]. However, the metal toxicity parameters are often expressed for oxides or salts, which often exhibit a different degradation profile compared with those of MOFs. Nevertheless, one could propose that MOFs designed for bioapplications should contain cations that have high daily requirements in the body, which is an illustrative parameter for the accepted toxicity threshold. For instance, the high daily requirements of cations such as Mg^{2+} , Ca^{2+} , Fe^{3+} or Zn^{2+} [54-57], make them interesting candidates for biomedical applications. In addition, the toxicity of the cation is strongly related to its possible accumulation in the body. Thus, some inert metals such as zirconium can be easily removed by the body [58], and thus be considered non-toxic.

Notwithstanding, MOFs also contain an organic part, which must also be biocompatible. However, considering the almost infinite number of organic ligands, each organic moiety might be treated independently.

Although 1st level toxicological considerations can be achieved by considering the reported toxicity data of the isolated constituent of the MOFs (organic and inorganic), toxicological data about MOFs is very scarce, and this factor might be a clear limiting step to any development in this field.

The cytotoxicity of a range of MOFs in different cell lines has nevertheless been reported. Ruiz-Molina *et al.* studied the behavior of Zn(1,4-bis(imidazol-1-ylmethyl)benzene) (Zn(bix)) PCPs in human promyelocytic leukemia HL-60 cells. After the treatment with the PCPs, the cell survival rate was 80 % [59].

Zanella *et al.* studied the behavior of copper ions and 3,5-bis(pyridin-3-ylmethylamino)benzoate (5–100 $\mu\text{g}\cdot\text{mL}^{-1}$) towards breast cancer MCF-7 cells, obtaining IC₅₀ values slightly higher than other Cu-based polymers, probably due to the interaction of the PCP and the disaggregation of the metal ions of the PCP. The same material also showed potent *in vitro* cytotoxicity against cervical cancer HeLa cells and human lung NCI-H446 cancer cells [60].

The stability of thin films of the porous copper terephthalate SURMOF-2 has recently been studied by Hanke *et al.* A high stability of SURMOF-2 was found in pure water and in artificial seawater, which differs from those obtained when introducing the MOF in PBS and in DMEM cell culture medium, in which a rapid dissolution was observed. Moreover, no adverse effects on the adhesion of SURMOF-2 on fibroblasts were observed, indicating that this material was biocompatible [61].

The cytotoxicity of PCPs made from Tb(III) ions and (diaminedichlorodisuccinato) Pt(IV) complexes was tested in HT-29 cells (human colon colorectal adenocarcinoma) and after 72 h no appreciable cell death was observed, linked to the scarce entry of Pt(IV) ions inside the cell [62].

Liu *et al.* introduced two antitumour N-containing BPs into Ca-based crystalline particles and coated the entire particle with single lipid bilayers. The authors studied their cytotoxicity in human non-small cell lung H460 cancer cells, observing no cell death due to the impossibility of entering the cells, which was not the case when using lipid-coated coordination polymer, probably because of the fusion of the cationic lipid bilayers with cell membranes [42].

Geranmayeh *et al.* synthesized a novel zinc terephthalate MOF and evaluated its cytotoxicity in human amniotic epithelial hAEC cells, showing a low cytotoxic effect in a wide range of concentration (up to 1 mM) and time intervals (up to 72 h) [63].

The cytotoxicity of the porous Fe-MOF NPs based on the endogenous ligand fumarate MIL-88A(Fe) or exogenous trimesate MIL-100(Fe) has been evaluated in recent years [22; 64; 65], exhibiting very low IC_{50} values, comparable with those of currently available nanoparticulated systems [66-70]. A more recent study has systematically evaluated the cytotoxicity of a large series of porous nanoMOFs with different compositions and structures in two different cell lines (J774 and HeLa), concluding that (i) the MOFs NPs exhibit low cytotoxicity, comparable to that of other commercialized nanosystems, and (ii) a strong dependence between the MOF composition and the cytotoxicity occurs. The less toxic particles were the Fe-MOFs with the lower hydrophilic/hydrophobic balance and the most toxic the Zn-MOF. Moreover, MIL-100(Fe) cell penetration studies were carried out showing a very fast internalization in J774 when compared to the HeLa cell line (Figure 2) [71].

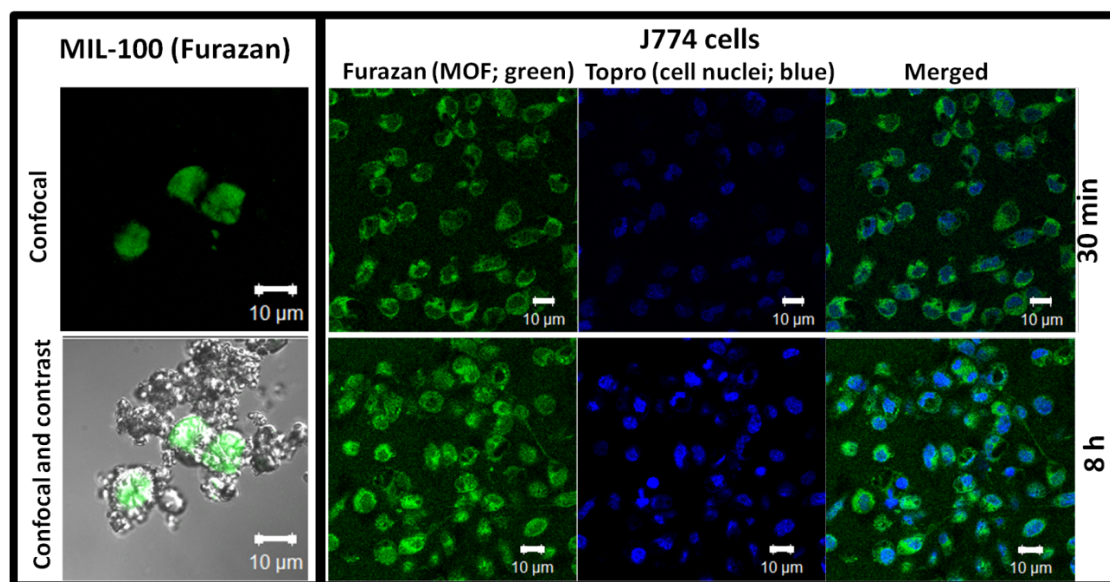


Figure 2. Confocal microscopy images of the micrometric MIL-100(Fe) particles encapsulating the green fluorophore furazan (left column). Cellular uptake kinetics of nanometric MIL-100(Fe) grafted with furazan done in J774 mouse macrophage cells after 30 min and 8 h (right).

However, it is well-known that cytotoxicity is not always related to *in vivo* toxicity. To the best of our knowledge, the only study regarding MOF *in vivo* toxicity has been carried out by some of us, using high doses of porous iron(III) carboxylates, based on three carboxylates with different polarities: MIL-100 (trimesate), MIL-88A (fumarate) and MIL-88B_4CH₃ (tetramethylterephthalate). MOF NPs together with the linkers alone were intravenously administered to rats and their toxicity and ADME (Absorption Distribution Metabolism Excretion) profile evaluated. The biochemical and enzymatic

parameters as well as histological cuts were evaluated, showing an absence of acute and subacute toxicity. The uncoated MOF NPs were rapidly captured mainly by the liver and spleen and then progressively degraded. Notably, both the iron excess and the exogenous linkers were directly removed by urine and dejections [52]. Although these results are very encouraging, similar systematic toxicological evaluations are strongly needed for a larger number of MOFs that have shown promising properties in biomedicine.

3. MOFs FOR THERAPEUTICS

Among the large variety of possible MOF bioapplications, this chapter will however be focused on the controlled delivery of therapeutic molecules (Figure 1).

The active molecule can be incorporated in the MOF in three different ways: (i) the active ingredient is adsorbed and entrapped inside the pores [72; 73], (ii) incorporating an endogenous and/or active compound as a constitutive part, either organic or inorganic, of the MOF architecture itself, leading to so-called BioMOFs [44] or (iii) by a combination of the first two methods if the BioMOF is porous.

3.1 BioMOFs

Although the incorporation of endogenous and/or active cations and/or ligands into a MOF's network is not new [74], their use in therapeutics as drug carriers is very recent [44]. Imaz *et al.* recently published a review on this topic, defining Metal-Biomolecule MOFs with the unique criterion of the presence of a biomolecule within its structure [75]. Other reviews are those of McKinlay *et al.* [76; 77], Imaz *et al.* [75] and Novio *et al.* [59].

As in the case of BioMOFs, the therapeutically active molecule can be a structural motif of the lattice, in which the main advantage lies in avoiding multistep procedures to prepare the loaded material, maximizing the drug payload, and the use of well-established toxicity components. In addition, the porosity of the particle is not necessarily required, since the release of the active principle will occur throughout the degradation of the MOF. On the other hand, the synthesis and structure characterization of these solids might be time-consuming due to (i) the need to optimize the crystallization conditions to achieve a complete structure determination, (ii) elude the use of toxic solvents and (iii) control of the particle size.

An increasing number of endogenous or therapeutically active ligands have been used to prepare BioMOFs, including aminoacids (aa) [78; 79], peptides [80-83], nucleotides [84], nucleobases [50; 85]), γ -cyclodextrins [86], or small endogenous bioactive molecules [20;

44; 87-89]. Other more specific molecules, such as, nitrogen containing BPs [42; 90] and cisplatin prodrugs [73], among others, can be used. However, some among them involve highly toxic metals such as Co and Ni, which certainly will rule out their use in biomedicine. Notably, so far, BioMOFs based on biocompatible metals are still scarce.

Aa-based MOFs have been recently well explored [75]. However, very few studies dealing with their stability and release profiles under biological conditions and/or their biological activity have been reported [44; 89].

One can also mention the work of Lin's group using cisplatin derivative coordination polymers [62; 91]. Others have used MTX [41; 92], daunorubicin and Doxo coordination spheres [93].

Recently, the synthesis of bioactive phosphonate-containing MOFs has been extensively studied. These solids exhibit very interesting properties in therapeutics due to, among other things, their activity in anticancer treatment and/or bone repair. Vega *et al.* synthesized Na-alendronate crystals [94]. Later, Yoshinari *et al.* have reported the synthesis of $\text{Ca}_3(\text{PO}_4)_2$ -coated and BP immobilized Ti implants, suggesting that a thin coating of $\text{Ca}_3(\text{PO}_4)_2$ followed by BPs immobilization is effective in the promotion of osteogenesis on surfaces of dental implants [95]. Fernández *et al.*, synthesized a novel Ca-BP MOF with potential applications in bone repair [96]. Liu *et al.* have reported Ca-palmdronate and Ca-zoledronate 1D coordination polymers that were further functionalized with lipid bilayers with anisamide to increase their stability, biocompatibility and targeted drug delivery properties [42]. A very recent work reports the synthesis of a novel Ca-alendronate for a bone repair synergic effect. However, this solid exhibited no bioactivity due probably to its very high stability in the biological media, in agreement with the strong chelating bond nature of the phosphonate towards Ca^{2+} ions [90].

Other BioMOFs built up from other endogenous cations presenting a very good biocompatibility due to the important levels presented within the body, have also been reported and proposed for biomedical applications. Note also that some of them exhibit a biological effect, due to the cation with in some cases a synergetic effect between the cation and the linker (*i.e.* Ag and Zn as antibacterial agents). For instance, in the case of iron-containing bioactive MOFs, an Fe(III) nicotinate has been proposed for the controlled release of B_3 vitamin presenting pellagra-curative, vasodilating, and antilipemic properties [44]. Moreover, Fe(III) fumarate that possesses both an endogenous metal and ligand has already been tested as an oral iron complement. Kin *et al.* have also reported a 3D Fe(III) glutarate framework with potential applications in biomedicine [97].

Slenters *et al.* have described an Ag-nicotinate for dental and body implants applications. These materials showed antimicrobial activity, having a potential use in preventing implant infection [98; 99]. Alongside, Berchel *et al.* reported a Ag₃(3-phosphonobenzoate) with Gram positive and Gram negative antibacterial activity [100]. Similarly, a series of 3D silver coordination polymers based on 1,3,5-triaza-7-phosphaadamantane-7-oxide (PTA=O), a type of diamondoid building blocks and a phosphate derivative have shown antibacterial and antifungal properties [101].

Wang *et al.* prepared a new Cu-PCP based on the 4,4'-dicarboxy-2,2'-bipyridine (H₂dcbp) linker. Its antibacterial activity was assessed on particles exhibiting different shapes and evaluated on different bacteria, showing low minimum inhibitory concentration (MIC) values. Interestingly, the antibacterial activity seems to be strongly related to the particle shape [102].

The Zn-adeninate or BioMOF-1 possesses both a bioactive cation and an endogenous ligand [103]. Although its therapeutic activity has not been reported yet, this solid could present additional antibacterial properties.

Azobenzene derivatives are associated with an antimicrobial activity, which depend on the type of substitution [104; 105]. Thus, a 1D microporous 3D MOF (BioMIL-3) has been prepared based on the biocompatible Ca²⁺ and the 3,3',5,5'-azobenzenetetracarboxylate ligand. This solid exhibits coordinatively Ca²⁺ Lewis acid sites able to trap and deliver NO at a biological level [106]. Similarly, other MOFs based on biocompatible cations (*i.e.* Ca, Mg, Zn, Fe) azobenzene derivatives might be potentially of interest for this type of applications [107-110].

Other series of MOFs based on bioactive cations with imaging properties (Gd³⁺, Mn²⁺ or Fe³⁺) have also been reported [77; 111]. However, imaging applications have been skipped from this Book Chapter as it is mainly focused on MOFs as drug vehicles.

3.2 Active Ingredient Adsorption and Release from MOFs

In order to develop bioapplications of MOFs, one of the initial strategies was to exploit the porosity and the inner chemistry of the pores, with the aim of encapsulating active molecules that can be gradually released, without their early degradation before reaching the targeted organs. MOFs presented a suitable alternative to other mesoporous materials such as zeolites [112-115] and mesoporous silica particles [116], exhibiting in some cases, higher drug loadings and more controlled deliveries [72].

Unlike the case of BioMOFs where the immobilization of the drug is achieved during the synthesis process, encapsulation within porous MOFs is mainly performed post-

synthetically using the preformed MOF [22; 77]. Thus, we discuss below the impact of the parameters that govern both drug encapsulation and release.

As for most carrier systems, the main two basic criteria that govern encapsulation are: (i) the concordance between the size of the pores and the one of the molecule (hydrodynamic diameter) and (ii) their chemical compatibility. Pore size might appear as a limitation of MOFs in comparison with ordered mesoporous silica with larger pore sizes. However, several biocompatible mesoporous MOFs have been reported that might permit the encapsulation of a broad range of large molecules [117; 118] while achieving high loadings. Additionally, the easily tunable amphiphilic internal microenvironment of MOFs, with a polar (inorganic part) and apolar fraction (organic ligand), might be sufficient for the encapsulation of a large variety of hydrophobic/hydrophilic molecules [22; 119; 120].

Finally, the biodegradability of the MOF is a crucial parameter, since the MOF once administered will have to deliver its cargo to the desired site of action, release the encapsulated drug and then shall be eliminated from the body to avoid toxicity issues.

Several molecules have been encapsulated in MOFs and will be classified into the following groups: drugs, cosmetics, enzymes, toxins and gases. This Book Chapter will exclusively focus on drugs (Table 1) and cosmetics.

Drugs

The proof of concept was reported by some of us in 2006 encapsulating the analgesic and anti-inflammatory ibuprofen (Ibu) within the rigid mesoporous Cr(III) carboxylates MIL-100 and MIL-101 [72]. A typical drug encapsulation is performed by impregnation, suspending the MOF in a solution containing the molecule to be encapsulated. Whereas exceptionally high loadings were obtained (up to 1.40 g Ibu·g⁻¹), the release of the total cargo in 3 or 6 days was achieved in a controlled manner from the pelletized solids. Later on, the use of flexible microporous Fe(III) and Cr(III) terephthalate MIL-53 allowed a better control of the drug release with very slow releases of Ibu (3 weeks) and predictable zero-order kinetics, with smaller Ibu encapsulated amounts (20 wt %) due to the lower pore volume [30].

Recently, Cunha *et al.* have also reported the encapsulation of Ibu within a series of functionalized rigid microporous Zr(IV) terephthalate UiO-66 type MOFs [121].

Rodrigues *et al.* also studied the encapsulation of Ibu in Zn terephthalate MOFs. After 8 days of contact between the MOF and the drug, Ibu loadings up to 44.5 wt % were reached. This study was then extended to other molecules such as antibiotics, gentamicin and amoxicillin, with an emphasis on the analysis of energetics of the host-guest

interactions. However, no information dealing with the drug releases was given [122]. Here, one could have tentatively expected an antimicrobial synergic effect between the Zn and the encapsulated antibiotic, but this was not investigated.

Table 1. Drugs encapsulated in different MOFs.

MOF	Drug	Loading (%)	Application	Reference
MIL-100(Cr)	Ibu	35	Anti-inflammatory/ analgesic	[72]
MIL-101(Cr)		1.38*		[72]
MIL-53(Cr)		22		[72]
MIL-53(Fe)		21		[72]
UiO-66(Zr)		35		[121]
Zn(BDC)(H ₂ O) ₂		45		[122]
HKUST-1(Cu)	Nimesulide	20		[130]
MIL-101(Fe)	ESCP	13	Antitumoral	[123]
MIL-100(Fe)	Doxo	9		[72]
Zn(bix)		21		[124]
MIL-100(Fe)	Bu	25		[72]
Zn(bix)	Camptothecin	21		[124]
Zn(bix)	Daunomycin	21		[124]
ZIF-8(Zn)	5-FU	45		[125]
Zn-based MOF (TATAT chiral linker)		50		[126]
MOF-1(Zn)		37		[127]
MOP-15(Cu)		24		[128]
Cu-BTC(Cu)		82		[129]
MIL-100(Fe)	CDV	16	Antiviral	[72]
MIL-101_NH ₂ (Fe)		42		[72]
MIL-100(Fe)	AZT-Tp	24	Antiretroviral	[51; 72]
MIL-101(Fe)_NH ₂		42		[72]

* Encapsulation expressed in g of drug *per* g of MOF

Some of the most relevant illnesses in research are AIDS and cancer, due to their high worldwide morbidity and mortality ratios. Several porous Fe(III) carboxylates were chosen to host challenging antitumor (Busulfan-Bu and Doxo) and antiviral (azidothymidine triphosphate; AZT-Tp and cidofovir; CDV) (Figure 3) [22], drugs that exhibit severe physicochemical and physiological drawbacks, such as poor aqueous solubility and stability [131; 132], very low bioavailability accompanied by important toxicity in side organs.

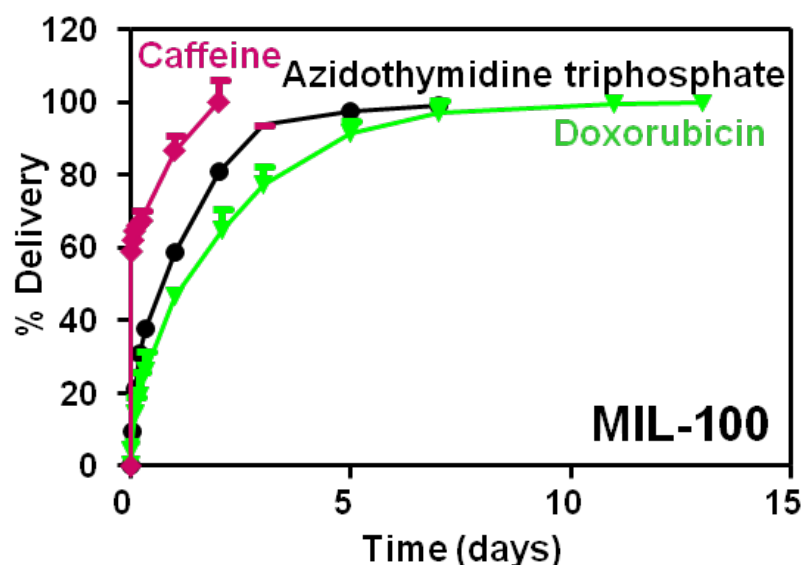


Figure 3. Drug delivery profiles of 3 different drugs in iron(III) carboxylate MIL-100 NPs: the antiretroviral azidothymidine triphosphate (AZT-Tp; ●), the antitumoral doxorubicin (DOXO; ▼) and the cosmetic caffeine (Caf; ◆). Caffeine shows a faster delivery from the MOF (MIL-100) when compared to the other 2 drugs, which show a more sustained release.

Very high loadings were achieved in all cases [22]. In particular, the mesoporous Fe(III) aminoterephthalate MIL-101-NH₂ NPs internalized record loadings up to 42 wt % of CDV and AZT-Tp, being much higher than in any other nanoparticulated system [12; 72]. Moreover, MIL-100(Fe) NPs showed exceptional drug capacities, with maximum loadings of 25, 9, 16 and 24 wt % for Bu, Doxo, CDV and AZT-Tp, respectively (Table 1).

Moreover, the antiretroviral AZT-Tp and the antitumor Doxo were progressively released from MIL-100(Fe) NPs under simulated physiological conditions (PBS, 37 °C) in 5 and 14 days, respectively, as a consequence of a combination of strong host-guest interactions and diffusion processes (see Section 3.3) [12; 51]. The slow release of Doxo, over up to 2 weeks, seems to be related to its hydrophobic character [133]. In the case of AZT-Tp, a direct coordination of the drug on the unsaturated metal sites of MIL-100(Fe) led to a sustained release of AZT-Tp, triggered by the phosphates from PBS [51; 134].

On the other hand, Bu showed a much faster release, albeit longer than the one obtained from polymer nanocarriers, within less than 8 h [22]. Using both experimental and computing simulation techniques, authors nevertheless proposed the use of flexible and/or amino-functionalized MOFs for an improved controlled release of Bu [64]. Imaz *et al.* studied the encapsulation of antitumor agents (Doxo, camptothecin and daunomycin) in a Zn-based MOF Zn(bix), leading to encapsulation efficiencies of 21 %. The release

profile (PBS, 37 °C) of the drugs was however rather fast, as almost 80 % of the total charge was released within 8 h [124].

Taylor-Pashow *et al.* also studied the encapsulation of an antitumor prodrug ethoxysuccinate-cisplatin (ESCP) using silica coated MIL-101(Fe)-NH₂ NPs, leading to an important loading of 13 wt % (Table 5). Their aim was to use the MOF for theranostics, *i.e.* both as a drug carrier and a contrast agent. The release of the drug (PBS, 37 °C) was achieved in a controlled manner within 80 h [123].

Within the past few years, several studies have focused on the development of new dosage forms of the antitumor agent 5-fluorouracil (5-FU) using Zn or Cu based MOFs in order to decrease its side effects. Sun *et al.* first proposed several Zn-based MOFs for the successful delivery of 5-FU [125], such as ZIF-8 (45.5 wt %), leading to an efficient pH-sensitive drug delivery system. Under acidic conditions (pH=5) a release of 85 % of the total load was obtained in 12 h, whereas in neutral pH (PBS, pH=7.4), the particles showed a more sustained release with a complete delivery after 1 week. Similarly, the same authors achieved loadings of almost 50 wt % of 5-FU using a Zn-MOF containing an achiral ligand [126]. Wang *et al.* also encapsulated 5-FU in MOF-1 ([Zn₃(L)(H₂O)₂].3DMF·7H₂O) (L=1,2,3,4,5,6-hexakis(3-carboxyphenyloxymethylene)benzene)), reaching a loading of 37 wt % with a controlled delivery within 72 h in deionized water at room temperature [127]. Concerning the encapsulation of 5-FU in Cu-MOFs, Wang *et al.*, loaded the drug following a stepwise assembly of copper based Metal-Organic Polyhedron (MOP). The encapsulation loading was of 23.76 wt % with however a very fast release of almost 80 % of the cargo (PBS, 37 °C) within 7.5 h [128]. More recently, Santos Lucena *et al.* encapsulated 5-FU within the porous copper trimesate CuBTC obtaining a remarkable capacity of 0.82 g 5-FU·g MOF⁻¹, and a release of 80 % of the cargo within 50 h (PBS, 37 °C) [129].

Finally, Ke *et al.*, reported the encapsulation of the anti-inflammatory agent nimesulide, which can also be used as an anticancer agent, in HKUST-1 NPs coupled to Fe₃O₄ nanorods in an attempt to associate diagnostics and therapeutics [130]. A 20 wt % loading capacity was obtained together with a very long release profile of 11 days (PBS, 37 °C).

Cosmetics

In 2010, the cosmetic industry's worldwide sales reached \$170 billion dollars. Moreover, the percentages of skin care and fragrances represented 27 and 10 %, respectively, illustrating its importance. Here we describe representative examples of the potential applications of MOFs as cosmetic molecule carriers.

Cosmetic molecules such as urea, caffeine (Caf), benzophenone-3 and benzophenone-4 with different activities have been encapsulated in Fe(III) or Zr(IV) carboxylate MOFs [119; 120]. In particular Caf, a xanthine alkaloid commonly found in commercialized creams such as topic cellulite reducer [135], is currently in the spotlight of several investigations. Its encapsulation is a challenge for the cosmetic industry due to its high tendency to crystallize leading to poor drug loadings (<5 wt %), as well as uncontrolled releases, with a subsequent low efficiency [136; 137]. Caf entrapping reached exceptional payloads (up to 50 wt % in MIL-100) [138]. Other rigid porous MOFs, based on either Fe(III) or Zr(IV), were also tested resulting into important Caf loadings, which were strongly dependent of the MOF structure and composition [121; 138; 139]. In addition, Caf was successfully incorporated into flexible porous MOFs, such as the functionalized iron(III) terephthalates MIL-53 or MIL-88B type structures, with loading rates reaching 30 and 25 wt %, respectively [138; 139]. Progressive releases were achieved under simulated topical conditions (water pH=6.3, 37°C). This is particularly the case of MIL-100(Fe) and UiO-66(Zr), which appear as very promising carriers for the topical administration of Caf, in agreement with their very high payloads together with progressive releases [138] (Figure 3). Recently, Liédana *et al.*, have also reported the encapsulation and release of Caf from ZIF-8. The authors obtained a slightly lower loading capacity than the best one obtained by Cunha *et al.* (28 *vs.* 50 wt %, respectively) [140]. However, a much more controlled release in water was achieved with the Zn-MOF (27 *vs.* 9 days for a delivery of 60 % Caf from MIL-53(Fe) in the same conditions [138]), probably due to the combination of narrow pores and hydrophobic character of ZIF-8.

Apart from the encapsulation of skin care products Vaughn *et al.* have also been working on the encapsulation and release of fragrances. Ethyl butyrate and *D*-limonene were loaded and progressively released through a moisture-triggered process [141]. This proof of concept provides an attractive opportunity for the controlled release fragrance formulations, as well as for the encapsulation of thermolabile molecules with medicinal properties.

3.3 Understanding

The aim of this Section is to tackle the driving forces that govern the most crucial processes for the use of MOFs in drug delivery. Despite the growing literature concerning the encapsulation and release of active ingredients (AI), only few works have focused on the understanding of this topic as a function of both the adsorbate and MOF physicochemical properties.

Encapsulation

The drug encapsulation process is typically performed by *ex situ* impregnation, suspending the dried MOF into a solution containing the biologically active molecule. Alternatively, Liédana *et al.* recently reported a one-step synthesis and encapsulation method [140], achieving a higher Caf loading in the ZIF-8, when compared to simple *ex situ* impregnation (28 *vs.* 4 wt %, respectively). This is probably related to the matter of Caf size ($\sim 7.6 \times 6.1 \text{ \AA}$), which makes the diffusion of the drug through the very narrow windows of the MOF harder ($\varnothing \sim 3.4 \text{ \AA}$). In addition, the very slow release in water (27 days) was then achieved through the flexible character of the framework induced by a rotation of the spacer. Therefore, in the case of MOFs possessing windows with a smaller size than the drug, this method could represent a nice alternative in order to reach higher loadings and longer releases. However, we must bear in mind that this might require synthesis conditions that are compatible with the stability of the adsorbate upon the synthetic conditions.

Concerning the usual *ex situ* impregnation route, this process depends on several physicochemical and structural parameters, such as the experimental conditions, the chemical structure of the adsorbate and the composition and structure of the MOF (*i.e.* porosity, reactive groups, tortuosity) [121].

The impact of experimental parameters on the encapsulation rate has been reported [22; 30; 72; 138]. It was shown that higher drug concentrations, longer times, higher temperatures or successive impregnations increase the drug encapsulation rates.

If one considers the role of the solvent during the encapsulation process, several parameters must be considered. First, as the library of available solvents remains limited for biomedical applications due to toxicity issues, most of the studies use water and ethanol. However, the often-low solubility of the adsorbate as well as the MOF degradability might limit their use. For instance, the insolubility and instability of the antitumour drug Bu required its encapsulation using acetonitrile or dichloromethane [64]. In such cases, the removal of the toxic solvent might be easy with no impact on the stability of the encapsulated drug.

Another study dealt with the loading of Caf in several biocompatible MOFs using either aqueous or EtOH Caf solutions, resulting in significant differences between the materials. It was proposed that for rigid MIL-100(Fe) or MIL-127(Fe) MOFs, EtOH could block the windows due to its coordination on the coordinatively unsaturated (CUS) sites, and therefore, limit the diffusion of Caf [138]. Moreover, the heat of adsorption of EtOH in MOFs, are typically higher than those of water [142; 143], which decreases the loading

capacity of Caf from EtOH solution. In the case of flexible MIL-53(Fe), EtOH only can fully open the pores opening allowing easier diffusion of Caf into the 1D pore system [144]. Gaudin *et al.* developed for the first time a quantitative structure activity relationship (QSAR) approach to rationalize the encapsulation of bioactive molecules in MOFs [139]. Thus, Caf was adsorbed into a series of isoreticular flexible MIL-88B(Fe), wherein the organic linker is functionalized by a large variety of polar and apolar functional groups. The experimental Caf uptake was used as a data set for the prediction to be related through a microscopic interpretation of the main descriptors (physicochemical properties of the linker) that govern the Caf loading. Individual QSAR models showed that, tuning the polarity and the H-donor capacity of the organic linker, one could enhance the Caf encapsulation, suggesting that the functional groups serve as anchoring points for the drug molecules [139].

Later, additional QSAR studies using a series of functionalized UiO-66(Zr) solids and two active molecules (Caf and Ibu), evidenced that when the MOF topology or the nature of the bioactive molecule and the solvent are modified, the descriptors that govern the drug loadings are different [121].

Another study analyzed the impact of phosphorylation of the antiretroviral AZT over its encapsulation rate in MIL-100(Fe) NPs [134], evidencing that the increase of the encapsulation kinetics and loading is inherently related to the degree of phosphorylation. This is due to the direct binding of the phosphate groups on the iron Lewis acid CUS [51; 134].

Release

Prior to analyzing the parameters that drive the drug release, we must be aware of the limitations arising from the drug solubility and the MOF scaffold degradability. The drug delivery is indeed mainly governed by: (i) the MOF degradation under the physiological conditions, (ii) the drug diffusion through the pores and (iii) the drug-matrix and drug-solvent interactions. The influence of these parameters was evidenced with the antiretroviral AZT-Tp [77]. First of all, this drug was more rapidly released from more instable MIL-101(Fe)-NH₂ NPs than from MIL-100(Fe) NPs. Second, very fast releases were also observed when the drug was exclusively adsorbed on the outer surface of MOFs which exhibited pore sizes smaller than the drug dimensions. On the other hand, the drug was progressively released in a controlled manner when encapsulated within the pores of more stable MOFs (*i.e.* MIL-100(Fe) NPs), evidencing the influence of the drug diffusion. The drug diffusivity depends both on the pore architecture (*i.e.* pore size, tortuosity) and

on the drug-MOF interactions [138]. Finally, the effect of the drug-matrix interactions was evidenced through the slower release kinetics of the AZT-Tp from MIL-100(Fe) NPs compared to its non-phosphorylated analogue AZT, associated with the stronger interactions between the phosphate group and the CUS, as mentioned above.

In addition, the release profile of a given drug-MOF couple depends on the release conditions (*i.e.* composition, temperature and stirring), as well as on the targeted administration route. This is well illustrated by the release of AZT-Tp from MIL-100(Fe) NPs in 3 different media, in which the release of AZT-Tp can only be achieved in phosphate-containing conditions, due to the replacement of the AZT-Tp interacting with the CUS by phosphates [51].

Similarly, a very fast Caf release occurred under simulated serum conditions (PBS; pH=7.4; 37 °C), a process which is mainly governed by the MOF degradation, whereas under topical simulated conditions (deionized water; pH=6.3; 37 °C), progressive releases were achieved, being mainly governed by the degree of Caf mobility and MOF-Caf interactions [138].

3.4 Theranostics

A very appealing application of MOFs is theranostics, which encompasses the diagnosis, usually done by different imaging techniques, and the therapeutics, by targeting the release of a drug. Although some important relevant results dealing with theranostics have been achieved during the last 7 years, this Section will only relate the key features of these applications, which are out of the scope of this work, focused on the adsorption and release of active compounds.

However, some very relevant works in this field have to be mentioned. First, we highlight the W. Lin's group contribution [145]. They proposed several magnetic resonance imaging (MRI) contrasts agents based on functionalized prodrug-containing Pt(IV)-MOF, some rare-earth coordination polymers [43; 91, 146, 147], Mn(II)-MOFs [148], as well as sophisticated DSCP-loaded dye-grafted and silica-coated MIL-101(Fe)-NH₂ [62] and ESCP-loaded amino-functionalized Fe₃(μ₃-O)Cl(H₂O)₂(BDC)₃ particles associated to a fluorophore [123] (See Section 3.2). They also proposed Zr-MOFs with [Ru(5,5'-(CO₂)₂-bpy)(bdy)₂] (bdy=2,2-bipyridine) as connecting points, resulting into an important cellular uptake in human lung tumoral cell line (H460) [149].

Rowe *et al.* have also published a MTX-containing Gd-based MOFs coated by several copolymers of a fluorophore [150; 151].

In addition, some of us have proposed biocompatible and degradable iron(III) carboxylates, which combine high drug loadings and progressive releases with favorable MRI relaxivities [22].

3.5 Efficacy

One step further is to evaluate the efficacy of the MOFs using both *in vitro* and *in vivo* tests. Although the results in this area are still scarce, they are very encouraging.

First, the efficacy of the encapsulated drug or pro-drug is of the utmost importance, as it will provide the therapeutic effect. Most of the disclosed activity tests concern the evaluation of the antitumour capacity of anticancer containing MOFs. Thus, the efficacy of Bu-loaded MIL-100(Fe) NPs was tested on three different cell lines, evidencing a similar antitumour activity in all cell lines for the free and encapsulated drug [22; 64]. Similarly, Santos Lucena *et al.* confirmed the high toxicity of the 5-FU loaded in a Cu-BTC using three cells lines [129]. Following this concept, Huxford *et al.* have studied several targeted lipid-coated or not Zn, Zr and Gd-based MOFs containing MTX on Jurkat human acute lymphoblastic leukemia (ALL), observing that the coated Gd-MOFs exhibited a better efficiency than non-coated ones [41]. Imaz *et al.* studied the activity of Doxo, camptothecin and daunomycin encapsulated in the Zn(bix) in HL-60 cells, observing a potential efficacy as the encapsulated Doxo possessed the same effect as the free drug [124].

Lin's group studied the *in vitro* antitumoral activity of several Pt(IV) based MOFs. First, the silica-coated Tb-cisplatin prodrug DSCP NPs (NCP-1) NPs showed an *in vitro* antitumour activity exclusively after their surface coating with the cyclic peptide C(RGDfK), which targets a type of integrin overexpressed in cancer [62]. Silica-coated amino-exchanged MIL-101(Fe) NPs, covalently incorporating first an optical imaging contrast agent and then a Pt(IV) prodrug were also evaluated *in vitro*, resulting in the same antitumour activity of the Pt(IV) prodrug as a free or encapsulated drug in HT-29 cell line [73].

Regarding theranostics, Zr-based MOF NCP-2 (containing [Ru 5,5'-(CO₂)₂-bpy (bpy)₂]) showed its potential use as contrast agent due to experiments done in the human-derived lung H460 cancer cell line [149].

Other interesting efficacy tests have been performed using antiretroviral-containing MOFs. The activity of the AZT-Tp encapsulated in MIL-100(Fe) NPs was evaluated on HIV-1-LAI-infected peripheral blood mononuclear cells (PBMC), demonstrating the higher anti-HIV activity of the AZT-TP-loaded MIL-100(Fe) NPs. This happened contrary

to the fact that the highly hydrophilic free drug cannot cross the cell membrane unlike AZT-Tp-containing MIL-100(Fe) NPs [51].

4. CONCLUSIONS

Pharmacy is an evolving science, which is nowadays focusing on personally-tailored treatments for each patient. In this sense, new drug delivery systems have been developed within the past two decades. Among them, MOFs are nice candidates owing to their ability to incorporate important loadings of several biologically active compounds either within their porosity or within the hybrid network itself. In addition, the progressive release of the active molecule can be achieved under physiological conditions through a combination of framework degradation, drug diffusion and host-guest interactions. Also, some of them possess contrast agents properties either directly, within their structure (inorganic or organic fractions), or through a grafting of active molecules on their surface (external or internal porosity), making these systems interesting candidates for theranostics.

MOFs can also be shaped to produce surface-engineered NPs, films, patches or pellets, which are required to develop formulations to the different administration routes.

Finally, although some of these structures are biodegradable and may be toxic, these points will be fully addressed in the near future through *in vitro* and *in vivo* evaluations, including ADME evaluation and efficacy tests. In this sense, formulations might be specifically adapted to each administration route.

REFERENCES

- [1] Baillie, A.J., Coombs, G.H., Dolan, T.F., Hunter, C.A., Laakso, T., Sjöholm, I., and Stjärnkvist, P. (1987) Biodegradable microspheres: Polyacryl starch microparticles as a delivery system for the antileishmanial drug, sodium stibogluconate. *J. Pharm. Pharmacol.*, **39** (10), 832-835.
- [2] Harmia, T., Speiser, P., and Kreuter, J. (1986) A solid colloidal drug delivery system for the eye: encapsulation of pilocarpin in nanoparticles. *J. Microencapsul.*, **3** (1), 3-12.
- [3] Adair, J.H., Parette, M.P., Altinoğlu, E.İ., and Kester, M. (2010) Nanoparticulate alternatives for drug delivery. *ACS Nano*, **4** (9), 4967-4970.
- [4] Banerjee, D., and Sengupta, S. (2011) Chapter 12 - Nanoparticles in cancer chemotherapy, In *Progress in Molecular Biology and Translational Science*, (ed. V. Antonio), Academic Press, Waltham, pp. 489-507.
- [5] Diebold, Y., and Calonge, M. (2010) Applications of nanoparticles in ophthalmology. *Prog. Retin. Eye Res.*, **29** (6), 596-609.

- [6] (2009) See Special Issue. Guest Editors J.R. Long and O.M. Yaghi. *Chem. Soc. Rev.*, **38** (5), 1201-1508.
- [7] (2012) See Special Issue. Guest Editors H.-C. Zhou, J.R. Long and O.M. Yaghi. *Chem. Rev.*, **112** (2), 673-1268.
- [8] Furukawa, H., Cordova, K.E., O'Keeffe, M., and Yaghi, O.M. (2013) The chemistry and applications of metal-organic frameworks. *Science*, **341** (6149), 1230444.
- [9] Hoskins, B.F., and Robson, R. (1989) Infinite polymeric frameworks consisting of three dimensionally linked rod-like segments. *J. Am. Chem. Soc.*, **111** (15), 5962-5964.
- [10] Ferey, G., and Serre, C. (2009) Large breathing effects in three-dimensional porous hybrid matter: facts, analyses, rules and consequences. *Chem. Soc. Rev.*, **38** (5), 1380-1399.
- [11] Uemura, K., Matsuda, R., and Kitagawa, S. (2005) Flexible microporous coordination polymers. *J. Solid State Chem.*, **178** (8), 2420-2429.
- [12] Horcajada, P., Serre, C., McKinlay, A.C., and Morris, R.E. (2011) Biomedical applications of metal-organic frameworks, In *Metal-Organic Frameworks: Applications from Catalysis to Gas Storage* (Ed. D. Farrusseng), Wiley-VCH Verlag GmbH & Co. KGaA, Weinheim, pp. 213-250.
- [13] Pachfule, P., Das, R., Poddar, P., and Banerjee, R. (2011) Solvothermal synthesis, structure, and properties of metal organic framework isomers derived from a partially fluorinated link. *Cryst. Growth Des.*, **11** (4), 1215-1222.
- [14] Baghbanzadeh, M., Carbone, L., Cozzoli, P.D., and Kappe, C.O. (2011) Microwave-assisted synthesis of colloidal inorganic nanocrystals. *Angew. Chem. Int. Edit.*, **50** (48), 11312-11359.
- [15] Yang, W., Zhang, L., Hu, Y., Zhong, Y., Wu, H.B., and Lou, X.W. (2012) Microwave-assisted synthesis of porous Ag₂S-Ag hybrid nanotubes with high visible-light photocatalytic activity. *Angew. Chem. Int. Edit.*, **51** (46), 11501-11504.
- [16] Bowmaker, G.A. (2013) Solvent-assisted mechanochemistry. *Chem. Commun.*, **49** (4), 334-348.
- [17] Haque, E., Khan, N.A., Park, J.H., and Jhung, S.H. (2010) Synthesis of a metal-organic framework material, iron terephthalate, by ultrasound, microwave, and conventional electric heating: a kinetic study. *Chem. Eur. J.*, **16** (3), 1046-1052.
- [18] Martinez Joaristi, A., Juan-Alcañiz, J., Serra-Crespo, P., Kapteijn, F., and Gascon, J. (2012) Electrochemical synthesis of some archetypical Zn²⁺, Cu²⁺, and Al³⁺ metal organic frameworks. *Cryst. Growth Des.*, **12** (7), 3489-3498.
- [19] Zhao, Y., Zhang, J., Han, B., Song, J., Li, J., and Wang, Q. (2011) Metal-organic framework nanospheres with well-ordered mesopores synthesized in an ionic liquid/CO₂/surfactant system. *Angew. Chem. Int. Edit.*, **50** (3), 636-639.
- [20] Chalati, T., Horcajada, P., Gref, R., Couvreur, P., and Serre, C. (2011) Optimisation of the synthesis of MOF nanoparticles made of flexible porous iron fumarate MIL-88A. *J. Mater. Chem.*, **21** (7), 2220-2227.
- [21] García-Márquez, A., Demessence, A., Platero-Prats, A.E., Heurtaux, D., Horcajada, P., Serre, C., Chang, J.S., Ferey, G., de la Pena-O'Shea, V.A., Boissiere, C., Grosso, D., and Sanchez, C. (2012)

Green microwave synthesis of MIL-100(Al, Cr, Fe) nanoparticles for thin-film elaboration. *Eur. J. Inorg. Chem.* **2012** (32), 5165-5174.

[22] Horcajada, P., Chalati, T., Serre, C., Gillet, B., Sebrie, C., Baati, T., Eubank, J.F., Heurtaux, D., Clayette, P., Kreuz, C., Chang, J.-S., Hwang, Y.K., Marsaud, V., Bories, P.-N., Cynober, L., Gil, S., Férey, G., Couvreur, P., and Gref, R. (2010) Porous metal-organic-framework nanoscale carriers as a potential platform for drug delivery and imaging. *Nat. Mater.*, **9** (2), 172-178.

[23] Horcajada, P. (2013) Functionalized and extra-large porous iron (III) tri- or dicarboxylates with MIL-100/101 topologies. Dissertation.

[24] Carne-Sanchez, A., Imaz, I., Cano-Sarabia, M., and MasPOCH, D. (2013) A spray-drying strategy for synthesis of nanoscale metal-organic frameworks and their assembly into hollow superstructures. *Nat. Chem.*, **5** (3), 203-211.

[25] Garcia-Marquez, A., Horcajada, P., Grosso, D., Férey, G., Serre, C., Sanchez, C., and Boissiere, C. (2013) Green scalable aerosol synthesis of porous metal-organic frameworks. *Chem. Commun.*, **49** (37), 3848-3850.

[26] Witters, D., Vergauwe, N., Ameloot, R., Vermeir, S., De Vos, D., Puers, R., Sels, B., and Lammertyn, J. (2012) Digital microfluidic high-throughput printing of single metal-organic framework crystals. *Adv. Mater.*, **24** (10), 1316-1320.

[27] Puigmarti-Luis, J., Rubio-Martinez, M., Hartfelder, U., Imaz, I., MasPOCH, D., and Dittrich, P.S. (2011) Coordination polymer nanofibers generated by microfluidic synthesis. *J. Am. Chem. Soc.*, **133** (12), 4216-4219.

[28] Hatakeyama, W., Sanchez, T.J., Rowe, M.D., Serkova, N.J., Liberatore, M.W., and Boyes, S.G. (2011) Synthesis of gadolinium nanoscale metal-organic framework with hydrotropes: manipulation of particle size and magnetic resonance imaging capability. *ACS Appl. Mater. Interfaces*, **3** (5), 1502-1510.

[29] Pang, M., Cairns, A.J., Liu, Y., Belmabkhout, Y., Zeng, H.C., and Eddaoudi, M. (2013) Synthesis and integration of Fe-SOC-MOF cubes into colloidosomes via a single-step emulsion-based approach. *J. Am. Chem. Soc.*, **135** (28), 10234-10237.

[30] Horcajada, P., Serre, C., Maurin, G., Ramsahye, N.A., Balas, F., Vallet-Regí, M., Sebban, M., Taulelle, F., and Férey, G. (2008) Flexible porous metal-organic frameworks for a controlled drug delivery. *J. Am. Chem. Soc.*, **130** (21), 6774-6780.

[31] Ananthoji, R., Eubank, J.F., Nouar, F., Mouttaki, H., Eddaoudi, M., and Harmon, J.P. (2011) Symbiosis of zeolite-like metal-organic frameworks (rho-ZMOF) and hydrogels: composites for controlled drug release. *J. Mater. Chem.*, **21** (26), 9587-9594.

[32] Bradshaw, D., Garai, A., and Huo, J. (2012) Metal-organic framework growth at functional interfaces: thin films and composites for diverse applications. *Chem. Soc. Rev.*, **41** (6), 2344-2381.

[33] Betard, A., and Fischer, R.A. (2012) Metal-organic framework thin films: from fundamentals to applications. *Chem. Rev.*, **112** (2), 1055-1083.

[34] Falcaro, P., Buso, D., Hill, A.J., and Doherty, C.M. (2012) Patterning techniques for metal organic frameworks. *Adv. Mater.*, **24** (24), 3153-3168.

- [35] Morris, R.E., and Wheatley, P.S. (2008) Gas storage in nanoporous materials. *Angew. Chem. Int. Edit.*, **47** (27), 4966-4981.
- [36] Li, D., and Xia, Y. (2004) Electrospinning of nanofibers: reinventing the wheel? *Adv. Mater.*, **16** (14), 1151-1170.
- [37] Ostermann, R., Cravillon, J., Weidmann, C., Wiebcke, M., and Smarsly, B.M. (2011) Metal-organic framework nanofibers via electrospinning. *Chem. Commun.*, **47** (1), 442-444.
- [38] Rose, M., Böhringer, B., Jolly, M., Fischer, R., and Kaskel, S. (2011) MOF processing by electrospinning for functional textiles. *Adv. Eng. Mater.*, **13** (4), 356-360.
- [39] Cohen, S.M. (2011) Postsynthetic methods for the functionalization of metal-organic frameworks. *Chem. Rev.*, **112** (2), 970-1000.
- [40] Gref, R., Agostoni, V., Daoud-Mahammed, S., Rodriguez-Ruiz, V., Malanga, M., Jicsinszki, L., Horcajada, P., and Serre, C. (2012) Modification de la surface de nanoparticules hybrides. FR12/55065 and issued May 31, 2012.
- [41] Huxford, R.C., de Krafft, K.E., Boyle, W.S., Liu, D., and Lin, W.B. (2012) Lipid-coated nanoscale coordination polymers for targeted delivery of antifolates to cancer cells. *Chem. Sci.*, **3** (1), 198-204.
- [42] Liu, D., Kramer, S.A., Huxford-Phillips, R.C., Wang, S., Della Rocca, J., and Lin, W. (2012) Coercing biphosphonates to kill cancer cells with nanoscale coordination polymers. *Chem. Commun.*, **48** (21), 2668-2670.
- [43] Rieter, W.J., Taylor, K.M.L., and Lin, W. (2007) Surface modification and functionalization of nanoscale metal-organic frameworks for controlled release and luminescence sensing. *J. Am. Chem. Soc.*, **129** (32), 9852-9853.
- [44] Miller, S.R., Heurtaux, D., Baati, T., Horcajada, P., Greneche, J.-M., and Serre, C. (2010) Biodegradable therapeutic mofs for the delivery of bioactive molecules. *Chem. Commun.*, **46** (25), 4526-4528.
- [45] Betard, A., Zacher, D., and Fischer, R.A. (2010) Dense and homogeneous coatings of CPO-27-M type metal-organic frameworks on alumina substrates. *CrystEngComm.*, **12** (11), 3768-3772.
- [46] Canioni, R., Roch-Marchal, C., Secheresse, F., Horcajada, P., Serre, C., Hardi-Dan, M., Ferey, G., Greneche, J.-M., Lefebvre, F., Chang, J.-S., Hwang, Y.-K., Lebedev, O., Turner, S., and Van Tendeloo, G. (2011) Stable polyoxometalate insertion within the mesoporous metal organic framework MIL-100(Fe). *J. Mater. Chem.*, **21** (4), 1226-1233.
- [47] Dhakshinamoorthy, A., Alvaro, M., Horcajada, P., Gibson, E., Vishnuvarthan, M., Vimont, A., Grenèche, J.-M., Serre, C., Daturi, M., and Garcia, H. (2012) Comparison of porous iron trimesates basolite F300 and MIL-100(Fe) as heterogeneous catalysts for lewis acid and oxidation reactions: roles of structural defects and stability. *ACS Catal.*, **2** (10), 2060-2065.
- [48] Wu, H., Yildirim, T., and Zhou, W. (2013) Exceptional mechanical stability of highly porous zirconium metal-organic framework UiO-66 and its important implications. *J. Phys. Chem. Lett.*, **4** (6), 925-930.

- [49] Kandiah, M., Nilsen, M.H., Usseglio, S., Jakobsen, S., Olsbye, U., Tilset, M., Larabi, C., Quadrelli, E.A., Bonino, F., and Lillerud, K.P. (2010) Synthesis and stability of tagged UiO-66 Zr-MOFs. *Chem. Mater.*, **22** (24), 6632-6640.
- [50] Sansone, F., Rossi, A., Del Gaudio, P., De Simone, F., Aquino, R.P., and Lauro, M.R. (2009) Hesperidin gastroresistant microparticles by spray-drying: preparation, characterization, and dissolution profiles. *AAPS Pharm. Sci. Tech.*, **10** (2), 391-401.
- [51] Agostoni, V., Chalati, T., Horcajada, P., Willaime, H., Anand, R., Semiramoth, N., Baati, T., Hall, S., Maurin, G., Chacun, H., Bouchemal, K., Martineau, C., Taulelle, F., Couvreur, P., Rogez-Kreuz, C., Clayette, P., Monti, S., Serre, C., and Gref, R. (2013) Towards an improved anti-HIV activity of NRTI via metal-organic frameworks nanoparticles. *Adv. Healthc. Mater.*, DOI: 10.1002/adhm.201200454.
- [52] Baati, T., Njim, L., Neffati, F., Kerkeni, A., Bouttemi, M., Gref, R., Najjar, M.F., Zakhama, A., Couvreur, P., Serre, C., and Horcajada, P. (2013) In depth analysis of the *in vivo* toxicity of nanoparticles of porous iron(III) metal-organic frameworks. *Chem. Sci.*, **4** (4), 1597-1607.
- [53] http://rais.ornl.gov/cgi-bin/tools/TOX_search (Accessed May 2013).
- [54] <http://www.nlm.nih.gov/medlineplus/ency/article/002423.htm> (Accessed September 2013).
- [55] <http://www.nlm.nih.gov/medlineplus/magazine/issues/winter11/articles/winter11pg12.html> (Accessed September 2013).
- [56] <http://ods.od.nih.gov/factsheets/Iron-HealthProfessional/> (Accessed September 2013).
- [57] <http://ods.od.nih.gov/factsheets/Zinc-HealthProfessional/> (Accessed September 2013).
- [58] <http://toxnet.nlm.nih.gov/cgi-bin/sis/search/a?dbs+hsdb:@term+@DOCNO+7347> (Accessed May 2013).
- [59] Novio, F., Simmchen, J., Vázquez-Mera, N., Amorín-Ferré, L., and Ruiz-Molina, D. (2013) Coordination polymer nanoparticles in medicine. *Coord. Chem. Rev.*, **257** (19-20), 2839-2847.
- [60] Zanella, A., Gandin, V., Porchia, M., Refosco, F., Tisato, F., Sorrentino, F., Scutari, G., Rigobello, M., and Marzano, C. (2011) Cytotoxicity in human cancer cells and mitochondrial dysfunction induced by a series of new copper(I) complexes containing tris(2-cyanoethyl)phosphines. *Invest. New Drugs*, **29** (6), 1213-1223.
- [61] Hanke, M., Arslan, H.K., Bauer, S., Zybalyo, O., Christophis, C., Gliemann, H., Rosenhahn, A., and Wöll, C. (2012) The biocompatibility of metal-organic framework coatings: an investigation on the stability of SURMOFs with regard to water and selected cell culture media. *Langmuir*, **28** (17), 6877-6884.
- [62] Rieter, W.J., Pott, K.M., Taylor, K.M.L., and Lin, W. (2008) Nanoscale coordination polymers for platinum-based anticancer drug delivery. *J. Am. Chem. Soc.*, **130** (35), 11584-11585.
- [63] Geranmayeh, S., Abbasi, A., Zarnani, A.-H., and Skripkin, M.Y. (2013) A novel trinuclear zinc metal-organic network: synthesis, x-ray diffraction structures, spectroscopic and biocompatibility studies. *Polyhedron*, **61**, 6-14.
- [64] Chalati, T., Horcajada, P., Couvreur, P., Serre, C., Ben Yahia, M., Maurin, G., and Gref, R. (2011) Porous metal organic framework nanoparticles to address the challenges related to busulfan encapsulation. *Nanomedicine*, **6** (10), 1683-1695.

- [65] Agostoni, V., Horcajada, P., Rodriguez-Ruiz, V., Willaime, H., Couvreur, P., Serre, C., and Gref, R. (2013) "Green" fluorine-free mesoporous iron(III) trimesate nanoparticles for drug delivery. *Green Mater.*, **1** (4), 209-217.
- [66] Lunov, O., Syrovets, T., Büchele, B., Jiang, X., Röcker, C., Tron, K., Nienhaus, G.U., Walther, P., Mailänder, V., Landfester, K., and Simmet, T. (2010) The effect of carboxydextran-coated superparamagnetic iron oxide nanoparticles on c-Jun N-terminal kinase-mediated apoptosis in human macrophages. *Biomaterials*, **31** (19), 5063-5071.
- [67] Hsiao, J.-K., Chu, H.-H., Wang, Y.-H., Lai, C.-W., Chou, P.-T., Hsieh, S.-T., Wang, J.-L., and Liu, H.-M. (2008) Macrophage physiological function after superparamagnetic iron oxide labeling. *NMR Biomed.*, **21** (8), 820-829.
- [68] Vu-Quang, H., Yoo, M.-K., Jeong, H.-J., Lee, H.-J., Muthiah, M., Rhee, J.H., Lee, J.-H., Cho, C.-S., Jeong, Y.Y., and Park, I.-K. (2011) Targeted delivery of mannan-coated superparamagnetic iron oxide nanoparticles to antigen-presenting cells for magnetic resonance-based diagnosis of metastatic lymph nodes *in vivo*. *Acta Biomater.*, **7** (11), 3935-3945.
- [69] Li, M., Kim, H.S., Tian, L., Yu, M.K., Jon, S., and Moon, W.K. (2012) Comparison of two ultrasmall superparamagnetic iron oxides on cytotoxicity and MR imaging of tumors. *Theranostics* **2** (1), 76-85.
- [70] Soma, C.E., Dubernet, C., Barratt, G., Benita, S., and Couvreur, P. (2000) Investigation of the role of macrophages on the cytotoxicity of doxorubicin and doxorubicin-loaded nanoparticles on M5076 cells *in vitro*. *J. Control Release*, **68** (2), 283-289.
- [71] Tamames-Tabar, C., Cunha, D., Imbuluzqueta, E., Ragon, F., Serre, C., Blanco-Prieto, M.J., and Horcajada, P. (2013) Cytotoxicity of nanoscaled metal-organic frameworks. *J. Mater. Chem. B*, DOI: 10.1039/C3TB20832J.
- [72] Horcajada, P., Serre, C., Vallet-Regí, M., Sebban, M., Taulelle, F., and Férey, G. (2006) Metal-organic frameworks as efficient materials for drug delivery. *Angew. Chem. Int. Edit.*, **45** (36), 5974-5978.
- [73] Huxford, R.C., Della Rocca, J., and Lin, W. (2010) Metal-organic frameworks as potential drug carriers. *Curr. Opin. Chem. Biol.*, **14** (2), 262-268.
- [74] Serre, C., Millange, F., Surblé, S., and Férey, G. (2004) A route to the synthesis of trivalent transition-metal porous carboxylates with trimeric secondary building units. *Angew. Chem. Int. Edit.*, **43** (46), 6285-6289.
- [75] Imaz, I., Rubio-Martinez, M., An, J., Sole-Font, I., Rosi, N.L., and MasPOCH, D. (2011) Metal-biomolecule frameworks (MBioFs). *Chem. Commun.*, **47** (26), 7287-7302.
- [76] McKinlay, A.C., Morris, R.E., Horcajada, P., Férey, G., Gref, R., Couvreur, P., and Serre, C. (2010) BioMOFs: Metal-organic frameworks for biological and medical applications. *Angew. Chem. Int. Edit.*, **49** (36), 6260-6266.
- [77] Horcajada, P., Gref, R., Baati, T., Allan, P.K., Maurin, G., Couvreur, P., Férey, G., Morris, R.E., and Serre, C. (2011) Metal-organic frameworks in biomedicine. *Chem. Rev.*, **112** (2), 1232-1268.

- [78] Vaidhyanathan, R., Bradshaw, D., Rebilly, J.-N., Barrio, J.P., Gould, J.A., Berry, N.G., and Rosseinsky, M.J. (2006) A family of nanoporous materials based on an amino acid backbone. *Angew. Chem. Int. Edit.*, **45** (39), 6495-6499.
- [79] Ong, T.T., Kavuru, P., Nguyen, T., Cantwell, R., Wojtas, Ł., and Zaworotko, M.J. (2011) 2:1 Cocrystals of homochiral and achiral amino acid zwitterions with Li⁺ salts: water-stable zeolitic and diamondoid metal–organic materials. *J. Am. Chem. Soc.*, **133** (24), 9224-9227.
- [80] Rabone, J., Yue, Y.-F., Chong, S.Y., Stylianou, K.C., Bacsá, J., Bradshaw, D., Darling, G.R., Berry, N.G., Khimyak, Y.Z., Ganin, A.Y., Wiper, P., Claridge, J.B., and Rosseinsky, M.J. (2010) An adaptable peptide-based porous material. *Science*, **329** (5995), 1053-1057.
- [81] Manton, A., Massüger, L., Rabu, P., Palivan, C., McCusker, L.B., and Taubert, A. (2008) Metal–peptide frameworks (MPFs): “bioinspired” metal organic frameworks. *J. Am. Chem. Soc.*, **130** (8), 2517-2526.
- [82] Liu, C., Li, T., and Rosi, N.L. (2012) Strain-promoted “click” modification of a mesoporous metal–organic framework. *J. Am. Chem. Soc.*, **134** (46), 18886-18888.
- [83] Afonso, R., Mendes, A., and Gales, L. (2012) Peptide-based solids: porosity and zeolitic behavior. *J. Mater. Chem.*, **22** (5), 1709-1723.
- [84] An, J., Farha, O.K., Hupp, J.T., Pohl, E., Yeh, J.I., and Rosi, N.L. (2012) Metal-adeninate vertices for the construction of an exceptionally porous metal-organic framework. *Nat. Commun.*, **3**, 604-608.
- [85] Stylianou, K.C., Warren, J.E., Chong, S.Y., Rabone, J., Bacsá, J., Bradshaw, D., and Rosseinsky, M.J. (2011) CO₂ selectivity of a 1D microporous adenine-based metal-organic framework synthesised in water. *Chem. Commun.*, **47** (12), 3389-3391.
- [86] Smaldone, R.A., Forgan, R.S., Furukawa, H., Gassensmith, J.J., Slawin, A.M.Z., Yaghi, O.M., and Stoddart, J.F. (2010) Metal–organic frameworks from edible natural products. *Angew. Chem. Int. Edit.*, **49** (46), 8630-8634.
- [87] Dybtsev, D.N., Nuzhdin, A.L., Chun, H., Bryliakov, K.P., Talsi, E.P., Fedin, V.P., and Kim, K. (2006) A homochiral metal–organic material with permanent porosity, enantioselective sorption properties, and catalytic activity. *Ang. Chem. Int. Ed.*, **45** (6), 916-920.
- [88] Thushari, S., Cha, J.A.K., Sung, H.H.Y., Chui, S.S.Y., Leung, A.L.F., Yen, Y.-F., and Williams, I.D. (2005) Microporous chiral metal coordination polymers: hydrothermal synthesis, channel engineering and stability of lanthanide tartrates. *Chem. Commun.* **44**, 5515-5517.
- [89] Miller, S.R., Horcajada, P., and Serre, C. (2011) Small chemical causes drastic structural effects: the case of calcium glutarate. *CrystEngComm.*, **13** (6), 1894-1898.
- [90] Alvarez, E., Garcia-Marquez, A., Devic, T., Steunou, N., Serre, C., Bonhomme, C., Gervais, C., Izquierdo-Barba, I., Vallet-Regi, M., Laurencin, D., Mauri, F., and Horcajada, P. (2013) A biocompatible calcium bisphosphonate coordination polymer: towards a metal-linker synergistic therapeutic effect? *CrystEngComm.* **15** (46), 9899-9905.
- [91] Della Rocca, J., Liu, D., and Lin, W. (2012) Are high drug loading nanoparticles the next step forward for chemotherapy? *Nanomedicine*, **7** (3), 303-305.

- [92] Xing, L., Cao, Y., and Che, S. (2012) Synthesis of core-shell coordination polymer nanoparticles (CPNs) for pH-responsive controlled drug release. *Chem. Commun.*, **48** (48), 5995-5997.
- [93] Xing, L., Zheng, H., and Che, S. (2011) A pH-responsive cleavage route based on a metal-organic coordination bond. *Chem. Eur. J.*, **17** (26), 7271-7275.
- [94] Vega, D., Baggio, R., and Garland, M.T. (1996) Monosodium 4-amino-1-hydroxy-1,1-butanediylidiphosphonate trihydrate (alendronate). *Acta Cryst. C*, **52** (9), 2198-2201.
- [95] Yoshinari, M., Oda, Y., Inoue, T., Matsuzaka, K., and Shimono, M. (2002) Bone response to calcium phosphate-coated and bisphosphonate-immobilized titanium implants. *Biomaterials*, **23** (14), 2879-2885.
- [96] Fernandez, D., Vega, D., and Goeta, A. (2003) Alendronate zwitterions bind to calcium cations arranged in columns. *Acta Crystallogr. C*, **59** (Pt 12), m543-545.
- [97] Kim, Y., Nam, H.J., and Jung, D.-Y. (2009) Three-dimensional iron glutarate with five- and six-coordinated iron (II)-oxygen networks. *Chem. Lett.*, **38** (1), 72-73.
- [98] Slenters, T.V., Sagué, J.L., Brunetto, P.S., Zuber, S., Fleury, A., Mirolo, L., Robin, A.Y., Meuwly, M., Gordon, O., Landmann, R., Daniels, A.U., and Fromm, K.M. (2010) Of chains and rings: synthetic strategies and theoretical investigations for tuning the structure of silver coordination compounds and their applications. *Materials*, **3** (5), 3407-3429.
- [99] Slenters, T.V., Hauser-Gerspach, I., Daniels, A.U., and Fromm, K.M. (2008) Silver coordination compounds as light-stable, nano-structured and anti-bacterial coatings for dental implant and restorative materials. *J. Mater. Chem.*, **18** (44), 5359-5362.
- [100] Berchel, M., Gall, T.L., Denis, C., Hir, S.L., Quentel, F., Elleouet, C., Montier, T., Rueff, J.-M., Salaun, J.-Y., Haelters, J.-P., Hix, G.B., Lehn, P., and Jaffres, P.-A. (2011) A silver-based metal-organic framework material as a 'reservoir' of bactericidal metal ions. *New J. Chem.*, **35** (5), 1000-1003.
- [101] Kirillov, A.M., Wiczorek, S.W., Lis, A., da Silva, M., Florek, M., Krol, J., Staroniewicz, Z., Smolenski, P., and Pombeiro, A.J.L. (2011) 1,3,5-triaza-7-phosphaadamantane-7-oxide (PTA=O): new diamondoid building block for design of three-dimensional metal-organic frameworks. *Cryst. Growth Des.*, **11** (7), 2711-2716.
- [102] Wang, K., Geng, Z., Yin, Y., Ma, X., and Wang, Z. (2011) Morphology effect on the luminescent property and antibacterial activity of coordination polymer particles with identical crystal structures. *CrystEngComm.*, **13** (16), 5100-5104.
- [103] An, J., Gelb, S.J., and Rosi, N.L. (2009) Cation triggered drug release from a porous zinc-adeninate metal-organic framework. *J. Am. Chem. Soc.*, **131** (24), 8376-8377.
- [104] Badawi, A.M., Azzam, E.M.S., and Morsy, S.M.I. (2006) Surface and biocidal activity of some synthesized metallo azobenzene isothiuronium salts. *Bioorg. Med. Chem.*, **14** (24), 8661-8665.
- [105] Kato, T.A., Matsuda, T., Matsui, S., Mizutani, T., and Saeki, K. (2002) Activation of the aryl hydrocarbon receptor by methyl yellow and related congeners: structure-activity relationships in halogenated derivatives. *Biol. Pharm. Bull.*, **25** (4), 466-471.

- [106] Miller, S.R., Alvarez, E., Fradcourt, L., Devic, T., Wuttke, S., Wheatley, P.S., Steunou, N., Bonhomme, C., Gervais, C., Laurencin, D., Morris, R.E., Vimont, A., Daturi, M., Horcajada, P., and Serre, C. (2013) A rare example of a porous Ca-MOF for the controlled release of biologically active NO. *Chem. Commun.*, **49** (71), 7773-7775.
- [107] Chen, Z.-F., Zhang, Z.-L., Tan, Y.-H., Tang, Y.-Z., Fun, H.-K., Zhou, Z.-Y., Abrahams, B.F., and Liang, H. (2008) Coordination polymers constructed by linking metal ions with azodibenzoate anions. *CrystEngComm.*, **10** (2), 217-231.
- [108] Tang, Y.-Z., Tan, Y.-H., Chen, S.-H., Chao, Y.-W., and Wang, P. (2008) Synthesis, characterization and crystal structures of two alkaline-earth metal complexes of olsalazine. *J. Coord. Chem.*, **61** (8), 1244-1252.
- [109] Lee, Y.-G., Moon, H.R., Cheon, Y.E., and Suh, M.P. (2008) A comparison of the H₂ sorption capacities of isostructural metal-organic frameworks with and without accessible metal sites: [Zn₂(abtc)(dmf)₂]₃ and [Cu₂(abtc)(dmf)₂]₃ versus [Cu₂(abtc)]₃. *Angew. Chemie Int. Edit.*, **47** (40), 7741-7745.
- [110] Dhakshinamoorthy, A., Alvaro, M., Chevreau, H., Horcajada, P., Devic, T., Serre, C., and Garcia, H. (2012) Iron(III) metal-organic frameworks as solid lewis acids for the isomerization of [small alpha]-pinene oxide. *Catal. Sci. Technol.*, **2** (2), 324-330.
- [111] Vivero-Escoto, J.L., Huxford-Phillips, R.C., and Lin, W. (2012) Silica-based nanoprobe for biomedical imaging and theranostic applications. *Chem. Soc. Rev.*, **41** (7), 2673-2685.
- [112] Dyer, A., Morgan, S., Wells, P., and Williams, C. (2000) The use of zeolites as slow release anthelmintic carriers. *J. Helminthol.*, **74** (2), 137-141.
- [113] Horcajada, P., Márquez-Álvarez, C., Rámila, A., Pérez-Pariente, J., and Vallet-Regí, M. (2006) Controlled release of ibuprofen from dealuminated faujasites. *Solid State Sci.*, **8** (12), 1459-1465.
- [114] Arruebo, M., Fernández-Pacheco, R., Uruñosa, S., Arbiol, J., Ibarra, M.R., and Santamaría, J. (2006) Sustained release of doxorubicin from zeolite-magnetite nanocomposites prepared by mechanical activation. *Nanotechnology*, **17** (16), 4057-4064.
- [115] Uglea, C., Albu, I., Vatanaju, A., Croitoru, M., Antoniu, S., Panaitescu, L., and Ottenbrite, R.M. (1994) Drug delivery systems based on inorganic materials: I. Synthesis and characterization of a zeolite-cyclophosphamide system. *J. Biomater. Sci. Polym. Ed.*, **6** (7), 633-637.
- [116] Vallet-Regí, M., Balas, F., and Arcos, D. (2007) Mesoporous materials for drug delivery. *Angew. Chemie Int. Edit.*, **46** (40), 7548-7558.
- [117] Xuan, W., Zhu, C., Liu, Y., and Cui, Y. (2012) Mesoporous metal-organic framework materials. *Chem. Soc. Rev.*, **41** (5), 1677-1695.
- [118] Song, L., Zhang, J., Sun, L., Xu, F., Li, F., Zhang, H., Si, X., Jiao, C., Li, Z., Liu, S., Liu, Y., Zhou, H., Sun, D., Du, Y., Cao, Z., and Gabelica, Z. (2012) Mesoporous metal-organic frameworks: design and applications. *Energy Environ. Sci.*, **5** (6), 7508-7520.
- [119] Horcajada, P., Serre, C., Gref, R., Férey, G., and Couvreur, P. (2008) Organic/inorganic hybrid nanoparticulates made from iron carboxylates. PCT/FR2008/001366 and issued Oct. 1, 2008.

- [120] Horcajada, P., Serre, C., Gref, R., Férey, G., and Couvreur, P. (2008) Solid inorganic/organic hybrid with modified surface. PCT/FR2008/001367 and issued Oct. 1, 2008.
- [121] Cunha, D., Gaudin, C., Colinet, I., Horcajada, P., Maurin, G., and Serre, C. (2013) Rationalization of the entrapping of bioactive molecules into a series of functionalized porous zirconium terephthalate MOFs. *J. Mater. Chem. B*, **1** (8), 1101-1108.
- [122] Rodrigues, M.O., de Paula, M.V., Wanderley, K.A., Vasconcelos, I.B., Alves, S., and Soares, T.A. (2012) Metal organic frameworks for drug delivery and environmental remediation: a molecular docking approach. *Int. J. of Quantum Chem.*, **112** (20), 3346-3355.
- [123] Taylor-Pashow, K.M.L., Rocca, J.D., Xie, Z., Tran, S., and Lin, W. (2009) Postsynthetic modifications of iron-carboxylate nanoscale metal-organic frameworks for imaging and drug delivery. *J. Am. Chem. Soc.*, **131** (40), 14261-14263.
- [124] Imaz, I., Rubio-Martinez, M., Garcia-Fernandez, L., Garcia, F., Ruiz-Molina, D., Hernando, J., Puentes, V., and Maspocho, D. (2010) Coordination polymer particles as potential drug delivery systems. *Chem. Commun.*, **46** (26), 4737-4739.
- [125] Sun, C.-Y., Qin, C., Wang, X.-L., Yang, G.-S., Shao, K.-Z., Lan, Y.-Q., Su, Z.-M., Huang, P., Wang, C.-G., and Wang, E.-B. (2012) Zeolitic imidazolate framework-8 as efficient pH-sensitive drug delivery vehicle. *Dalton Trans.*, **41** (23), 6906-6909.
- [126] Sun, C.-Y., Qin, C., Wang, C.-G., Su, Z.-M., Wang, S., Wang, X.-L., Yang, G.-S., Shao, K.-Z., Lan, Y.-Q., and Wang, E.-B. (2011) Chiral nanoporous metal-organic frameworks with high porosity as materials for drug delivery. *Adv. Mater.*, **23** (47), 5629-5632.
- [127] Wang, Y., Yang, J., Liu, Y.-Y., and Ma, J.-F. (2013) Controllable syntheses of porous metal-organic frameworks: encapsulation of In III cations for tunable luminescence and small drug molecules for efficient delivery. *Chem. Eur. J.*, **19** (43), 14591-14599.
- [128] Wang, H.-N., Meng, X., Yang, G.-S., Wang, X.-L., Shao, K.-Z., Su, Z.-M., and Wang, C.-G. (2011) Stepwise assembly of metal-organic framework based on a metal-organic polyhedron precursor for drug delivery. *Chem. Commun.*, **47** (25), 7128-7130.
- [129] Lucena, F.R.S., de Araújo, L.C.C., Rodrigues, M.d.D., Silva, T.G., Pereira, V.R.A., Militão, G.C.G., Fontes, D.A.F., Neto, P.J.R., da Silva, F.F., and Nascimento, S.C. (2013) Induction of cancer cell death by apoptosis and slow release of 5-fluoracil from metal-organic frameworks Cu-BTC. *Biomed. Pharmacother.*, **67** (8), 707-713.
- [130] Ke, F., Yuan, Y.-P., Qiu, L.-G., Shen, Y.-H., Xie, A.-J., Zhu, J.-F., Tian, X.-Y., and Zhang, L.-D. (2011) Facile fabrication of magnetic metal-organic framework nanocomposites for potential targeted drug delivery. *J. Mater. Chem.*, **21** (11), 3843-3848.
- [131] Vassal, G., Deroussent, A., Challine, D., Hartmann, O., Koscielny, S., Valteau-Couanet, D., Lemerle, J., and Gouyette, A. (1992) Is 600 mg/m² the appropriate dosage of busulfan in children undergoing bone marrow transplantation? *Blood*, **79** (9), 2475-2479.
- [132] Vassal, G., Gouyette, A., Hartmann, O., Pico, J.L., and Lemerle, J. (1989) Pharmacokinetics of high-dose busulfan in children. *Cancer Chemother. Pharmacol.*, **24** (6), 386-390.

- [133] Xu, J., Zhao, Q., Jin, Y., and Qiu, L. High loading of hydrophilic/hydrophobic doxorubicin into polyphosphazene polymersome for breast cancer therapy. *Nanomed. Nanotech. Biol. Med.* DOI: 10.1016/j.nano.2013.08.004.
- [134] Agostoni, V., Anand, R., Monti, S., Hall, S., Maurin, G., Horcajada, P., Serre, C., Bouchemal, K., and Gref, R. (2013) Impact of phosphorylation on the encapsulation of nucleoside analogues within porous iron(III) metal-organic framework MIL-100(Fe) nanoparticles. *J. Mater. Chem. B*, **1** (34), 4231-4242.
- [135] Doucet, O., Ferrero, L., Garcia, N., and Zastrow, L. (1998) O/W emulsion and W/O/W multiple emulsion: physical characterization and skin pharmacokinetic comparison in the delivery process of caffeine. *Int. J. Cosmet. Sci.*, **20** (5), 283-295.
- [136] Touitou, E., Junginger, H.E., Weiner, N.D., Nagai, T., and Mezei, M. (1994) Liposomes as carriers for topical and transdermal delivery. *J. Pharm. Sci.*, **83** (9), 1189-1203.
- [137] Bolzinger, M.A., Briançon, S., Pelletier, J., Fessi, H., and Chevalier, Y. (2008) Percutaneous release of caffeine from microemulsion, emulsion and gel dosage forms. *Eur. J. Pharm. Biopharm.*, **68** (2), 446-451.
- [138] Cunha, D., Ben Yahia, M., Hall, S., Miller, S.R., Chevreau, H., Elkaïm, E., Maurin, G., Horcajada, P., and Serre, C. (2013) Rationale of drug encapsulation and release from biocompatible porous metal-organic frameworks. *Chem. Mater.*, **25** (14), 2767-2776.
- [139] Gaudin, C., Cunha, D., Ivanoff, E., Horcajada, P., Cheve, G., Yasri, A., Loget, O., Serre, C., and Maurin, G. (2012) A quantitative structure activity relationship approach to probe the influence of the functionalization on the drug encapsulation of porous metal-organic frameworks. *Microporous Mesoporous Mater.*, **157**, 124-130.
- [140] Liédana, N., Galve, A., Rubio, C., Téllez, C., and Coronas, J. (2012) Caf@ZIF-8: one-step encapsulation of caffeine in MOF. *ACS Appl. Mater. Interfaces*, **4** (9), 5016-5021.
- [141] Vaughn, J., Wu, H., Efremovska, B., Olson, D.H., Mattai, J., Ortiz, C., Puchalski, A., Li, J., and Pan, L. (2013) Encapsulated recyclable porous materials: An effective moisture-triggered fragrance release system. *Chem. Commun.*, **49** (51), 5724-5726.
- [142] Devautour-Vinot, S., Maurin, G., Henn, F., Serre, C., and Férey, G. (2010) Water and ethanol desorption in the flexible metal organic frameworks, MIL-53 (Cr, Fe), investigated by complex impedance spectroscopy and density functional theory calculations. *Phys. Chem. Chem. Phys.*, **12** (39), 12478-12485.
- [143] Bourrelly, S., Moulin, B., Rivera, A., Maurin, G., Devautour-Vinot, S., Serre, C., Devic, T., Horcajada, P., Vimont, A., Clet, G., Daturi, M., Lavalley, J.-C., Loera-Serna, S., Denoyel, R., Llewellyn, P.L., and Férey, G. (2010) Explanation of the adsorption of polar vapors in the highly flexible metal organic framework MIL-53(Cr). *J. Am. Chem. Soc.*, **132** (27), 9488-9498.
- [144] Walton, R.I., Munn, A.S., Guillou, N., and Millange, F. (2011) Uptake of liquid alcohols by the flexible Fe(III) metal-organic framework MIL-53 observed by time-resolved in situ X-ray diffraction. *Chem. Eur. J.*, **17** (25), 7069-7079.
- [145] Wang, C., Liu, D., and Lin, W. (2013) Metal-organic frameworks as a tunable platform for designing functional molecular materials. *J. Am. Chem. Soc.*, **135** (36), 13222-13234.

[146] Rieter, W.J., Taylor, K.M.L., An, H., Lin, W., and Lin, W. (2006) Nanoscale metal-organic frameworks as potential multimodal contrast enhancing agents. *J. Am. Chem. Soc.*, **128**, 90242-99025.

[147] Della Rocca, J., Liu, D., and Lin, W. (2013) Nanoscale metal-organic frameworks for biomedical imaging and drug delivery. *Accounts Chem. Res.*, **44** (10), 957-968.

[148] Taylor, K.M.L., Rieter, W.J., and Lin, W. (2008) Manganese-based nanoscale metal-organic frameworks for magnetic resonance imaging. *J. Am. Chem. Soc.*, **130** (44), 14358-14359.

[149] Liu, D., Huxford, R.C., and Lin, W. (2011) Phosphorescent nanoscale coordination polymers as contrast agents for optical imaging. *Angew. Chemie Int. Edit.*, **123** (16), 3780-3784.

[150] Rowe, M.D., Chang, C.-C., Thamm, D.H., Kraft, S.L., Harmon, J.F., Vogt, A.P., Sumerlin, B.S., and Boyes, S.G. (2009) Tuning the magnetic resonance imaging properties of positive contrast agent nanoparticles by surface modification with raft polymers. *Langmuir*, **25** (16), 9487-9499.

[151] Rowe, M.D., Thamm, D.H., Kraft, S.L., and Boyes, S.G. (2009) Polymer-modified gadolinium metal-organic framework nanoparticles used as multifunctional nanomedicines for the targeted imaging and treatment of cancer. *Biomacromolecules*, **10** (4), 983-993.

HYPOTHESIS AND OBJECTIVES
HIPÓTESIS Y OBJETIVOS

HYPOTHESIS AND OBJECTIVES

The treatment of cancer and other infectious illnesses is very diverse and depends on several factors, socioeconomic amidst others. Thus, we can find a series of *in vitro* high efficacy drugs with however many disadvantages, which limit their clinical use (*i.e.* low specificity and high toxicity, among others).

For this reason, one of the current objectives in pharmaceutical technology is to find adequate drug delivery systems (DDS) with more secure (in terms of toxicity) and effective drugs, together with an improvement of the patients' life quality. In this sense, the drug encapsulation in biodegradable nanoparticles is reporting very good results.

Therefore, the **general objective** of this PhD Thesis work is based on the design, synthesis and biomedical evaluation of porous coordination polymers or Metal-Organic Frameworks (MOFs), which are biodegradable hybrid materials with a wide range of applications and that could be an interesting alternative in drug delivery, due to their high porosity and versatile composition, able to load and release divers therapeutic molecules. The chosen drugs for this work are: (i) a natural origin antitumoral drug (genistein), which will be encapsulated within the MOF porosity, as well as (ii) two antibiotic agents, azelaic acid (AZA) and zinc, which will create the MOF structure.

To achieve this final objective, the work has been divided in **3 partial objectives**, listed in the next points:

- 1) The synthesis and characterisation of a series of MOF nanoparticles based on *a priori* low toxic metals (Fe, Zr, Zn), as well as the evaluation of their cytotoxicity and cell uptake, with the objective of selecting the more suitable nanoparticles for the encapsulation of drugs (**Chapter 1**).
- 2) The encapsulation and the *in vitro* release of the soy isoflavone genistein in a series of iron(III) and zirconium(IV) based-MOFs and its pharmacokinetic and biodistribution evaluation in mice (**Chapter 2**).
- 3) The synthesis and characterisation of a novel zinc azelate MOF, together with the evaluation of its antibacterial properties for the treatment of different skin pathologies (**Chapter 3**).

HIPÓTESIS Y OBJETIVOS

El tratamiento del cáncer y de las enfermedades infecciosas depende de muchos factores, entre ellos los socioeconómicos. Para el tratamiento de estas enfermedades, se dispone de fármacos con una buena eficacia *in vitro* pero cuyo uso en clínica se ve limitado debido a su baja especificidad y/o alta toxicidad.

Por ello, uno de los principales objetivos de la tecnología farmacéutica, se centra en la vehiculización de fármacos, con el fin de disminuir su toxicidad y aumentar su eficacia, lo que redundaría en una mejor calidad de vida para los pacientes.

El **objetivo general** de este proyecto de Tesis es el diseño, síntesis y evaluación de los materiales híbridos cristalinos o *Metal-Organic Frameworks* (MOFs). Estos materiales micro o nanoparticulados biodegradables, presentan un amplio abanico de aplicaciones en la administración de fármacos. En este trabajo, se han vehiculizado varios principios activos. Por un lado, la genisteína, molécula de origen natural con propiedades antitumorales, se ha encapsulado en la porosidad de los MOFs y, por otro, el ácido azelaico y el zinc, dos agentes antibacterianos, que se han combinado formando un nuevo MOF bioactivo.

Para conseguir este objetivo general fue necesario abordar los siguientes estudios:

- 1) La síntesis, caracterización, evaluación de la citotoxicidad y penetración celular de una serie de nanoMOFs, con el fin de seleccionar los sistemas más adecuados para la encapsulación de fármacos (**Capítulo 1**).
- 2) La encapsulación de la isoflavona genisteína en una serie de MOFs porosos a base de hierro(III) y zirconio(IV), así como el estudio de su liberación *in vitro* y su perfil farmacocinético, incluyendo su biodistribución en ratones (**Capítulo 2**).
- 3) La síntesis, caracterización, biodegradación y eficacia antibacteriana de un nuevo BioMOF (BioMIL-5), que contiene ácido azelaico y zinc en su composición y que puede ser utilizado como antibiótico en patologías de la piel (**Capítulo 3**).

CHAPTER 1

CYTOTOXICITY OF NANOSCALED METAL-ORGANIC FRAMEWORKS

GENERAL OBJECTIVES AND AUTHOR CONTRIBUTIONS

C. Tamames-Tabar, D. Cunha, E. Imbuluzqueta, F. Ragon, C. Serre, M. J. Blanco-Prieto and P. Horcajada, *Journal of Materials Chemistry B*, 2014, 2, 262-271.

Metal-Organic Frameworks (MOFs) have recently emerged as promising materials for their use in biomedicine, in particular as drug delivery systems (DDS). However, prior to any biomedical application, their toxicity and biological interactions need to be assessed.

Therefore, a series of 14 MOF nanoparticles (NPs) based on different structures and compositions (metal=Fe, Zr and Zn; linkers=imidazolate and different carboxylates), were chosen to fulfil cytotoxicity studies in two commonly used cell lines: (i) murine macrophage cells (J774), a cell line of choice in cellular penetration assays, and (ii) foetal cervical carcinoma cells (HeLa), due to the potential dermal applications of MOFs. Later, the best candidate in terms of low cytotoxicity, the mesoporous iron(III) trimesate MIL-100 NPs, was chosen for further cellular uptake assays with the aim of better understanding the interaction of this MOF NPs with these two different cell lines.

This work has been divided in the following parts for a better comprehension of the reader: (i) synthesis and characterisation of a series of 14 MOF NPs, as well as the adsorption of a green fluorophore (here-called furazan) in MIL-100 NPs porosity for allowing to observe the cellular penetration by fluorescence confocal microscopy, (ii) the cytotoxicity evaluation of MOFs in J774 and HeLa cell lines during 24 h, discussing the influence of different parameters (MOF topology, composition and size) on their *in vitro* toxicity and (iii) the cellular uptake tests of MIL-100 NPs engrafted with furazan in both cell lines as a function of time.

All the authors have contributed in this work. C. Tamames-Tabar has synthesised and characterised all the MOF NPs (except for MIL-127, ZIF-8 and UiO-66 NPs), has encapsulated furazan in MIL-100, fulfilled the cytotoxicity tests and the cellular uptake studies, as well as has contributed in the writing of the article manuscript. Dr. D. Cunha has synthesised MIL-127 and ZIF-8 NPs, has collaborated in cytotoxicity evaluations and in the article manuscript. Dr. E. Imbuluzqueta has actively participated in cytotoxicity evaluations, cellular uptake studies and in the article writing. Dr. F. Ragon has synthesised and fully characterised the UiO-66 NPs. Dr. C. Serre has actively contributed in the article manuscript. Finally, Dr. M. J. Blanco-Prieto and Dr. P. Horcajada have actively supervised all the work and contributed in the article manuscript.

CYTOTOXICITY OF NANOSCALED METAL-ORGANIC FRAMEWORKS

Cristina Tamames-Tabar, †^{a,b} Denise Cunha, †^a Edurne Imbuluzqueta, †^b Florence Ragon,^a
Christian Serre,^a María J. Blanco-Prieto*^b and Patricia Horcajada*^a

^a*Institut Lavoisier, UMR CNRS 8180, Université de Versailles Saint-Quentin-en-Yvelines, 45 Avenue des Etats-Unis, 78035 Versailles Cedex, France.*

^b*Departamento de Farmacia y Tecnología Farmacéutica, Facultad de Farmacia, Universidad de Navarra, Irunlarrea 1, 31008 Pamplona, Spain.*

† CTT, DC and EI contribute equally to this work.

Journal of Materials Chemistry B, 2014, 2, 262-271.

Corresponding authors*

M. J. Blanco-Prieto: Departamento de Farmacia y Tecnología Farmacéutica, Facultad de Farmacia, Universidad de Navarra, Irunlarrea 1, 31008 Pamplona, Spain; Fax: 34 948425649; Tel: 34 948425600 Ext. 806519; E-mail: mjblanco@unav.es

P. Horcajada: Institut Lavoisier, UMR CNRS 8180, Université de Versailles Saint-Quentin-en-Yvelines, 45 Avenue des Etats-Unis, 78035 Versailles Cedex, France ; Fax: 33 (0) 139256652; Tel: 33 (0) 1 39254371; E-mail: horcajada@chimie.uvsq.fr

ABSTRACT

A series of fourteen porous Metal-Organic Frameworks (MOFs) with different compositions (Fe, Zn, Zr; carboxylates or imidazoles) and structures have been successfully synthesised at the nanoscale and fully characterised by XRPD, FTIR, TGA, N₂ porosimetry, TEM, DLS and ζ -potential. Their toxicological assessment was performed using two different cell lines: human epithelial cells from foetal cervical carcinoma (HeLa) and murine macrophage cell line (J774). It appears that MOF nanoparticles (NPs) exhibit a low cytotoxicity, comparable to those of other commercialised nanoparticulated systems, the less toxic being the Fe carboxylate and the more toxic the zinc imidazole NPs. The cytotoxicity values, higher in J774 cells than in HeLa cells, are mainly function of their composition and cell internalisation capacity. Finally, cell uptake of one of the most relevant Fe-MOF-NPs for drug vectorisation has been investigated by confocal microscopy studies, and indicates faster cell penetration kinetics within J774 compared to HeLa cells.

1. INTRODUCTION

Metal-Organic Frameworks or MOFs, are still considered as being a hot research topic in material chemistry¹ as illustrated through their highly porous hybrid character built up from inorganic units and organic polycomplexing linkers. Their easily tuneable structure, composition and porosity allow a careful switching of their physico-chemical properties. This huge chemical and structural versatility makes them promising candidates for main relevant applications such as gas storage, separation, heat transformation, catalysis and sensing, among others^{1,2}. Recently, their use in biomedicine has been proposed³, including contrast agents for imaging techniques⁴ and the encapsulation for controlled delivery of molecules, such as drugs⁵, cosmetics⁶ and biologically active gases (NO, H₂S, etc)⁷.

Control of MOF particle size in the nanometric range⁸ has paved the way for their use in nanotechnology⁹. Noteworthy, nanoscale non-toxic porous iron(III)-based MOFs with engineered cores and surfaces have been proposed as nanocarriers for the controlled delivery of antitumoral and anti-HIV drugs, with additional imaging properties^{9b,10}. Also, they enable the progressive release of the drug into the cells^{9b}. However, prior to any bioapplication of MOF nanoparticles (NPs), their toxicity has to be established¹¹. Up to now, the available toxicity information remains still very scarce, mostly related either to the inorganic and organic precursors, or *in vitro* cytotoxicity studies¹². For instance, Lin and co-workers have reported values of the half maximal inhibitory concentration (IC₅₀) of 46 µg·mL⁻¹ for the silica-coated MIL-101-NH₂-Br-BODIPY NPs on human colon adenocarcinoma cells (HT-29). However, both the fluorophore moiety and the silica coating of these NPs might also influence their cytotoxicity¹⁰. Additionally, the *in vitro* toxicity of lanthanide-based MOFs¹³ was carried out in human colon adenocarcinoma (HT-29) and in acute lymphoblastic leukaemia human cells, showing important cytotoxicity values (IC₅₀ ~10 and 15 µg·mL⁻¹, respectively), due *a priori* to the linkers' antitumoral own activity.

Finally, the only reported *in vivo* studies so far, concern the intravenous injection of high doses (up to 220 mg·Kg⁻¹) of three porous iron(III) carboxylate NPs based on different organic linkers. All the studied parameters (serum, enzymatic, histological, etc.) evidenced a lack of severe acute and subacute (150 mg·Kg⁻¹ for four consecutive days) toxicity. NPs were rapidly captured by the liver and spleen and then, degraded into their constitutive components (iron and carboxylate ligand), allowing the direct removal in around 15 days of iron and exogenous linkers by the urine and faeces without any metabolism^{9b,14}. Note that biodistribution and elimination kinetics might depend on

the MOF nature. Thus, despite these encouraging results, further studies must be performed on different MOF structures taking special attention to their long-term toxicity. Therefore, we propose here to investigate the cytotoxicity of a series of benchmarked MOF NPs, using two different cell lines, in order to evaluate the influence of their topology, composition, biological stability, particle size and surface charge in regard to their cell toxicity. The chosen MOF NPs are here: (i) the cubic-zeotype mesoporous MIL-100 and MIL-101 solids (MIL: Material of Institut Lavoisier) built up from trimers of iron(III) octahedra and tricarboxylic acids (trimesate, BTC) for MIL-100 or 2-amino or 2,5-dimethyl terephthalates (BDC-NH₂ or BDC-2CH₃) for MIL-101-NH₂ and -2CH₃, respectively), which all exhibit a very high porous character^{9b,15}; (ii) the cubic structure Soc-MOF (Fe) or MIL-127, based on iron(III) octahedra trimers and 3,3',5,5'-azobenzene-tetracarboxylate anions (Tabz)¹⁶; (iii) the cubic structure UiO-66 (UiO: Oslo University) based on zirconium(IV) oxoclusters and terephthalate anions (BDC)¹⁷; (iv) the flexible series of isorecticular MIL-88¹⁸, built from iron(III) oxo-centered trimers connected by dicarboxylate bridges (fumarate for MIL-88A; terephthalate for MIL-88B). In addition, the physico-chemical properties and porosity of these solid are tuned through the grafting different organic functional groups on the aromatic ring of the terephthalate linker, such as NH₂, NO₂, CH₃, 2CH₃ and 4CH₃ (for MIL-88B-NH₂, -NO₂, -CH₃, -2CH₃ and -4CH₃, respectively)¹⁸ and finally, (v) the cubic architecture ZIF-8 (ZIF-8: Zeolitic Imidazolate Framework) based on a microporous zinc 2-methyl-imidazolate¹⁹.

The present work aims to: (i) evaluate the cytotoxicity of MOFs in human cervical cancer cell line (HeLa) and in mouse macrophage cell line (J774) by the MTT assay²⁰ and (ii) study the cellular uptake of MIL-100(Fe) using the same cells, taking into account its exceptional drug loadings and controlled releases^{6,9b,21} HeLa cells were chosen due to possible dermal applications of MOFs containing cosmetic agents^{6,22} and J774 for being a cell line of choice for cellular uptake studies.

2. EXPERIMENTAL SECTION

2.1 Material Synthesis

NPs of MIL-100(Fe)^{9b}, MIL-101-NH₂^{9b}, MIL-101-2CH₃²³, MIL-88A^{19b} MIL-88B-4CH₃^{9b}, ZIF-8¹⁹, MIL-88B-CH₃¹⁸, MIL-88B-2CH₃¹⁸ and MIL-88B-2CF₃¹⁸ were prepared as previously reported. Nanometric MIL-127, UiO-66, MIL-88B, MIL-88B-NH₂ and MIL-88B-NO₂ were synthesised by different methods (round bottom flask or microwave

assisted hydro/solvothermal route; see SI pages 94-98). Microwave-assisted syntheses were done using a MARS-CEM® microwave (USA).

For fluorophore ((*R*)-(-)-4-(3-Aminopyrrolidino)-7-nitrobenzofurazan, furazan) encapsulation, 1 mg of the dehydrated MIL-100(Fe) microparticles (MPs) or NPs (100 °C overnight) was suspended into 200 µL of a 32 µg·mL⁻¹ furazan aqueous solution under rotational stirring for 2 h at room temperature (RT). The particles were later recovered by centrifugation (15000 *g*/15 min) and washed with deionised water.

2.2 Material Characterisation

X-ray powder diffraction (XRPD) patterns were collected using a SIEMENS D5000 diffractometer (Siemens, Germany) (θ -2 θ) using Cu K α _{1,2} radiation ($\lambda \sim 1.54056$ Å) from 5 to 15 ° (2 θ) using a step size of 0.04 ° and 4 s per step in continuous model (page 98). Fourier-Transformed Infrared (FTIR) spectra were obtained with a Thermo Nicolet spectrometer (Thermo, USA) and were recorded from 4000-400 cm⁻¹ at RT (page 99). Approximately 5-10 mg of each sample were used for thermogravimetric analysis (TGA) measurements and were analysed under an O₂ flow (20 mL·min⁻¹) with a Perkin Elmer Diamond TGA/DTA STA 6000 running from 20 to 600 °C with a scan rate of 2 °C·min⁻¹ (page 99). Nitrogen porosimetry of the rigid materials was carried out with a Belsorp mini II® porosimeter (BEL Japan Inc.) (page 99). Morphological analysis was done with a Transmission Electron Microscopy (TEM) Darwin 208 Philips 60-80-100 kV coupled to an AMT camera (page 77). Particle size and polydispersity index (PDI) were measured in phosphate buffer solution (PBS) 0.271 mM pH 7.2 by dynamic light scattering (DLS) and surface charge (ζ -potential) by laser Doppler electrophoresis using a Zetasizer Nano-ZS® analyser system (Malvern Instruments, UK) (pages 76 and 101).

For the experimentally estimated log P, 1 mg of each linker was added to 1 mL of water and 1 mL of *n*-octanol and maintained at 37 °C under rotational stirring overnight. Then, both fractions were separated by centrifugation (8000 *g*/15 min) and the amount of each linker in each fraction was measured by an Agilent 8453 Ultraviolet Spectrophotometer (Agilent Technologies, USA) (page 82).

Finally, for furazan delivery studies, 5 mg of furazan-grafted MIL-100(Fe)_NPs were suspended in 1 mL of RPMI cell culture medium under stirring at 37 °C to simulate *in vitro* conditions. Aliquots of 20 µL were collected every 30 min and the amount of delivered furazan was quantified by fluorescence spectroscopy using a Cary® Uv-VIS-NIR Spectrophotometer (Varian, USA) at λ_{em} and λ_{ex} of 535 and 500 nm, respectively (page 78).

2.3 Cell Culture and Cytotoxicity Assays

J774 cell line (ATCC TIB-67) was maintained in RPMI 1640 medium supplemented with glutamax®, 10% of heat-inactivated foetal bovine serum and 1% of antibiotic antimycotic solution. HeLa cells (ATCC CCL-2) were cultured in DMEM medium supplemented with 1% of *L*-glutamine, 10% of heat-inactivated foetal bovine serum and 1% of antibiotic antimycotic solution. Both cell lines were grown at 37 °C in a humidified 5% CO₂ atmosphere and passaged twice a week (at 80% of confluence) at a density of 5x10⁴ cells·cm⁻².

The cytotoxic activity of the NPs and their constitutive linkers was analysed by the MTT assay²⁰, being the amount of linker tested, the molar equivalent of its amount in the NP. 24 h prior the assay, the cells were seeded in 96-well plates at a density of 1x10⁴ cells *per* well. The treatments (MOF NPs and linkers) were prepared at a 10-fold higher concentration (due to a direct 1/10 direct dilution in the well, as 20 µL of treatments were added to a final volume of 200 µL *per* well). They were solubilised (in the case of the linkers) or dispersed (in the case of the MOF NPs) in cell culture medium containing 0.5% of DMSO. Then they were added to the cells at different concentrations (up till a final concentration of 2.5 mg·mL⁻¹) and kept 24 h at 37 °C with 5% CO₂ atmosphere. Cytotoxicity was determined after 24 h by adding the MTT reactant (0.5 mg·mL⁻¹ in PBS, incubation at 37 °C during 2 h) followed by 200 µL of DMSO to each well. The plates were read at λ=540 nm.

Finally, it was determined that a DMSO concentration of 0.5%, corresponding to the maximum amount added to homogenise the treatments, was not toxic²⁴. Also, the cell culture medium pH was measured before and after each MTT assay, being the pH variations minimal (see SI, pages 74-75).

2.4 Cellular Penetration Assays: Confocal Microscopy

For MIL-100(Fe)_NPs uptake studies, J774 and HeLa cells were seeded at a density of 1x10⁵ cells *per* well on glass coverslips placed in 24-well plates. After 24 h, cells were washed with PBS and incubated with 0.25 mg of furazan-engrafted MIL-100(Fe)_NPs in complete cell culture medium. Untreated cells and cells treated with 10 µg·mL⁻¹ of free furazan were included as controls. After appropriate incubation times, cells were extensively washed with PBS to remove the excess of non-internalised material, fixed in 4% *p*-formaldehyde for 5 min and incubated with the nuclear dye TOPRO-3 (1:1000 in PBS, 5 min). Finally, coverslips were mounted with Dako Fluorescent mounting medium

onto glass slides and cells were examined using a Zeiss LSM 510 META confocal microscope with a Plan-Apochromat AN objective (Carl Zeiss Microscope Systems, Zena, Germany) equipped with an Ar laser at 488 nm together with a filter at 505 nm. The images were analysed using the LSM Image Browser Carl Zeiss Advanced Imaging Microscopy Release 4.2 software.

3. RESULTS AND DISCUSSION

3.1 Synthesis and Characterisation of MOFs

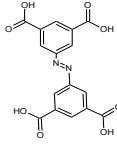
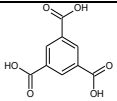
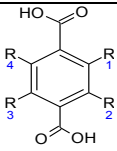
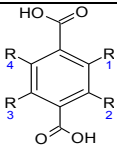
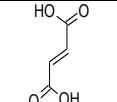
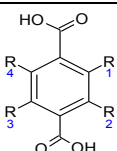
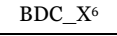
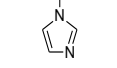
Fourteen types of MOF NPs (Tab. 1, page 76) with different structures and compositions have been successfully synthesised, as first confirmed by XRPD, which show the characteristic Bragg peaks of the bulk MOFs with broadness, in agreement with the smaller crystal size (Fig. S1, page 98).

Noteworthy, some synthesis routes were slightly modified in order to obtain high yields (>70%) of small and well monodispersed NPs (Tab. 1, page 76). This is the case for the MIL-88B-NH₂ and MIL-88B-NO₂ solids, previously obtained as MPs by solvothermal route¹⁸. However, this required the use of toxic solvents such as *N,N'*-dimethylformamide or methanol (*i.e.* MIL-127, MIL-101-2CH₃, UiO-66, MIL-88B, MIL-88B-CH₃, -2CH₃ and -4CH₃). Thus, before studying the *in vitro* toxicity of the NPs, purification and/or activation steps (see SI, pages 94-98) were carried out to avoid the presence of remaining traces of toxic solvent. TGA and FTIR spectra both confirmed the absence of any impurities (residual organic linker or solvents) in the final products (Tab. S1 and Fig. S2, page 99). Moreover, except for the flexible porous MIL-88 type solids, which showed no accessible porosity in their dehydrated (closed) form, the permanent porosity of rigid MOF-NPs was evaluated by nitrogen adsorption at 77 K, leading to results close to those of the bulk materials (Tab. S2, page 99)^{15-17,19}.

Concerning the resulting particle sizes, most NPs exhibited mean diameters close to 100 nm associated with low polydispersity indexes (PdI<0.2) (Tab. 1, page 76). In contrast, MIL-127 NPs presented a higher particle size (476±82 nm) with a high PdI as consequence of an important aggregation process in solution. Similarly, ZIF-8 and UiO-66 NPs exhibited larger dimensions in solution (DLS) than in their dry state (TEM) (~60 and 30 *vs.* 100 and 90 nm, respectively), due to an aggregation effect, as also evidenced by TEM (Fig. 1, page 77). Indeed, TEM images showed rather small and monodispersed NPs bearing different morphologies. Well-faceted crystals with more or less elongated hexagonal morphology or octahedral-cubic shape were observed for respectively the MIL-

88 solids or MIL-100/101/127 NPs, whereas ZIF-8 and UiO-66 NPs disclosed a spherical morphology associated with an important aggregation.

Tab. 1 Physico-chemical characterisation of MOF NPs (particle size and ζ -potential), and their IC₅₀ values at 24 h in J774 and HeLa cells.

MOF NPs	M ¹	L ²	R _n ³	Size (nm)	ζ -pot (mV)	IC ₅₀ (mg·mL ⁻¹)				
						HeLa		J774		
						MOF NPs	L ²	MOF NPs	L ²	
MIL-127	Fe		-	476±82	-38.5±2.0	>2.00	0.80±0.02	0.44±0.02	0.82±0.17	
MIL-100			-	120±40	-18.3±0.6	1.10±0.15	2.00±0.06	0.70±0.02	>1.00	
MIL-101_2CH ₃			(CH ₃) _{1,3} (H) _{2,4}	120±15	-24.2±2.1	>2.50	>1.70	0.17±0.01	0.08±0.01	
MIL-101_NH ₂			(NH ₂) ₁ ,(H) ₂₋₄	100±18	-27.4±1.5	>1.00	0.60±0.01	0.07±0.002	0.02±0.004	
MIL-88A			-	105±15	-25.0±4.3	0.015±0.005	0.03±0.003	0.05±0.002	0.40±0.01	
MIL-88B			(H) ₁₋₄	100±20	-23.5±1.8	1.26±0.08	0.80±0.02	0.37±0.08	0.43±0.03	
MIL-88B_CH ₃			(CH ₃) ₁ ,(H) ₂₋₄	75±20	-22.8±2.2	>2.00	1.05±0.03	0.37±0.01	0.24±0.02	
MIL-88B_2CH ₃			(CH ₃) _{1,3} (H) _{2,4}	100±20	-26.0±0.4	2.10±0.08	>1.70	0.36±0.03	0.08±0.01	
MIL-88B_4CH ₃			(CH ₃) ₁₋₄	120±20	-41.3±0.6	0.69±0.02	>2.00	0.08±0.01	0.42±0.01	
MIL-88B_2CF ₃			(CF ₃) _{1,3} (H) _{2,4}	105±30	-53.2±7.3	>2.00	1.12±0.08	0.41±0.01	0.57±0.01	
MIL-88B_NH ₂			(NH ₂) ₁ ,(H) ₂₋₄	115±20	-25.7±1.6	1.10±0.02	0.60±0.01	0.45±0.03	0.02±0.004	
MIL-88B_NO ₂			(NO ₂) ₁ ,(H) ₂₋₄	130±15	-28.4±0.7	>2.00	>2.00	0.03±0.001	0.17±0.01	
UiO-66		Zr		(H) ₁₋₄	100±20	-26.3±1.5	0.40±0.01	0.80±0.02	0.06±0.001	0.43±0.03
ZIF-8		Zn		-	90±15	-11.0±0.6	0.10±0.01	1.40±0.02	0.025±0.001	>1.00

¹M: Metal; ²L: Linker; ³R_n: Functionalisations; ⁴Tabz: Azobenzene-tetracarboxylic acid; ⁵BTC: 1,3,5-benzenetricarboxylic acid; ⁶BDC_X: 1,4-dicarboxylic acid or terephthalic acid; ⁷FUM: fumaric acid; ⁸MI: 2-methylimidazolate.

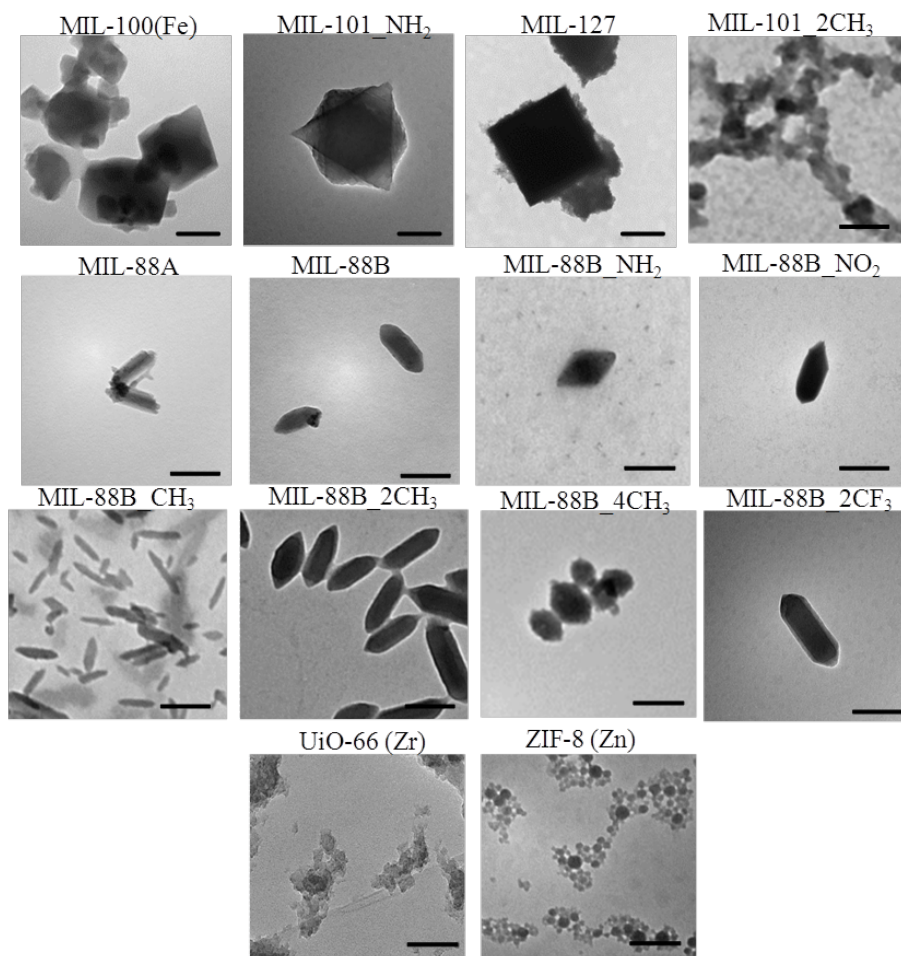


Fig. 1 Transmission Electron Microscope (TEM) images of MOF NPs. Scale bars correspond to 100 nm.

Alongside with particle sizes in the same range, all MOF NPs exhibited negative surface charges in PBS, being the most negative the hydrophobic solids MIL-88B_2CF₃ and MIL-88B_4CH₃ (-53.2 ± 7.3 and -41.3 ± 0.6 mV). Interestingly, analysis of the (CH₃)_n functionalised MIL-88B NPs suggests that the increase in the number of methyl groups *per* spacer leads to more negatively charged particles (-22.8 ± 2.2 , -26.0 ± 0.4 and -41.3 ± 0.6 mV for $n=2$, 3 and 4, respectively). In addition, the zeta potential has been also determined in DMEM cell culture media + 10% FBS (see Tab. S3, page 101), evidencing less negative surface charges. These less negative values, in agreement with the zeta potential value obtained for the medium alone (-8.32 ± 0.25 mV), indicate the adsorption of proteins presented in the medium and might permit the interaction between and the NPs and the cell membrane.

With the aim to visualise the NPs inside the cells and further study their interactions with cells, a fluorophore was associated to the MIL-100(Fe)_NPs. Furazan was selected since: (i) it possesses functional groups (amino, nitro and heterocyclic heteroatoms), *a priori*

able to strongly interact with the unsaturated metal sites (CUS) of MIL-100(Fe) NPs, preventing the leaching during the *in vitro* tests; (ii) it bears small dimensions (5.5 x 10.6 x 3.7 Å) allowing furazan to be trapped within the pores (windows size ~8.6 and 4.7 x 5.7 Å); (iii) its high aqueous solubility (3.14 mg·mL⁻¹) and (iv) its easy and sensible detection and quantification.

First, furazan (Fig. 2A) was loaded into the MIL-100(Fe)_MPs crystals (~1-5 μm) to allow its location within the particles. A simple impregnation of the MPs within a furazan aqueous solution (see Experimental Section, page 73) was carried out to ensure its homogeneous distribution within the pores, as evidenced by confocal microscopy (Fig. 2C). Then, MIL-100(Fe)_NPs were similarly functionalised achieving a furazan grafting of around 11.4% wt, as confirmed by fluorescence spectroscopy. Although the microscopy resolution did not allow distinguishing the location of the furazan within the NPs, it can be considered that the fluorophore was homogeneously distributed within the pores, similarly to the MPs.

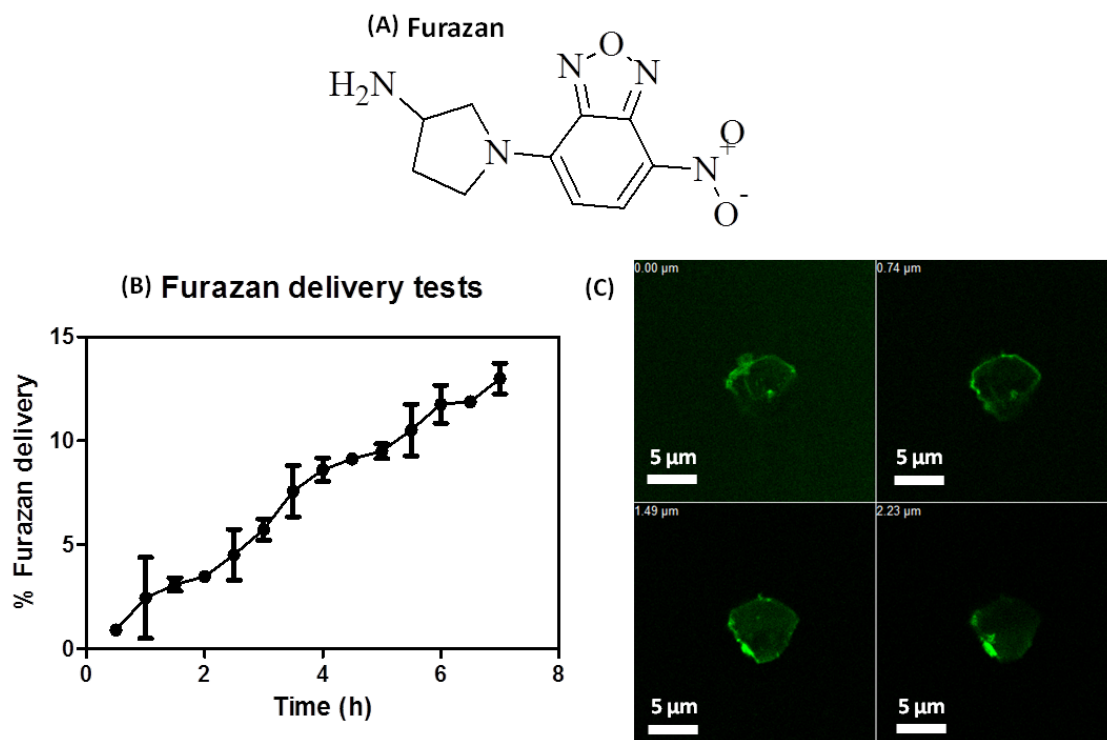


Fig. 2 Chemical structure of furazan (A; top). Delivery profile of furazan from MIL-100(Fe) NPs in RPMI cell culture medium at 37 °C ($n=3$; mean±SD) (B; left). Furazan-engrafted MIL-100(Fe)_MP stack at different depths (0.00, 0.74, 1.49 and 2.23 μm), showing homogeneous furazan engrafting observed by confocal microscopy (C; right).

Finally, the stability of the grafting was evaluated by incubating the furazan-loaded MIL-100(Fe)_NPs in cell culture media. The released furazan was quantified by fluorescence spectroscopy (Fig. 2B, page 78). Furazan showed a slow delivery from the NPs, with less than 5 and 15% of the grafted furazan (0.02 and 0.06 mg per 100 mg of dehydrated MIL-100(Fe)_NPs) released after the first 2 and 7 h, respectively. Consequently, the stability of the loaded furazan within the NPs is high enough to follow the cellular penetration of the furazan-grafted MIL-100(Fe)_NPs within different cell lines.

3.2 Cytotoxicity Evaluation

The high chemical and/or structural versatility (metal, organic linker, structure of the MOFs) introduces many factors that shall impact the resulting cytotoxicity. Furthermore, cytotoxicity was studied using HeLa and J774 cells (Tab. 1, page 76), finding a cell type specific response to the treatments, which was attributed to the different phagocytic characteristics of the used lines, as it will be further considered.

Effect of the Topology

Interestingly, the cytotoxicity of polymorphs (identical composition but different crystalline structure) such as the iron amino-terephthalates MIL-88B_NH₂ and MIL-101_NH₂ or the iron 2,5-dimethylterephthalates MIL-88B_2CH₃ and MIL-101_2CH₃, was not different (IC₅₀=1.10 *vs.* 1.0 mg·mL⁻¹ and 2.1 *vs.* 2.5 mg·mL⁻¹, respectively), indicating a poor effect of the topology.

Effect of the Metal

On the whole, the toxicity depends on the nature of the metal with the Zn-based MOFs being more toxic (ZIF-8: IC₅₀ (HeLa)=0.10 mg·mL⁻¹; (J774)=0.025 mg·mL⁻¹) followed by Zr-MOFs UiO-66 NPs (IC₅₀ (J774)=0.06 mg·mL⁻¹; IC₅₀ (HeLa)=0.40 mg·mL⁻¹) and finally the less toxic Fe-based MOFs NPs (Tab. 1, page 76).

Both Zn and Fe are related to important biological functions²⁵, and are present in the body in relatively significant amounts (~4 g)²⁶. Although Zn is an endogenous element, it is well-known to induce considerable cellular toxicity, as a consequence of its capacity to compete with Fe and Ca ion channels, modifying their metabolism and therefore, leading to cellular damage²⁷. Despite the high cytotoxicity values disclosed by ZIF-8, these hybrid NPs exhibited IC₅₀ values comparable to those of other Zn oxide NPs²⁸. In addition,

Karlsson *et al.* evidenced an important cytotoxic effect of ZnO NPs in human lung epithelial A549 cell line due to their considerable ability to cause DNA damage²⁹. Recent toxicological studies suggested that Zn toxicity is related with the rather high solubility of Zn²⁺ ions³⁰. Here, we expect that ZIF-8 NPs are progressively degraded into Zn²⁺ and methyl-imidazolate (pK_a ~7.0 and 14.5) in cell culture media (pH ~7.4 in presence of phosphates) as well as in endosomal environment (pH ~6.5-4.5 and enzymes). Therewith, the high toxicity values of ZIF-8 could arise from competition of Zn²⁺ with Fe²⁺ and Ca²⁺ cations through ion channels and/or DNA damage.

The Fe cytotoxicity, evidenced in J774 cells, was also comparable to those of Fe oxide NPs widely used as contrast agents³¹. However, Fe toxicity is generally related with different factors. First, it is well known that Feⁿ⁺ ions can generate reactive oxygen species (ROS) through the Fenton or Harber-Weiss reaction when in contact with cells³². Noteworthy, redox active metals and ROS pathways alter the plasma membrane potential, provoking changes in the gene expression³³ and cell cycle regulation³⁴, finalising with cellular death or apoptosis. Additionally, the formation of ROS could also be the consequence of the membrane lipid peroxidation by NPs, inducing cell damage³⁵. Finally, the intense Fe traffic in mitochondria, enabling the synthesis of heme and Fe-S clusters involved in the cellular respiration, could be also affected by an iron overload³⁶. Therefore, the Fe sensibility of each cell type, same as their capability to avoid the trigger of these mechanisms and their consequent cell damages, will define which cell type will be the most affected. Despite the possibility of Feⁿ⁺ ions inducing toxicity, there are nowadays numerous examples of Fe oxide particles having very secure profiles, such as USPIO and SPIO with different coatings (poly(ethylene glycol) (PEG)³⁷, carboxydextran³⁸, mannan³⁹, dextran⁴⁰, etc.

Although the impact of Zr⁴⁺ ions has not been studied as wide as Feⁿ⁺ or Zn²⁺, previous investigations reported several coumarin Zr⁴⁺ complexes as antiproliferative agents⁴¹. Their IC₅₀ values were of approximately 0.04 mg·mL⁻¹ for the highly soluble Zr⁴⁺ salt (ZrCl₄) in acute myeloid leukaemia derived HL-60 and in chronic myeloid leukaemia LAMA-84 cells, a value which was in total agreement with the important toxicity found in J774 cells (IC₅₀=0.06 mg·mL⁻¹).

Effect of the Organic Linker

The influence of the organic constitutive linker has been mainly evaluated using isostructural Fe-based MOFs bearing various functionalised terephthalate linkers (BDC_X; Tab. 1, page 76).

One shall keep here in mind that during their degradation process at pH 7.4 and in presence of phosphate groups, the linkers might be progressively replaced by oxo or hydroxo groups and/or phosphates and released to the media as polycarboxylate anions ($pK_a \sim 3-5$). Degradation studies, performed on DMEM medium + 10% FBS by elemental analysis, showed however that except for the MIL-101_2CH₃ and MIL-88B_2CH₃, the rest of the NPs did not exhibit a significant degradation after 24 h, which could be related with a protective effect of the proteins adsorbed on the MOF outer surface. For MIL-101_2CH₃ and MIL-88B_2CH₃ NPs, a partial degradation was observed corresponding to 18.3 ± 1.6 and $11.1 \pm 7.1\%$, respectively.

Comparing the IC₅₀ values in J774 cells, the values were in agreement with the cytotoxicity for some ligands, supporting that the cytotoxicity of MOF NPs was on the whole related to the one of their constitutive organic linkers. Nonetheless, this profile was not followed for the BDC_CH₃, BDC_2CH₃ and BDC_NH₂ MOF materials. Here again, this might be due to the internalisation of nanoparticles by endocytosis whereas linker molecules could follow other cell penetration pathways.

When analysing the results in HeLa cells, it can be pointed out that in general, linkers are “safe” considering their IC₅₀ values above 1.00 mg·mL⁻¹, except for BDC_NH₂, Tazb and BDC with nevertheless high IC₅₀ values ranging between 0.60 and 0.80 mg·mL⁻¹. However, this cytotoxicity profile cannot be observed for the fumarate linker, as it is the most toxic one (IC₅₀=0.03 mg·mL⁻¹), comparable with our cytotoxicity values using the J774 cells (IC₅₀=0.40 mg·mL⁻¹), which clearly differs from our *in vivo* data^{9b,14}. MIL-88A NPs showed a low IC₅₀, comparable with currently other available nanoparticulated systems⁴². However, our cytotoxicity values are here unexpectedly high, when taking into account the endogenous character of fumarate, and the absence of any *in vivo* toxicity for the MIL-88A_NPs^{9b}.

Moreover, our previous *in vivo* toxicity studies evidenced the lack of toxicity of MIL-88A, MIL-100 and MIL-88B-4CH₃_NPs, built up from linkers exhibiting different polarities. After the intravenous administration of high doses of these MOFs, a fast Fe removal and a dependent excretion rate of the ligands, following their hydrophobic-hydrophilic character, was observed^{9b,14}. Hydrophobic BDC_4CH₃ was slowly removed, due to its association with lipid droplets into macrophages (liver and spleen), whereas hydrophilic BTC linker was fast excreted in urine due to its high polarity. Interestingly, hydrophilic FUM was not removed since this endogenous molecule can be reused in the Krebs cycle.

In our study, the hydrophobic/hydrophilic balance (log P) of the constitutive organic linker can be related to the MOF NPs cytotoxicity. Indeed, with the exception of MIL-88A_NPs, a roughly linear tendency between the partition coefficients (experimentally

estimated log P) and cytotoxicity expressed in IC_{50} value can be deduced (Fig. 3). However, this non perfect correlation means that the hydrophobic-hydrophilic balance is not the only parameter ruling the cytotoxicity of MOF NPs.

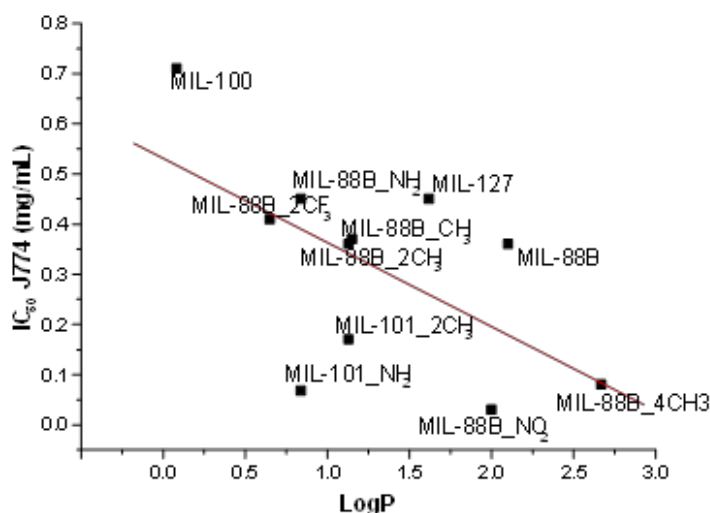


Fig. 3 Representation of the IC_{50} values of MOF NPs in J774 cells vs. the log P values of their constitutive ligands.

The hydrophilic MIL-100(Fe)_NPs showed almost absence of cytotoxicity with IC_{50} values of $0.70 \text{ mg}\cdot\text{mL}^{-1}$ in J774 cells, in agreement with our *in vivo* results. In contrast, MIL-88A and MIL-88B_4CH₃ showed almost 10 times lower IC_{50} values for the same cell line, in agreement with our MIL-88A previous values^{9b}. Furthermore, even though these values correspond to a relatively higher cytotoxicity when compared to other Fe MOF NPs, the absence of a significant *in vivo* toxicity indicates that, the *in vitro* toxicity does not necessarily involve a severe toxicity in a complete organism, possessing specific clearance systems, specialised on the removal of exogenous compounds.

Finally, the cytotoxicity values of polar functionalised MOF-NPs (MIL-101_NH₂ and MIL-88B_NH₂) on HeLa cells were higher than the apolar dimethyl-functionalised MOF-NPs. Interestingly, the IC_{50} values obtained in HeLa cells were dramatically higher ($>1 \text{ mg}\cdot\text{mL}^{-1}$) than those corresponding to J774 cells ($<0.7 \text{ mg}\cdot\text{mL}^{-1}$). These differences could be explained by the intrinsic properties of the two cell lines. First, the unregulated cell growth characteristics of cancer cells⁴³, might lead to a higher resistance to external agents⁴⁴. Secondly, cytotoxicity might also be related to the cell internalisation capacity of the particles, being higher in specialised cells, such as macrophages.

3.3 Cell Penetration Studies

In light of the cytotoxicity findings, MIL-100(Fe) was chosen to deepen cell penetration studies. This MOF was selected due to its green synthesis, low toxicity profile and excellent performances on drug encapsulation and release^{9b}, being therefore a good candidate as a future drug nanocarrier.

In order to investigate its cellular internalisation in J774 macrophages and epithelial HeLa cells, confocal microscopy images of the cells treated with fluorescent MIL-100(Fe)_NPs were taken at different times. As seen on Fig. 4 (page 84), the kinetics of uptake was different for the different studied cell lines, being faster in the case of J774 cells that showed a high fluorescence at early incubation times (30 min), than for HeLa cells, in which fluorescence appeared more progressively. This variability of uptake kinetics for the same particle has also been reported by other authors and was attributed to their different phagocytic activity⁴⁵.

Although there are no comparable results with MOFs in cellular penetration, the cellular uptake of iron oxides such as SPIONs in macrophages has been deeply studied. Hsiao *et al.*, analysed the morphological and physiological changes in murine macrophages when adding Ferucarbotran (Resovist[®]) to cells, demonstrating a particle accumulation in the membrane-bound organelles^{38b}. Also, the PEG coating of SPIONs provides more positively charged surface particles, reducing the cellular uptake. However, due to the antifouling properties of PEG³⁷, PEGylated SPIONs have a lower cellular uptake by macrophages⁴⁶.

In our case, images taken at different incubation times ($t=30$ min, 1 h and 8 h) showed a rapid and easy internalisation of the hybrid NPs inside J774 cells. Interestingly, fluorescence was detected in J774 cells immediately after their contact with the NPs, and remained during the 24 h of the study (not shown). Also, no significant differences in cell internalisation were observed when comparing 30 min and 1 h of incubation with the MOF, as also observed by Lunov *et al.* after 30 min and 6 h of incubation of macrophages with SPIONs^{42a}. Besides, internalised NPs were localised in cytoplasmatic organelles, such as lysosomes, where they remained up to 24 h^{38a}. Further investigations by the same group indicated that lysosomal enzymes might degrade the dextran coating and the exposed redox-active Fe_3O_4 would catalyse the generation of ROS, finalising with cellular damage.

In contrast, after 30 min and 1 h of incubation with the MIL-100(Fe)_NPs, almost no fluorescence was observed in HeLa cells. However, despite HeLa are not specialised in

phagocytosis, an intense fluorescence was observed after 8 h of incubation that lasted at least for 24 h (data not shown).

Moreover, the polarity of furazan was also an important feature since this could modify its cell penetration as a free moiety. Furazan showed a quite hydrophilic polar structure meaning that cell permeation of this fluorophore was reduced in a lipophilic membrane. As observed in Fig. 4, both controls showed no free fluorophore inside, being the fluorophore entrance into the cells only possible through encapsulation within the pores of MIL-100(Fe). Also, although there is a furazan release from MIL-100(Fe)_NPs, the remaining amount after 8 h is still significant enough for a good localisation of the particles and study their cellular uptake, as shown in Fig. 2 (page 78).

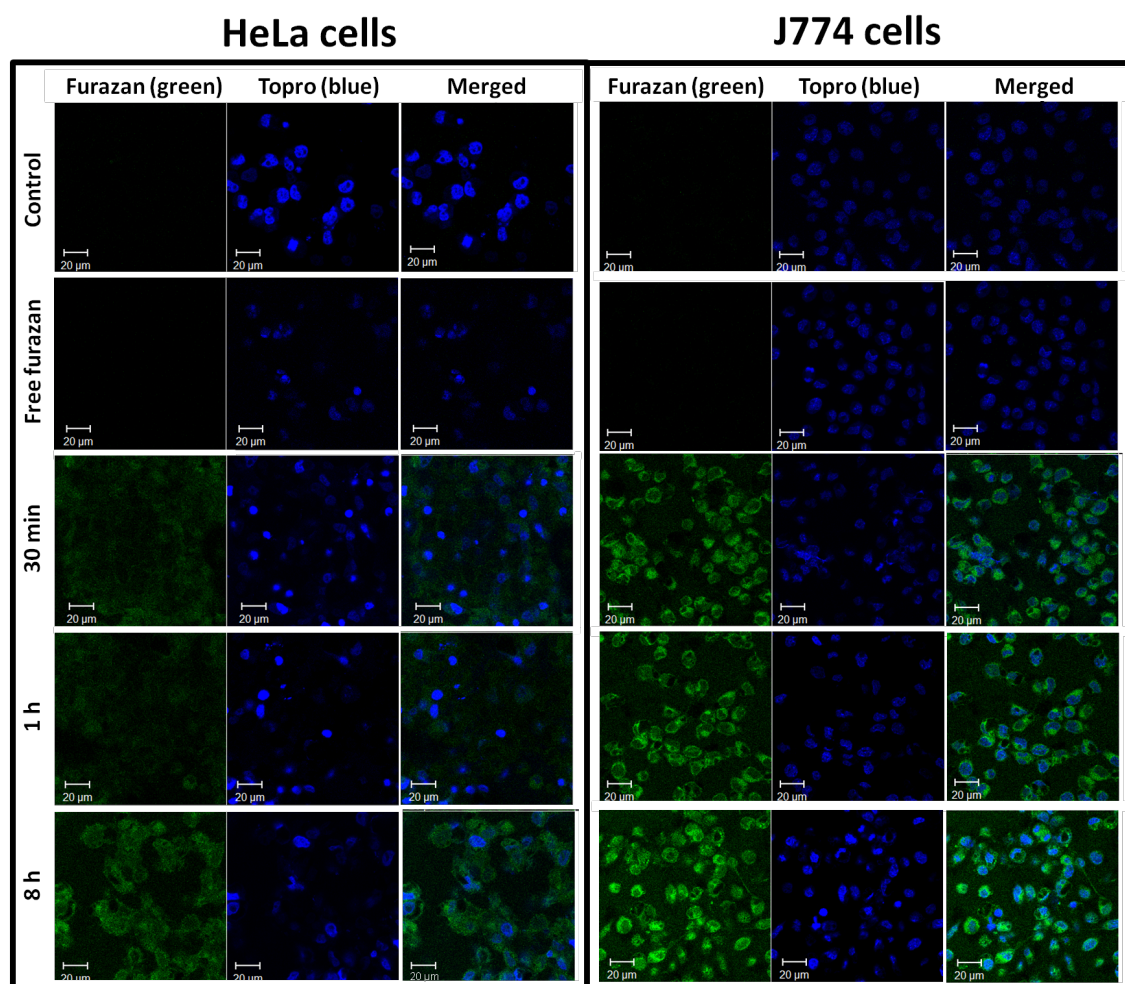


Fig. 4 Confocal microscopy images of HeLa (left) and J774 (right) cells containing furazan-engrafted MIL-100(Fe)_NPs disassembled in furazan (green; left), topro (blue; centre) and merged (right) channels. The images have been taken at different times: 30 min, 1 h and 8 h. Moreover, 2

controls were made: cells and cells together with free furazan. The scale bar corresponds to 20 μm . All the images were taken at 63X.

To further determine whether these NPs were internalised into the cells, confocal microscopy images were taken at different depths of the Z-axis. As can be seen in Fig. 5 (page 86), after 8 h of incubation of the NPs with the cells, the green fluorescence was observed at the different levels, corroborating that NPs were internalised by the cells and not only externally adsorbed at the cell membrane. Finally, it can be suggested that the higher cytotoxicity of the NPs observed in J774 cells compared to HeLa cells is probably related to: (i) their faster internalisation in J774 and therefore, (ii) the larger residence time of the NPs inside these cells and (iii) metabolic pathways that take place in different parts of the cell. It is important to consider that, if exogenous materials remain a longer time inside the cells, the possibility to create cell damage increases. As NPs remain longer in J774 than in HeLa cells, it is expected that the NPs will be more toxic in J774 cells.

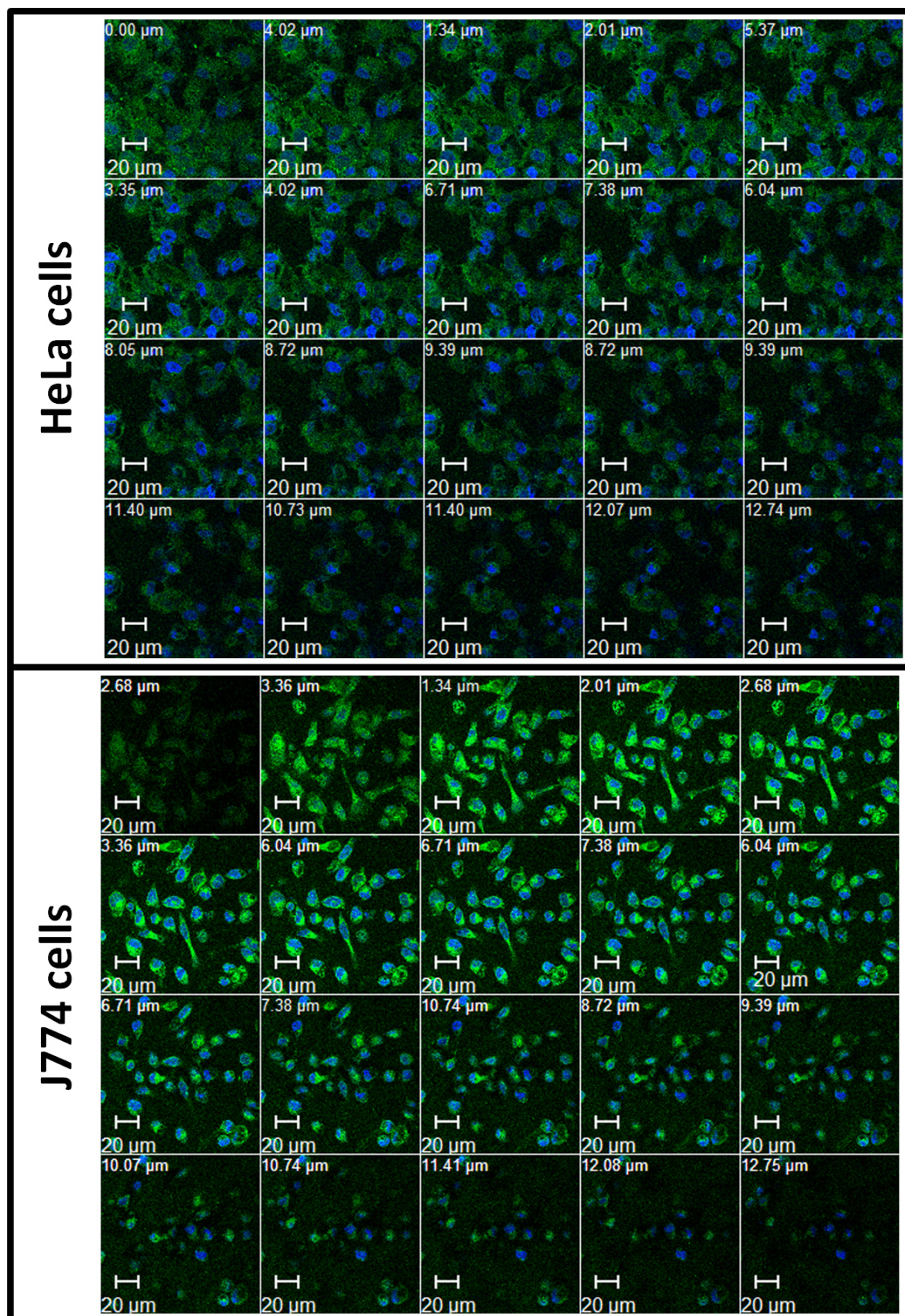


Fig. 5 Confocal images at different depths in the Z-axis of HeLa cells (top) and J774 cells (bottom) after 8 h of incubation with furazan-loaded MIL-100(Fe)_NPs. The scale bars correspond to 20 μm. All the images are taken at 63X.

4. CONCLUSIONS

A series of 14 MOFs were successfully synthesised at the nanoscale and fully characterised, exhibiting a crystalline structure and porosity comparable with their respective bulk materials.

The cytotoxicity of these MOFs NPs was evaluated by the MTT assay using two cell lines (J774 and HeLa), indicating low toxicity values similar to those of other currently commercialised nanometric systems. Indeed, cytotoxicity was observed to strongly depend on the MOF composition such as: (i) the nature of the metal, being the less toxic for the Fe-based MOFs, compared with the Zr- or Zn-MOFs NPs and (ii) the constitutive organic linker, being the hydrophobic/hydrophilic balance an important parameter.

In addition, the higher cytotoxicity observed in J774 cells compared to HeLa cells was mainly attributed to the faster internalisation of NPs in the macrophage line. Moreover, the stable fluorophore grafting within MIL-100(Fe)_NPs allowed to evaluate the cell uptake by confocal fluorescence microscopy, indicating an immediate cell internalisation in J774 mouse macrophages, faster than in epithelial HeLa cell line, in agreement with their different phagocytic activity.

ACKNOWLEDGEMENTS

The authors thank E. Garbayo for her technical assistance during confocal microscopy studies and V. Agostoni, R. Gref and P. Couvreur for the *in vitro* training. C. Tamames-Tabar would like to acknowledge the Asociación de Amigos de la Universidad de Navarra for the fellowship grant. This work was partially supported by FEUN (Fundación Empresa Universidad de Navarra) and the CNRS funding, the EU funding through the ERC-2007-209241-BioMOFs ERC (C.S., P.H., D.C.) and the French ANR project VIRMIL (ANR-2010-RMNP-004-01; P.H., C.S.).

NOTES AND REFERENCES

^aInstitut Lavoisier, UMR CNRS 8180, Université de Versailles Saint-Quentin-en-Yvelines, 45 Avenue des Etats-Unis, 78035 Versailles Cedex, France.

Fax: 33 (0) 139256652; Tel: 33 (0) 1 39254371; E-mail: horcajada@chimie.uvsq.fr

^bDepartamento de Farmacia y Tecnología Farmacéutica, Facultad de Farmacia, Universidad de Navarra, Irunlarrea 1, 31008 Pamplona, Spain.

Fax: 34 948425649; Tel: 34 948425600 Ext. 806519; E-mail: mjblanco@unav.es

† CTT, DC and EI contribute equally to this work.

* MJBP and PH are equal senior authors.

‡ Electronic Supplementary Information (ESI) available: [The supplementary information contains the synthesis of the non-commercialised linkers, the MOF syntheses and the MOF characterisation. See DOI: 10.1039/c3tb20832j].

REFERENCES

- ¹See Special Issues: (a) Guest Editors J.R. Long and O.M. Yaghi. *Chem. Soc. Rev.*, 2009, 38, 1201; (b) Guest Editors H.-C. Zhou, J.R. Long and O.M. Yaghi. *Chem. Rev.*, 2012, 112, 673.
- ²See Special Issue: Guest Editor C.A. Reed. *Acc. Chem. Res.*, 2005, 38, 215.
- ³P. Horcajada, R. Gref, T. Baati, P. K. Allan, G. Maurin, P. Couvreur, G. Férey, R. E. Morris and C. Serre, *Chem. Rev.*, 2012, 112, 1232.
- ⁴W. J. Rieter, K. M. L. Taylor, H. An, W. Lin and W. Lin, *J. Am. Chem. Soc.*, 2006, 128, 9024.
- ⁵P. Horcajada, C. Serre, M. Vallet-Regí, M. Sebban, F. Taulelle and G. Férey, *Angew. Chem. Int. Ed.*, 2006, 45, 5974.
- ⁶C. Gaudin, D. Cunha, E. Ivanoff, P. Horcajada, G. Chevé, A. Yasri, O. Loget, C. Serre and G. Maurin, *Micropor. Mesopor. Mater.*, 2012, 157, 124.
- ⁷B. Xiao, P. S. Wheatley, X. Zhao, A. J. Fletcher, S. Fox, A. G. Rossi, I. L. Megson, S. Bordiga, L. Regli, K. M. Thomas and R. E. Morris, *J. Am. Chem. Soc.*, 2007, 129, 1203.
- ⁸A. Carne, C. Carbonell, I. Imaz and D. MasPOCH, *Chem. Soc. Rev.*, 2011, 40, 291.
- ⁹(a) J. Gómez-Herrero and F. Zamora, *Adv. Mater.*, 2011, 23, 5311; (b) P. Horcajada, T. Chalati, C. Serre, B. Gillet, C. Sebrie, T. Baati, J. F. Eubank, D. Heurtaux, P. Clayette, C. Kreuz, J.-S. Chang, Y. K. Hwang, V. Marsaud, P.-N. Bories, L. Cynober, S. Gil, G. Férey, P. Couvreur and R. Gref, *Nat. Mater.*, 2010, 9, 172; (c) A. Demessence, P. Horcajada, C. Serre, C. Boissiere, D. Grosso, C. Sanchez and G. Férey, *Chem. Commun.*, 2009, 7149.
- ¹⁰K. M. L. Taylor-Pashow, J. D. Rocca, Z. Xie, S. Tran and W. Lin, *J. Am. Chem. Soc.*, 2009, 131, 14261.
- ¹¹Regulation (EC) No 1907/2006; OJ L 396 of 30. 12. 2006.
- ¹²T. Chalati, P. Horcajada, P. Couvreur, C. Serre, M. Ben Yahia, G. Maurin and R. Gref, *Nanomedicine*, 2011, 6, 1683.
- ¹³(a) W. J. Rieter, K. M. Pott, K. M. L. Taylor and W. Lin, *J. Am. Chem. Soc.*, 2008, 130, 11584; (b) R. C. Huxford, K. E. deKrafft, W. S. Boyle, D. Liu and W. Lin, *Chem. Sci.*, 2012, 3, 198.
- ¹⁴T. Baati, L. Njim, F. Neffati, A. Kerkeni, M. Bouttemi, R. Gref, M. F. Najjar, A. Zakhama, P. Couvreur, C. Serre and P. Horcajada, *Chem. Sci.*, 2013, 4, 1597.
- ¹⁵(a) P. Horcajada, S. Surble, C. Serre, D.-Y. Hong, Y.-K. Seo, J.-S. Chang, J.-M. Grenèche, I. Margiolaki and G. Férey, *Chem. Commun.*, 2007, 2820; (b) G. Férey, C. Mellot-Draznieks, C. Serre, F. Millange, J. Dutour, S. Surblé and I. Margiolaki, *Science*, 2005, 309, 2040.

- ¹⁶(a) Y. Liu, J. F. Eubank, A. J. Cairns, J. Eckert, V. C. Kravtsov, R. Luebke and M. Eddaoudi, *Angew. Chem. Int. Edit.*, 2007, 46, 3278; (b) A. Dhakshinamoorthy, M. Alvaro, H. Chevreau, P. Horcajada, T. Devic, C. Serre and H. Garcia, *Catal. Sci. Technol.*, 2012, 2, 324.
- ¹⁷J. H. Cavka, S. Jakobsen, U. Olsbye, N. Guillou, C. Lamberti, S. Bordiga and K. P. Lillerud, *J. Am. Chem. Soc.*, 2008, 130, 13850.
- ¹⁸(a) C. Serre, C. Mellot-Draznieks, S. Surblé, N. Audebrand, Y. Filinchuk and G. Férey, *Science*, 2007, 315, 1828; (b) T. Chalati, P. Horcajada, R. Gref, P. Couvreur and C. Serre, *J. Mater. Chem.*, 2011, 21, 2220; (c) P. Horcajada, F. Salles, S. Wuttke, T. Devic, D. Heurtaux, G. Maurin, A. Vimont, M. Daturi, O. David, E. Magnier, N. Stock, Y. Filinchuk, D. Popov, C. Riekkel, G. Férey and C. Serre, *J. Am. Chem. Soc.*, 2011, 133, 17839.
- ¹⁹A. Demessence, C. Boissiere, D. Grosso, P. Horcajada, C. Serre, G. Férey, G. J. A. A. Soler-Illia and C. Sanchez, *J. Mater. Chem.*, 2010, 20, 7676.
- ²⁰T. Mosmann, *J. Immunol. Methods*, 1983, 65, 55.
- ²¹(a) Horcajada, C. Serre, R. Gref, G. Férey, P. Couvreur, PCT applications PCT/FR2008/001366, 01 october 2008; (b) P. Horcajada, C. Serre, R. Gref, G. Férey, P. Couvreur, PCT applications PCT/FR2008/001367, 01 october 2008.
- ²²D. Cunha, C. Gaudin, I. Colinet, P. Horcajada, G. Maurin and C. Serre, *J. Mater. Chem. B*, 2013, 1, 1101.
- ²³P. Horcajada, Private Communication.
- ²⁴K. Sumida, Y. Igarashi, N. Toritsuka, T. Matsushita, K. Abe-Tomizawa, M. Aoki, T. Urushidani, H. Yamada, Y. Ohno, *Hum. Exp. Toxicol.*, 2011, 30(10), 1701.
- ²⁵J. C. Rutherford and A. J. Bird, *Eukaryotic Cell*, 2004, 3, 1.
- ²⁶L. L. Brunton, D. K. Blumenthal, I. L. O. Buxton and K. Parker, *Goodman & Gilman's Manual of Pharmacology and Therapeutics*, United States of America: McGraw-Hill Professional, 2008.
- ²⁷J. Borovanský and P. A. Riley, *Chem. Biol. Interact.*, 1989, 69, 279.
- ²⁸R. Wahab, N. Kaushik, A. Verma, A. Mishra, I.H. Hwang, Y.-B. Yang, H.-S. Shin and Y.-S. Kim, *J. Biol. Inorg. Chem.*, 2011, 16, 431.
- ²⁹H.L. Karlsson, P. Cronholm, J. Gustafsson and L- Möller, *Chem. Res. Toxicol.*, 2008, 21, 1726.
- ³⁰T. J. Brunner, P. Wick, P. Manser, P. Spohn, R. N. Grass, L. K. Limbach, A. Bruinink and W. J. Stark, *Environ. Sci. Technol.*, 2006, 40, 4374.
- ³¹M. Mahmoudi, A. Simchi and M. Imani, *J. Phys. Chem. C*, 2009, 113, 9573.
- ³²(a) M. T. Nuñez, M. A. Garate, M. Arredondo, V. Tapia and P. Muñoz, *Biol. Res.*, 2000, 33, 133; (b) M. C. R. Symons and J. M. C. Gutteridge, *Free Radicals and Iron: Chemistry, Biology and Medicine*, Oxford University Press, Oxford, 1998.
- ³³V. Mallikarjun, D. J. Clarke and C. J. Campbell, *Free Radical Bio. Med.*, 2012, 53, 280.
- ³⁴(a) S. J. H. Soenen and M. De Cuyper, *Contrast Media Mol. Imaging*, 2009, 4, 207; (b) M. W. Hentze, M. U. Muckenthaler and N. C. Andrews, *Cell*, 2004, 117, 285; (c) Y. C. Taylor and A. M. Rauth, *Cancer Res.*, 1978, 38, 2745.
- ³⁵B. F. Trump, J. M. Valigorsky, A. U. Arstila, W. J. Menger, T. D. Kinney, *Am. J. Pathol.*, 1973, 72, 295.

- ³⁶M. Mahmoudi, S. Laurent, M. A. Shokrgozar and M. Hosseinkhani, *ACS Nano*, 2011, 5, 7263.
- ³⁷I. M. Nnebe, R. D. Tilton and J. W. Schneider, *J. Colloid Interface Sci.*, 2004, 276, 306.
- ³⁸(a) O. Lunov, T. Syrovets, B. Büchele, X. Jiang, C. Röcker, K. Tron, G. U. Nienhaus, P. Walther, V. Mailänder, K. Landfester and T. Simmet, *Biomaterials*, 2010, 31, 5063; (b) J.-K. Hsiao, H.-H. Chu, Y.-H. Wang, C.-W. Lai, P.-T. Chou, S.-T. Hsieh, J.-L. Wang and H.-M. Liu, *NMR Biomed.*, 2008, 21, 820.
- ³⁹H. Vu-Quang, M.-K. Yoo, H.-J. Jeong, H.-J. Lee, M. Muthiah, J. H. Rhee, J.-H. Lee, C.-S. Cho, Y. Y. Jeong and I.-K. Park, *Acta Biomater.*, 2011, 7, 3935.
- ⁴⁰M. Li, H. S. Kim, L. Tian, M. K. Yu, S. Jon and W. K. Moon, *Theranostics* 2012, 2, 76.
- ⁴¹I. Kostova and G. Momekov, *Eur. J. Med. Chem.*, 2006, 41, 717.
- ⁴²C. E. Soma, C. Dubernet, G. Barratt, S. Benita and P. Couvreur, *J Control. Release*, 2000, 68, 283.
- ⁴³A. S. Arbab, L. A. Bashaw, B. R. Miller, E. K. Jordan, B. K. Lewis, H. Kalish and J. A. Frank, *Radiology*, 2003, 229, 838.
- ⁴⁴G. Cairo, L. Bardella, L. Schiaffonati, P. Arosio, S. Levi and A. Bernelli-Zazzera, *Biochem Bioph Res Co*, 1985, 133, 314.
- ⁴⁵S. Recalcati, D. Taramelli, D. Conte and G. Cairo, *Blood*, 1998, 91, 1059.
- ⁴⁶(a) C. Hoskins, A. Cuschieri and L. Wang, *J Nanobiotechnol.*, 2012, 10, 15; (b) U. I. Tromsdorf, N. C. Bigall, M. G. Kaul, O. T. Bruns, M. S. Nikolic, B. Mollwitz, R. A. Sperling, R. Reimer, H. Hohenberg, W. J. Parak, S. Förster, U. Beisiegel, G. Adam and H. Weller, *Nano Letters*, 2007, 7, 2422.

SUPPLEMENTARY INFORMATION
CYTOTOXICITY OF NANOSCALED METAL-ORGANIC
FRAMEWORKS

SUPPLEMENTARY INFORMATION

CYTOTOXICITY OF NANOSCALED METAL-ORGANIC FRAMEWORKS

Cristina Tamames-Tabar, ^{†a,b} Denise Cunha, ^{†a} Edurne Imbuluzqueta, ^{†b} Florence Ragon,^a
Christian Serre,^a María J. Blanco-Prieto^{*b} and Patricia Horcajada^{*a}

^a*Institut Lavoisier, UMR CNRS 8180, Université de Versailles Saint-Quentin-en-Yvelines, 45
Avenue des Etats-Unis, 78035 Versailles Cedex, France.*

^b*Departamento de Farmacia y Tecnología Farmacéutica, Facultad de Farmacia, Universidad de
Navarra, Irunlarrea 1, 31008 Pamplona, Spain.*

[†] CTT, DC and EI contribute equally to this work.

Journal of Materials Chemistry B, 2014, 2, 262-271.

1. REACTANTS

The organic linkers 1,3,5-benzenetricarboxylic acid (BTC), fumaric acid (FUM), 2-nitroterephthalic acid (BDC_NO₂), 2-aminoterephthalic acid (BDC_NH₂) were purchased at Sigma-Aldrich (France). The metallic precursors iron (III) chloride hexahydrate (FeCl₃·6H₂O), iron (III) perchlorate hydrate (Fe(ClO₄)₃·6H₂O) and zinc nitrate hexahydrate (Zn(NO₃)₂·6H₂O) were acquired at Sigma-Aldrich (France) whereas zirconium oxychloride (ZrOCl₂·8H₂O) was acquired at Alfa Aesar (France). The solvents for organic syntheses hydrogen chloride (HCl), absolute ethanol (EtOH abs), ethanol 96.2 (EtOH 96.2), sulphuric acid (H₂SO₄), chloroform (CHCl₃), dichloromethane (DCM) and *N,N*-dimethylformamide (DMF) were purchased at Carlo Erba (Italy), and sodium hydroxide (NaOH) was obtained at Alfa Aesar (France). Furazan ((*R*)-(-)-4-(3-aminopyrrolidino)-7-nitrobenzofuran) and the MTT reactant (3-(4,5-dimethylthiazol-2-yl)-2,5-diphenyltetrazolium bromide) were acquired at Sigma-Aldrich (France). Cell culture reagents were acquired at Gibco[®] (France). *N*-octanol was purchased at Merck (Germany). For confocal studies, TOPRO-3 (Invitrogen[™]) was acquired at Life Technologies (France).

5-nitroisophthalic acid (BDC_NO₂): Sigma Aldrich; sodium hydroxide (NaOH): Alfa Aesar; aluminium: Sigma Aldrich; glucose: Sigma Aldrich; hydrogen chloride (HCl): Carlo

Erba; H₂SO₄ 95%: Carlo Erba; sodium nitrite (NaNO₂) and toluene: Acros; chloroform (CHCl₃): Carlo Erba; *N,N*-dimethylformamide (DMF): Carlo Erba; ethanol (EtOH): VWR; methanol (MeOH): Carlo Erba; Acetone: Carlo Erba; iron (III) perchlorate hexahydrate (Fe(ClO₄)₃·6H₂O): Sigma Aldrich; iron (III) chloride hexahydrate (FeCl₃·6H₂O): Alfa Aesar; zirconyl (IV) chloride (ZrOCl₂): Alfa Aesar; zinc nitrate hexahydrate (Zn(NO₃)₂·6H₂O): Sigma Aldrich; fumaric acid: Sigma Aldrich; 1,4-terephthalic acid (BDC): Sigma Aldrich; 1,3,5-benzenetricarboxylic acid (BTC): BASF; 2-methyl-terephthalonitrile: Sigma Aldrich; 1,2,4,5-tetramethylbenzene: Sigma Aldrich; 2-amino-terephthalic acid (BDC-NH₂): Alfa Aesar; 2-nitroterephthalic acid (BDC-NO₂): Alfa Aesar; 2-methylimidazole: Alfa Aesar.

2. SYNTHESIS OF THE ORGANIC LINKERS

The non-commercialised organic linkers 3,3',5,5'-azobenzene tetracarboxylic acid (Tazb; S2.1 SI¹), dimethylterephthalic acid (BDC_2CH₃; S 2.4²), 2,3,5,6-tetramethylterephthalic acid (BDC_4CH₃; S 2.10^{3, 4}) and 2,5-diperfluoroterephthalic acid (BDC_2CF₃; S 2.11⁵) were synthesised following the published methods.

3. MATERIAL SYNTHESIS

3.1. MIL-127_nano or (Fe₃O(OH)(H₂O)₃[(C₁₆N₂O₈H₆)₃ n·H₂O)

537 mg of 3,3',5,5'-azobenzene tetracarboxylic acid¹ and 15 mL of DMF were added into a 50 mL round bottom flask and set into reflux in order to dissolve all the components. 810 mg of FeCl₃·6H₂O were added to the prior mixture. After 1 h of reflux, the nanoparticles (NPs) were collected by centrifugation (10,500 rpm/15 min) and then washed with EtOH 96.2% in order to eliminate remaining DMF. The activation was performed by suspending the NPs in DMF at 50 °C during 1 h, continued by four washes with EtOH.

3.2. MIL-100_nano or (Fe₃O(OH)(H₂O)₂[(CO₂)₃C₆H₃]₂ n·H₂O)

The synthesis of MIL-100_NPs has been performed according to the published procedure⁶. 845 mg of 1,3,5-BTC (BTC) together with 2,425 mg of FeCl₃·6H₂O and 20 mL of distilled water were added into a Teflon lined autoclave. After 10 min of gentle magnetic stirring, the mixture was sealed and heated at 130 °C for 4 min in a microwave oven (at 400 W; Mars-5, CEM) with a heating temperature of 2 min. The NPs were recovered by

centrifugation (10,500 rpm/15 min). The activation was performed by suspending the NPs in 20 mL of EtOH 96.2%, repeating this washing procedure 7 times till disappearance of the free acid.

3.3. MIL-100_ **micro** or $(\text{Fe}_3\text{O}(\text{H}_2\text{O})_2\text{OH}[\text{C}_6\text{H}_3(\text{CO}_2)_3]_2 n \cdot \text{H}_2\text{O})$

The synthesis of micrometric MIL-100 has been performed according to the published procedure⁷. 210 mg of 1,3,5-BTC together with 270 mg of $\text{FeCl}_3 \cdot 6\text{H}_2\text{O}$ and 5 mL of distilled water held at 130 °C in a Teflon-lined autoclave for 3 days. The light-orange solid product was recovered by filtration and washed with deionised water. A treatment in hot deionised water (80 °C) for 3 h was applied to decrease the amount of residual trimesic acid (typically, 1 g of MIL-100(Fe) in 350 mL of water).

3.4. MIL-101_ **2CH₃_ nano** or $(\text{Fe}_3\text{O}(\text{OH})(\text{H}_2\text{O})_2[(\text{CO}_2)_2\text{C}_6\text{H}_2(\text{CH}_3)_2]_3 n \cdot \text{H}_2\text{O})$

194 mg of 2,5-dimethylterephthalic acid² together with 354 mg of $\text{Fe}(\text{ClO}_4)_3 \cdot 6\text{H}_2\text{O}$ and 5 mL of DMF were added into a Parr bomb and heated at 100 °C for 15 h. The orange NPs were recovered by centrifugation (10,500 rpm/15 min). The activation was performed suspending the NPs 5 times in 20 mL of EtOH 96.2% for 10 min.

3.5. MIL-101_ **NH₂_ nano** or $(\text{Fe}_3\text{O}(\text{OH})(\text{H}_2\text{O})_2[(\text{CO}_2)_2\text{C}_6\text{H}_3\text{NH}_2]_3 n \cdot \text{H}_2\text{O})$

The synthesis of MIL-101_ **NH₂** NPs has been performed according to the published procedure⁸. 90.5 mg of 2-aminoterephthalic acid (BDC_ **NH₂**) together with 135 mg of $\text{FeCl}_3 \cdot 6\text{H}_2\text{O}$, 25 mL of EtOH 96.2% and 0.25 mL of HCl 1 M were placed into a Teflon-liner and heating till reaching a temperature of 60 °C during 40 min and maintaining the temperature plateau for 5 min under microwave irradiation at 400 W. The obtained brown precipitated was recovered by centrifugation at 10,500 rpm for 10 min. The activation was performed by suspending the NPs in 20 mL of EtOH 96.2%, repeating this process 4 times.

3.6. MIL-88A_ **nano** or $(\text{Fe}_3\text{O}(\text{OH})(\text{H}_2\text{O})_2[(\text{CO}_2)_2\text{C}_2\text{H}_2]_3 n \cdot \text{H}_2\text{O})$

290 mg of fumaric acid (FUM) together with 675 mg of $\text{FeCl}_3 \cdot 6\text{H}_2\text{O}$ and 25 mL of distilled water were added to a Teflon tube. After 10 minutes of gentle magnetic stirring, the Teflon tube was inserted inside the microwave and heated at 80 °C for 10 min (600 W), as

previously reported⁹. Then, the obtained precipitated was recovered by centrifugation at 10,500 rpm for 10 min. The activation was performed in EtOH 96.2 by adding 20 mL of the solvent during 4 times.

3.7. MIL-88B_nano or $(\text{Fe}_3\text{O}(\text{OH})(\text{H}_2\text{O})_2[(\text{CO}_2)_2\text{C}_6\text{H}_4]_3 n \cdot \text{H}_2\text{O})$

The synthesis of MIL-101_NH₂_NPs has been performed according to the published procedure^{10, 11}. 332 mg of terephthalic acid (BDC) together with 344 mg of iron(III) acetate and 10 mL of MeOH were added into a Parr bomb, heated in an oven at 100 °C for 2 h and then, a fast cool down. Then, the orange solid was recovered by filtration. The activation was made by washing the NPs with 20 mL of EtOH 96.2% for 10 min, repeating this protocol 3 times.

3.8. MIL-88B_CH₃_nano or $(\text{Fe}_3\text{O}(\text{OH})(\text{H}_2\text{O})_2[(\text{CO}_2)_2\text{C}_6\text{H}_3(\text{CH}_3)]_3 n \cdot \text{H}_2\text{O})$

The synthesis of MIL-88B_CH₃_nano has been performed according to the published procedure⁴. 180 mg of 2-methylterephthalic acid¹² together with 354 mg of $\text{Fe}(\text{ClO}_4)_3 \cdot 6\text{H}_2\text{O}$ and 5 mL of MeOH were placed in a Teflon-lined autoclave (23 mL) for 3 days at 100 °C. Then, the brown solid was recovered by centrifugation (10,500 rpm/15 min). The activation was performed by suspending the in 20 mL of EtOH twice (16 h).

3.9. MIL-88B_2CH₃_nano or $(\text{Fe}_3\text{O}(\text{OH})(\text{H}_2\text{O})_2[(\text{CO}_2)_2\text{C}_6\text{H}_2(\text{CH}_3)_2]_3 n \cdot \text{H}_2\text{O})$

The synthesis of MIL-88B_2CH₃_nano has been performed according to the published procedure⁴. 194 mg of 2,5-dimethylterephthalic acid² together with 354 mg of $\text{Fe}(\text{ClO}_4)_3 \cdot 6\text{H}_2\text{O}$ and 5 mL of MeOH were placed in a Teflon-lined autoclave (23 mL) for 3 days at 100 °C. Then, the brown solid was recovered by centrifugation (10,000 rpm/15 min). The activation of this material has 2 steps: a first wash with 5 mL of DMF twice (1 h) and then washed with 20 mL of absolute EtOH.

3.10. MIL-88B_4CH₃_nano or $(\text{Fe}_3\text{O}(\text{OH})(\text{H}_2\text{O})_2[(\text{CO}_2)_2\text{C}_6(\text{CH}_3)_4]_3 n \cdot \text{H}_2\text{O})$

MIL-88B_4CH₃_nano was prepared as previously reported⁸. 116 mg of 2,3,5,6-tetramethylterephthalic acid³ together with 270 mg of $\text{FeCl}_3 \cdot 6\text{H}_2\text{O}$ and 10 mL of DMF with 0.4 mL of NaOH 2M were added into a Parr bomb. The mixture was placed in a in a Teflon-lined autoclave (23 mL) at 100 °C for 2 h. After cooling the Paar bomb under

water, the solid was recovered by centrifugation at 10,500 rpm for 10 min. The activation of this material was made by washing with 3 times with 20 mL of EtOH for 10 min.

3.11. MIL-88B_2CF₃_nano or (Fe₃O(OH)(H₂O)₂[(CO₂)₂C₆H₂(CF₃)₂]₃ n·H₂O)

The synthesis of MIL-88B_2CF₃ has been performed according to the published procedure⁴. 775 mg of 2,5-trifluoromethylterephthalic acid⁵ together with 675 mg of FeCl₃·6H₂O and 25 mL of absolute EtOH were added into a Teflon tube and then heated at 100 °C for 30 min and maintaining the temperature plateau at 100 °C during 5 min using a microwave oven (400 W). The sample was recovered by centrifugation at 10,500 rpm for 10 min and activated in cold acetone (1 g MIL-88B_2CF₃ in 25 mL of cold acetone) under stirring during 4 h.

3.12. MIL-88B_NH₂_nano or (Fe₃O(OH)(H₂O)₂[(CO₂)₂C₆H₃(NH₂)]₃ n·H₂O)

534 mg of BDC_NH₂ together with 405 mg of FeCl₃·6H₂O and 25 mL of EtOH were added into a Teflon tube and then inserted inside the microwave and heated at 100 °C for 40 min and maintaining at the temperature plateau of 100 °C during 5 min (800 W). The sample was recovered by centrifugation at 10,500 rpm for 10 min and activated in 3 steps: 20 mL of DMF, then 20 mL of MeOH twice and finally 20 mL of EtOH 96.2%.

3.13. MIL-88B_NO₂_nano or (Fe₃O(OH)(H₂O)₂[(CO₂)₂C₆H₃(NO₂)]₃ n·H₂O)

1,055 mg of 2-nitroterephthalic acid (BDC_NO₂) together with 1,350 mg of FeCl₃·6H₂O and 25 mL of distilled water were added into a Teflon tube then inserted inside the microwave and heated at 100 °C for 90 min maintaining then the sample at a temperature plateau of 100 °C during 5 min (400 W). The sample was recovered by centrifugation at 10,500 rpm for 10 min and the activation was performed by suspending the solid in 20 mL of EtOH 96.2% heating at 100 °C for 30 min and maintaining at 100 °C temperature plateau during 5 min in the microwave (400 W). This protocol was repeated twice.

3.14. UiO-66_nano or (Zr₆O₄(OH)₄(H₂O)₂[(CO₂)₂C₆H₄]₆ n·H₂O)

A solution of 0.83 g of 1,4-BDC, 1.6 g of ZrOCl₂·8H₂O, 25 mL of DMF and 0.8 mL of HCl 37% were placed into a Teflon-liner steel autoclave at 150 °C during 2 h in a 100 mL round bottom flask under continuous magnetic stirring. The activation of UiO-66 had three

steps, a first with 5 mL of DMF, a second with 20 mL of MeOH, both overnight and under continuous magnetic stirring and finally a last step washing with 20 mL of EtOH 96.2%. After each step, the particles were centrifuged at 10,500 rpm during 20 min.

3.15. ZIF-8_nano or $[\text{Zn}(\text{C}_4\text{H}_6\text{N}_2)_2 n \cdot \text{H}_2\text{O}]$

ZIF-8 nanoparticles were synthesised according to the published procedure¹³. A solution of zinc nitrate hexahydrate 2,933 g of $\text{Zn}(\text{NO}_3)_2 \cdot 6\text{H}_2\text{O}$ in 200 mL of MeOH was rapidly poured into a solution of 6,489 g 2-methylimidazole in 200 mL of MeOH under vigorous stirring at room temperature. The mixture slowly turns turbid and after 1 h the nanocrystals were separated from the milky dispersion by centrifugation at 10,500 rpm for 15 min. The activation was performed readily redispersing the material in absolute EtOH and recovering by centrifugation. Three washing cycles of the redispersion in absolute EtOH/centrifugation were carried out to activate the material.

4. MATERIAL CHARACTERISATION

4.1. X-Ray Powder Diffraction (XRPD)

XRPD patterns were collected in a SIEMENS D5000 diffractometer (Siemens, Germany) (θ - 2θ) using Cu $K\alpha_1$ radiation ($\lambda=1.54056$ angstroms) from 5 to 13 ° (2θ) using a step size of 0.04 ° and 4 s per step in continuous mode (Fig. S1).

Note that XRPD patterns of some of the nanometric flexible structures differ from their micrometric analogues due to the different pore opening (pore content) as a consequence of their flexible structure⁴.

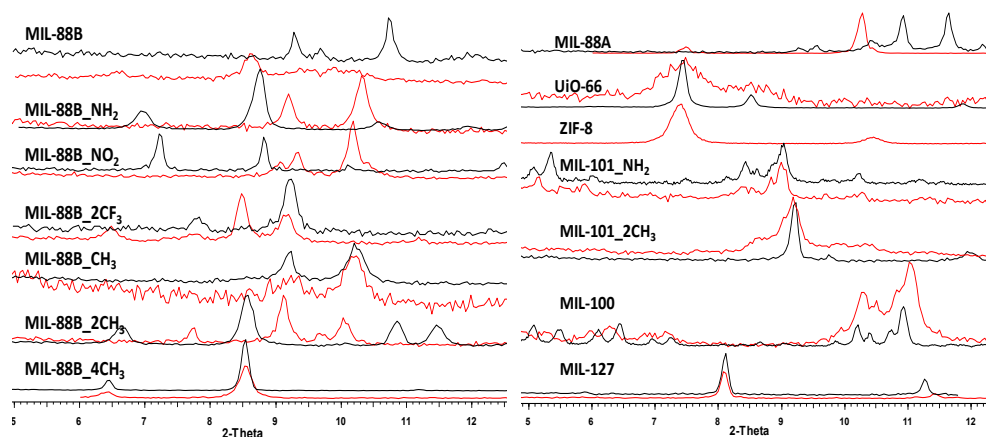


Fig. S1 XRPD patterns of the MOF micro (black) and nanoparticles (red) after their activation.

4.2. Infrared Spectroscopy (FTIR)

A small amount of solids was analysed by a Thermo Nicolet spectrometer (Thermo, USA). The spectra were recorded from 4,000-400 cm^{-1} at room temperature (Fig. S2).

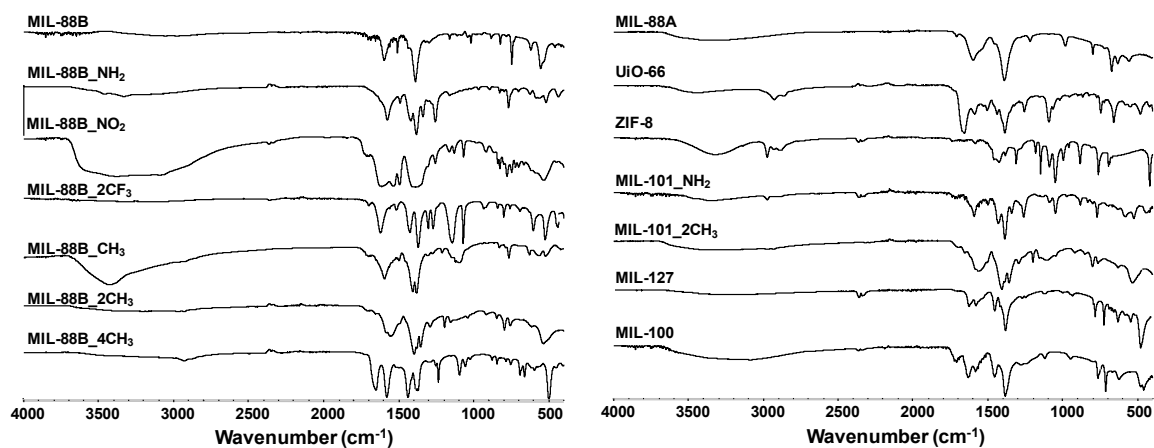


Fig. S2 Infrared spectroscopy spectra of the materials after their activation.

4.3. Thermogravimetric Analysis (TGA)

Approximately 5-10 mg of each sample was used for TGA measurements. Samples were analysed under an oxygen flow ($20 \text{ mL}\cdot\text{min}^{-1}$) using a Perkin Elmer Diamond TGA/DTA STA 6000 running from room temperature to $600 \text{ }^\circ\text{C}$ with a scan rate of $2 \text{ }^\circ\text{C}\cdot\text{min}^{-1}$ (Tab. S1).

Tab. S1 Theoretical and experimental (estimated by TGA) composition of the MOF NPs.

MOF Sample	%M _x O _x	
	Theoretical (anhydrous form)	Experimental (anhydrous form)
MIL-127_nano	32.8	29.8
MIL-100_nano	39.0	40.8
MIL-101_2CH ₃ _nano	31.1	26.3
MIL-101_NH ₂ _nano	32.5	32.2
MIL-88A_nano	44.2	49.0
MIL-88B_nano	34.6	39.0
MIL-88B_CH ₃ _nano	32.6	30.9

MIL-88B_2CH ₃ _nano	31.1	25.3
MIL-88B_4CH ₃ _nano	27.9	26.6
MIL-88B_2CF ₃ _nano	21.9	20.5
MIL-88B_NH ₂ _nano	32.5	38.0
MIL-88B_NO ₂ _nano	26.1	22.0
UiO-66_nano	44.4	46.5
ZIF-8_nano	35.8	36.0

*M_xO_y corresponding to Fe₂O₃, ZnO and ZrO₂ according to the XRPD.

4.4. Nitrogen Sorption Porosimetry

N₂ isotherms were obtained at 77 K using a Belsorp Mini (Bel, Japan). Prior to the analysis, approximately 40-60 mg of activated rigid samples were evacuated for 12-24 h at 200 °C under vacuum (Tab. S2).

Tab. S2 BET surface area and pore volume of rigid materials.

MOF sample	S _{BET} (m ² .g ⁻¹)	V _p (cm ³ .g ⁻¹)
MIL-127_nano	650	0.41
MIL-100_nano	1900	0.98
MIL-101_2CH ₃ _nano	1780	1.22
MIL-101_NH ₂ _nano	1840	0.85
UiO-66_nano	1010	0.40
ZIF-8_nano	1700	0.66

4.5. pH Variations

Despite the buffering capacity of the cell culture media, the polycarboxylate anions present on the external surface together with the release of the linker upon degradation are expected to induce changes in the pH media and therefore, possibly affect the cell-specific metabolic toxic effects. Thus, the pH of the media was followed during the MTT assay. Except for the BDC linker that exhibited a pH variation up to 1 unit (pH=6), the rest of the linkers led to a lower change in pH (~7). Despite the pH variation, the cytotoxicity of BDC was not severe (IC₅₀=0.43 mg·mL⁻¹) when compared to other linkers (IC₅₀ (BDC_NH₂)=0.02; (BTC)>1.00 mg·mL⁻¹; see Tab. 1, page 76). Additionally, both cell lines can grow at those pH values, in agreement with the lack of influence of the pH, within the

considered range, over the toxicity of MOF NPs¹⁴. Finally, no significant cytotoxicity differences have been observed whatever the linker, suggesting that the pH is not a main factor of the cytotoxicity for the HeLa and J774 cells.

4.6. Zeta Potential

Zeta potential measurements were made to all the MOFs used in this study in DMEM cell culture medium + 10% FBS using a Zetasizer Nano-ZS® analyser (Malvern Instruments, UK).

Tab. S3 Results from the zeta potential measurements done in PBS and in DMEM cell culture medium + 10% FBS.

Zeta potential (mV)	PBS	DMEM
MIL-100_nano	-18.3 ± 0.6	-8.1 ± 0.2
MIL-127_nano	-38.5 ± 2.0	-8.9 ± 0.2
MIL-101_2CH ₃ _nano	-24.2 ± 2.1	-14.7 ± 0.7
MIL-101-NH ₂ _nano	-27.4 ± 1.5	-8.1 ± 0.4
MIL-88A_nano	-25.0 ± 4.3	-10.7 ± 0.7
MIL-88B_nano	-23.5 ± 1.8	-9.8 ± 0.4
MIL-88B_CH ₃ _nano	-22.8 ± 2.2	-9.5 ± 0.2
MIL-88B_2CH ₃ _nano	-26.0 ± 0.4	-10.2 ± 0.4
MIL-88B_4CH ₃ _nano	-41.3 ± 0.6	-11.0 ± 0.5
MIL-88B_2CF ₃ _nano	-53.7 ± 7.3	-10.8 ± 0.6
MIL-88B_NH ₂ _nano	-25.7 ± 1.6	-8.0 ± 0.2
MIL-88B_NO ₂ _nano	-28.4 ± 0.7	-7.7 ± 0.7
UiO-66_nano	-26.3 ± 1.5	-11.5 ± 0.5
ZIF-8_nano	-11.0 ± 0.6	-8.7 ± 1.2

4.7. Degradation Tests

Degradation tests of all the studied MOF NPs were carried out during 24 h in DMEM cell culture medium + 10% FBS. The selected time of the study was 24 h, which was the time used for the cytotoxicity evaluation *via* the MTT assay. Here, 2 mL of DMEM cell culture medium + 10% FBS at 37 °C was added to 1 mg of MOF NPs (C=500 µg·mL⁻¹). The samples were maintained at 37 °C during 24 h and after that time, they were centrifuged in an Eppendorf minispin centrifuge (Eppendorf, Germany) during 10 min at 6000 *g*.

Then, the supernatants were collected for elemental analysis, in which the % of C and N were measured.

5. REFERENCES

- ¹A. Dhakshinamoorthy, M. Alvaro, H. Chevreau, P. Horcajada, T. Devic, C. Serre and H. Garcia, *Catal. Sci. Technol.*, 2012, 2, 324-330.
- ²S. M. Ngola, P. C. Kearney, S. Mecozzi, K. Russell and D. A. Dougherty, *J. Am. Chem. Soc.*, 1999, 121, 1192-1201.
- ³J. N. Moorthy, P. Mal, N. Singhal, P. Venkatakrishnan, R. Malik and P. Venugopalan, *J. Org. Chem.*, 2004, 69, 8459-8466.
- ⁴P. Horcajada, F. Salles, S. Wuttke, T. Devic, D. Heurtaux, G. Maurin, A. Vimont, M. Daturi, O. David, E. Magnier, N. Stock, Y. Filinchuk, D. Popov, C. Riekkel, G. Férey and C. Serre, *J. Am. Chem. Soc.*, 2011, 133, 17839-17847.
- ⁵Y. Kim and T. M. Swager, *Chem. Commun.*, 2005, 0, 372-374.
- ⁶A. García Márquez, A. Demessence, A. E. Platero-Prats, D. Heurtaux, P. Horcajada, C. Serre, J.-S. Chang, G. Férey, V. A. de la Peña-O'Shea, C. Boissière, D. Grosso and C. Sanchez, *Eur. J. Inorg. Chem.*, 2012, 2012, 5165-5174.
- ⁷R. Canioni, C. Roch-Marchal, F. Secheresse, P. Horcajada, C. Serre, M. Hardi-Dan, G. Férey, J.-M. Greneche, F. Lefebvre, J.-S. Chang, Y.-K. Hwang, O. Lebedev, S. Turner and G. Van Tendeloo, *J. Mater. Chem.*, 2011, 21, 1226-1233.
- ⁸P. Horcajada, T. Chalati, C. Serre, B. Gillet, C. Sebrie, T. Baati, J. F. Eubank, D. Heurtaux, P. Clayette, C. Kreuz, J.-S. Chang, Y. K. Hwang, V. Marsaud, P.-N. Bories, L. Cynober, S. Gil, G. Férey, P. Couvreur and R. Gref, *Nat. Mater.*, 2010, 9, 172-178.
- ⁹T. Chalati, P. Horcajada, R. Gref, P. Couvreur and C. Serre, *J. Mater. Chem.*, 2011, 21, 2220-2227.
- ¹⁰P. Horcajada, C. Serre, R. Gref, G. Férey, P. Couvreur, PCT applications PCT/FR2008/001367, 01 october 2008.
- ¹¹P. Horcajada, C. Serre, R. Gref, G. Férey, P. Couvreur, PCT applications PCT/FR2008/001366. 01 october 2008.
- ¹²L. Anzalone and J. A. Hirsch, *J. Org. Chem.*, 1985, 50, 2128-2133.
- ¹³A. Demessence, C. Boissiere, D. Grosso, P. Horcajada, C. Serre, G. Férey, G. J. A. A. Soler-Illia and C. Sanchez, *J. Mater. Chem.*, 2010, 20, 7676-7681.
- ¹⁴(a) J.-M. Michot, F. Van Bambeke, M.-P. Mingeot-Leclercq and P. M. Tulkens, *Antimicrob. Agents Ch.*, 2004, 48, 2673-2682; (b) C. G. Mackenzie, J. B. Mackenzie and P. Beck, *J. Biophys. Biochem. Cytol.*, 1961, 9, 141-156.

CHAPTER 2

METAL-ORGANIC FRAMEWORKS: NEW DELIVERY SYSTEMS FOR GENISTEIN ADMINISTRATION

GENERAL OBJECTIVES AND AUTHOR CONTRIBUTIONS

C. Tamames-Tabar, F. Salles, C. Martineau, G. Maurin, C. Serre, P. Horcajada and M.J. Blanco-Prieto^a

This Chapter advocates the use of porous MOFs for drug delivery. Considering the important loadings of different therapeutic molecules achieved with different MOFs as well as their low cytotoxicity, evidenced in Chapter 1, a series Fe- and Zr-based porous MOFs have been proposed for encapsulating a drug. The chosen drug is genistein (GEN), a natural soy isoflavone aglycone, exhibiting interesting anticancer, antiangiogenic, and antioxidant properties. However, this molecule has a very low bioavailability due to several factors, in which first-pass metabolism is one of the main issues. The fact of encapsulating GEN within a MOF, could overcome its low bioavailability, with in addition more controlled releases.

The work in this Chapter has been divided in the following objectives: (i) the encapsulation of GEN in a series of 7 micro or nanometric MOFs together with a complete characterisation of each formulation, (ii) the release of GEN under simulated physiological conditions and (iii) the evaluation of its pharmacokinetics and biodistribution profiles in a mouse *in vivo* model in comparison to the free drug.

Several authors have worked in this Chapter. C. Tamames-Tabar has fulfilled the initial GEN physico-chemical tests, together with the encapsulation and release studies, as well as the *in vivo* tests. Dr. F. Salles and Prof. G. Maurin have been performed the computing simulation studies. Dr. C. Serre has been involved in material characterisation. Dr. C. Martineau has made the NMR characterisation of the formulations. Dr. P. Horcajada and Dr. M.J. Blanco-Prieto have supervised the entire work fulfilled in this Chapter.

METAL-ORGANIC FRAMEWORKS: NEW DELIVERY SYSTEMS FOR GENISTEIN ADMINISTRATION

C. Tamames-Tabar^{a,b}, F. Salles, C. Martineau^b, G. Maurin^c, C. Serre^b, P. Horcajada^b, M.J.
Blanco-Prieto^a

^a*Department of Pharmacy and Pharmaceutical Technology, School of Pharmacy, University of
Navarra, Irunlarrea 1, 31008 Pamplona, Spain.*

^b*Institut Lavoisier, UMR CNRS 8180, Université de Versailles Saint-Quentin-en-Yvelines, 45
Avenue des Etats-Unis, 78035 Versailles Cedex, France.*

^c*Institut Charles Gerhardt Montpellier UMR 5253 CNRS UM2, UM1, Université Montpellier 2,
Place E. Bataillon, 34095 Montpellier Cedex 05, France.*

Corresponding authors*

P. Horcajada: Institut Lavoisier, UMR CNRS 8180, Université de Versailles Saint-
Quentin-en-Yvelines, 45 Avenue des Etats-Unis, 78035 Versailles Cedex, France; Fax: 33
(0) 139256652; Tel: 33 (0) 1 39254371; E-mail: horcajada@chimie.uvsq.fr

M. J. Blanco-Prieto: Departamento de Farmacia y Tecnología Farmacéutica, Facultad de
Farmacia, Universidad de Navarra, Irunlarrea 1, 31008 Pamplona, Spain; Fax: 34
948425649; Tel: 34 948425600 Ext. 806519; E-mail: mjblanco@unav.es

ABSTRACT

Metal-Organic Frameworks (MOFs) in both micrometric and nanometric scale, are appealing systems for drug delivery, depending on the administration route and/or the bioapplications, among several factors. Genistein (GEN), a bioflavonoid from the family of isoflavones, has a wide variety of applications, such as chemopreventive, antioxidant and antiangiogenic. First, a GEN encapsulation study by simple *ex situ* impregnation, in a broad series of Fe- and Zr-based MOFs has been fulfilled, obtaining reproducible 174 μg GEN·mg formulation⁻¹ for rigid mesoporous iron(III) carboxylate MIL-100(Fe) nanoparticles (NPs). Subsequently, *in vitro* GEN delivery studies carried out in PBS showed in general, a sustained GEN release. GEN-entrapped MIL-100(Fe)_NPs were selected for short term pharmacokinetic and biodistribution studies in mice. Results showed higher plasmatic levels of GEN for an extended period of time, as well as an increase in pharmacokinetic parameters such as drug oral bioavailability. Moreover, the MOF worked as a shelter for GEN, impeding its metabolization.

Keywords: MOFs, Genistein, Drug Delivery, Pharmacokinetics

1. INTRODUCTION

Nowadays, there is a general trend in coming back to nature, regarding nutrition and therapeutics. Bioflavonoids or phytoestrogens are in vogue. In particular, the bioflavonoid genistein (GEN), which is found in many fruits, vegetables, legumes and plant leaves [Bennett *et al.*, 2004], has a wide array of compelling applications in therapeutics [Polkowski and Mazurek, 2000]. Among them, probably the best-known activity of GEN is as chemopreventive and anticancer agent [Sarkar and Li, 2006]. In sharp contrast with the currently used cytotoxic drugs, GEN antitumoral activity does not present any toxicity due to its different action mechanism based on the alterations GEN makes in the cell cycle (*i.e.* apoptosis or inhibition of the cell proliferation), by inhibition of topoisomerase II (topo II) [Azarova *et al.*, 2010; Bandele and Osheroff, 2007], by blockage of protein tyrosine kinase (PTK) [Yu *et al.*, 2012; Sánchez *et al.*, 2009; Akiyama *et al.*, 1987] or by the alterations in the phosphatidylinositol (PI) turnover [Makishima *et al.*, 1991]. In the last years, several studies have shown its benign effect in leukaemia [Azarova *et al.*, 2010; Li *et al.*, 2010; Sánchez *et al.*, 2009], breast cancer [Banerjee *et al.*, 2008; Lamartiniere *et al.*, 2002; Lamartiniere, 2000] and prostate cancer [Banerjee *et al.*, 2008; Lamartiniere *et al.*, 2002], among others, as well as in metastasis [Pavese, Farmer and Bergan, 2010].

In addition, GEN inhibits the production of reactive oxygen species (ROS) [Sánchez *et al.*, 2009], blocks multidrug resistance proteins [Castro and Altenberg, 1997; Versantvoort, Rhodes and Twentyman, 1996], suppresses bone degradation [Ming, Chen and Xian, 2013] and decreases cardiovascular-related diseases [Yu *et al.*, 2012]. Finally, it could also be used for the treatment of cystic fibrosis [Lansdell *et al.*, 2000], allergic processes [Brzezińska-Błaszczyk, Pietrzak and Misiak-Tłoczek, 2007], obesity [Behloul and Wu, 2013], skin photoaging [Polito *et al.*, 2012] and as a neuroprotective agent [Liao *et al.*, 2013] owing to enthralling results.

Despite all the promising properties GEN possesses, several important drawbacks limit their clinical use, including its very low water solubility and its low bioavailability (F). Its low F is mainly related to: (i) an important first-pass metabolism and enterohepatic recycling [Kobayashi *et al.*, 2013; Chen, Lin and Hu, 2003; Liu and Hu, 2002], (ii) an important serum protein binding [Bolli *et al.*, 2010], (iii) a low absorption when orally administered (notwithstanding, aglycones are more rapidly absorbed when contrasted to glycones, role connected to the sugar moiety) [Setchell *et al.*, 2001] and (iv) the effect of efflux proteins, which prevent GEN blood absorption [Chan, Lowes and Hirst, 2004]. Rationally, the encapsulation of GEN can overcome the previously described drawbacks, achieving a secure and effective drug dosage form (DDS) [Adair *et al.*, 2010].

Nanotechnology embraces new approaches in therapeutics, encompassing many different drug carriers at the nanometric scale [Adair *et al.*, 2010], a growing field due to the interdisciplinary work of diverse research areas.

In the last years, GEN has been entrapped in different polymeric (amylase, PLGA or eudragit) [Tang *et al.*, 2011; Shin *et al.*, 2010; Cohen *et al.*, 2008], or lipid NPs [Pham, Brownlow and Elbayoumi, 2013], achieving drug loadings up to 11.3 μg of GEN *per mg* of formulation. Also, PEG- or PVA-based MPs have reached GEN capacities of 6 μg of GEN *per mg* of formulation [Zhang, Gao and Xu, 2013; Motlekar, Khan and Youan, 2006].

Metal-Organic Frameworks or MOFs, obtained at both the micro- and nanometric scale depending on their synthesis conditions [Lee, Kim and Ahn, 2013], are based on inorganic units and organic polycomplexant linkers. Their high structural and composition versatility together with a high porosity and an amphiphilic internal environment, make them interesting potential candidates for several chemical and industrial processes, such as: heat transformation [Mahata, Prabu and Natarajan, 2008], catalysis, sensing, gas storage and separation [Special Issue Chem Rev, 2012]. More recently, MOFs have been revealed as promising candidates for biomedical applications [Novio *et al.*, 2013; Horcajada *et al.*, 2012; Della Rocca, Liu and Lin, 2011]. MOFs have been proposed for (i) the encapsulation and delivery of several drugs [He *et al.*, 2014; Cunha *et al.*, 2013b; Sun *et al.*, 2012; Ke *et al.*, 2011; Horcajada *et al.*, 2010], cosmetics [Cunha *et al.*, 2013a; Liédana *et al.*, 2012], biologically active gases [Hinks *et al.*, 2010; Xiao *et al.*, 2007], enzymes [Liu *et al.*, 2013; Lykourinou *et al.*, 2011] and toxins [de Oliveira *et al.*, 2013; Hasan, Choi and Jhung, 2013; Khan, Hasan and Jhung, 2013]; (ii) their use in imaging [Wang *et al.*, 2013; Rieter *et al.*, 2006] and theranostics [Wang *et al.*, 2013; Wang, Liu and Lin, 2013; Della Rocca, Liu and Lin, 2011].

In this work we propose the encapsulation and controlled release of GEN from a series of 7 highly porous MOFs bearing different topologies and compositions, based on *a priori* biocompatible metal (*i.e.* Fe, Zr) dicarboxylates with pore sizes compatible with the GEN dimensions (12x5x2 Å). To that purpose, four different MOF topologies were studied (Figure 1): (i) the cubic-zeotype MIL-100 (MIL stands for Material of Institut Lavoisier), built up from iron(III) octahedra trimers connected by trimesate anions, exhibiting a very important porosity (BET or Brunauer-Emmett-Teller surface: $S_{\text{BET}} \sim 2400 \text{ m}^2 \cdot \text{g}^{-1}$, pore volume $V_p \sim 1.2 \text{ cm}^3 \cdot \text{g}^{-1}$) and two types of mesocages (25 and 29 Å) accessible through microporous windows ($\sim 4.7 \times 5.5$ and 8.6 Å) [Horcajada *et al.*, 2007]; (ii) the hexagonal MIL-88C architecture based on iron(III) octahedra trimers and 2,6-naphthalendicarboxylate anions creating a network of microporous tunnels and cages. MIL-88C presents a reversible flexible structure able to reversibly adapt its pore size in

the presence of different stimuli from a closed form (unit cell volume= $V_{u.c.} \sim 2100 \text{ \AA}^3$) to an open form ($V_{u.c.} \sim 5700 \text{ \AA}^3$; $\emptyset \sim 13 \text{ \AA}$) [Serre *et al.*, 2007]; (iii) the cubic UiO-66 materials (UiO for Oslo University), based on zirconium (Zr) oxoclusters and 4,4'-biphenyldicarboxylate (UiO-66_BPDC), 2,6-naphthalendicarboxylate (UiO-66_NDC) or terephthalate anions (UiO-66) bearing different functional groups on the aromatic benzyl ring (UiO-66_X for X=2CF₃ or NH₂). UiO-66_BPDC, UiO-66_NDC and UiO-66 solids possess octahedral (23, 14 and 11 Å, respectively) and tetrahedral cavities (~11.5, 11 and 8 Å, respectively) accessible through microporous triangular windows (~8, 8 and 5–7 Å, respectively) with $S_{BET} \sim 2500, 1700$ and $1200 \text{ m}^2 \cdot \text{g}^{-1}$ and pore volumes of ~0.8, 0.7 and $0.5 \text{ cm}^3 \cdot \text{g}^{-1}$, respectively [Katz *et al.*, 2013; Zhang *et al.*, 2013a; Barcia *et al.*, 2011; Cavka *et al.*, 2008]; and finally, (iv) the tetragonal MIL-140C solid, based on complex zirconium oxide chains and 4,4'-biphenyldicarboxylate, which possesses 1D triangular channels of ~7 Å ($S_{BET} \sim 700 \text{ m}^2 \cdot \text{g}^{-1}$, $V_p \sim 0.5 \text{ cm}^3 \cdot \text{g}^{-1}$) [Guillerm *et al.*, 2012].

The pharmacokinetics (PK) and F of GEN-loaded MIL-100(Fe) nanoparticles (NPs) were evaluated in female BALB/C mice.

2. EXPERIMENTAL SECTION

2.1 Genistein Encapsulation and *In Vitro* Release

MOFs Synthesis

Several MOFs were used for achieving high GEN payload formulations. Hence, micrometric UiO-66_2CF₃(Zr)_MPs [Cunha *et al.*, 2013b], UiO-66_NH₂(Zr)_MPs [Cunha *et al.*, 2013b], UiO-66_NDC(Zr)_MPs [Garibay and Cohen, 2010], UiO-66_BPDC(Zr)_MPs [Schaate *et al.*, 2011; Cavka *et al.*, 2008] and MIL-140C(Zr)_MPs [Guillerm *et al.*, 2012] were synthesised according to the already published methods (see SI). Nanometric MIL-100(Fe)_NPs were prepared as previously reported [Garcıa-Marquez *et al.*, 2012]. Finally, MIL-88C(Fe)_NPs were solvothermally prepared in EtOH by a microwave method (see SI, pages 138-139).

Genistein Encapsulation

After a broad preliminary GEN encapsulation screening, in which several parameters were changed (*i.e.* solvents, functionalisation, temperature, contact time and molar ratio,

among others), the best results were obtained with a series of Zr-based and Fe-based MOFs.

In the case of Zr-based solids, GEN was entrapped by suspending the previously dehydrated micrometric materials in a GEN solution in DCM ($0.65 \text{ mg}\cdot\text{mL}^{-1}$) maintaining a material:drug molar ratio of 1:2 under stirring for 24 h (see SI and Table S2, page 140). After the encapsulation, the drug-containing solids were recovered by filtration and dried at $100 \text{ }^\circ\text{C}$.

Contrary to the Zr-based MOFs, in the case of Fe-based MOFs, the encapsulation parameters were particular to each MOF. Hence, the flexible MIL-88C(Fe)_NPs were suspended in a GEN ethanol solution ($1 \text{ mg}\cdot\text{mL}^{-1}$). Alongside, the water-exchanged rigid MIL-100(Fe)_NPs were suspended in an aqueous solution of the GEN dicalcium salt denoted GCa ($1.14 \text{ mg}\cdot\text{mL}^{-1}$; see SI page 140). In all the cases, the material:drug molar ratio was maintained at 1:2 during 24 h. Finally, the GEN containing nanoMOF dispersion was centrifuged during min at $21130 g$ during 15 min.

Its drug payload was quantified by thermogravimetric analysis (TGA; Table S4, Figure S3, pages 144-145), high performance liquid chromatography (HPLC; Table S4, page 144) and elemental analysis (EA; Table S4, page 144). Moreover, the solids were characterised before and after the drug loading by X-ray powder diffraction (XRPD; Figure S1, page 142), dynamic light scattering (DLS; Table S3, page 143), ζ -potential (Table S3, page 143), N_2 adsorption porosimetry (Table S5, Figure S4, page 146), Fourier-transform infrared spectroscopy (FTIR; Figure S5, pages 147-148), solid state ^{13}C -nuclear magnetic resonance (NMR; Figure S6, page 149) and computing simulation (see SI, page 149-150).

Genistein In Vitro Release

For the *in vitro* GEN release studies, 1 mg of GEN-containing MOF (formulation) was suspended in 15 mL of a PBS solution (pH 7.2), kept under bidimensional rotation at $37 \text{ }^\circ\text{C}$, under sink conditions. After different incubation times, a supernatant aliquot of 7.5 mL (half of the total volume) was recovered by centrifugation ($15000 g$ for 15 min) and replaced with the same volume of fresh medium already set at $37 \text{ }^\circ\text{C}$. The aliquot was filtered using a $0.22 \text{ }\mu\text{m}$ pore diameter filter and stored at $4 \text{ }^\circ\text{C}$ until HPLC analysis. After a basic treatment (1 mL of NaOH 0.5 M was added to 1 mL of PBS supernatant and was maintained during 2 h), the amount of released GEN was quantified by HPLC (see SI and Table S6, pages 150-151).

After the complete release, the formulation pellet was first characterised by XRPD. Latter, it was suspended in 1 mL of NaOH 0.01 M and maintained under rotational stirring for 7 h to then estimate the amount of non-released GEN (see SI and Table S7, pages 150-155).

2.2. Pharmacokinetic and Bioavailability Profile of GEN and GEN-loaded MIL-100(Fe)_NPs

The PK and F study of the encapsulated GEN was performed in female BALB/mice (6–8 weeks old; 20 ± 1 g body weight, Harlan Ibérica, Spain). All experimental procedures were reviewed and approved by the Animal Experimentation Ethics Committee of the University of Navarra (Spain). In the study, mice ($n=6$) were housed in cages and maintained at 22-25 °C and at 20% relative humidity with a 12 h light/dark cycle. In addition, their feed had traces of GEN (up to 20 mg GEN·Kg⁻¹ of product). Therefore, 12 h prior to the experiment start, during the first 24 h and 12 h prior blood extraction, mice were deprived from their diet (Harlan Teklad 2014, Harlan Ibérica, Spain), surrogated by soy-free jelly-based nutrition (Resource®, Nestlé Health Science, Spain). Moreover, mice had drinking water *ad libitum* (See SI, pages 150).

The experiment was divided in 3 time groups regarding the end point of the experiment (4, 24 and 48 h). Alongside, the animals were divided in free and in encapsulated GEN, which in all the cases was administered by a single oral administration (p.o.). In the case of the free GEN group, a single dose of 100 µL of a homogeneous GEN solution (30 mg·Kg⁻¹) containing 10% DMSO, 25% PEG 400 and 65% of water for injection was administered [Tamames-Tabar *et al.*, 2013]. In the case of the encapsulated GEN, a single dose of 100 µL of GEN-loaded MIL-100(Fe)_NPs (30 mg·Kg⁻¹) was suspended and administered in the same conditions as in the free GEN group.

Blood samples were collected at different times (0.25, 0.5, 1, 2, 4, 6, 8, 24 and 48 h) in EDTA-coated tubes to avoid blood coagulation. Just after blood extraction, the samples were centrifuged at 5000 *g* for 10 min at 4 °C and plasma was kept at -80 °C until sample analysis. All the PK parameters (C_{max} , T_{max} , $t_{1/2}$, MRT and F) resulting from the comparison between the free and encapsulated GEN, were obtained with the WinNonLin® software (Certara, USA). Mice were sacrificed at 4, 24, and 48 h post-administration and their kidneys, spleens and livers were removed, homogenised with 1 mL of PBS pH 7.4 and kept at -80 °C until sample analysis [Tamames-Tabar *et al.*, 2013].

3. RESULTS AND DISCUSSION

3.1 GEN Encapsulation and *In Vitro* Release

GEN Encapsulation

GEN encapsulation was performed by simple impregnation by suspending the powdered MOF, in either their micro (Zr-based MOFs) or nanometric form (Fe-based MOFs), into a concentrated solution of GEN (Figure 1). The GEN loading was quantified by combining three different techniques, TGA, HPLC and elemental analysis. Different parameters were modified (the solvent, encapsulation temperature and number of consecutive impregnations) for optimising the encapsulation conditions.

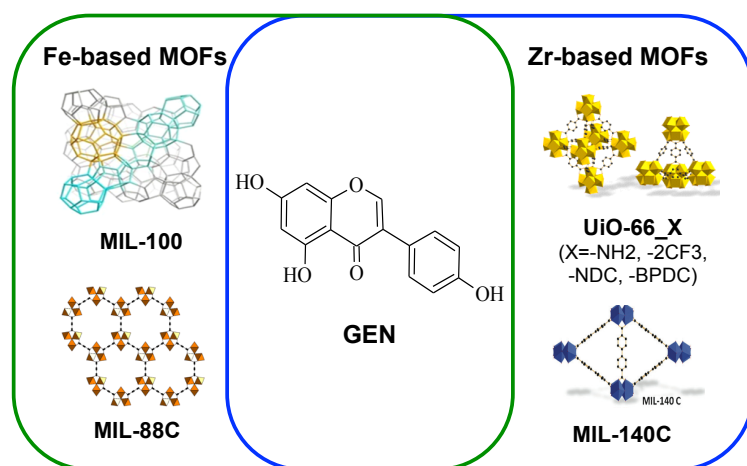


Figure 1. Scheme of the best genistein (GEN) encapsulations with Fe-based MOFs (MIL-100 and MIL-88C NPs) and Zr-based MOFs (UiO-66 and MIL-140C MPs).

Firstly, EtOH and DCM were selected due to the high GEN experimental solubility (~ 1.3 and $2.0 \text{ mg}\cdot\text{mL}^{-1}$, respectively), their low toxicity values (rat oral lethal dose 50; $\text{LD}_{50} = 7060$ and $2100 \text{ mg}\cdot\text{Kg}^{-1}$, respectively) [MSDS, 2014; US Environmental Protection Agency, 1994] and their easy removal at low temperature ($< 80 \text{ }^\circ\text{C}$; see Table S1, page 140). The GEN encapsulation in the Zr-based MOFs was significantly higher when GEN-DCM solution was used rather than ethanol solutions (*i.e.* ~ 160 vs. $\sim 2 \text{ } \mu\text{g GEN}\cdot\text{mg formulation}^{-1}$ for the UiO-66_2CF₃ and non-functionalised UiO-66, in DCM and EtOH, respectively). As previously suggested [Cunha *et al.*, 2013a], this lower encapsulation rate when using an EtOH solution could be related with the presence of coordinatively unsaturated metal sites (CUS) in the UiO-66 solids [Cavka *et al.*, 2008]. EtOH could coordinate these CUS

reducing the free aperture of the windows and then the drug diffusion. In contrast, in the MIL-88C(Fe)_NPs, EtOH led to higher GEN loadings than DCM, (~ 201.7 vs. $51.0 \mu\text{g GEN}\cdot\text{mg formulation}^{-1}$). This higher GEN cargo might be related to the pore opening of this flexible MOF [Serre *et al.*, 2007]. In EtOH, MIL-88C(Fe)_NPs exhibited a large pore form (space group P-62c; $a\sim 18.68 \text{ \AA}$, $c\sim 18.76$, $V\sim 5670 \text{ \AA}^3$), more accessible to GEN, whereas in DCM the structure is closer (space group P-62c; probable cell parameters: $a\sim 13.44 \text{ \AA}$, $c\sim 23.02$, $V\sim 3600 \text{ \AA}^3$), which could hinder the GEN diffusion through the pores. Finally, in the case of MIL-100(Fe)_NPs both EtOH and DCM, led to poor GEN loadings (~ 18.3 and $17.8 \mu\text{g GEN}\cdot\text{mg formulation}^{-1}$, respectively), followed with the presence of free recrystallized GEN in the case of DCM encapsulation, as observed by XRPD. Therefore, a new strategy was developed to improve the GEN loadings in MIL-100(Fe)_NPs. A dicalcium salt of GEN (denoted GCa) was prepared in order to increase its water solubility (from $0.8 \mu\text{g}\cdot\text{mL}^{-1}$ to $1.4 \text{ mg}\cdot\text{mL}^{-1}$, both at $37 \text{ }^\circ\text{C}$) (See SI, pages 139-141), allowing the use of biofriendly and low cost aqueous solutions for the GEN encapsulation. Interestingly, higher encapsulation rates were achieved using GEN aqueous solution at moderate temperature (~ 174 vs. $\sim 18 \mu\text{g GEN}\cdot\text{mg formulation}^{-1}$ for GCa in water at $37 \text{ }^\circ\text{C}$ and GEN in EtOH at RT, respectively), as the drug diffusion throughout the MIL-100(Fe)_NPs' porosity was directly related with the temperature. Higher temperatures up to $100 \text{ }^\circ\text{C}$ led however to a partial degradation of the MOF structure, ruling out their use (results not shown). In addition, elemental analysis measurements showed the presence of a small percentage of calcium. Considering that the pH of the encapsulation medium decreases from an initial pH of 8 to 6.6, owing to the presence of partially coordinated trimesate linkers located in the outer surface of MIL-100(Fe)_NPs and the pK_a of GEN (7.2, 10.0 and 13.1) [Bellido *et al.*, 2014; Zielonka, Gebicki and Gryniewicz, 2003], this value might correspond to *ca.* 8% of the total encapsulated GEN as the monocalcium form. Although in a small proportion, the presence of a salt could improve the GEN bioavailability due to the better aqueous solubility of this fraction [Serajuddin, 2007].

With the exception of the UiO-66_NH₂(Zr)_MPs, several consecutive impregnations (up to 3 successive impregnations) did not lead to significant higher GEN payloads. However, almost twice of the initial GEN capacity of the UiO-66_NH₂(Zr)_MPs was achieved in a second impregnation (159.3 ± 47.7 vs. $336.0\pm 25.0 \mu\text{g GEN}\cdot\text{mg formulation}^{-1}$). Interestingly, Cunha *et al.* have not observed any influence of the reimpregnation process, suggesting that the caffeine cargo was maximal (*i.e.* ~ 50 wt% in MIL-100(Fe) corresponding to a pore occupation of $\sim 90\%$) [Cunha *et al.*, 2013b]. The dramatic increase of the GEN payload after a second impregnation in UiO-66(Zr)_NH₂ might be associated with a partial filling

of the pores in the first encapsulation, remaining still available a fraction of the porosity for housing GEN.

Table 1. GEN loadings together with the BET surface and micropore volume for the different GEN formulations.

MOF	GEN Loading		Raw MOF			Formulation	
	$\text{\textcircled{S}}\mu\text{g}\cdot\text{mg form.}^{-1}$	$\text{\textcircled{L}}\text{Mol}\cdot\text{mol}^{-1}$	Windows size (Å)	Pore Volume ($\text{cm}^3\cdot\text{g}^{-1}$)*	BET Surface ($\text{m}^2\cdot\text{g}^{-1}$)	Pore Volume ($\text{cm}^3\cdot\text{g}^{-1}$)*	BET Surface ($\text{m}^2\cdot\text{g}^{-1}$)
MIL-100(Fe)_NPs	174.0±24.9	0.48	4.7*5.5 & 8.6	0.30	620	0.04	20
MIL-88C(Fe)_NPs [†]	201.7±51.7	0.79	13	1.6 [†]	4100 [†]	-	-
UiO-66_NH ₂ (Zr)_MPs	159.3±47.7	1.23	5-7	0.34	680	**	**
	335.9±24.8*	3.28				0.06	110
UiO-66_2CF ₃ (Zr)_MPs	157.0±44.8	1.71	5-7	0.23	500	0.05	80
UiO-66_NDC(Zr)_MPs	329.3±45.7	3.57	8	0.72	1110	0.03	30
UiO-66_BPDC(Zr)_MPs	337.7±24.9	4.00	8	0.64	1240	0.02	30
MIL-140C(Zr)_MPs	225.6±88.2	0.37	7	0.80	1620	0.01	20

$\text{\textcircled{S}}$ μg of GEN *per* mg of formulation

$\text{\textcircled{L}}$ mol of GEN *per* mol of dry and empty MOF

*corresponding to a two successive impregnation processes.

**in progress

[†] theoretical values estimated by computing simulation (see SI).

Important GEN loadings ranging from 160 to 340 $\mu\text{g}\cdot\text{mg formulation}^{-1}$ were achieved using MOFs, depending on the topology and nature of the MOF. These values are in total agreement with the encapsulation rates obtained for similar materials and other drugs (10-40 wt% in MIL-100(Fe) and UiO-66(Zr) solids) [He *et al.*, 2014; Agostoni *et al.*, 2013a; Cunha *et al.*, 2013b; Gaudin *et al.*, 2012; Chalati *et al.*, 2011; Horcajada *et al.*, 2011; Horcajada *et al.*, 2008; Horcajada *et al.*, 2006]. Although the works dealing with the GEN entrapping are still scarce, these encapsulation rates are higher than those previously reported using other drug carriers such as polymeric (*i.e.* PLGA, PVA, PEG) and lipid particles, which reached maximum loadings of 11.3 $\mu\text{g}\cdot\text{mg formulation}^{-1}$ [Pham, Brownlow and Elbayoumi, 2013; Zhang, Gao and Xu, 2013; Tang *et al.*, 2011; Shin *et al.*, 2010; Cohen *et al.*, 2008; Motlekar, Khan and Youan, 2006]. If we compare the obtained values with the encapsulation of other bioflavonoids, such as daidzein, quercetin and kaempferol in different polymeric and lipid DDS [Scalia *et al.*, 2013; Ghosh *et al.*, 2011; Tzeng *et al.*, 2011; Ge *et al.*, 2007], the GEN payloads in MOFs are in the same range. Therefore, GEN-MOF formulations seem to be promising candidates for the GEN administration.

With the exception of the flexible MIL-88C(Fe) solid, which showed a close porosity (not accessible to the nitrogen adsorption), all the rigid solids after the GEN incorporation showed almost no residual porosity, confirming the presence of GEN inside their pores occupying almost 83-99% of the total porosity. The payload seems to be related with the pore volume and surface of the solids (Table 1, page 116). For a better comparison, we have considered the amount of the GEN encapsulated within the MOF (mol GEN·mol⁻¹ of dry and empty solid; Table 1) as a function of the initial pore volume of the MOF. Interestingly, one mol of GEN seems to fill a similar volume in each MOF (0.002 mol GEN·cm⁻³), with the exception of MIL-88C(Fe)_NPs. In fact, the considered pore volume of MIL-88C(Fe)_NPs structure corresponds to the totally open form, which is not the case in presence of GEN, as previously evidenced by XRPD. This observation indicates that the main parameter governing the encapsulation loading of GEN is the pore volume of the MOF.

XRPD patterns confirm that all the formulations preserved their crystalline structure after the GEN impregnation (Figure S1, page 140), with no significant difference in the broadening of the Bragg peaks. In addition, no reflections corresponding to the free recrystallised GEN were observed, being consistent with the GEN entrapping inside the MOF porosity. Remarkably, after the GEN encapsulation in the flexible MIL-88C(Fe)_NPs, the main peaks position of the XRPD patterns was completely modified, indicating a different pore opening due to the efficient GEN entrapping inside the pores. Unit cell parameters of the GEN-containing MIL-88C(Fe)_NPs are currently being indexed using Dicsvol to a hexagonal cell, probably corresponding to a partially open GEN-containing MIL-88C form (cell volume ~3800 Å³).

Force-field-based Monte Carlo (GCMC) simulations were first employed, to evaluate the theoretical GEN uptake for MIL-100(Fe)_NPs and MIL-88C(Fe)_NPs in order to check if the maximum theoretical loading has been experimentally achieved. In both cases, the experimental GEN cargoes are much lower than the theoretical ones (0.21 *vs.* 0.84 g GEN·g⁻¹ of dry empty MIL-100(Fe)_NPs and 0.25 *vs.* 1.32 g GEN·g⁻¹ of dry empty MIL-88C(Fe)_NPs). First, GCMC estimations have considered the totally open form of the MIL-88C(Fe)_NPs structure, which is not the case, being a partially open form filled with GEN (5670 *vs.* 3800 Å³), as previously shown by XRPD. Second, regarding the MIL-100(Fe)_NPs, the theoretical loading (0.84 g·g⁻¹) was estimated by assuming a full accessibility of both small and large cages. However, considering that the dimensions of GEN (11.7x5.3x2.0 Å) are quite close to the windows size (~4.7x5.5 Å) of the small cage, one can rationally expect that only the large cages will be accessible to GEN adsorption. Thus, blocking the volume of the small cages (54%), we can roughly estimate an

encapsulation rate of $0.38 \text{ g}\cdot\text{g}^{-1}$, which continuous being larger than the experimental payload. Finally, the differences between the experimental laboratory values and the theoretical computing calculations, might be due to not considering the coadsorption phenomenon of the encapsulation solvent within the MOF porosity during the GEN entrapping, fact that happened experimentally. Hence, probably overestimating the saturation determined experimentally.

Finally, particle size and surface charge were estimated by means of DLS and ζ -potential (Table S3, page 143). Although no significant differences were observed regarding particle size, the formulations depicted a general tendency in becoming more negative, except for UiO-66_BPDC(Zr)_MPs. This last solid exhibited a quite important initial negative charge ($-24.42\pm 0.35 \text{ mV}$), which became more neutral, but still negative in presence of GEN ($-5.86\pm 0.75 \text{ mV}$). In all the cases, the negative surface might be related with the presence of GEN, also adsorbed on the outer surface of the MOF particles.

In Vitro Release

GEN release was evaluated by suspending the GEN-containing MOFs in a phosphate buffer solution (PBS 0.04 M at pH=7.2) at 37°C under continuous stirring. The released GEN was quantified after a basic treatment by HPLC (See SI, Tables S6 and S7, pages 150-155). Moreover, to study the MOF structural degradation under the release conditions, the constitutive organic linker was motorised by HPLC and the solids recovered after 3 days of the GEN release were characterized by XRPD (page 142).

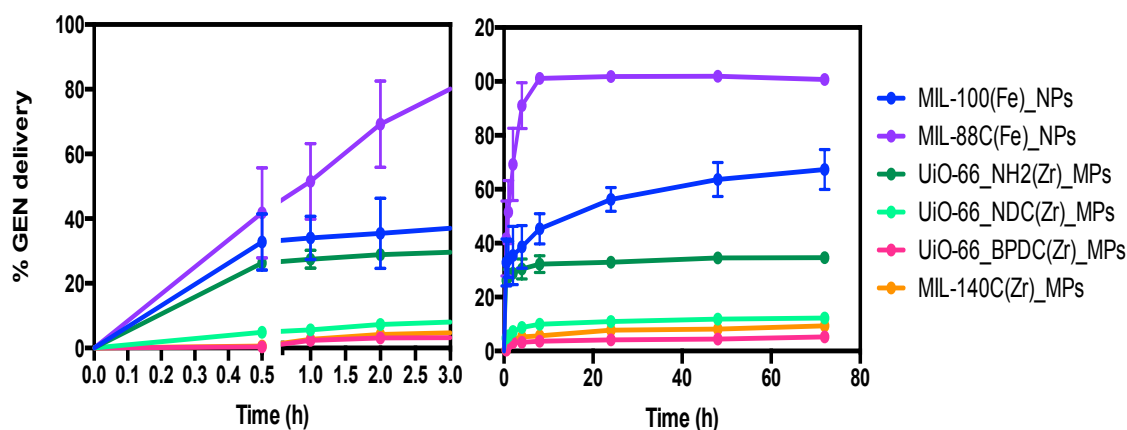


Figure 2. GEN delivery profiles from different Fe-based MOF NPs (MIL-100 and MIL-88C) and Zr-based MOF MPs (UiO-66_X (X=-NH₂, -NDC, -BPDC) and MIL-140C) during 3 days after the addition of a NaOH 0.5 M solution to the existing GEN in PBS supernatants. We have displayed the release results up to 3 days, as the following data are in a plateau.

With the exception of flexible MIL-88C(Fe)_NPs, whose total cargo was delivered in a controlled manner within 2 days, GEN was progressively released from the MOFs in around 3 days, in which GEN release reached a plateau, which was maintained for several weeks (6 weeks; Figure 2, Table S7, pages 120 and 154, respectively). The observed slow release kinetics, in the same time-range than other previously reported for similar MOF structures [He *et al.*, 2014; Agostoni *et al.*, 2013a; Cunha *et al.*, 2013a; Horcajada *et al.*, 2011], are also comparable to the *in vitro* release profiles reported for other GEN and other bioflavonoid formulations [Sun *et al.*, 2014; Cohen *et al.*, 2008; Ge *et al.*, 2007]. This observation suggests that the hydrophobic character of the drug is involved in the controlled release of GEN.

The release kinetics can be ordered from the faster to slower as follows: MIL-88C(Fe)_NPs > MIL-100(Fe)_NPs > UiO-66_NH₂(Zr)_MPs >> UiO-66_NDC(Zr)_MPs > UiO-66_BPDC(Zr)_MPs > MIL-140C(Zr)_MPs. At a first sign, NPs seem to faster release the GEN, in agreement with shorter diffusions. In addition, the GEN was slower delivered from the more hydrophobic solids (UiO-66_NDC(Zr)_MPs, UiO-66_BPDC(Zr)_MPs, MIL-140C(Zr)_MPs) regardless to their pore size (Table 1, page 118). This could be related with the diffusion of the aqueous release medium through the pores, slowing down the GEN exchange, and is supported by the important hydrophobicity of the GEN.

Apart from the effect of the drug/medium diffusion, controlled released of GEN from MOFs has been previously associated to other two parameters: MOF degradation under physiological conditions and the formation of specific host-guest interactions between the drug and the MOF [Horcajada *et al.*, 2012]. Thus, we will try to bring some light to the degradation kinetics in order to understand the more relevant parameters affecting the GEN release rate.

First, the formation of specific interaction was investigated by computing simulation DFT, FTIR and solid state ¹³C-CPMAS NMR (cross polarisation magic angle spin nuclear magnetic resonance). From DFT calculations, the GEN conformation inside the pores has been estimated, evidencing that the main interactions between the Fe-MOF NPs and the GEN correspond to π -stacking interactions between the aromatic ring of the GEN moieties and the trimesate or naphthalene cycles of the MIL-100(Fe)_NPs and MIL-88C(Fe)_NPs, respectively, as illustrated in Figure 3. In addition, the terminal OH atoms of the iron trimer in MIL-88C(Fe)_NPs seem to establish additional interactions through the formation of hydrogen bondings with the 7-hydroxy-group of the GEN.

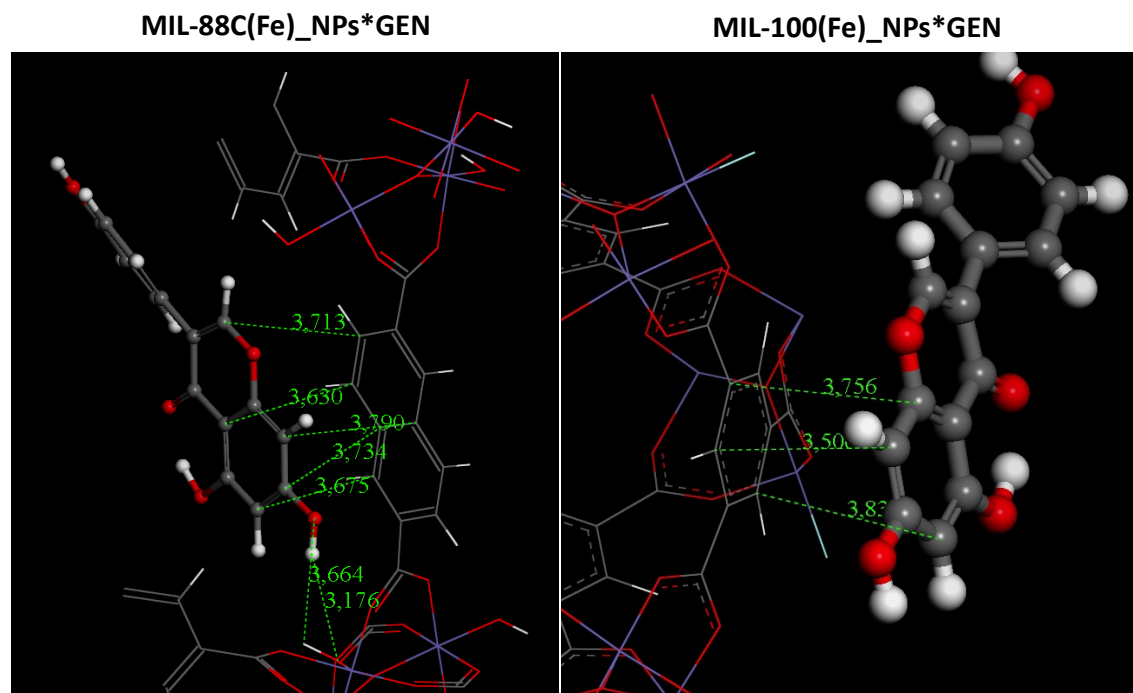


Figure 3. DFT-optimised structures of MIL-100(Fe)_NPs and MIL-88C(Fe)_NPs in presence of GEN. Characteristic GEN/MOF interacting distances are reported in Angstrom (in green).

In agreement with DFT calculations, FTIR showed a shift of $\nu/\delta(\text{C}=\text{C})$ bands at around 1500 cm^{-1} , which could be in accordance with the formation of π -interactions (Figure S5, pages 147-148). Also, the formation of hydrogen bonding interactions through the Fe-OH of the MIL-88C(Fe)_NPs and the HO-GEN seems to be supported by a slight shift of the $\nu(\text{Fe}-\text{O})$ band from 487 to 491 cm^{-1} . Furthermore, Zr-based MOFs exhibit a significant positive shift of the $\nu(\text{Zr}-\text{O})$ band, suggesting the formation of specific interactions between the metal sites of the Zr-MOFs and the hydroxyl groups of the GEN (Figure S5, pages 147-148).

Further characterisation has been performed by means of solid state ^{13}C -CPMAS NMR on the GEN-loaded Zr-based MOFs. Although the NMR characterisation is currently in progress, some preliminary results have been obtained with the UiO-66- $\text{NH}_2(\text{Zr})$ _MPs before and after the GEN encapsulation. The presence of GEN in the UiO-66- $\text{NH}_2(\text{Zr})$ _MPs loaded sample is confirmed by the ^{13}C CPMAS NMR spectrum (Figure S6, page 149). As observed for the caffeine-loaded UiO-66- $\text{NH}_2(\text{Zr})$ [Devautour-Vinot *et al.*, 2013], the incorporation of species in the pores of the MOFs induces local modification of the structure, which in turn results in a broadening of the ^{13}C lines of the UiO-66(Zr), compared to the parent MOF.

On the other hand, it is well-known that metal carboxylate MOFs can degrade in presence of phosphate buffer, as a consequence of the replacement of the carboxylate-metal bonds by the more complexant phosphate groups [Horcajada *et al.*, 2010]. Thus, the degradation of the MOFs was evaluated during the GEN release analysing the constitutive organic ligand delivered to the medium (Figure S8, pages 153-154). Constitutive ligands were progressively released from the GEN-containing MOFs, corresponding to partial MOF degradation, ranging from 10 to 30% depending on the structure and nature of the MOF. In agreement to this partial degradation, XRPD patterns of the MOFs after the GEN release have shown either a peak broadening (UiO-66-NH₂(Zr)_MPs and UiO-66-NDC(Zr)_MPs), consistent with a partial degradation of the crystalline structure, or a complete or almost total loss of long-range order (MIL-100(Fe)_NPs, MIL-88C(Fe)_NPs, UiO-66-BPDC(Zr)_MPs and MIL-140C(Zr)_MPs; Figure S1, page 142).

Finally, the GEN released from the MOFs seems to be a consequence of the drug diffusion (hydrophobic GEN and MOF), the MOF carrier degradation, the formation of drug-matrix interactions and drug diffusion. Among the different formulations, MIL-100(Fe)_NPs was revealed as a very promising MOF carrier for GEN release since it showed a long release profile, interesting for a clinical perspective.

3.2 Pharmacokinetic and Bioavailability Profile of GEN and GEN-loaded MIL-100(Fe) NPs

Prior any clinical use of a drug or formulation, a series of preclinical studies have to be fulfilled. In this path, we studied the behaviour of one of the previously described GEN-MOF formulations: MIL-100(Fe)_NPs. This particular formulation was selected to carry out this experiment owing to: (i) having an optimal particle size for its administration (likewise MIL-88C(Fe)_NPs) and (ii) for exhibiting a long GEN *in vitro* release profile, unlike MIL-88C(Fe)_NPs. In addition, MIL-100(Fe)_NPs' acute *in vivo* toxicity [Baati *et al.*, 2013] and cytotoxicity [Tamames-Tabar *et al.*, 2014] have been recently published, displaying low *in vivo* and *in vitro* toxicity values, making it an ideal candidate for future clinical applications.

MIL-100(Fe)_NPs formulation was administered in a DMSO/PEG 400/NaCl solution (10:25:65, v/v). This highly stable formulation permitted a suitable dispersion of the NPs together with a very low GEN release (only 10% of the total cargo is released after 6 h; Figure S9, page 156).

In order to assess this Fe-based formulation, we administered the same single p.o. dose (D=30 mg·Kg⁻¹) of free and encapsulated GEN (in MIL-100(Fe)_NPs) to BALB/C female

mice (See Experimental Section 2.3., pages 155-156). The study was divided in two parts: (i) the PK profile of free and encapsulated GEN and (ii) the F of free and encapsulated GEN in different mouse organs.

GEN Pharmacokinetics

The PK results after a single p.o. administration of 30 mg·Kg⁻¹ of GEN and GEN-loaded MIL-100(Fe)_NPs are displayed in Figure 4, where the concentration of GEN in mouse plasma is plotted against time. As it can be observed, there is a large difference among the profiles of both encapsulated and free GEN, not only in GEN levels, but also regarding time.

The T_{max} was reached 4 h post-administration of both free and encapsulated GEN, where the maximal concentration values of the drug (C_{max}) were 171.25 and 2123.29 ng·mL⁻¹, respectively. Moreover, 8 h post-administration, a decrease of GEN levels was observed for both groups, being more pronounced in the case of the encapsulated drug (36.47 and 1643.88 ng·mL⁻¹ for free and encapsulated GEN after 8 h, respectively). Later, the GEN plasmatic levels corresponded to the GEN released from MIL-100(Fe)_NPs (1292.85 and 120.07 ng·mL⁻¹ for 24 and 48 h, respectively), values that decreased until undetectable levels at 72 h post-administration. This had a similar profile to the one observed by King and Bursill, in which GEN was quickly eliminated from plasma, dropping to residual levels 12-24 h after a soy meal consumption, evidencing a short t_{1/2} [King and Bursill, 1998].

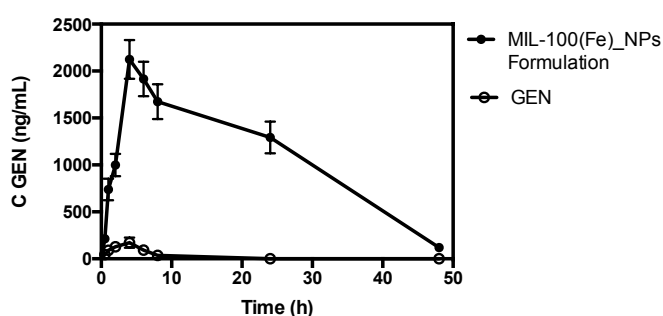


Figure 4. Time-plasma concentration curve data of GEN (empty circles) and of MIL-100(Fe)_NPs formulation (filled circles) after a single oral administration of 30 mg·Kg⁻¹ ($n=6$) during 48 h. Interestingly, the administration of our formulation, increased by 12-fold the drug plasmatic levels (~170 vs. ~2100 ng·mL⁻¹ for free and encapsulated GEN, respectively), incremented 4-fold the mean residence time (MRT, 3.82 vs. 16.23 h for free and encapsulated GEN, respectively) and raised by 5.5-fold the drug half life (t_{1/2}, 1.79 vs. 10.12

h for free and encapsulated GEN, respectively). Most importantly, the insertion of GEN inside MIL-100(Fe)_NPs, enhanced the relative bioavailability by 62-fold (AUC \sim 900 *vs.* \sim 52600 ng·h·mL⁻¹ for both orally administered free and encapsulated GEN, respectively), as well as the absolute bioavailability by \sim 25% (AUC \sim 52600 *vs.* \sim 212000 ng·h·mL⁻¹ for encapsulated GEN p.o. and free GEN i.v.) [Tamames-Tabar *et al.*, 2013]. This value was very similar to the one obtained by Yang *et al.*, which after the oral administration of free GEN to mice (D=20 mg·Kg⁻¹) was of 23.4% [Yang *et al.*, 2010].

GEN Biodistribution

Alongside the PK study, the tissue distribution was expressed as the GEN concentration after the p.o. administration of a single dose of 30 mg·Kg⁻¹ ($n=6$). Animals were sacrificed 4, 24 and 48 h post-administration. Free GEN was only found in liver 4 h post-administration (0.58 ± 0.47 μ g GEN·g tissue⁻¹). The large standard deviations in liver, suggested important interindividual differences. Moreover, and as seen in Figure 4 (page 124), the amount of free drug in mouse plasma at 4h was very low. This fact, together with its low $t_{1/2}$, could indicate that the amount of free drug distributed to other organs (*i.e.* kidneys) could be under the LOQ of the quantification technique [Tamames-Tabar *et al.*, 2013].

Rationally, due to the metabolic pathways GEN suffers in liver and in intestine [Steensma, 2006], we expected higher drug levels coming from the encapsulated group at 4 h. However, as the T_{max} was 4 h post-administration and the organs were analysed at the same time, it was suggested that after 4 h, no GEN tissue distribution due to the drug release (from the MOF) was achieved. In addition, the fact of discerning a higher encapsulated GEN accumulation in spleen after 24 h (1.28 ± 0.28 μ g GEN·g tissue⁻¹), could indicate that the MOFs had been sequestered by macrophages, and therefore, concentrate in this organ. Later, low GEN levels were observed in kidneys 48 h post-administration (0.16 ± 0.02 μ g GEN·g tissue⁻¹). These isoflavone levels could come from the released drug from MIL-100(Fe)_NPs, particles which were previously accumulated in spleen, and then eliminated via kidneys.

In conclusion, the encapsulation of GEN inside MIL-100(Fe)_NPs, protected from its metabolisation, and therefore, was detected for a longer time when compared to the free drug. Moreover, these encouraging results obtained after the p.o. administration of this formulation, make an appealing advance in the framework of MOFs, as well as in drug delivery.

4. CONCLUSION

In this study, we have accomplished reproducible MOF-GEN formulations with loads between 160-340 $\mu\text{g GEN}\cdot\text{mg formulation}^{-1}$, values that are in the scope of other reported MOF formulations. Moreover, this GEN load is higher when compared to other reported GEN and bioflavonoid formulations, except for kaempferol. The *in vitro* release studies, showed that GEN exhibited long release profiles within MOFs when compared to other reported MOF formulations, with the exception of MIL-88C(Fe)_NPs. Furthermore, an important complexation between the drug and the MOF has been observed, due to a relevant drug-host interaction. The addition of a strong base, allowed quantifying the total GEN released. This slow release profile has been also described for other bioflavonoids, most probably due to its high hydrophobicity.

The *in vivo* evaluation of MIL-100(Fe)_NPs in a mouse model showed that after the administration of the encapsulated drug p.o., higher plasmatic levels for an extended period of time were observed, as well as an increase in pharmacokinetic parameters, such as, the drug oral bioavailability, amidst among others. Moreover, the MOF worked as a shelter for GEN, impeding its metabolisation. Hence, GEN levels were detected in organs up to 48 h post-administration.

ACKNOWLEDGEMENTS

Authors thank the technical support of F. Ragon for MOF synthesis guidance, D. Cunha for supplying various MOFs, M. A. Campanero for HPLC assessment and E. Imbuluzqueta and H. Lana for technical support with the *in vivo* experiments. Authors would like to acknowledge Asociación de Amigos de la Universidad de Navarra for the predoctoral grant of C.T-T. This work was partially supported by FeUN (Fundación Empresa Universidad de Navarra) and the CNRS funding and the EU funding through the ERC-2007-209241-BioMOFs ERC (C.S., P.H.).

REFERENCES

- Adair, J.H.; Parette, M.P.; Altinoğlu, E.İ.; Kester, M., **2010**. Nanoparticulate alternatives for drug delivery. *ACS Nano*, 4(9): 4967-4970.
- Agostoni, V.; Chalati, T.; Horcajada, P.; Willaime, H.; Anand, R.; Semiramo, N.; Baati, T.; Hall, S.; Maurin, G.; Chacun, H.; Bouchemal, K.; Martineau, C.; Taulelle, F.; Couvreur, P.; Rogez-Kreuz,

- C.; Clayette, P.; Monti, S.; Serre, C.; Gref, R., **2013**. Towards an improved anti HIV activity of NRTI via metal-organic frameworks nanoparticles. *Adv. Healthc. Mater.*, 2(12): 1630-1637.
- Agostoni, V.; Anand, R.; Monti, S.; Hall, S.; Maurin, G.; Horcajada, P.; Serre, C.; Bouchemal, K.; Gref, R., **2013**. Impact of phosphorylation on the encapsulation of nucleoside analogues within porous iron(III) metal-organic framework MIL-100(Fe) nanoparticles. *J. Mater. Chem. B*, 1(34): 4231-4242.
- Akiyama, T.; Ishida, J.; Nakagawa, S.; Ogawara, H.; Watanabe, S.; Itoh, N.; Shibuya, M.; Fukami, Y., **1987**. Genistein, a specific inhibitor of tyrosine-specific protein kinases. *J. Biol. Chem.*, 262(12): 5592-5595.
- Azarova, A.M.; Lin, R.-K.; Tsai, Y.-C.; Liu, L.F.; Lin, C.-P.; Lyu, Y.L., **2010**. Genistein induces topoisomerase II beta- and proteasome-mediated DNA sequence rearrangements: implications in infant leukemia. *Biochem. Biophys. Res. Commun.*, 399(1): 66-71.
- Baati, T.; Njim, L.; Neffati, F.; Kerkeni, A.; Bouttemi, M.; Gref, R.; Najjar, M.F.; Zakhama, A.; Couvreur, P.; Serre, C.; Horcajada, P., **2013**. In depth analysis of the *in vivo* toxicity of nanoparticles of porous iron(III) metal-organic frameworks. *Chem. Sci.*, 4: 1597-1607.
- Bárcia, P.S.; Guimarães, D.; Mendes, P.A.P.; Silva, J.A.C.; Guillerm, V.; Chevreau, H.; Serre, C.; Rodrigues, A.E., **2011**. Reverse shape selectivity in the adsorption of hexane and xylene isomers in MOF UiO-66. *Microporous Mesoporous Mater.*, 139(1): 67-73.
- Bandle, O.J.; Osheroff, N., **2007**. Bioflavonoids as poisons of human topoisomerase II α and II β . *Biochemistry*, 46(20): 6097-6108.
- Banerjee, D.; Sengupta, S., **2011**. Nanoparticles in cancer chemotherapy. *Prog. Mol. Biol. Transl. Sci.*, 104: 489-507.
- Banerjee, S.; Li, Y.; Wang, Z.; Sarkar, F.H., **2008**. Multi-targeted therapy of cancer by genistein. *Cancer Lett.*, 269(2): 226-242.
- Behloul, N.; Wu, G., **2013**. Genistein: promising therapeutic agent for obesity and diabetes treatment. *Eur. J. Pharmacol.*, 698(1-3): 31-38.
- Bellido, E.; Guillevic, M.; Hidalgo, T.; Santander-Ortega, M.J.; Serre, C.; Horcajada, P., **2014**. Understanding the colloidal stability of the mesoporous MIL-100(Fe) nanoparticles in physiological media. *Langmuir*, 30(20): 5911-5920.
- Bennett, J.O.; Yu, O.; Heatherly, L.G.; Krishnan, H.B., **2004**. Accumulation of genistein and daidzein, soybean isoflavones implicated in promoting human health, is significantly elevated by irrigation. *J. Agric. Food Chem.*, 52(25): 7574-7579.
- Bolli, A.; Marino, M.; Rimbach, G.; Fanali, G.; Fasano, M.; Ascenzi, P., **2010**. Flavonoid binding to human serum albumin. *Biochem. Biophys. Res. Commun.*, 398(3): 444-449.
- Brzezińska-Błaszczyk, E.; Pietrzak, A.; Misiak-Tłoczek, A.H., **2007**. Tumor necrosis factor (TNF) is a potent rat mast cell chemoattractant. *J. Interferon Cytokine Res.*, 27(11): 911-920.
- Bury, K.; Neugebauer, D., **2014**. Novel self-assembly graft copolymers as carriers for anti-inflammatory drug delivery. *Int. J. Pharm.*, 460(1-2): 150-157.
- Castro, A.F.; Altenberg, G.A., **1997**. Inhibition of drug transport by genistein in multidrug-resistant cells expressing P-glycoprotein. *Biochem. Pharmacol.*, 53(1): 89-93.

- Cavka, J.H.; Jakobsen, S.; Olsbye, U.; Guillou, N.; Lamberti, C.; Bordiga, S.; Lillerud, K.P., **2008**. A new zirconium inorganic building brick forming metal organic frameworks with exceptional stability. *J. Am. Chem. Soc.*, 130(42): 13850-13851.
- Chalati, T.; Horcajada, P.; Couvreur, P.; Serre, C.; Ben Yahia, M.; Maurin, G.; Gref, R., **2011**. Porous metal organic framework nanoparticles to address the challenges related to busulfan encapsulation. *Nanomedicine (UK)*, 6(10): 1683-1695.
- Chan, L.M.S.; Lowes, S.; Hirst, B.H., **2004**. The ABCs of drug transport in intestine and liver: efflux proteins limiting drug absorption and bioavailability. *Eur. J. Pharm. Sci.*, 21(1): 25-51.
- Chen, J.; Lin, H.; Hu, M., **2003**. Metabolism of flavonoids via enteric recycling: role of intestinal disposition. *J. Pharm. Exp. Ther.*, 304(3): 1228-1235.
- Cohen, R.; Orlova, Y.; Kovalev, M.; Ungar, Y.; Shimoni, E., **2008**. Structural and functional properties of amylose complexes with genistein. *J. Agric. Food Chem.*, 56(11): 4212-4218.
- Cunha, D.; Ben Yahia, M.; Hall, S.; Miller, S.R.; Chevreau, H.; Elkaïm, E.; Maurin, G.; Horcajada, P.; Serre, C., **2013**. Rationale of drug encapsulation and release from biocompatible porous Metal–Organic Frameworks. *Chem. Mater.*, 25(14): 2767-2776.
- Cunha, D.; Gaudin, C.; Collinet, I.; Horcajada, P.; Maurin, G.; Serre, C., **2013**. Rationalization of the entrapping of bioactive molecules into a series of functionalized porous zirconium terephthalate MOFs. *J. Mater. Chem. B.*, 1(8): 1101-1108.
- Della Rocca, J.; Liu, D.; Lin, W., **2011**. Nanoscale metal–organic frameworks for biomedical imaging and drug delivery. *Accounts Chem. Res.*, 44(10): 957-968.
- de Oliveira, C.A.F.; da Silva, F.F.; Jimenez, G.C.; da S. Neto, J.F.; de Souza, D.M.B.; de Souza, I.A.; Junior, S.A., **2013**. MOF@activated carbon: a new material for adsorption of aldicarb in biological systems. *Chem. Commun.*, 49(58): 6486-6488.
- Devautour-Vinot, S.; Martineau, C.; Diaby, S.; Ben-Yahia, M.; Miller, S.; Serre, C.; Horcajada, P.; Cunha, D.; Tautelle, F.; Maurin, G., **2013**. Caffeine confinement into a series of functionalised porous zirconium MOFs: a joint experimental/modeling exploration. *J. Phys. Chem. C.*, 117(22): 11694-11704.
- Diebold, Y.; Calonge, M., **2010**. Applications of nanoparticles in ophthalmology. *Prog. Retin. Eye Res.*, 29(6): 596-609.
- Garibay, S.; Cohen, S.M., **2010**. Isoreticular synthesis and modification of frameworks with the UiO-66 topology. *Chem. Commun.*, 46(41): 7700-7702.
- Gaudin, C.; Cunha, D.; Ivanoff, E.; Horcajada, P.; Chevé, G.; Yasri, A.; Loget, O.; Serre, C.; Maurin, G., **2012**. A quantitative structure activity relationship approach to probe the influence of the functionalization on the drug encapsulation of porous metal-organic frameworks. *Micropor. Mesopor. Mater.*, 157: 124-130.
- Ge, Y.-B.; Chen, D.-W.; Xie, L.-P.; Zhang, R.-Q., **2007**. Optimized preparation of daidzein-loaded chitosan microspheres and *in vivo* evaluation after intramuscular injection in rats. *Int. J. Pharm.*, 338(1-2): 142-151.
- Ghosh, S.; Dungdung, S.R.; Chowdhury, S.T.; Mandal, A.K.; Sarkar, S.; Ghosh, D.; Das, N., **2011**. Encapsulation of the flavonoid quercetin with an arsenic chelator into nanocapsules enables the

simultaneous delivery of hydrophobic and hydrophilic drugs with a synergistic effect against chronic arsenic accumulation and oxidative stress. *Free Radic. Biol. Med.*, 51(10): 1893-1902.

Guillerm, V.; Ragon, F.; Dan-Hardi, M.; Devic, T.; Vishnuvarthan, M.; Campo, B.; Vimont, A.; Clet, G.; Yang, Q.; Maurin, G.; Férey, G.; Vittadini, A.; Gross, S.; Serre, C., **2012**. A series of isorecticular, highly stable, porous zirconium oxide based metal-organic frameworks. *Angew. Chem. Int. Edit.*, 51(37): 9267-9271.

Hasan, Z.; Choi, E.-J.; Jhung, S. H., **2013**. Adsorption of naproxen and clofibrac acid over a metal-organic framework MIL-101 functionalized with acidic and basic groups. *Chem. Eng. J.*, 219: 537-544.

He, C.; Lu, K.; Liu, D.; Lin, W., **2014**. Nanoscale metal-organic frameworks for the co-delivery of cisplatin and pooled siRNAs to enhance therapeutic efficacy in drug-resistant ovarian cancer cells. *J. Am. Chem. Soc.* 136(14): 5181-5184.

Hinks, N.J.; McKinlay, A.C.; Xiao, B.; Wheatley, P.S.; Morris, R.E., **2010**. Metal organic frameworks as NO delivery materials for biological applications. *Micropor. Mesopor. Mater.*, 129(3): 330-334.

Horcajada, P.; Gref, R.; Baati, T.; Allan, P.K.; Maurin, G.; Couvreur, P.; Férey, G.; Morris, R.E.; Serre, C., **2012**. Metal-organic frameworks in biomedicine. *Chem. Rev.*, 112(2): 1232-1268.

Horcajada, P.; Serre, C.; McKinlay, A.C.; Morris, R.E., **2011**. "Biomedical applications of metal-organic frameworks" in *Metal-Organic Frameworks: Applications from Catalysis to Gas Storage*, ed. D. Farrusseng, Wiley-VCH Verlag GmbH & Co. KGaA, Weinheim, pp. 213-250.

Horcajada, P.; Chalati, T.; Serre, C.; Gillet, B.; Sebrie, C.; Baati, T.; Eubank, J.F.; Heurtaux, D.; Clayette, P.; Kreuz, C.; Chang, J.-S.; Hwang, Y.K.; Marsaud, V.; Bories, P.-N.; Cynober, L.; Gil, S.; Férey, G.; Couvreur, P.; Gref, R., **2010**. Porous metal-organic-framework nanoscale carriers as a potential platform for drug delivery and imaging. *Nat. Mater.*, 9(2): 172-178.

Horcajada, P.; Serre, C.; Maurin, G.; Ramsahye, N.A.; Balas, F.; Vallet-Regi, M.; Sebban, M.; Taudelle, F.; Férey, G., **2008**. Flexible porous metal-organic frameworks for a controlled drug delivery. *J. Am. Chem. Soc.*, 130(21): 6774-6780.

Horcajada, P.; Surblé, S.; Serre, C.; Hong, D.-H.; Seo, Y.-H.; Chang, J.-S.; Grenèche, J.-M.; Margiolaki, I.; Férey, G., **2007**. Synthesis and catalytic properties of MIL-100(Fe), an iron (III) carboxylate with large pores. *Chem. Commun.*, 27: 2820-2822.

Horcajada, P.; Serre, C.; Vallet-Regí, M.; Sebban, M.; Taulelle, F.; Férey, G., **2006**. Metal-organic frameworks as efficient materials for drug delivery. *Angew. Chem. Int. Edit.*, 45(36): 6120-6124.

Huxford, R.C.; Della Rocca, J.; Lin, W., **2010**. Metal-organic frameworks as potential drug carriers. *Curr. Opin. Chem. Biol.*, 14(2): 262-268.

Katz, M.J.; Brown, Z.J.; Colón, Y.J.; Siu, P.W.; Scheidt, K.A.; Snurr, R.Q.; Hupp, J.T.; Farha, O.K., **2013**. A facile synthesis of UiO-66, UiO-67 and their derivatives. *Chem. Commun.*, 49: 9449-9451.

Ke, F.; Yuan, Y.-P.; Qiu, L.-G.; Shen, Y.-H.; Xie, A.-J.; Zhu, J.-F.; Tian, X.-Y.; Zhang, L.-D., **2011**. Facile fabrication of magnetic metal-organic framework nanocomposites for potential targeted drug delivery. *J. Mater. Chem.*, 21(11): 3843-3848.

- Keskin, S.; Kizilel, S., **2010**. Biomedical applications of metal organic frameworks. *Ind. Eng. Chem. Res.*, 50(4): 1799-1812.
- Khan, N. A.; Hasan, Z.; Jhung, S. H., **2013**. Adsorptive removal of hazardous materials using metal-organic frameworks (MOFs): a review. *J. Hazardous Mater.*, 244-245: 444-456.
- King, R. A.; Bursill, D. B., **1998**. Plasma and urinary kinetics of the isoflavones daidzein and genistein after a single soy meal in humans. *Am. J. Clin. Nutr.*, 67(5): 867-872.
- Kobayashi, S.; Shinohara, M.; Nagai, T.; Konishi, Y., **2013**. Transport mechanisms of soy isoflavones and their microbial metabolites dihydrogenistein and dihydrodaidzein across monolayers and membranes. *Pharmaceut. Anal. Acta*, 4(4): 227-233.
- Lamartiniere, C.A.; Cotroneo, M.S.; Fritz, W.A.; Wang, J.; Mentor-Marcel, R.; Elgavish, A., **2002**. Genistein chemoprevention: timing and mechanisms of action in murine mammary and prostate. *J. Nutr.*, 132(3): 552S-558S.
- Lamartiniere, C.A., **2000**. Protection against breast cancer with genistein: a component of soy. *Am. J. Clin. Nutr.*, 71(6): 1705S-1707.
- Lansdell, K.A.; Cai, Z.; Kidd, J.F.; Sheppard, D.N., **2000**. Two mechanisms of genistein inhibition of cystic fibrosis transmembrane conductance regulator Cl⁻ channels expressed in murine cell line. *J. Phys.*, 524(2): 317-330.
- Lee, Y.-R.; Kim, J.; Ahn, W.-S., **2013**. Synthesis of metal-organic frameworks: a mini review. *Korean J. Chem. Eng.*, 30(9): 1667-1680.
- Li, W.; Frame, L.T.; Hirsch, S.; Cobos, E., **2010**. Genistein and hematological malignancies. *Cancer Lett.*, 296(1): 1-8.
- Liao, W.; Jin, G.; Zhao, M.; Yang, H., **2013**. The effect of genistein on the content and activity of α - and β -secretase and protein kinase c in $\alpha\beta$ -injured hippocampal neurons. *Basic Clin. Pharmacol. Toxicol.*, 112(3): 182-185.
- Liédana, N.; Galve, A.; Rubio, C.; Téllez, C.; Coronas, J., **2012**. Caf@ZIF-8: one-step encapsulation of caffeine in MOF. *ACS Appl. Mater. Interfaces*, 4(9): 5016-5021.
- Liu, W.-L.; Lo, S.-H.; Singco, B.; Yang, C.-C.; Huang, H.-Y.; Lin, C.-H., **2013**. Novel trypsin-FITC@MOF bioreactor efficiently catalyzes protein digestion. *J. Mater. Chem. B*, 1(7): 928-932.
- Liu, Y.; Hu, M., **2002**. Absorption and metabolism of flavonoids in the caco-2 cell culture model and a perused rat intestinal model. *Drug Metab. Dispos.*, 30(4): 370-377.
- Lykourinou, V.; Chen, Y.; Wang, X.-S.; Meng, L.; Hoang, T.; Ming, L.-J.; Musselman, R.L.; Ma, S., **2011**. Immobilization of MP-11 into a mesoporous metal-organic framework, MP-11@mesomof: a new platform for enzymatic catalysis. *J. Am. Chem. Soc.*, 133(27): 10382-10385.
- Mahata, P.; Prabu, M.; Natarajan, S., **2008**. Role of temperature and time in the formation of infinite -M-O-M- linkages and isolated clusters in MOFs: a few illustrative examples. *Inorg. Chem.*, 47(19): 8451-8463.
- Makishima, M.; Honma, Y.; Hozumi, M.; Sampi, K.; Hattori, M.; Umezawa, K.; Motoyoshi, K., **1991**. Effects of inhibitors of protein tyrosine kinase activity and/or phosphatidylinositol turnover on differentiation of some human myelomonocytic leukemia cells. *Leuk. Res.*, 15(8): 701-708.

- Ming, L.-G.; Chen, K.-M.; Xian, C.J., **2013**. Functions and action mechanisms of flavonoids genistein and icariin in regulating bone remodeling. *J. Cell. Physiol.*, 228(3): 513-521.
- Motlekar, N.; Khan, M.A.; Youan, B.-B.C., **2006**. Preparation and characterization of genistein containing poly(ethylene glycol) microparticles. *J. Appl. Pol. Sci.*, 101(3): 2070-2078.
- MSDS Data Sheet. **2014**. Last consulted May 2014. (http://www.spectrex.com/html_files2/pdf/MSDSXDRedSolution.pdf)
- National Cancer Institute. **2013**. Last consulted May 2013. (<http://nano.cancer.gov/>)
- Novio, F.; Simmchen, J.; Vázquez-Mera, N.; Amorín-Ferré, L.; Ruiz-Molina, D., **2013**. Coordination polymer nanoparticles in medicine. *Coord. Chem. Rev.*, 257(19–20): 2839-2847.
- Pavese, J.M.; Farmer, R.L.; Bergan, R.C., **2010**. Inhibition of cancer cell invasion and metastasis by genistein. *Cancer Metastasis Rev.*, 29(3): 465-482.
- Pham, J.; Brownlow, B.; Elbayoumi, T., **2013**. Mitochondria-specific pro-apoptotic activity of genistein lipidic nanocarriers. *Mol. Pharm.*, 10(10): 3789-3800.
- Polito, F.; Marini, H.; Bitto, A.; Irrera, N.; Vaccaro, M.; Adamo, E.B.; Micali, A.; Squadrito, F.; Minutoli, L.; Altavilla, D., **2012**. Genistein aglycone, a soy-derived isoflavone, improves skin changes induced by ovariectomy in rats. *Br. J. Pharmacol.*, 165(4): 994-1005.
- Polkowski, K.; Mazurek, A.P., **2000**. Biological properties of genistein. A review of *in vitro* and *in vivo* data. *Acta Pol. Pharm.*, 57(2): 135-155.
- Rieter, W.J.; Taylor, K.M.L.; An, H.; Lin, W.; Lin, W., **2006**. Nanoscale metal–organic frameworks as potential multimodal contrast enhancing agents. *J. Am. Chem. Soc.*, 128(28): 9024-9025.
- Sánchez, Y.; Calle, C.; de Blas, E.; Aller, P., **2009**. Modulation of arsenic trioxide-induced apoptosis by genistein and functionally related agents in U937 human leukaemia cells. Regulation by ROS and mitogen-activated protein kinases. *Chemico-Biological Interactions*, 182(1): 37-44.
- Sarkar, F.H.; Li, Y., **2006**. Using chemopreventive agents to enhance the efficacy of cancer therapy. *Cancer Res.*, 66(7): 3347-3350.
- Scalia, S.; Trotta, V.; Traini, D.; Young, P.M.; Sticozzi, C.; Cervellati, F.; Valacchi, G., **2013**. Incorporation of quercetin in respirable lipid microparticles: Effect on stability and cellular uptake on A549 pulmonary alveolar epithelial cells. *Colloids Surf. B*, 112: 322-329.
- Schaate, A.; Roy, P.; Godt, A.; Lippke, J.; Waltz, F.; Wiebcke, M.; Behrens, P., **2011**. Modulated synthesis of Zr-based metal-organic frameworks: from nano to single crystals. *Chem. Eur. J.*, 17(24): 6643-6651.
- Serajuddin, A.T.M., **2007**. Salt formation to improve drug solubility. *Adv. Drug. Deliv. Rev.*, 59(7):603-616.
- Serpe, L., **2007**. “Conventional chemotherapeutic drug nanoparticles for cancer treatment”. Nanotechnologies for the Life Sciences, Wiley-VCH Verlag GmbH & Co. KGaA. DOI: 10.1002/9783527610419.ntlsoo60.
- Serre, C.; Mellot-Draznieks, C.; Surblé, S.; Audebrand, N.; Filinchuk, Y.; Férey, G., **2007**. Role of solvent-host interactions that lead to very large swelling of hybrid frameworks. *Science*, 315(5820): 1828-1831.

- Setchell, K.D.R.; Brown, N.M.; Desai, P.; Zimmer-Nechemias, L.; Wolfe, B.E.; Brashear, W.T.; Kirschner, A.S.; Cassidy, A.; Heubi, J.E., **2001**. Bioavailability of pure isoflavones in healthy humans and analysis of commercial soy isoflavone supplements. *J. Nutr.*, 131(4 Suppl): 1362S-1375S.
- Shin, J.; Shin, K.; Lee, H.; Nam, J.-B.; Jung, J.-E.; Ryu, J.-H.; Han, J.-H.; Suh, K.-D.; Kim, Y.-J.; Shim, J.; Kim, J.; Han, S.-H.; Char, K.; Kim, Y.M.; Chung, J.H.; Lee, M.J.; Kang, B.C.; Kim, J.-W., **2010**. Non-invasive transdermal delivery route using electrostatically interactive biocompatible nanocapsules. *Adv. Mater.*, 22(6): 739-743.
- Special Issue **2012**. Guest Editors J.R. Long and O.M. Yaghi. *Chem. Rev.*, 112: 673-1268.
- Steensma, A., **2006**. Bioavailability of genistein and its glycoside genistin. PhD Thesis (Wageningen University, The Netherlands).
- Sun, M.; Nie, S.; Pan, X.; Zhang, R.; Fan, Z.; Wang, S., **2014**. Quercetin-nanostructured lipid carriers: characteristics and anti-breast cancer activities *in vitro*. *Colloids Surf. B*, 113: 15-24.
- Sun, C.-Y.; Qin, C.; Wang, X.-L.; Yang, G.-S.; Shao, K.-Z.; Lan, Y.-Q.; Su, Z.-M.; Huang, P.; Wang, C.-G.; Wang, E.-B., **2012**. Zeolitic imidazolate framework-8 as efficient pH-sensitive drug delivery vehicle. *Dalton Trans.*, 41(23): 6906-6909.
- Tamames-Tabar, C.; Cunha, D.; Imbuluzqueta, E.; Ragon, F.; Serre, C.; Blanco-Prieto, M.J.; Horcajada, P., **2014**. Cytotoxicity of nanoscaled metal-organic frameworks. *J. Mater. Chem. B.*, 2: 262-271.
- Tamames-Tabar, C.; Imbuluzqueta, E.; Campanero, M.A.; Horcajada, P.; Blanco-Prieto, M.J., **2013**. A simple and robust high-performance liquid chromatography coupled to a diode-array detector method for the analysis of genistein in mouse tissues. *J. Chrom. B.*, 935: 47-53.
- Tang, J.; Xu, N.; Ji, H.; Liu, H.; Wang, Z.; Wu, L., **2011**. Eudragit nanoparticles containing genistein: formulation, development, and bioavailability assessment. *Int. J. Nanomedicine*, 6: 2429-2435.
- Tzeng, C.-W.; Yen, F.-L.; Wu, T.-H.; Ko, H.-H.; Lee, C.-W.; Tzeng, W.-S.; Lin, C.-C., **2011**. Enhancement of dissolution and antioxidant activity of kaempferol using a nanoparticle engineering process. *J. Agric. Food Chem.*, 59(9): 5073-5080.
- U.S. Environmental Protection Agency **1994**. Last consulted May 2014. (http://www.epa.gov/chemfact/s_dcm.txt)
- Versantvoort, C.H.; Rhodes, T.; Twentyman, P.R., **1996**. Acceleration of MRP-associated efflux of rhodamine 123 by genistein and related compounds. *Br. J. Cancer*, 74(12): 1949-1954.
- Wang, C.; Liu, D.; Lin, W., **2013**. Metal-organic frameworks as a tunable platform for designing functional molecular materials. *J. Am. Chem. Soc.*, 135(36): 13222-13234.
- Wang, Y.; Yang, J.; Liu, Y.-Y.; Ma, J.-F., **2013**. Controllable syntheses of porous metal-organic frameworks: encapsulation of LnIII cations for tunable luminescence and small drug molecules for efficient delivery. *Chem. Eur. J.*, 19(43): 14591-14599.
- Xiao, B.; Wheatley, P.S.; Zhao, X.; Fletcher, A.J.; Fox, S.; Rossi, A.G.; Megson, I.L.; Bordiga, S.; Regli, L.; Thomas, K.M.; Morris, R.E., **2007**. High-capacity hydrogen and nitric oxide adsorption and storage in a metal-organic framework. *J. Am. Chem. Soc.*, 129(5): 1203-1209.

- Yang, Z.; Zhu, W.; Gao, S.; Xu, H.; Wu, B.; Kulkarni, K., **2010**. Simultaneous determination of genistein and its four phase II metabolites in blood by a sensitive and robust UPLC-MS/MS method: application to an oral bioavailability study of genistein in mice. *J. Pharm. Biomed. Anal.*, 53(1): 81-89.
- Yu, X.; Zhu, J.; Mi, M.; Chen, W.; Pan, Q.; Wei, M., **2012**. Anti-angiogenic genistein inhibits VEGF-induced endothelial cell activation by decreasing PTK activity and MAPK activation. *Med. Oncol.*, 29(1): 349-357.
- Zhang, Y.; Gao, B.; Xu, Z., **2013**. Adsorption properties of polyvinyl-alcohol-grafted particles toward genistein driven by hydrogen-bond interaction. *J. Phys. Chem. B*, 117(18): 5730-5736.
- Zhang, W.; Huang, H.; Liu, D.; Yang, Q.; Xiao, Y.; Ma, Q.; Zhong, C., **2013**. A new metal-organic framework with high stability based on zirconium for sensing small molecules. *Micropor. Mesopor. Mater.*, 171: 118-124.
- Zhang, W.; Li, X.; Ye, T.; Chen, F.; Sun, X.; Kong, J.; Yang, X.; Pan, W.; Li, S., **2013**. Design, characterization, and *in vitro* cellular inhibition and uptake of optimized genistein-loaded NLC for the prevention of posterior capsular opacification using response surface methodology. *Int. J. Pharm.*, 454(1): 354-366.
- Zhou, S.; Hu, Y.; Zhang, B.; Teng, Z.; Gan, H.; Yang, Z.; Wang, Q.; Huan, M.; Mei, Q., **2008**. Dose-dependent absorption, metabolism, and excretion of genistein in rats. *J. Agric. Food Chem.*, 56(18): 8354-8359.

SUPPLEMENTARY INFORMATION
METAL-ORGANIC FRAMEWORKS: NEW DELIVERY
SYSTEMS FOR GENISTEIN ADMINISTRATION

SUPPLEMENTARY INFORMATION**METAL-ORGANIC FRAMEWORKS: NEW DELIVERY SYSTEMS FOR
GENISTEIN ADMINISTRATION**

C. Tamames-Tabar^{a,b}, F. Salles, C. Martineau^b, G. Maurin^c, C. Serre^b, P. Horcajada^b, M.J. Blanco-Prieto^a

^a*Department of Pharmacy and Pharmaceutical Technology, School of Pharmacy, University of Navarra, Irunlarrea 1, 31008 Pamplona, Spain.*

^b*Institut Lavoisier, UMR CNRS 8180, Université de Versailles Saint-Quentin-en-Yvelines, 45 Avenue des Etats-Unis, 78035 Versailles Cedex, France.*

^c*Institut Charles Gerhardt Montpellier UMR 5253 CNRS UM2, UM1, Université Montpellier 2, Place E. Bataillon, 34095 Montpellier Cedex 05, France.*

1. CHEMICALS AND REAGENTS

Dimethylsulphoxyde (DMSO), HPLC quality methanol (MeOH) and triethanolamine (TEA) were purchased from Merck (Germany). Dichloromethane (DCM) was acquired from Acros Organics (Belgium). Ethanol (96.2%, EtOH), acetone and *N,N'*-dimethylformamide (DMF) were purchased from Carlo Erba (Italy). Formic acid, monopotassium phosphate (KH₂PO₄), sodium chloride (NaCl), 7-ethoxycoumarin and poly(ethylene glycol) 400 (PEG 400) were purchased from Sigma-Aldrich (Spain). Genistein (GEN) was purchased from LC Laboratories (USA). Hydrochloric acid at 37% (HCl) and acetic acid (HAc) were purchased from Scharlau (Spain). Disodium phosphate (Na₂HPO₄) was purchased from Prolabo (Spain). Ultrapure water was used for all the experiments.

The organic linkers for the MOF synthesis 2-aminoterephthalate (BDC-NH₂), 1,3,5-benzenetricarboxylic acid (BTC), 2,6-naphthalenedicarboxylic acid (NDC) and 4,4'-biphenyldicarboxylic acid (BPDC), as well as the metal precursors (iron(III) chloride hexahydrate (FeCl₃·6H₂O) and zirconium(IV) chloride (ZrCl₄)) were purchased from Sigma-Aldrich (France). The organic linker 2,5-diperfluoromethyl terephthalic acid (BDC-2CF₃) was synthesised as previously reported [Kim and Swager, 2005].

2. MOF SYNTHESIS

2.1 Iron(III) Trimesate Nanoparticles (MIL-100(Fe)_NPs) or $\text{Fe}_3\text{O}(\text{OH})(\text{H}_2\text{O})_2[(\text{CO}_2)_3\text{C}_6\text{H}_3]_2 \cdot n\text{H}_2\text{O}$: The synthesis of MIL-100(Fe)_NPs has been performed according to the published procedure via microwave-assisted method [Garcia-Marquez *et al.*, 2012]. Briefly, 845 mg of 1,3,5-benzenetricarboxylic acid (BTC) were added to 20 mL of distilled water, followed by the addition of 2425 mg of the inorganic precursor iron(III) chloride hexahydrate ($\text{FeCl}_3 \cdot 6\text{H}_2\text{O}$). After, its activation was performed by suspending the NPs in 20 mL of EtOH, repeating this washing procedure 7 times. The resulting activated NPs were kept wet. Synthesis yield ~87%.

2.2 Iron(III) 2,6-Naphthalendicarboxylate Nanoparticles (MIL-88C(Fe)_NPs) or $\text{Fe}_3\text{O}(\text{OH})(\text{H}_2\text{O})_2[(\text{CO}_2)_2\text{C}_{10}\text{H}_6]_3 \cdot n\text{H}_2\text{O}$: MIL-88C(Fe)_NPs was synthesised according to the reported method [Serre *et al.*, 2007]. Briefly, a solution containing 432 mg of NDC in 40 mL of EtOH 96.2% was prepared. Next, 400 μL of TEA and 114 μL of HAc were added to the prior mix until total dissolution of the linker after 10 min of gentle magnetic stirring. Finally, 540 mg of $\text{FeCl}_3 \cdot 6\text{H}_2\text{O}$ were added. The mixture was sealed and heated at 85 °C for 5 min in a microwave oven (at 400 W; Mars-5, CEM) with a heating ramp of 40 sec. The MIL-88C(Fe)_NPs, recovered by centrifugation (10000 *g*/15 min), were activated suspending the NPs in 20 mL of EtOH, repeating this washing procedure 7 times. The resulting activated NPs were kept wet (in EtOH). Synthesis yield ~60%.

2.3 Zirconium(IV) Aminoterephthalate Microparticles (UiO-66-NH₂(Zr)_MPs) or $\text{Zr}_6\text{O}_4(\text{OH})_4[(\text{CO}_2)_2\text{C}_6\text{H}_3(\text{NH}_2)]_6 \cdot n\text{H}_2\text{O}$: UiO-66-NH₂(Zr)_MPs were prepared after the reported method [Cunha *et al.*, 2013]. Briefly, 494 mg of 2-aminoterephthalic acid (BDC-NH₂) were added to 3 mL of DMF, followed by the addition of 231 mg of the inorganic precursor zirconium(IV) chloride ZrCl_4 by solvothermal method. Finally, 200 mg of the recovered solid were suspended into 100 mL of DMF overnight, followed by the same procedure in MeOH. Synthesis yield ~70%.

2.4 Zirconium(IV) 2,5-Diperfluoromethylterephthalate Microparticles (UiO-66-2CF₃(Zr)_MPs) or $\text{Zr}_6\text{O}_4(\text{OH})_4[(\text{CO}_2)_2\text{C}_6\text{H}_2(\text{2CF}_3)_2]_6 \cdot n\text{H}_2\text{O}$: UiO-66-2CF₃(Zr)_MPs were prepared as previously reported [Cunha *et al.*, 2013]. Briefly, 302 mg of the organic linker perfluoroterephthalic acid (BDC-2CF₃) were added to 3 mL of DMF, followed by the addition of 231 mg of the inorganic precursor ZrCl_4 by solvothermal

method. Finally, 200 mg of the recovered solid were suspended into 100 mL of DMF overnight, followed by the same procedure in MeOH. Synthesis yield ~61%.

2.5 Zirconium(IV) 2,6-Naphthalendicarboxylate Microparticles (UiO-66_NDC(Zr)_MPs) or $Zr_6O_4(OH)_4[(CO_2)_2C_{10}H_6]_6 \cdot n \cdot H_2O$: The synthesis of UiO-66_NDC(Zr)_MPs was performed after the reported method [Garibay and Cohen, 2010]. Briefly, 216 mg of NDC and 117 mg of $ZrCl_4$ were placed in a 25 mL Teflon-lined steel autoclave. After, 2.5 mL of DMF and 143 μ L of AcH were added. The autoclave was sealed and heated at 220 °C (1h heating ramp) for 6 h. The sample was recovered by filtration and activated following 2 steps. First, the solid was dispersed in 100 mL of DMF at RT under stirring overnight. Second, the same procedure was repeated twice using MeOH. Synthesis yield ~55%.

2.6 Zirconium(IV) 4,4'-Biphenyldicarboxylate Microparticles (UiO-66_BPDC(Zr)_MPs) or $Zr_6O_4(OH)_4[(CO_2)_2C_{12}H_8]_6 \cdot n \cdot H_2O$: The synthesis of UiO-66_BPDC(Zr)_MPs was performed after the reported method [Schaate *et al.*, 2011; Cavka *et al.*, 2008]. Briefly, 242 mg of BPDC and 117 mg of $ZrCl_4$ were placed in a 25 mL Teflon-lined steel autoclave. After, 2.5 mL of DMF and 143 μ L of HAc were added. The sealed autoclave was placed in an oven at 220 °C for 12 h. The solid, recovered by filtration, was activated as previously described for UiO-66_NDC(Zr)_MPs. Synthesis yield ~53%.

2.7 Zirconium(IV) 4,4'-Biphenyldicarboxylate Microparticles (MIL-140C(Zr)_MPs) or $Zr_8O_8(OH)_4[(CO_2)_2C_{12}H_8]_6 \cdot n \cdot H_2O$: MIL-140C(Zr)_MPs were prepared as previously reported [Guillerm *et al.*, 2012]. Briefly, 2422 mg of the organic linker H₂BPDC were added to 25 mL of DMF, followed by the addition of 1165 mg of the inorganic precursor $ZrCl_4$ by solvothermal method. The sample was activated in 200 mL of DMF at 100 °C overnight. Then, the sample was filtered and left overnight in 200 mL of MeOH under continuous stirring. Synthesis yield ~67%.

3. GENISTEIN ENCAPSULATION

As seen in Table S1 (page 140), 3 different solvents were used for GEN encapsulation.

GEN was entrapped into the Zr-based solids by suspending the previously dehydrated (100 °C overnight) powdered samples in a 0.65 mg·mL⁻¹ GEN solution in DCM protected from light at room temperature (RT) under magnetic stirring for 24 h (see Table S2, page

141). The molar ratio material: drug was 1:2. The drug-containing solids were recovered by filtration and dried at 100 °C.

20 mg of MIL-88C(Fe)_NPs (note that the NPs are weighted wet based on the wet:dry ratio previously determined from NPs dry at 100 °C overnight) were suspended in 11.93 mL of a GEN ethanol solution (1 mg·mL⁻¹) protected from light at RT under stirring for 24 h.

Table S1. Solubility of GEN, boiling point and toxicological data of the solvents DCM, EtOH and H₂O.

Solvent	GEN solubility* (mg·mL ⁻¹)	Boiling point (°C)	LD ₅₀ (mg·Kg ⁻¹)**
DCM	2.0	40	2100
EtOH	1.3	78	7060
H ₂ O	1.4***	100	-

* Solubility values at RT.

**LD₅₀ (Lethal Dose 50) after oral administration in rats.

*** Solubility value for GCa (GEN calcium salt at 37 °C)

Prior to the encapsulation, MIL-100(Fe)_NPs were exchanged twice in pure water. To improve the GEN aqueous solubility, a calcium genistein salt (denoted GCa) was synthesised as following. 54 mg of commercialised GEN, 14.80 mg of Ca(OH)₂ and 2 mL of distilled water were added to a glass vial and maintained at RT under magnetic stirring away from light exposure for 24 h. Then, the formed grey coloured solution was centrifuged at 5000 *g* for 10 min, obtaining a light-grey pellet which was further dried at 100 °C. Considering the pH of the solution (10.5) and the GEN pK_a values (7.2, 10.0 and 13.1) reported by Zielonka and coworkers [Zielonka, Gebicki and Gryniewicz, 2003], the obtained solid corresponds to the dicalcium salt of GEN. The experimental aqueous solubility at 37 °C of GCa is much higher than the commercial GEN (1.4 mg·mL⁻¹ vs. 0.8 µg·mL⁻¹) (Table S1). Then, 60 mg of MIL-100(Fe)_NPs (note that the NPs are weighted wet based on the wet:dry ratio previously determined from NPs dried at 100 °C overnight) were suspended in 43.86 mL of an aqueous solution of GCa (1.14 mg·mL⁻¹) protected from light at 37 °C under stirring for 24 h. In the case of MOF NPs, the GEN containing MOF dispersion was centrifuged during 15 min at 21130 *g*. The encapsulation experiments were done keeping the molar ratio MOF:GEN equal to 1:2 for all the solids (Table S2, page 141).

Table S2. Encapsulation protocol for each formulation.

MOF	MOF (mg)	Drug	Drug (mg)	Solvent	Solvent (mL)	T (°C)
MIL-100(Fe)_NPs	60.00	GCa*	49.82	H ₂ O	43.86	37
MIL-88C(Fe)_NPs	20.00	GEN	11.93	EtOH	11.93	RT
UiO-66_NH ₂ (Zr)_MPs	100.00	GEN	30.84	DCM	47.45	RT
UiO-66_2CF ₃ (Zr)_MPs	40.00	GEN	8.71	DCM	13.41	RT
UiO-66_NDC(Zr)_MPs	20.00	GEN	5.55	DCM	8.53	RT
UiO-66_BPDC(Zr)_MPs	40.00	GEN	10.27	DCM	15.81	RT
MIL-140C(Zr)_MPs	50.00	GEN	9.72	DCM	14.95	RT

*GCa a calcium GEN salt was used for MIL-100(Fe)_NPs formulation.

RT=room temperature

The adsorbed drug amount was quantified by thermogravimetric analysis (TGA; Table S4 and Figure S3, pages 144 and 145, respectively), high performance liquid chromatography (HPLC, Table S6, page 151) and elemental analysis (EA; Table S4, page 144). The solids before and after the drug entrapping were characterized by X-Ray Powder Diffraction (XRPD; Figure S1, page 142), Dynamic Light Scattering (DLS; Table S3, page 143), ζ -potential (Table S3, page 143), N₂ adsorption porosimetry (Table S5 and Figure S4, page 146), Fourier-Transformed Infrared Spectroscopy (FTIR; Figure S5, pages 147-148) and solid state ¹³C-Nuclear Magnetic Resonance (NMR; Figure S6, page 149).

3.1 XRPD

X-ray powder diffraction (XRPD) patterns were measured using a high-throughput Bruker D8 Advance diffractometer working on transmission mode and equipped with a focusing Göbel mirror producing CuK α radiation ($\lambda=1.5418$ Å) and a LYNXEYE detector. Data were collected at room temperature (RT), in the 2θ range 3–30°, with a 0.02° step width.

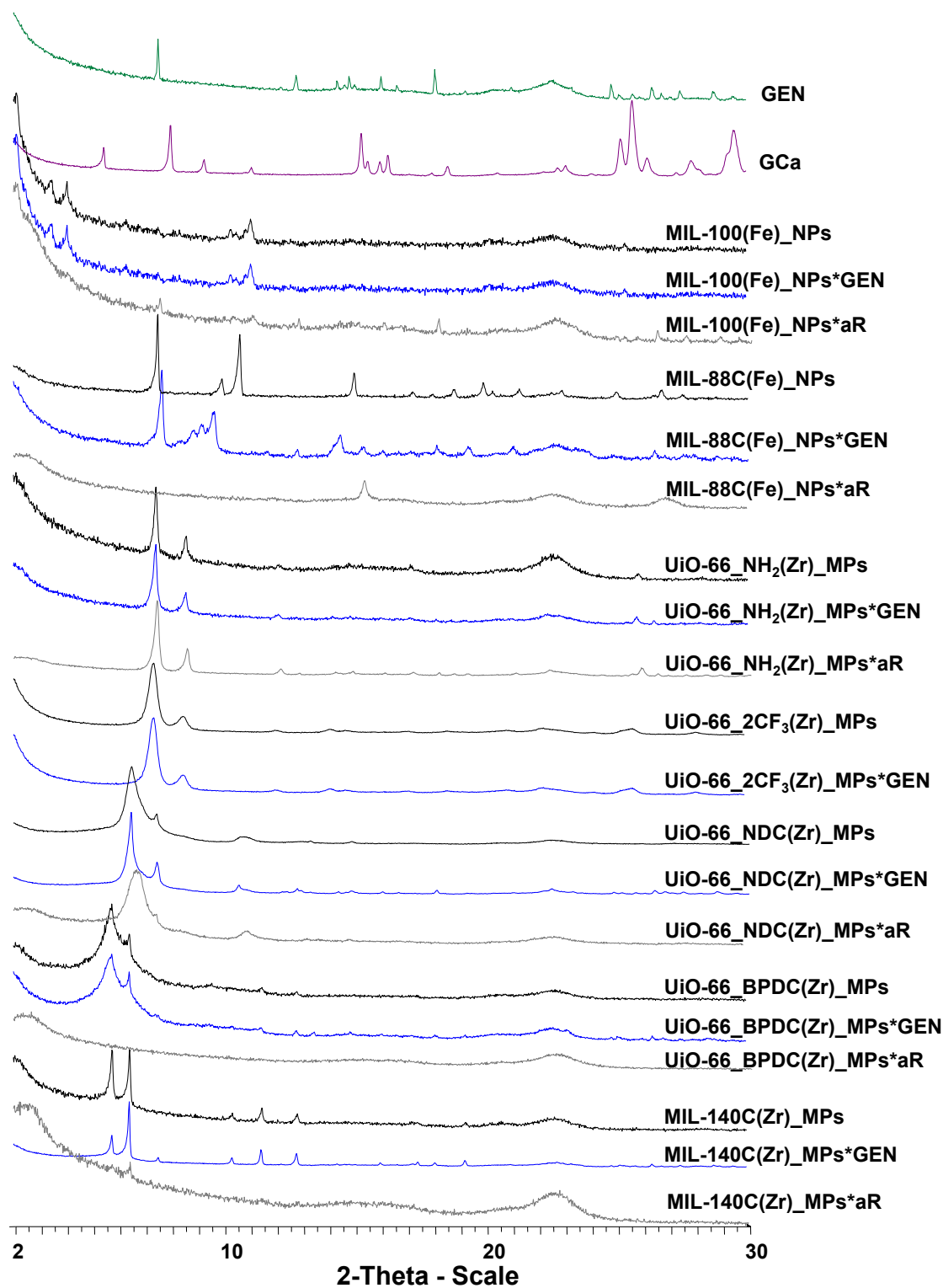


Figure S1. XRPD patterns of the raw (black), GEN-encapsulated (blue) and samples after *in vitro* release (grey). Commercial GEN (green) and GEN calcium salt or GCa (purple) are also displayed.

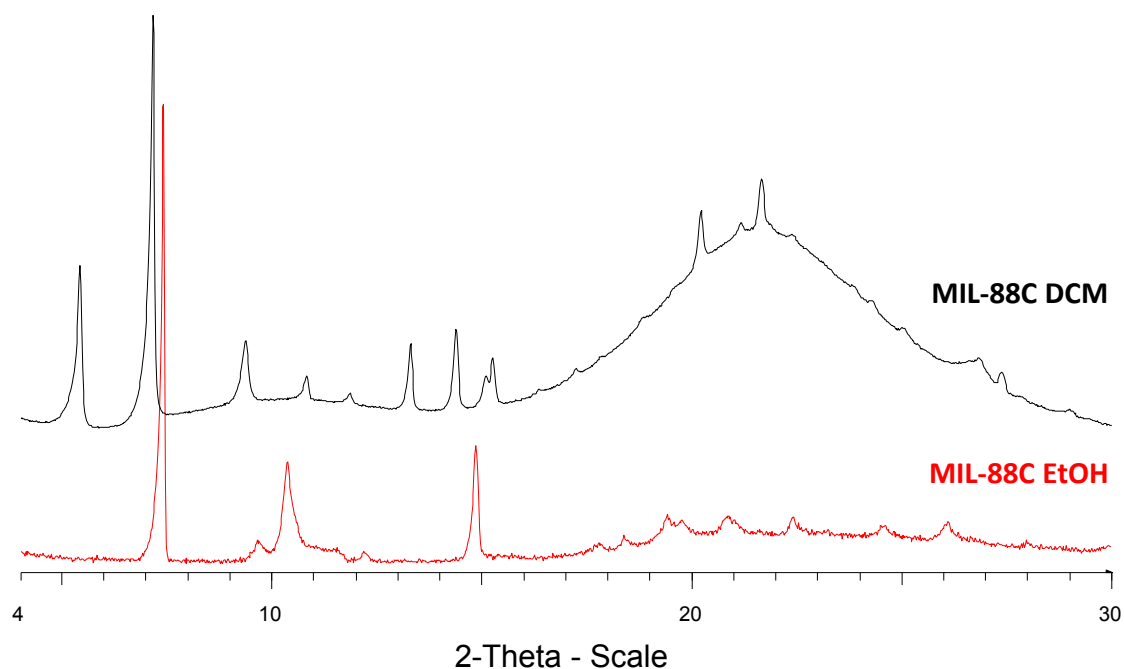


Figure S2. XRPD of the MIL-88C solid immersed in EtOH or DCM.

3.2 Particle Size and ζ -Potential

DLS particle size and ζ -potential measurements were carried out with a Zetasizer Nano Series Nano-ZS[®] from Malvern Instruments (UK). The particles were dispersed in ultrapure water by using a Microson[™] XL 2000 ultrasonic liquid processor (Qsonica, USA) during 30 seconds at 20 watt with amplitude of 30%.

Table S3. Particle size and ζ -potential in ultrapure water of the MOF solids before and after genistein encapsulation.

MOF	Particle size (nm)		ζ -potential (mV)	
	Raw MOF	Encapsulation	Raw MOF	Encapsulation
MIL-100(Fe)_NPs	128.4±15.0	139.4±16.9	20.2±1.3	-15.68±3.5
MIL-88C(Fe)_NPs	120.7±12.0	144.0±7.2	6.6±0.7	-13.90±2.0
UiO-66_NH ₂ (Zr)_MPs	-	-	-5.7±1.5	-6.34±1.0
UiO-66_2CF ₃ (Zr)_MPs	-	-	33.0±3.9	-18.1±2.36
UiO-66_NDC(Zr)_MPs	-	-	-18.0±3.0	-24.8±0.9
UiO-66_BPDC(Zr)_MPs	-	-	-24.4±0.3	-5.9±0.7
MIL-140C(Zr)_MPs	-	-	-15.7±3.7	-24.7±1.5

3.3 Genistein Quantification

The GEN encapsulation was determined by the combination of three different techniques, TGA, EA and HPLC. Approximately 5-10 mg of each sample were used for TGA measurements. Samples were analysed under an oxygen flow ($2\text{ }^{\circ}\text{C}\cdot\text{min}^{-1}$ scan rate) using a Perkin Elmer Diamond TGA/DTA STA 6000 running from RT to $600\text{ }^{\circ}\text{C}$ (USA).

HPLC analysis was performed with a RP-C₁₈ 3 μm Gemini NX 150 x 2.0 mm column from Phenomenex (USA), protected by a KJO-4282 Security Guard Cartridge from the same package from Phenomenex (USA), using a Agilent Technologies Series 1200 equipped with an Infinity Diode Array Detector HPLC system and controlled by ChemStation for LC 3D systems from Agilent Technologies (USA). The analysis was done with a mobile phase containing MeOH and formic acid (0.1%) at a ratio of 60:40 (v/v), at a flow rate of $0.160\text{ mL}\cdot\text{min}^{-1}$, an injection volume of $5\text{ }\mu\text{L}$, followed by needle wash, monitoring the GEN peaks at 260 nm (retention time of 5.3 min). The temperature of the analysis was not controlled (RT). The calibration curve for GEN was set in the interval of $0.01\text{-}10\text{ }\mu\text{g}\cdot\text{mL}^{-1}$, was $y=221.5x-3.2186$ (LOQ and LOD= $0.01\text{ }\mu\text{g}\cdot\text{mL}^{-1}$) ($R^2=0.9995$).

Table S4. Quantification of the GEN loading by TGA, EA and HPLC.

MOF	GEN (wt%)*		
	TGA**	EA	HPLC
MIL-100(Fe)_NPs	174.0 ± 24.9	18.4	76.4 ± 4.4
MIL-88C(Fe)_NPs	201.7 ± 51.7	22.2	26.5 ± 1.7
UiO-66_NH ₂ (Zr)_MPs	159.3 ± 47.7 $335.9\pm 24.8^{***}$	23.6	14.2 ± 3.2
UiO-66_2CF ₃ (Zr)_MPs	157.0 ± 44.8	16.5	15.3 ± 1.9
UiO-66_NDC(Zr)_MPs	329.3 ± 45.7	29.4	16.5 ± 1.6
UiO-66_BPDC(Zr)_MPs	337.7 ± 24.9	36.2	23.6 ± 2.2
MIL-140C(Zr)_MPs	225.6 ± 88.2	22.5	16.6 ± 2.5

*Values corresponding to the dry MOF without GEN.

**Values in $\mu\text{g GEN}\cdot\text{mg formulation}^{-1}$.

***Values of the second impregnation.

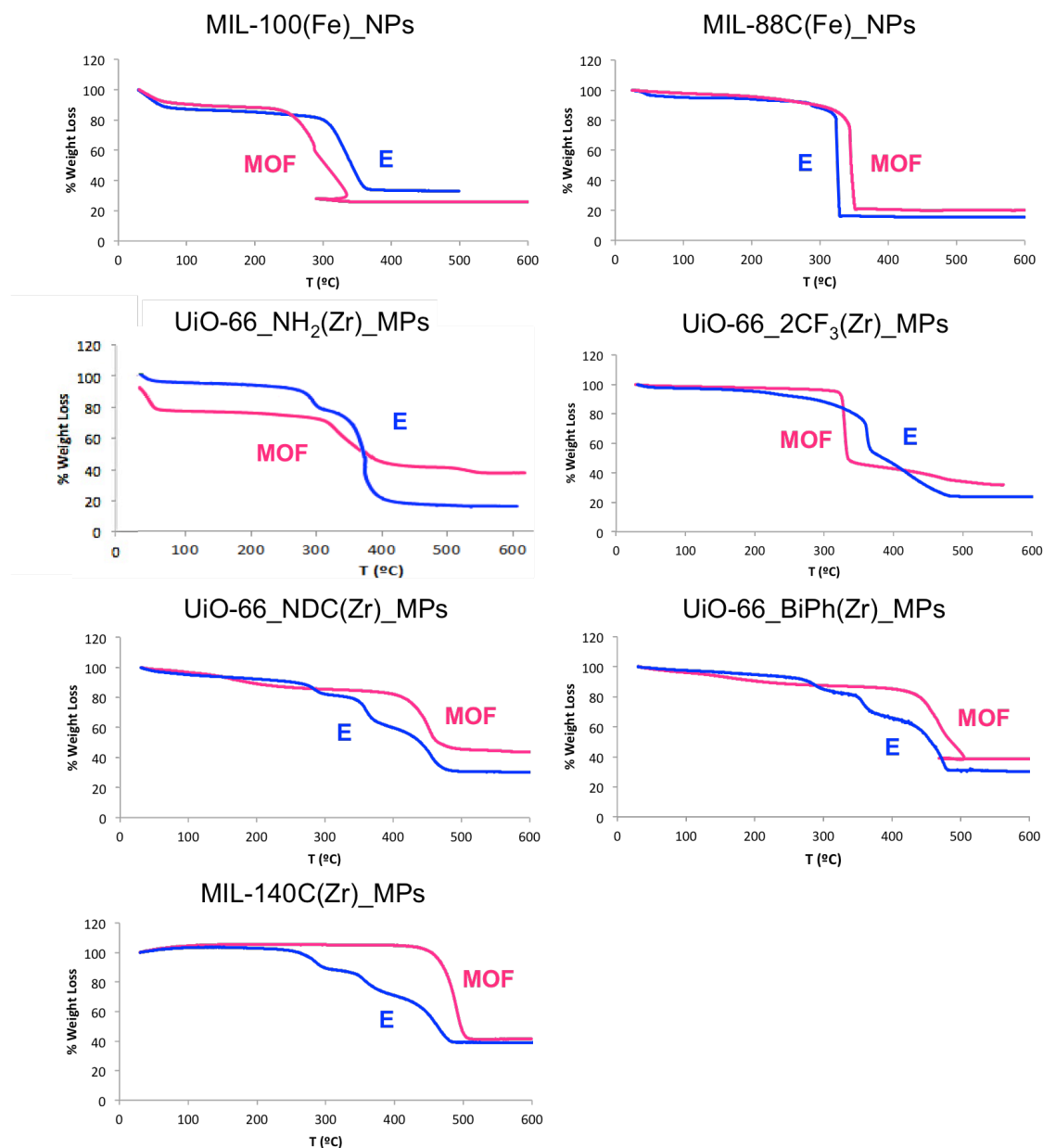


Figure S3. TGA results of the raw samples or MOF (pink) and of the formulation (blue).

3.4 N₂ Adsorption

The N₂ isotherms (Figure S3 and Table S5, pages 145 and 146) from the rigid MOFs were obtained at 77 K using a Belsorp Mini (Bel, Japan). Prior to the analysis, approximately 40-60 mg of the samples were evacuated at 200 °C under vacuum overnight.

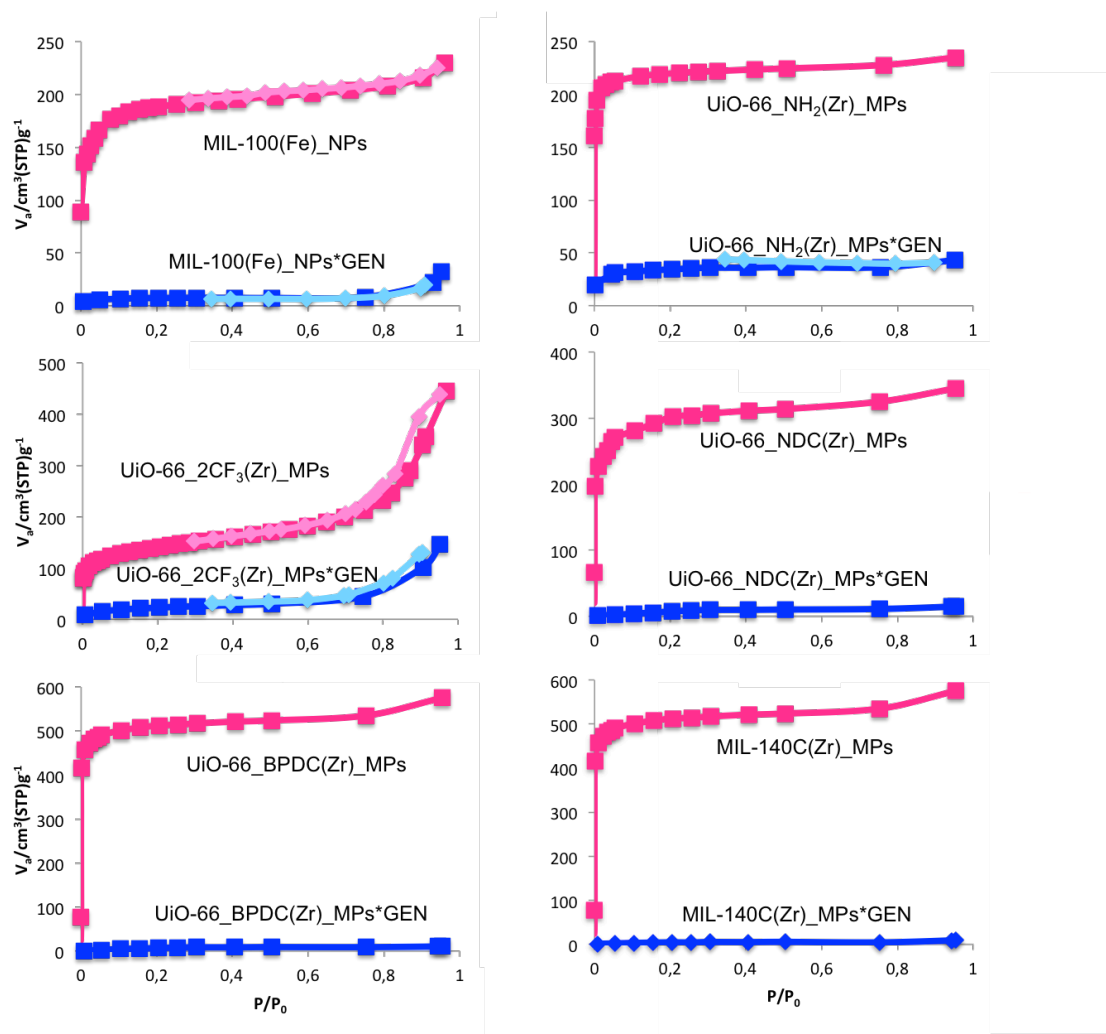


Figure S4. Nitrogen isotherms of all the rigid MOFs: adsorption of the raw (dark pink) and of the formulations (dark blue) and desorption of the raw (light pink) and of the formulations (light blue).

Table S5. BET surface area and micropore volume before and after the GEN encapsulation (denoted as raw MOF sample and formulation, respectively).

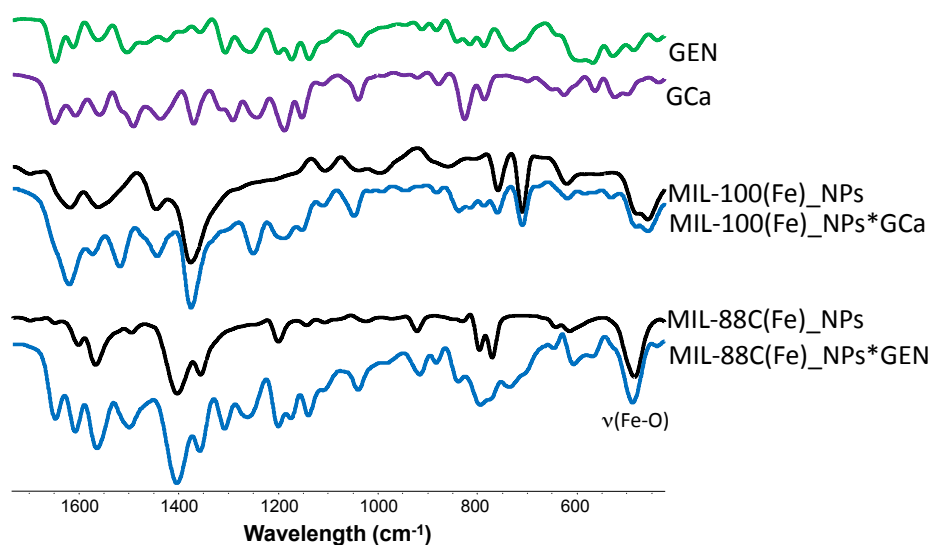
Samples	Raw MOF		Formulation	
	Pore Volume ($\text{cm}^3 \cdot \text{g}^{-1}$)*	BET Surface Area ($\text{m}^2 \cdot \text{g}^{-1}$)	Pore Volume ($\text{cm}^3 \cdot \text{g}^{-1}$)*	BET Surface Area ($\text{m}^2 \cdot \text{g}^{-1}$)
MIL-100(Fe)_NPs	0.30	620	0.04	20
UiO-66_NH ₂ (Zr)_MPs	0.34	680	0.06	110
UiO-66_2CF ₃ (Zr)_NPs	0.23	500	0.05	80
UiO-66_NDC(Zr)_NPs	0.72	1110	0.03	30
UiO-66_BPDC(Zr)_MPs	0.64	1240	0.02	30
MIL-140C(Zr)_MPs	0.80	1620	0.01	20

*Corresponding to micropore ($P/P_0 < 0.3$)

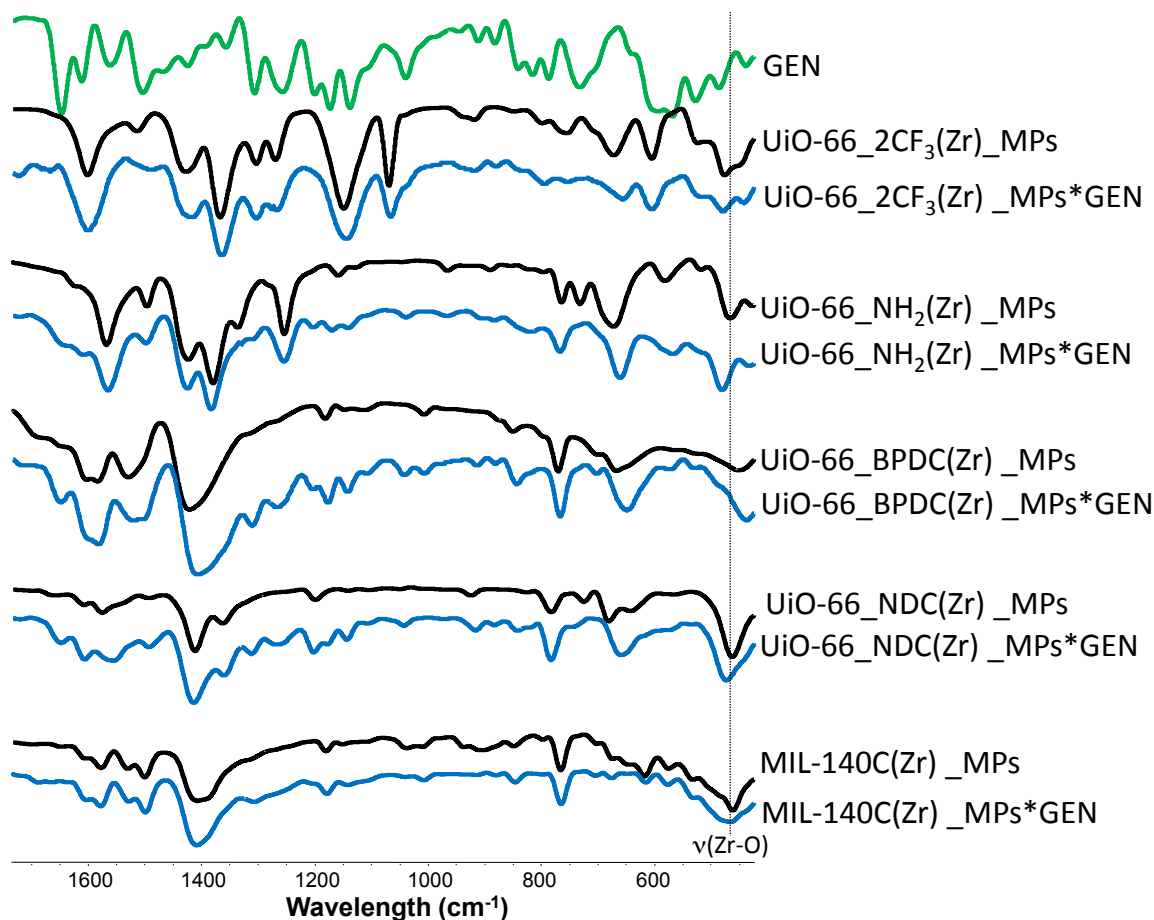
Note that the porosity of MIL-88C(Fe)_NPs is not accessible to nitrogen since its flexible structure remains close when dehydrated. The accessible surface area of the simulated structure model for MIL-88C(Fe)_NPs was estimated using the strategy previously reported by Düren *et al.* [Düren *et al.*, 2007]. This surface was calculated from the center of a nitrogen probe molecule rolling across the surface. While the diameter of the nitrogen probe molecule was considered to be 3.681 Å, the diameters of each atom constituting the MIL-88C structure were taken from the UFF forcefield. Using the same parametrization for the framework, the methodology of Gelb and Gubbins was further used to calculate the pore size distributions (PSD) for each modified structure [Gelb and Gubbins, 1999]. Thus, the theoretical values for the specific surface area and pore volume of MIL-88C(Fe)_NPs were 4070 m²·g⁻¹ and 1.57 cm³·g⁻¹, respectively.

3.5 FTIR

A small amount of solids was analysed by a Thermo Nicolet spectrometer (Thermo, USA). The spectrum was recorded from 4000-400 cm⁻¹.



(a)



(b)

Figure S5. (a) FTIR spectra of the raw samples (black) and encapsulated ones (blue) for the Fe-based MOFs. (b) FTIR spectra of the raw samples (black) and encapsulated ones (blue) for the Zr-based MOFs. GEN (Green) and GCa (purple**) are also displayed. The spectra from both figures are zoomed in the region from 1800 to 400 cm^{-1} .

3.6 Solid Stated ^{13}C -NMR

The ^{13}C cross-polarization (CP) MAS NMR spectra were acquired on a Avance 500 Bruker spectrometer ($B_0=11.7$ T, Larmor frequency of 500.1 and 125.7 MHz for ^1H and ^{13}C , respectively) using a 4 mm probe. The MAS frequency was set to 10 kHz, the recycle delay to 5 s for pure GEN and 1 s for the MOF samples, with 192 and about 10 000 transients accumulated, respectively. The contact time is 3.5 ms, the first ^1H 90° pulse was set to 3 μs , the radio-frequency fields of 50 and 60 kHz for ^{13}C and ^1H , respectively, during the CP transfer. ^1H 64-step small-phase incremental alternation (SPINAL-64) decoupling was implemented during the acquisition period of the ^{13}C NMR spectra. The ^{13}C chemical shifts are referenced to TMS.

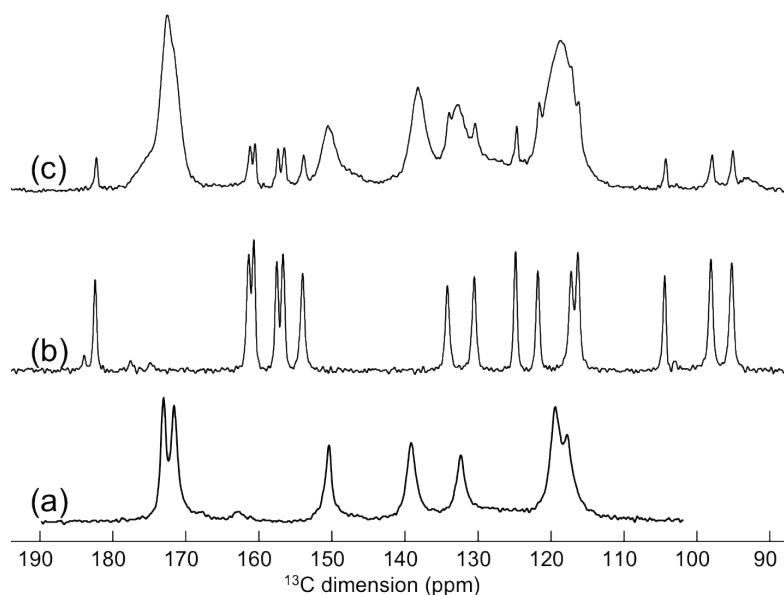


Figure S6. ^{13}C CPMAS NMR spectra of (a) UiO-66(Zr) $_{\text{NH}_2}$, (b) pure genistein and (c) UiO-66(Zr) $_{\text{NH}_2}$ loaded with genistein.

4. COMPUTING SIMULATION

The saturation for GEN was estimated using Grand Canonical Monte Carlo (GCMC) calculations. Using such calculations, it is possible to estimate the number of molecules present in the pores as a function of the chemical potential. It is also possible to elucidate the preferential adsorption sites for guest molecules on the solid framework. Partial charges and force field parameters have been implemented to run GCMC calculations. We performed all the simulations at 300 K with a simulation box large enough to use a cut-off equal to 12.5 Å with typically 5×10^6 Monte Carlo steps for both equilibration and prediction steps. Saturation is estimated at $P=10000$ kPa (such a high value allows us to assure the saturation to be accessed).

The framework was kept rigid, with atoms at the positions previously derived for the empty material during the whole adsorption process. Short range interactions have been estimated using a cut-off distance of 12.5 Å. The differential adsorption enthalpy at low coverage was calculated through the fluctuation over the number of particles in the system and from the internal energy. The parameters are given in the previous section.

The different crystallographic structures considered in this study are issued from literature for the functionalised and bare MIL-88 series [Horcajada *et al.*, 2011] and for the MIL-100 structure [Horcajada *et al.*, 2007]. In the GCMC calculations, the solid is supposed to be rigid and the unit cell parameters are therefore fixed. For this study, we have considered the largest unit cell structures for all solids.

The adsorbed GEN molecule has been optimised by Density Functional Theory (DFT) calculations and was considered in the GCMC calculations as rigid. It follows that no rearrangement of the confined molecules is possible in the MIL pores.

Regarding the solid, we used the Universal Forcefield (UFF) for Lennard Jones interatomic potentials, which is usually used to describe solid interactions [Rappé *et al.*, 1992] and Equalisation Electronegativity Method implemented in Material Studio to determine the partial charges distribution for the solid [Rappé and Goddard, 1991] In contrast, the UFF parameters and DFT partial charges are used for the adsorbate molecules.

In all calculations, we didn't take into account the effect of the solvent, probably overestimating the saturation determined experimentally.

5. GENISTEIN RELEASE

The first release assays were fulfilled in PBS pH 7.2 (KH₂PO₄ 15 mM, Na₂HPO₄ 27 mM and NaCl 1551 mM in 500 mL of ultrapure water; HCl was used to adjust the pH to 7.2) at 37 °C under SINK conditions (see the experimentally estimated solubility of GEN and constitutive organic linkers in PBS pH 7.2 at 37 °C, as displayed in Table S6; page 151). Therefore, 1 mg of each formulation was suspended in 15 mL of PBS pH 7.2 at 37 °C and kept under rotational stirring. After different incubation times, an aliquot of 7.5 mL of supernatant (half of the total volume) was recovered by centrifugation (15000 *g* for 15 min) and replaced with the same volume of fresh medium at 37 °C. The aliquot was filtered using a 0.22 µm pore diameter filter and stored at 4 °C until HPLC analysis.

The amount of released GEN was quantified by HPLC by using a calibration curve, which the mother solution was done in the release solution (or encapsulation solvent for their HPLC quantification) followed by successive dilutions in mobile phase (MeOH/Formic acid 0.1% 60/40 v/v). The chromatographic conditions are further summarised (Table S6; page 151):

- RP-C₁₈ 3 µm Gemini NX 150 x 2.0 mm column from Phenomenex (USA), protected by a KJO-4282 Security Guard Cartridge from the same package from Phenomenex (USA)
- Chromatographer: Agilent Technologies Series 1200 equipped with an Infinity Diode Array Detector HPLC system and controlled by ChemStation for LC 3D systems from Agilent Technologies (USA). (See the characteristic UV-Vis maximal absorption for GEN and organic linkers in Table S6; page 151).
- Mobile phase: MeOH/Formic acid 0.1% (60/40 v/v)

- Flow: 0.160 mL·min⁻¹
- Temperature: 25 °C
- Injection volume: 5 µL

Several GEN and organic ligand solutions in PBS were used as standards. The standard calibration curves for all analytes (GEN and the organic linkers) showed good correlation coefficients >0.99. See the characteristic retention times in Table S6. Moreover, the degradation of the solid was calculated according with the organic linker release, using the same method than for GEN and considering the maximum degradation (100%) when the total of the linker was released. In addition, the chromatographic conditions for all the monitorised solvents were exactly the same as the method described for GEN.

Table S6. Solubility and HPLC chromatographic details for the quantification of GEN and the organic linkers.

Analyte**	Solubility (µg·mL ⁻¹) *	Wavelength (λ, nm)	Linearity range (µg·mL ⁻¹)	rt (min)	Equation	R ²
GEN	27.8	260	0.010-10.00	5.30	y=185.40x + 3.05	0.9999
BTC MIL-100(Fe)_NPs	96.0	215	0.100-100.00	2.80	y=334.65x + 193.83	0.9977
BDC_NH₂ UiO-66_NH ₂ (Zr)_MPs	22.5	228	0.042-41.56	2.71	y=210.99x - 63.48	0.9993
NDC MIL-88C(Fe)_NPs UiO-66(Zr)_NDC_MPs	85.6	240	0.021-10.45	2.47	y=312.50x - 17.12	0.9995
BPDC UiO-66(Zr)_BPDC_MPs MIL-140C(Zr)_MPs	37.4	278	0.103-10.35	2.46	y=158.86x - 20.75	0.9985

*Solubility data in phosphate buffer saline (PBS) pH 7.2 at 37 °C.

**GEN (Genistein); BTC (1,3,5-benzenetricarboxylic acid or trimesic acid); BPDC (4,4'-biphenylcarboxylic acid); NDC (2,6-naphthalenedicarboxylic acid); BDC_NH₂ (2-aminoterephthalic acid).

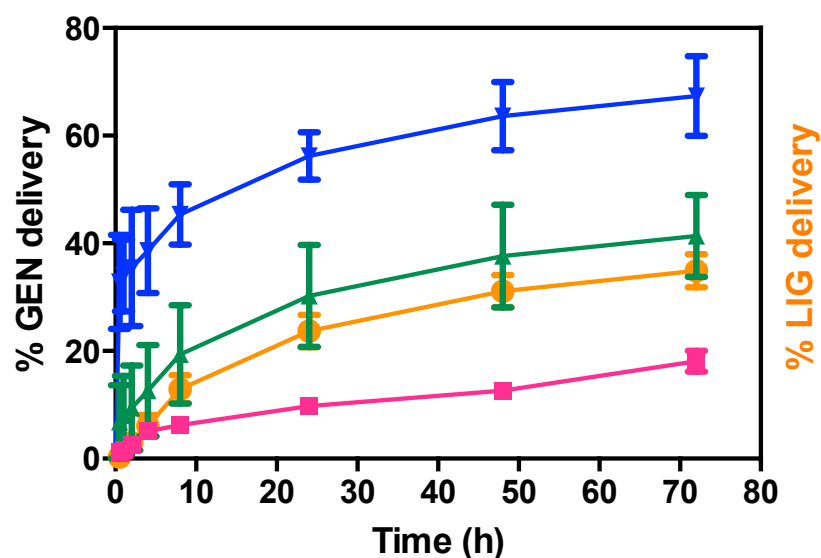


Figure S7. GEN release during 3 days from MIL-100(Fe)_NPs, depicting the GEN release in PBS conditions (■), after the addition of NaOH 0.01M to the PBS-GEN supernatant (▲) and after the addition of NaOH 0.5M to the PBS-GEN supernatant (▼). Moreover, the release of the organic linker BTC in PBS is also depicted (●).

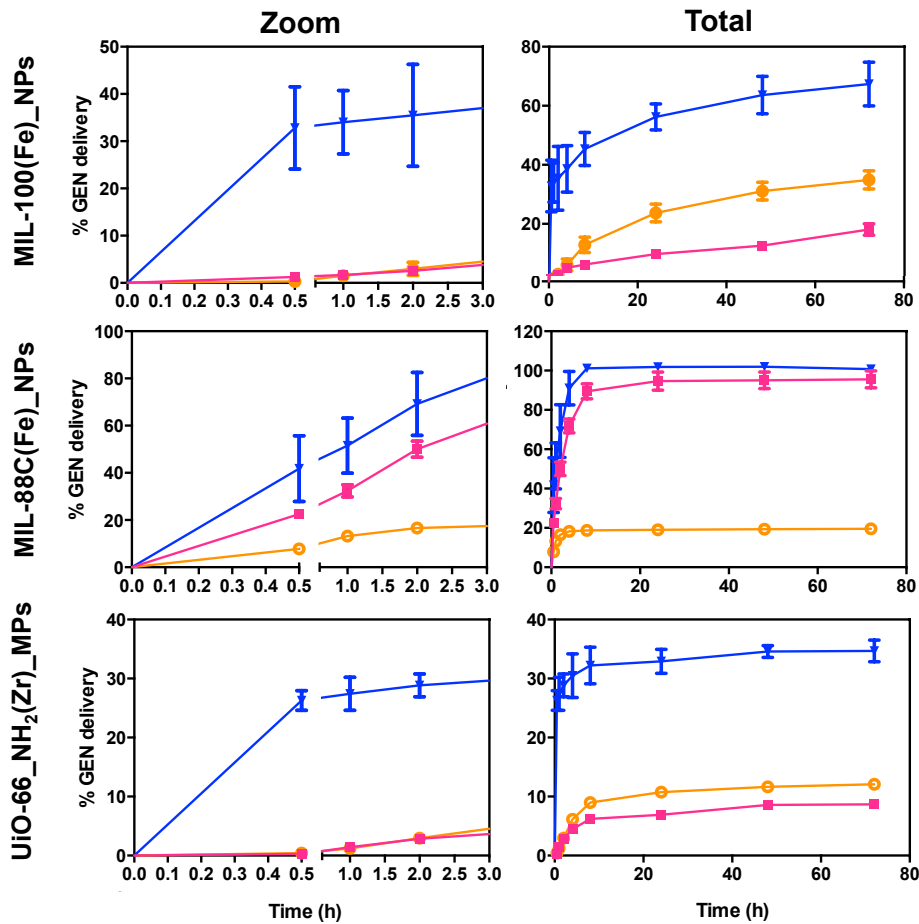
Due to the important complexing character of GEN, a complexation of around 45 and 20% of GEN with Fe and Zr, respectively, was determined by adding 1 mL of a GEN solution in mobile phase ($1 \text{ mg}\cdot\text{mL}^{-1}$) to 2 mg of the metal precursors $\text{FeCl}_3\cdot 6\text{H}_2\text{O}$ and ZrCl_4 . Considering the partial degradation of the MOF under the release conditions (PBS pH 7.2), Fe or Zr cations will be present in the PBS solution, leading to an underestimation of the released GEN. For this reason, the samples were previously treated with a base (NaOH) prior to their sample injection in the HPLC system. Therefore, 1 mL of the collected aliquots or GEN supernatants (from the GEN release in PBS) was added together with 1 mL of NaOH 0.5 M. Then, each sample was maintained for 2 h with the NaOH solution under rotational stirring, followed by 5 min vortex homogenisation and the sample centrifugation at $15000 g$ for 15 min. Thus, the supernatant was filtered through a $0.22 \mu\text{m}$ pore diameter filter and analysed by HPLC (see conditions above).

The results of this test evidenced that a fraction of GEN, which was released in PBS, was complexed with the MOF metallic core, as it can be observed in Figure 2 (page 120).

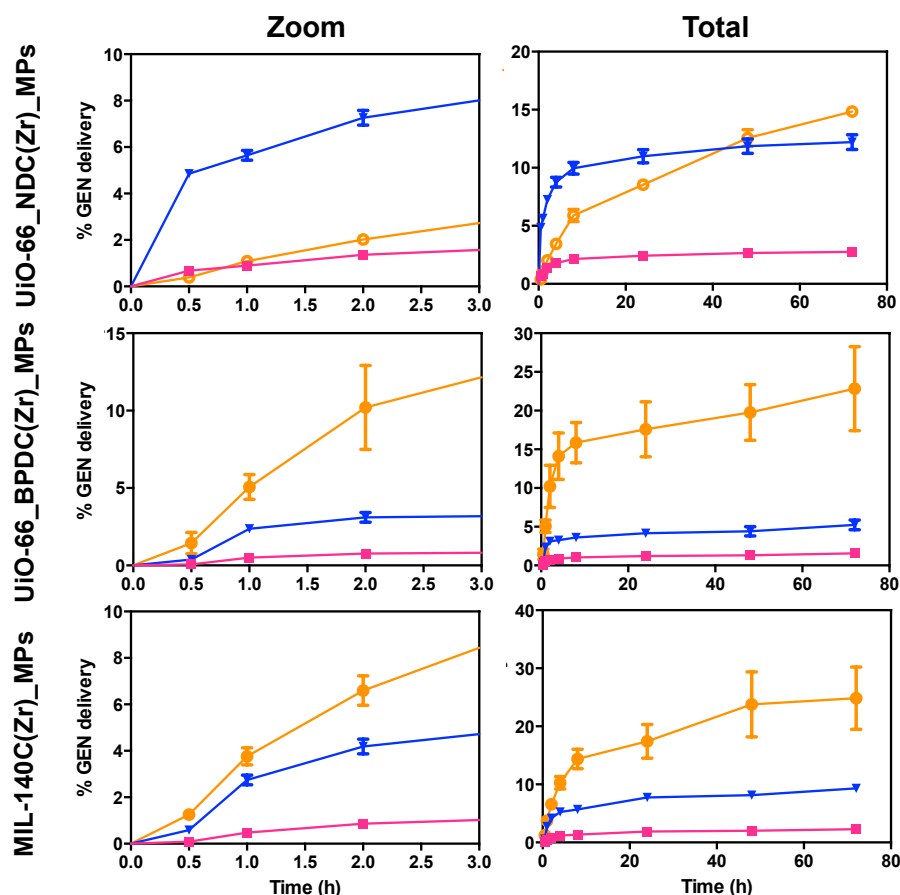
In order to quantify the possible non-released GEN into the MIL-100(Fe)_NPs solid, the pellet recovered after 3 days of GEN release in PBS was suspended in 1 mL of NaOH 0.01 M and maintained under rotational stirring for 7 h. A non-released GEN amount of ~72% (from the total initial loading) was afterwards detected, in agreement with a partial release of the GEN to the medium (an accumulative amount of ~90%), which was almost the

totality of the encapsulated amount. After observing these results, the same procedure was fulfilled for the rest of the formulations, showing almost complete release of GEN.

Additional future tests encompassing different NaOH treatments (*i.e.* different concentrations, amounts, temperatures and times) will be fulfilled for determining the best parameters for GEN delivery analysis.



(a)



(b)

Figure S8. (a) Delivery profiles of GEN in PBS (■), GEN in PBS after the addition of NaOH 0.5 M (▼) and the organic linker (●) for MIL-100(Fe)_NPs, MIL-88C(Fe)_NPs and UiO-66_NH₂(Zr)_MPs. (b) The same delivery profiles for UiO-66_NDC(Zr)_MPs, UiO-66_BPDC(Zr)_MPs and MIL-140C(Zr)_MPs.

Table S7. GEN loading and release quantification.

Formulation	Drug loading ($\mu\text{g}\cdot\text{mg form.}^{-1}$)	% Drug release			
		Released (Supernatant)		Non-released (Pellet)	Accumulative *
		Only PBS	Addition of NaOH 0.5M		
MIL-100(Fe)_NPs	174.0 \pm 24.9	18.1 \pm 1.9	67.4 \pm 7.4	23.6 \pm 1.5	91 \pm 2.8
MIL-88C(Fe)_NPs	201.7 \pm 51.7	95.7 \pm 4.4	100.8 \pm 0.3	0.9 \pm 0.3	100 \pm 0.5
UiO-66_NH ₂ (Zr)_MPs	159.3 \pm 47.7	8.7 \pm 0.3	34.7 \pm 1.8	46.8 \pm 3.0	81.5 \pm 1.6
UiO-66_NDC(Zr)_MPs	329.3 \pm 45.7	2.7 \pm 0.1	12.2 \pm 0.6	30.3 \pm 1.9	42.5 \pm 0.9
UiO-66_BPDC(Zr)_MPs	337.7 \pm 24.9	1.6 \pm 0.2	5.2 \pm 0.6	68.5 \pm 3.6	73.7 \pm 2.4
MIL-140C(Zr)_MPs	225.7 \pm 88.2	2.3 \pm 0.3	9.3 \pm 0.6	64.3 \pm 2.4	73.6 \pm 1.5

* Accumulative value by adding the values from the supernatant (PBS+NaOH 0.5 M) and the pellet (NaOH 0.01 M).

6. IN VIVO EXPERIMENTS

6.1 Animal Diet

One-day prior the start of the experiment, animals were weighted in order to calculate the amount of treatment that had to be administered to each mouse ($D=30 \text{ mg}\cdot\text{Kg}^{-1}$). Furthermore, animals were grouped in different cages ($n=6$), which corresponded to different experimental groups.

Just 12 h before the start of the experiment, the animal feed was subtracted from all the cages, due to the existing GEN amount in it, leaving the animals in fast for that time (12 h). Notwithstanding, water was kept in the cages *ad libitum*. Even if the animal feed didn't contain GEN traces, the protocol would have been the same, being standard to all pharmacokinetic/biodistribution studies.

The oral administration of 100 μL of treatment (free GEN or the GEN-MIL-100(Fe)_NPs formulation; $D=30 \text{ mg}\cdot\text{Kg}^{-1}$) was fulfilled to all the animals at time 0, continued by the blood extraction of the animals after 0.5, 1, 2, 4, 6, 8, 24 and 48 h the start of the experiment. Animals were fed with a soy-free jelly-based fed (Resource®, Nestlé Health Science) during the rest of the experiment. During the HPLC analysis [Tamames-Tabar *et al.*, 2013], no interferences between this jelly-based fed were observed.

6.2 Treatment Resuspension

Both GEN and the MIL-100(Fe)_NPs formulation were resuspended using the same protocol as previously published [Tamames-Tabar *et al.*, 2013]. Briefly, the resuspension solution contained DMSO/PEG 400/NaCl 0.9% (10:25:65, v/v). After 5 min of vortex homogenisation, all the treatments were correctly resuspended.

The GEN release from MIL-100(Fe)_NPs was quantified in the administration medium for 8 h. Although after 8 h around ~25% of the GEN was released, it is interesting to note that the GEN release was smaller than ~3% after 1 h (Figure S9, page 156). Therefore, the suspension of the GEN-containing MIL-100(Fe)_NPs in the DMSO/PEG 400/NaCl medium allowed the adequate *in vivo* administration of the formulation keeping the GEN cargo within the MOF porosity.

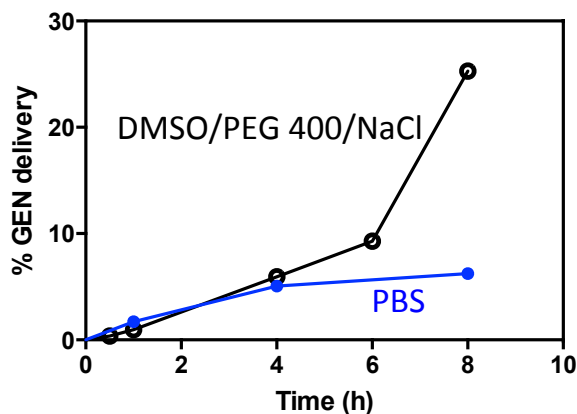


Figure S9. GEN release from MIL-100(Fe)_NPs in PBS (●) and in DMSO/PEG 400/NaCl (○).

REFERENCES

- Cavka, J.H.; Jakobsen, S.; Olsbye, U.; Guillou, N.; Lamberti, C.; Bordiga, S.; Lillerud, K.P., **2008**. A new zirconium inorganic building brick forming metal organic frameworks with exceptional stability. *J. Am. Chem. Soc.*, 130(42): 13850-13851.
- Cunha, D.; Gaudin, C.; Collinet, I.; Horcajada, P.; Maurin, G.; Serre, C., **2013**. Rationalization of the entrapping of bioactive molecules into a series of functionalized porous zirconium terephthalate MOFs. *J. Mater. Chem. B*, 1: 1101-1108.
- Düren, T.; Millange, F.; Férey, G.; Walton, K.S.; Snur, R.Q., **2007**. Calculating geometric surface areas as a characterization tool for metal-organic frameworks. *J. Phys. Chem. C*, 111(42): 15350-15356.
- García-Márquez, A.; Demessence, A.; Platero-Prats, A.E.; Heurtaux, D.; Horcajada, P.; Serre, C.; Chang, J.S.; Férey, G.; de la Pena-O'Shea, V.A.; Boissiere, C.; Grosso, D.; Sanchez, C., **2012**. Green microwave synthesis of MIL-100(Al, Cr, Fe) nanoparticles for thin-film elaboration. *Eur. J. Inorg. Chem.*, 2012(32): 5165-5174.
- Garibay, S.; Cohen, S.M., **2010**. Isoreticular synthesis and modification of frameworks with the UiO-66 topology. *Chem. Commun.*, 46(41): 7700-7702.
- Gelb, L.D.; Gubbins, K.E., **1999**. Pore size distributions in porous glasses: a computer simulation study. *Langmuir*, 15(2): 305-308.
- Guillerm, V.; Ragon, F.; Dan-Hardi, M.; Devic, T.; Vishnuvarthan, M.; Campo, B.; Vimont, A.; Clet, G.; Yang, Q.; Maurin, G.; Férey, G.; Vittadini, A.; Gross, S.; Serre, C., **2012**. A series of isoreticular, highly stable, porous zirconium oxide based metal-organic frameworks. *Angew. Chem. Int. Edit.*, 51(37): 9267-9271.
- Horcajada, P.; Salles, F.; Wuttke, S.; Devic, T.; Heurtaux, D.; Maurin, G.; Vimont, A.; Daturi, M.; David, O.; Magnier, E.; Stock, N.; Filinchuk, Y.; Popov, D.; Riekkel, C.; Férey, G.; Serre, C., **2011**. How linker's modification controls swelling properties of highly flexible iron(III) dicarboxylates MIL-88. *J. Am. Chem. Soc.*, 133(44): 17839-17847.

Horcajada, P.; Surble, S.; Serre, C.; Hong, D.Y.; Seo, Y.K.; Chang, J.S.; Greneche, J.M.; Margiolaki, I.; Férey, G., **2007**. Synthesis and catalytic properties of MIL-100(Fe), an iron(III) carboxylate with large pores. *Chem. Commun.*, 27, 2820-2822.

Kim, Y.; Swager, T.M., **2005**. Ultra-photostable n-type PPVs. *Chem. Commun.*, 3: 372-374.

Rappé, A.K.; Casewit, C.J.; Colwell, K.S.; Goddard, W.A., **1992**. UFF, a full periodic table force field for molecular mechanics and molecular dynamics simulations. *J. Am. Chem. Soc.*, 114(25): 10024-10035.

Rappé, A.K.; Goddard, W.A., **1991**. Charge equilibration for molecular dynamics simulations. *J. Phys. Chem.*, 95(8): 3358-3363.

Schaate, A.; Roy, P.; Godt, A.; Lippke, J.; Waltz, F.; Wiebcke, M.; Behrens, P., **2011**. Modulated synthesis of Zr-based metal-organic frameworks: from nano to single crystals. *Chem. Eur. J.*, 17: 6643-6651.

Serre, C.; Mellot-Draznieks, C.; Surblé, S.; Audebrand, N.; Filinchuk, Y.; Férey, G., **2007**. Role of solvent-host interactions that lead to very large swelling of hybrid frameworks. *Science*, 315(5820): 1828-1831.

Tamames-Tabar, C.; Imbuluzqueta, E.; Campanero, M.A.; Horcajada, P.; Blanco-Prieto, M.J., **2013**. A simple and robust high-performance liquid chromatography coupled to a diode-array detector method for the analysis of genistein in mouse tissues. *J. Chrom. B.*, 935: 47-53.

Zielonka, J.; Gebicki, J.; Gryniewicz, G., **2003**. Radical scavenging properties of genistein. *Free Radic. Biol. Med.*, 35(8): 958-965.

CHAPTER 3

A ZINC AZELATE MOF: COMBINING ANTIBACTERIAL EFFECT

GENERAL OBJECTIVES AND AUTHOR CONTRIBUTIONS

C. Tamames-Tabar, E. Imbuluzqueta, N. Guillou, C. Serre, S.R. Miller, E. Elkaïm, P. Horcajada. and M.J. Blanco-Prieto, Accepted in CrystEngComm.

As previously described in the first Chapter of this Thesis manuscript, the drug loading in MOF carriers can be achieved via two main strategies: (i) adsorbing the drug inside its pores or (ii) building a MOF whose components already possess the desired biological activity. This second strategy leads to biologically active MOFs, also known as BioMOFs, which are able to release their active components upon degradation. Thus, this Chapter is focussed on this interesting second approach.

Continuing with this path, we have worked in the green-synthesis and full structural characterisation of a zinc azelate (called BioMIL-5). Azelaic acid (AzA) and zinc are currently used in dermatology for the treatment of several skin disorders, such as hyperpigmentation and acne vulgaris. The idea of this work was to combine the activity of both components for future skin care applications.

Thus, we continued studying the degradation kinetics of the material in both water and in a bacterial broth (MHCA) media, in order to determine the controlled release of the active components. Then, its antibacterial activity was tested on bacteria commonly found in the skin (*S. epidermidis* and *S. aureus*). All the authors have actively contributed in this work. Dr. S.R. Miller has initially synthesised the BioMIL-5 and participated on its characterisation. C. Tamames-Tabar has worked in the synthesis optimisation, as well as fulfilled the degradation and microbiological evaluation of BioMIL-5. Dr. E. Imbuluzqueta has actively worked on the antibacterial studies. Dr. N. Guillou and Dr. C. Serre have performed the structural resolution of BioMIL-5. Dr. E. Elkaïm was involved in the synchrotron measurements for the determination of the crystalline structure. Finally, Dr. P. Horcajada and Dr. M.J. Blanco-Prieto have supervised the whole project.

A ZINC AZELATE MOF: COMBINING ANTIBACTERIAL EFFECT

Cristina Tamames-Tabar,^{a,b} Edurne Imbuluzqueta,^a Nathalie Guillou,^b Christian Serre,^b Stuart R. Miller,^b Erik Elkaïm,^c Patricia Horcajada^{*b} and María J. Blanco-Prieto^{*a}

^a*Department of Pharmacy and Pharmaceutical Technology, School of Pharmacy, University of Navarra, Irunlarrea 1, 31008 Pamplona, Spain.*

^b*Institut Lavoisier, UMR CNRS 8180, Université de Versailles Saint-Quentin-en-Yvelines, 45 Avenue des Etats-Unis, 78035 Versailles Cedex, France.*

^c*Cristal beamline, Soleil Synchrotron, L'Orme des Merisiers Saint Aubin BP4891192 Gif-sur-Yvette Cedex, France.*

Accepted in CrystEngComm

Keywords: Azelaic Acid, Zinc, Metal-Organic Frameworks, BioMOF, Antibacterial.

Corresponding Authors*

P. Horcajada: Institut Lavoisier, UMR CNRS 8180, Université de Versailles Saint-Quentin-en-Yvelines, 45 Avenue des Etats Unis, 78035 Versailles Cedex, France; Fax: 33(0) 139256652; Tel: 33(0) 139254371; E-mail: horcajada@chimie.uvsq.fr

M.J. Blanco-Prieto: Department of Pharmacy and Pharmaceutical Technology, School of Pharmacy, University of Navarra, Irunlarrea 1, 31008 Pamplona, Spain; Fax: 34 948425649; Tel: 34 948425600 Ext. 806519; E-mail: mjblanco@unav.es

ABSTRACT

A novel biocompatible and bioactive Metal-Organic Framework (BioMOF), named BioMIL-5 (Bioactive Materials from Institut Lavoisier), was hydrothermally synthesised from a Zn^{2+} salt and azelaic acid, both with interesting antibacterial and dermatological properties. Its structure was determined by high resolution X-ray powder diffraction, and further characterised by infrared spectroscopy, thermogravimetric analysis and elemental analysis. On the other hand, the determination of the minimal inhibitory concentration (MIC) and minimal bactericidal concentration (MBC) values of BioMIL-5 in *Staphylococcus aureus* and *Staphylococcus epidermidis*, demonstrated that the antimicrobial activity of the individual components of BioMIL-5 were maintained after its synthesis. Moreover, BioMIL-5 was found to be stable in water and in bacterial culture medium, especially in water, leading to the subsequent progressive release of its active constituents, AzA and Zn^{2+} ions. Interestingly, this slow active delivery allowed a control of the growth of a *S. epidermidis* suspension over 7 days. The high stability of this material and the maintenance of its antibacterial properties make BioMIL-5 a good candidate for future bioapplications, for skin care and in cosmetics.

1. INTRODUCTION

Metal-Organic Frameworks (MOFs) are a very versatile group of crystalline hybrids, due to their broad application fields, including catalysis, separation or gas storage, among others.¹ Although their first potential applications were mainly focused on these fields, in recent years, MOFs have also been directed towards biomedicine.² These have been evaluated as new controlled delivery systems for drugs,^{2a,3} cosmetics,⁴ or biologically active gases,⁵ encapsulation of enzymes⁶ and finally for imaging⁷ and theranostics.^{3a,8}

MOFs can work as drug controlled-release carriers by (i) entrapping the active molecule within their porosity³⁻⁶ or by (ii) incorporating the biomolecule as a constitutive part of their skeleton.^{2b,9} In this latter case, these are also known as BioMOFs (Bioactive Metal-Organic Frameworks). This latter strategy permits the use of therapeutically active molecules bearing multiple complexing groups, as well as bioactive cations (Ca^{2+} , $\text{Fe}^{2/3+}$, Ag^+ , Zn^{2+}), to build the BioMOF and then deliver the active compounds via framework degradation.¹⁰ While the best antibacterial activity has been validated for antibacterial-metal molecular complexes by combining different antibiotic drugs and metals,¹¹ to the best of our knowledge, no studies dealing with such combination have been published about MOFs. Indeed, studies reporting the antibacterial activity of MOFs are typically based on non-toxic antimicrobial cations (Zn^{2+} ,¹² $\text{Ag}^{+10a,13}$).

In particular, Zn^{2+} is an endogenous low-toxic transition metal cation¹⁴ widely used in dermatology, as a cicatrising agent and skin moisturiser with antidandruff, astringent, anti-inflammatory and antibacterial properties,¹⁵ but without controlled release.

On the other hand, azelaic acid (nonaedioic acid or AzA) exhibits antibacterial¹⁶ and anti-inflammatory¹⁷ properties and is regularly used as a routine treatment against acne vulgaris¹⁸ and rosacea.¹⁹ AzA has shown a great potential for the treatment of other skin pathologies such as malignant melanoma,²⁰ hyperpigmentation²¹ and melasma.²² However, it is poorly absorbed through the skin and requires several applications to maintain active levels for an extended period.²³

The combination of AzA and Zn^{2+} into a robust MOF would result into long drug release carriers. The development of such drug delivery systems could contribute to major technological progress for future bioapplications in dermatology and skin care.

In the present study, we report the synthesis of a new BioMOF, named BioMIL-5 (MIL stands for Materials of Institut Lavoisier), based on Zn^{2+} ions as inorganic nodes and AzA as the organic linker, both with very interesting properties for the dermatological treatment of various skin disorders. First, its structure was determined by means of high resolution X-ray powder diffraction data, further confirmed by physico-chemical

characterisations. The release of its active constitutive compounds was also assessed by stability tests of BioMIL-5 in water and in bacteria broth at 37 °C. Finally, the antibacterial activity of BioMIL-5 was evaluated by using 2 common Gram-positive bacteria normally found in skin (*S. aureus* and *S. epidermidis*).

2. EXPERIMENTAL SECTION

2.1. Chemicals and Reagents

Zinc nitrate hexahydrate ($\text{Zn}(\text{NO}_3)_2 \cdot 6\text{H}_2\text{O}$) and azelaic acid (AzA) were purchased from Sigma-Aldrich (Germany). All solvents, absolute ethanol (EtOH) and nitric acid 37% (HNO_3 37%) were acquired from Carlo Erba (Italy), except for the high performance liquid chromatography (HPLC) grade acetonitrile (AcN) and dimethylsulphoxide (DMSO) acquired from Merck KGaA (Germany). AzA-derivatisation was accomplished using 4-bromophenacyl bromide and *N,N*-diisopropylethylamine, both purchased from Sigma-Aldrich (Germany) and ammonium formate (NH_4HCO_2) purchased from AVOCADO Research Chemical Ltd. (UK). The Zn standard for atomic absorption spectroscopy 1 $\text{mg} \cdot \text{mL}^{-1}$ Zn in nitric acid TraceCERT® was purchased from Fluka (Switzerland). Both Mueller-Hinton cation adjusted broth (MHCA) and trypticase soy agar (TSA) were purchased from Becton Dickinson and Company (USA).

2.2. BioMIL-5 Synthesis and Characterization

BioMIL-5 synthesis: 297 mg of $\text{Zn}(\text{NO}_3)_2 \cdot 6\text{H}_2\text{O}$ (1 mmol) together with 47 or 188 mg of AzA (0.25 or 1 mmol) and 5 mL of MilliQ water were put inside a 23 mL Teflon Parr Bomb (Parr Instrument Company, USA) and incubated for 24 h at 200 °C in a Heraeus Oven (Thermo Scientific, USA) with a ramp to temperature of 1 h. Then, the particles were recovered by filtration and washed with water. Initial conditions based on a Zn:AzA stoichiometry of 1:0.25 led to a good crystalline solid used for structural determination but with the presence of a ZnO impurity.

Optimised synthetic conditions, based on a Zn:AzA stoichiometry equal to 1:1, yielded a pure BioMIL-5. The amount of recovered solid was approximately 150 mg (yield ~52%).

Structural Determination

No suitable single crystal with a sufficient size or quality for a structural investigation was available. High resolution X-ray powder diffraction data were then collected on the CRISTAL beamline at Soleil Synchrotron (Gif-sur-Yvette, France). A monochromatic beam was extracted from the U20 undulator beam by means of a Si(111) double monochromator. Its wavelength of 0.72528 Å was refined from a LaB₆ (NIST Standard Reference Material 660a) powder diagram recorded prior to the experiment. High angular resolution was obtained with, in the diffracted beam, a 21 perfect crystal Si(111) multi-analyzer similar to the one employed on beamline ID31 at ESRF.²⁴ The sample was loaded in a 0.7 mm capillary (Borokapillaren, GLAS, Schönwalde, Germany) mounted on a spinner rotating at about 5 Hz to improve the particles' statistics. Diffraction data were collected for less than 2 h in continuous scanning mode and the diffractogram was obtained from the precise superposition and addition of the 21 channels data.

Extractions from the peak positions, pattern indexing, Fourier difference calculations and Rietveld refinements were carried out with the TOPAS program.²⁵ Structural determination was performed with the EXPO package,²⁶ using EXTRA for extracting integrated intensities and SIR97 for direct-method structure solutions. 31 restraints on Zn-O, C-C and C-O distances were applied in order to maintain a suitable geometry during the refinement. Hydrogen atoms were introduced geometrically and not refined.

Fourier Transformed Infrared Spectroscopy (FTIR) was analysed on a Thermo Nicolet 6700 spectrometer (Thermo, USA) registering the spectra at a wavelength interval of 4000-400 cm⁻¹ at RT. Thermogravimetric analyses (TGA) were carried out using a Perkin Elmer Diamond STA 6000 apparatus (Perkin Elmer, USA) under oxygen gas with a heating rate of 3 °C·min⁻¹. Morphologic analysis of the crystals was carried out with a field-emission gun scanning electron microscope (FEG-SEM) JEOL JAMP 9500F (JEOL GmbH, Germany), dynamic light scattering (DLS) measurements with a Mastersizer S®(Malvern Instruments, UK).

2.3. BioMIL-5 Degradation and Release of AzA and Zn

For the BioMIL-5 degradation study and AzA and Zn²⁺ release monitoring, 1 mL of media (water or MHCA broth) was added to 4.3 mg of solid and kept inside an incubator under rotational stirring at 37 °C during 70 days. After different incubation times, the samples were removed from the incubator and centrifuged (14100 g/15 min). The pellet was characterised by means of FTIR, XRPD, SEM and DLS. The released amount of AzA and

Zn was quantified in the sample supernatant by high performance liquid chromatography (HPLC) and atomic absorption spectroscopy (AAS), respectively. The solubility values of AzA in both media at 37 °C were experimentally accomplished being 2.2 and 3.4 mg·mL⁻¹ for water and MHCA, respectively.

Quantification of AzA

AzA released from BioMIL-5 was analysed after its derivatisation by an HPLC system (Waters Alliance C2695) coupled to a photodiode array detector (PDA) (Waters E2998) and controlled by Empower software (Version 5.00, Waters Corporation, USA). The derivatisation was carried out by a previously described method²⁷ with minor modifications. Briefly, 1 mL of supernatant was added to 500 µL of 4-bromophenacyl bromide (50 mg·mL⁻¹ in AcN) and 200 µL of *N,N*-diisopropylethylamine. After their vortex mixing, samples were incubated at 60 °C during 30 min and analysed by HPLC.

The chromatographic separation was carried out using a Durashell C18 column (5 µm, 150 mm x 4.6 mm I.D., Agela Technologies Inc, USA) protected by a guard cartridge precolumn with the same packing material. For all the samples, an isocratic elution profile was established and the flow rate was set at 1 mL·min⁻¹. The mobile phase composition varied depending on the sample type, being 80% of AcN and 20% of NH₄HCO₂ 1 M (pH=5) for water samples and 50% of AcN and 50% of NH₄HCO₂ 1 M (pH=5) for MHCA broth samples. The injection volume was 20 µL and AzA was detected by UV absorbance at the wavelength of 250 nm. The standard curve was prepared by dilutions of a 1 mg·mL⁻¹ AzA mother solution in AcN.

Quantification of Zn

The Zn²⁺ content of the samples was analyzed using a Thermo Electron Corporation M Series atomic absorption spectrometer (Thermo Scientific, USA) with a Zn lamp at 213.9 nm using SOLAAR software (Thermo Scientific, USA). Samples were diluted 1:100 (in water/MHCA depending on the sample type) prior to analysis and the calibration curve was prepared by dilutions of the Zn²⁺ standard in HNO₃ 2%.

2.4. Antibacterial Activity Studies

Antibacterial properties of the synthesised BioMIL-5 were evaluated against *Staphylococcus aureus* ATCC (American Type Culture Collection) 25923 and

Staphylococcus epidermidis ATCC 12228. Experiments were performed with fresh bacteria previously incubated on TSA plates at 37 °C for 24 h.

First, minimal inhibitory concentration (MIC) and minimal bactericidal concentration (MBC) values for BioMIL-5 and its individual components (AzA and Zn) were determined in MHCA broth by broth microdilution method according to the CLSI recommendations.²⁸ Experiments were carried out by suspending BioMIL-5 in this medium at 37 °C, as well as the equivalent amounts of its individual components (1.1 and 3.2 mg, for Zn and AzA, per 4.3 mg of BioMIL-5 respectively). Briefly, stock concentrations of BioMIL-5, as well as the corresponding amounts of their constitutive ligand and metal (AzA and Zn), were prepared in 0.9% saline solution and further diluted in MHCA broth to different concentrations. Bacterial suspensions in 0.9% saline solution were adjusted to an optical density of 0.085 (600 nm) ($\sim 10^8$ colony forming units (CFU) \cdot mL⁻¹) with a Thermo Scientific Genesys 20 Spectrophotometer (Thermo Scientific, USA) and diluted 1:100 in MHCA broth. The real inoculum was determined by plating appropriate dilutions on TSA plates. Finally, 100 μ L of each treatment were mixed with 100 μ L of each bacterial suspension in 96-well plates resulting in final treatment concentrations ranging from 0.031 to 6 mg \cdot mL⁻¹. As a control for bacterial growth, treatment-free medium was also included. After incubation at 37 °C for 24 h, MICs were defined as the lowest concentration of drug that resulted in no visible bacterial growth. For MBC determination, aliquots of 20 μ L from the wells without visual bacterial growth were plated on TSA plates and incubated for 24 h at 37 °C. The minimum concentration that yielded more than 99.9% killing of the bacteria was defined as the MBC of each treatment.

On the other hand, in order to study the antibacterial properties of BioMIL-5 over time, a *S. epidermidis* suspension in MHCA broth (5×10^5 CFU \cdot mL⁻¹) was exposed to increasing concentrations of the BioMOF (0.9, 1.7 and 4.3 mg \cdot mL⁻¹) and bacterial growth was monitored at 37 °C and kept under stirring during 7 days. For comparing the previous results, the growth of non-treated bacteria was also monitored. At different incubation times, 100 μ L of each bacterial suspension were plated on TSA plates for colony counting. Results of CFU counts were transformed into logarithms and represented *vs.* time to obtain the bacterial growth curves.

3. RESULTS AND DISCUSSION

3.1. BioMIL-5 Synthesis and Characterisation

White-shining thin platelet-shaped crystals (5-10 μm , with a few larger ones of around 30 μm) of the zinc azelate BioMIL-5 were initially prepared using a hydrothermal route and a Zn:AzA stoichiometry of 1:0.25. BioMIL-5 crystallises in the orthorhombic unit cell ($a=47.288(1)$, $b=4.7297(2)$, $c=9.3515(3)$ \AA ; $V=2091.5(1)$ \AA^3). Systematic absences were consistent with the *Pcca* space group (n. 54). Unindexed lines observed on the powder pattern correspond to ZnO impurity due probably to the large excess of the Zn precursor (Zn:AzA=1:0.25). Its structural model was introduced in the next steps of the structural investigation. Direct methods calculations allowed location of one independent zinc atom with most of its environment with few carbons. This structural model was completed by successive difference Fourier calculations. At the final stage, Rietveld refinement for BioMIL-5 involved the following structural parameter: 45 atomic coordinates, 1 overall thermal factor and the scale factor. The anisotropic line broadening effect was modelled by using spherical harmonics and soft restraints were maintained on bond lengths and angles. The final Rietveld plot (Fig. S1, page 187) corresponds to satisfactory crystal structure model indicator ($R_{\text{Bragg}}=0.029$) and profile factors ($R_{\text{P}}=0.076$ and $R_{\text{WP}}=0.104$). The amount of ZnO was estimated at about 5 wt% (weight). The unit cell contains one independent Zn atom located in a general position and two independent organic moieties located on a mirror, leading to the chemical formula $\text{Zn}(\text{C}_9\text{O}_4\text{H}_{14})$. Crystallographic data are summarised in Tab. S1 (page 187).

This structure is very close to the one of the cobalt pimelate MIL-36 or $(\text{Co}(\text{C}_7\text{H}_{10}\text{O}_4))$.²⁹ Similar structures have been more recently reported based on a cobalt adipate $(\text{Co}(\text{C}_6\text{H}_8\text{O}_4))$ or a zinc glutarate $(\text{Zn}(\text{C}_5\text{H}_6\text{O}_4))$.³⁰ Each Zn atom is tetrahedrally coordinated by oxygen atoms coming from the carboxylate groups of 4 azelate ligands. This leads to an infinite grid in the (011) plane of ZnO_4 tetrahedra linked by bridging CO_2^- groups (see Fig. 1, page 173). The connection along the [100] direction is insured by the aliphatic chains giving rise to the neutral 3-D framework of BioMIL-5. Therefore, a non-porous framework is generated, with a clear segregation of the hydrophilic (carboxylate+Zn) and hydrophobic part (alkyl chains). The shortest C...C distances between adjacent walls are 3.65(1) \AA and 4.04 \AA , respectively, suggesting a rather close packing of the long alkyl chains of the azelate ligand.

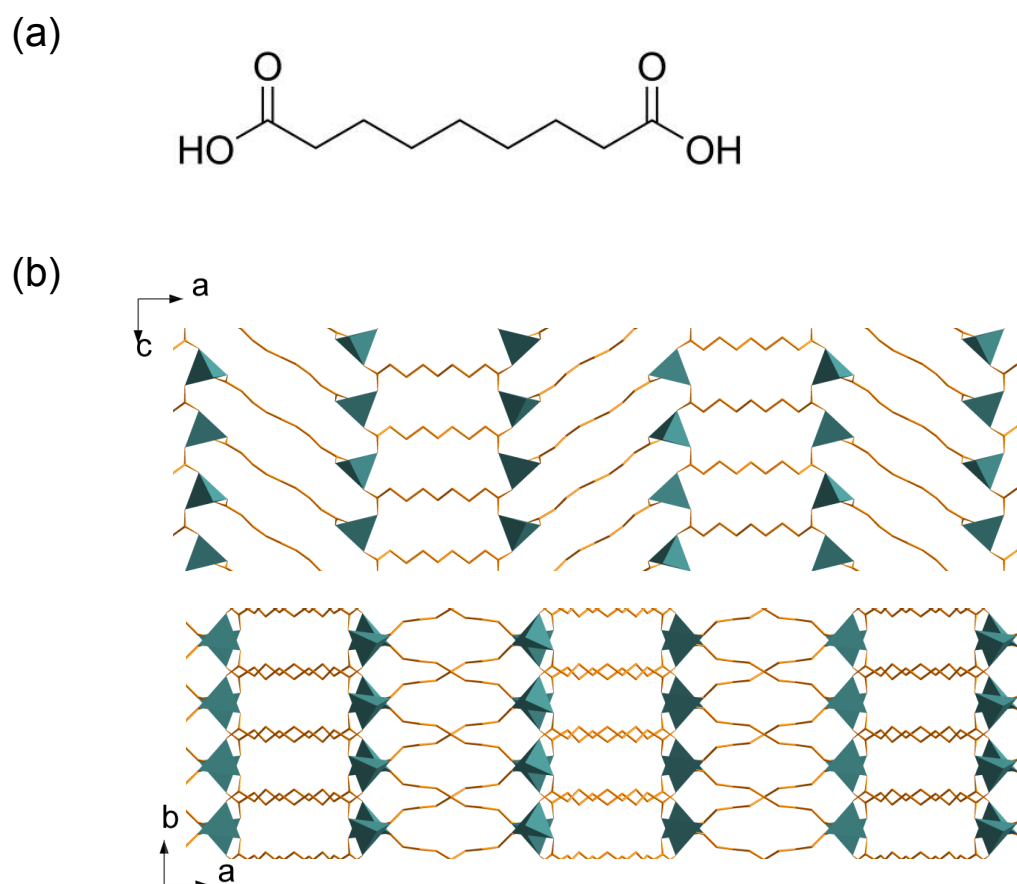


Fig. 1 (a) Structure of the organic linker: azelaic acid (Aza). (b) Projections of the crystal structure of BioMIL-5 along $[010]$ and $[001]$ directions. Zn polyhedral and carbon atoms are in green and yellow, respectively.

In order to prevent the formation of the ZnO impurity, synthetic conditions were further optimised by increasing the Zn:Aza ratio from 1:0.25 to 1:1. Thus, white-shining platelet-shaped crystals ($10 \pm 6 \mu\text{m}$; Fig. S2) of the pure zinc azelate BioMIL-5 were successfully synthesised using a biocompatible and green hydrothermal route, avoiding the use of any toxic additive. XRPD confirmed the identity and the purity of the whole polycrystalline product (Fig. 3, page 174).

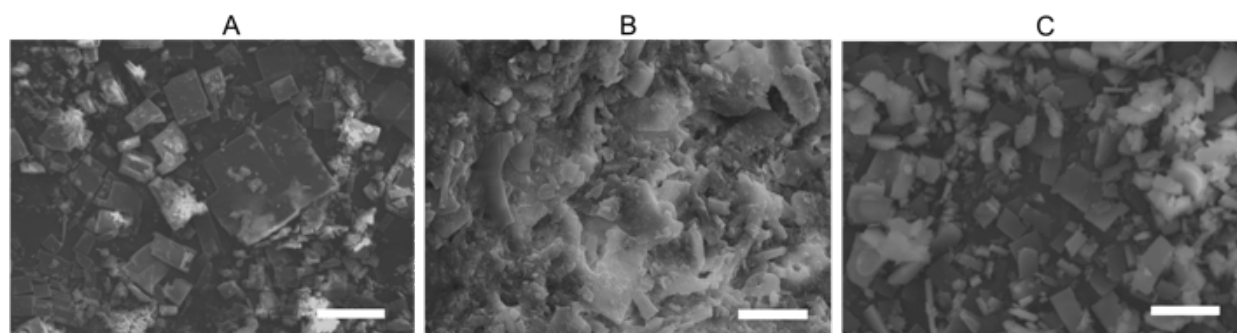


Fig. 2 SEM images of BioMIL-5 after synthesis (A), and after 70 days in Mueller Hinton Cation Adjusted broth or MHCA (B) and in water (C). The scale bar for all images is 10 μm .

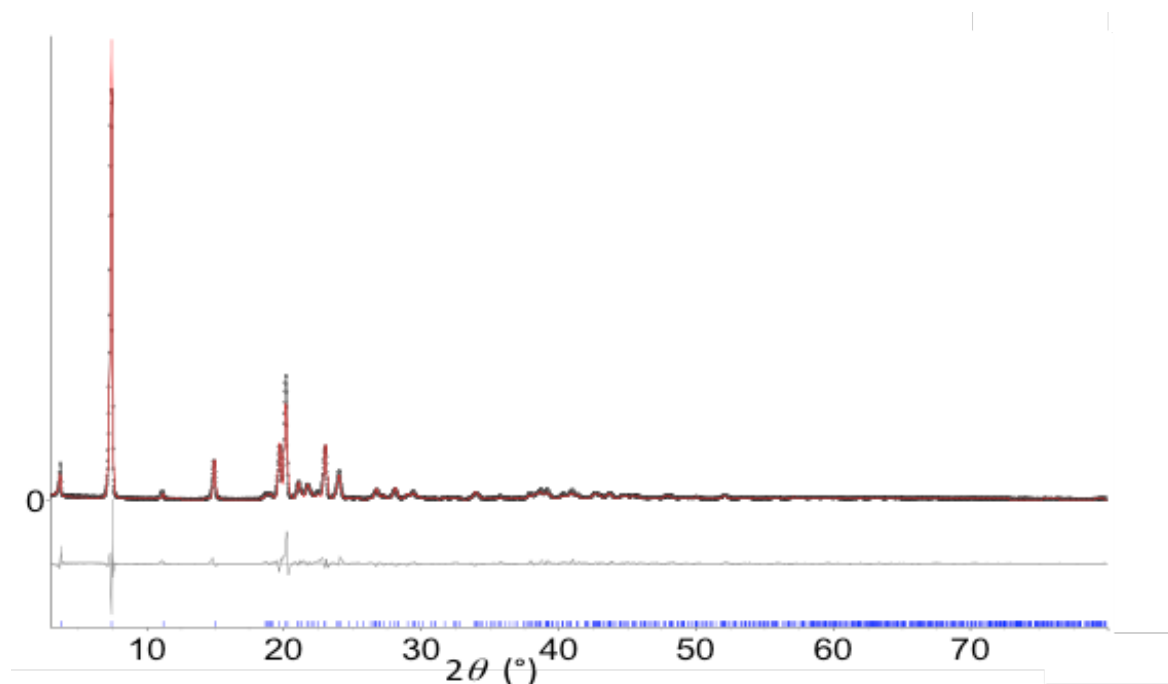


Fig. 3 Comparison of experimental (black points) and calculated (red line) patterns of BioMIL-5, confirming the purity of the solid. Laboratory X-ray powder diffraction data were collected on a Siemens D5000 diffractometer by using $\text{CuK}\alpha$ radiation. The pattern was scanned over an angular range 3-80° (2θ) with a step length of 0.02° (2θ).

TGA analysis showed the absence of any residual solvent as well as only one weight loss of 67.2 wt% at around 320 °C, corresponding to the combustion of the azelate ligand (Fig. S2, page 188), in agreement with the proposed structural formula (ZnO theo.=32.3 wt%; calc.=32.8 wt%).

Thermal stability of BioMIL-5 under air atmosphere reached 300 °C, as indicated by X ray powder thermodiffraction patterns, in agreement with TGA (Fig. S3, page 188).

FTIR spectrum of the BioMIL-5 showed the presence of $\nu(\text{C-O})$ at 1450 and 1550 cm^{-1} . In addition, the absence of the $\nu(\text{C=O})$ band at 1700 cm^{-1} confirmed the absence of free-remaining azelaic ligand (Fig. S5, page 190).

3.2. BioMIL-5 Degradation and Release of AzA and Zn

In order to assess whether BioMIL-5 will be able to progressively release its therapeutic constitutive molecules (Zn and AzA), the BioMIL-5 degradation was studied in 2 different

media: (i) MilliQ water for simulating skin conditions and (ii) MHCA bacteria broth, a more complex medium composed by many organic and inorganic nutrients (among them aminoacids, sugars, casein, inorganic salts, etc).³¹ This last medium will be further used to evaluate the MIC and MBC values (see Results and Discussion, Antibacterial Activity Studies, pages 177-179). Experiments were carried out suspending $4.3 \text{ mg}\cdot\text{mL}^{-1}$ of BioMIL-5 in these media at 37°C . The degradation and subsequent release of AzA and Zn^{2+} from BioMIL-5, was monitored by analyzing both supernatant and pellet at different incubation times (see Experimental Section, pages 169-170). Degradation is represented as the wt% of the linker released in the medium, considering 100% as the total degradation of the BioMOF that is when the entire amount of linker and metal that build the particles is released to the medium.

As can be seen in Fig. 4 (page 175), a perfect correlation was found between the degradation values obtained from the Zn^{2+} or AzA release in water (*i.e.* release of 6.9 ± 0.0 and $8.3\pm 0.3\%$ after 7 days or 56.6 ± 3.9 and $51.4\pm 0.1\%$ after 70 days for Zn and AzA, respectively). On the other hand, a slight difference between the degradation values estimated from either the Zn^{2+} or AzA release in the MHCA broth medium was observed (*i.e.* release of 14.8 ± 0.2 and $30.5\pm 0.0\%$ after 7 days or 100.8 ± 0.1 and $92.3\pm 0.0\%$ after 70 days for Zn and AzA, respectively). This might be related to the presence of components in the medium able to interact differently with the AzA and Zn^{2+} complexes.

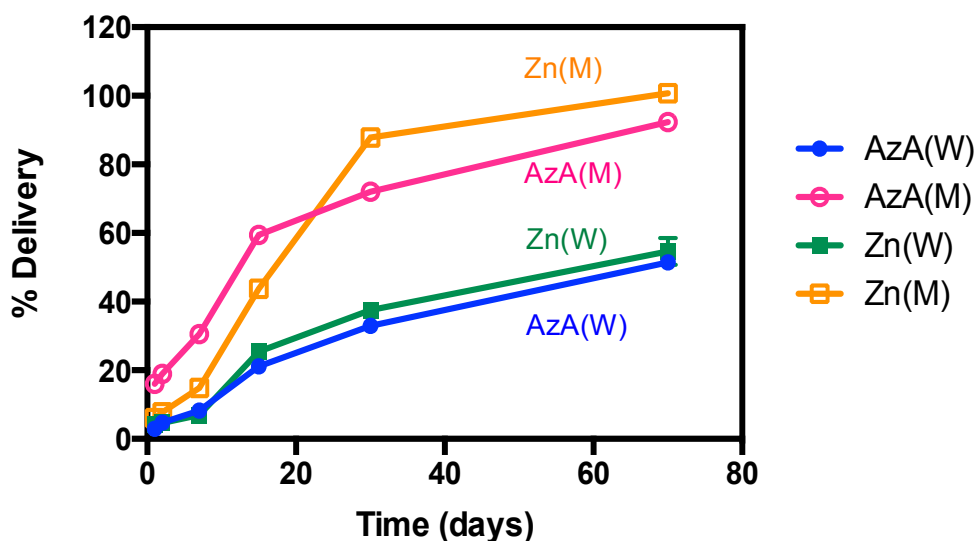


Fig. 4 Delivery profile of azelaic acid (AzA) and zinc (Zn) in Mueller Hinton Cation Adjusted broth or MHCA (M) and in water (W): AzA (M) (○), AZA (W) (●), Zn (M) (□) and Zn (W) (■).

As can be observed in Fig. 4 (page 175), BioMIL-5 degrades slowly and progressively in both media, the release in water being even slower than in MHCA broth. For instance, the degradation in water was found to be ~8 and ~55% after respectively 7 and 70 days of incubation, whereas in MHCA broth, the degradation was ~25 and ~95% after 7 and 70 days, respectively. The higher pH value obtained in MHCA in comparison with its value in MilliQ water (7.4 *vs.* 6.0), was several units above the pK_a of the azelate ligand ($pK_a=4.55$ and 5.41),³² and might favor the formation of Zn oxide/hydroxide and therefore, the degradation of the solid.³³ In addition, the presence of several aminoacids, sugars and salts, in particular some phosphate groups (present in the MHCA broth composition for casein hydrolysis)³¹ able to compete for the coordination of the Zn^{2+} cation with the azelate ligand, might explain the faster degradation of BioMIL-5 in MHCA. This fact is in total concordance with that already seen in other metal carboxylate MOFs when exposed to phosphate buffered saline.^{3b,34}

In this sense, FTIR spectra (Fig. S5, page 190) show an important intensity decrease on the bands at around 1450 and 1550 cm^{-1} , corresponding to the carboxylate bonds, as well as the presence of traces of free carboxylic bands ($\nu(C=O)$) at around 1700 cm^{-1} . These results, together with the apparition of new bands at 1000 cm^{-1} , which can be assigned to $\nu(P=O)$ bands, are in complete agreement with the degradation of BioMIL-5 in MHCA medium.

Furthermore, in both media, the BioMIL-5 was not fully degraded during the degradation process, as confirmed by the XRPD patterns depicted in Fig. S4 (page 189). Whereas BioMIL-5 did not show any significant variation even after 70 days of immersion in water, confirming the high stability, an important Bragg peak broadening was observed after 70 days in MHCA broth medium, consistent with a larger extent of degradation. Interestingly, despite the progressive degradation of BioMIL-5 in MHCA broth, with around 95% of their constitutive parts released to the medium, the small amount of remaining solid stays crystalline up to the end of the assay. The important stability of BioMIL-5 contrasts with other previously reported zinc dicarboxylates, such as the well-known MOF-5.³⁵ This is due both to the absence of pores in BioMIL-5 and its hydrophobic character.³⁶

Moreover, the morphological study showed that contrary to the large and polydispersed well-faceted crystals of BioMIL-5 sample ($9.83\pm 6.12 \mu m$), SEM images after degradation showed smaller more or less rounded-corners crystals after 70 days of degradation in water (3.00 ± 0.02 and $1.83\pm 1.17 \mu m$; Fig. 2, page 173). Note that for the BioMIL-5, very little solid was obtained after the degradation in MHCA, reflecting almost complete degradation. In accord with the SEM images, the particle sizes obtained by DLS

measurements, for BioMIL-5 before and after 70 days immersed in water and in MHCA broth were 6.00 ± 3.50 , 5.80 ± 0.45 and 0.78 ± 0.02 μm , respectively (note the important polydispersity of the sample, in agreement with the SEM observations, as well as the DLS measurement complexity considering the non-spherical form of the particles). This is consistent with the much higher degree of degradation of BioMIL-5 in MHCA broth than in water.

In light of these findings, one can presumably propose a degradation mechanism of BioMIL-5 in MHCA broth by erosion, in which the constitutive parts that are located on the external surface of the crystal are progressively released to the media, leading to a decrease on the crystal dimension without affecting the integrity of the crystalline framework.

3.3. Antibacterial Activity Studies

The antibacterial activity of BioMIL-5, as well as of its constituents (Zn and AzA), was first investigated by means of their MIC/MBC (MIC=Minimal Inhibitory Concentration; MBC=Minimal Bactericidal Concentration) determination against 2 Gram-positive bacteria present in the normal skin flora but which cause some skin disorders: *S. aureus* and *S. epidermidis* (see Experimental Section, pages 170-171).

MIC values for Zn, AzA and BioMIL-5 were 0.5, 1.5 and 1.7 $\text{mg}\cdot\text{mL}^{-1}$, respectively, and MBC values were 2.0, 3.0 and 4.3 $\text{mg}\cdot\text{mL}^{-1}$, respectively (Tab. 1, page 173). It is noteworthy that the biological activity of the original components of BioMIL-5 was maintained, not only after the hydrothermal synthesis conditions but also after the degradation of the hybrid network, releasing both Zn^{2+} and AzA in their active form.

Tab. 1 Minimal inhibitory concentration (MIC) and minimal bactericidal concentration (MBC) results in $\text{mg}\cdot\text{mL}^{-1}$ of azelaic acid (AzA), BioMIL-5 and in *S. aureus* and *S. epidermidis*.

Treatment	<i>S. aureus</i>		<i>S. epidermidis</i>	
	MIC	MBC	MIC	MBC
BioMIL-5	1.7	4.3	1.7	4.3
AzA	1.5	3.0	1.5	3.0
Zn	0.5	-	0.5	2.0

Some comments can be proposed regarding the MBC values. Although an antibacterial additive effect between AzA and Zn^{2+} could be expected by their combination in BioMIL-5,

no evidence supporting any synergistic activity was found. However, considering the different biological properties of AzA and Zn^{2+} , acting at different skin care levels (*i.e.* cicatrizing, antidandruff, astringent, anti-acne, etc), one could rationally expect, that by simultaneously targeting different pathophysiological events, the AzA and Zn^{2+} released from BioMIL-5, might provide complementary beneficial actions in the treatment of skin disorders.

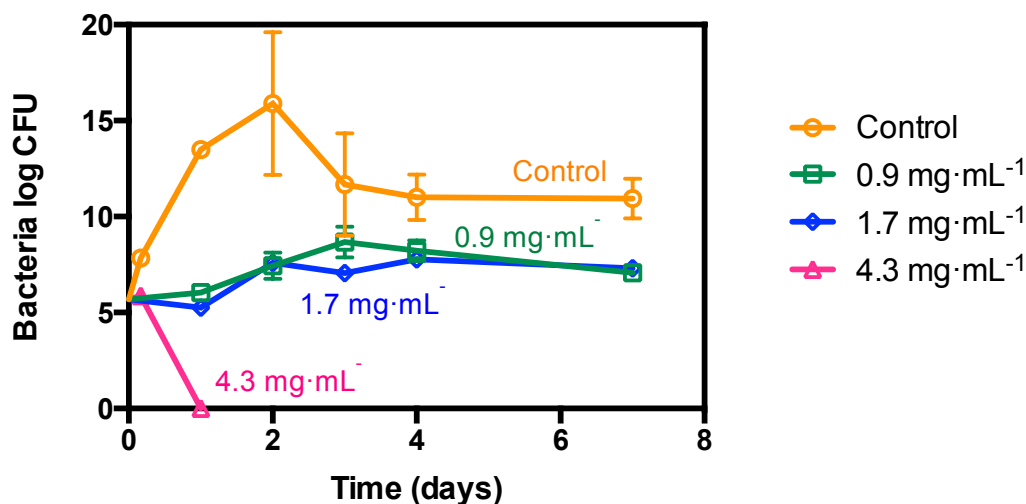


Fig. 5 Bacterial growth curves comparing the control group (○) with BioMIL-5 at different concentrations ($\text{mg}\cdot\text{mL}^{-1}$): 0.9 (□), 1.7 (◇) and $4.3 \text{ mg}\cdot\text{mL}^{-1}$ (△) after 1 week in *S. epidermidis*.

After determining the MIC/MBC values, the following step was to evaluate the influence of the slow release of both AzA and Zn^{2+} on the duration of the pharmacological effect of BioMIL-5. Therefore, the growth of a *S. epidermidis* suspension was monitored for 7 days in the absence or presence of 3 different BioMIL-5 concentrations (0.9, 1.7 and $4.3 \text{ mg}\cdot\text{mL}^{-1}$), in order to evaluate whether it had a time- or dose-dependent antibacterial profile. As depicted in Fig. 5, the presence of BioMIL-5 at the MIC ($1.7 \text{ mg}\cdot\text{mL}^{-1}$) but more interestingly at $0.5 \times \text{MIC}$ ($0.9 \text{ mg}\cdot\text{mL}^{-1}$), significantly reduced the growth rate of *S. epidermidis* and stopped it after 48 h of incubation, evidencing a concentration-dependent biological activity of BioMIL-5. At 48 h, the number of $\text{CFU}\cdot\text{mL}^{-1}$ was 7.76×10^{15} for the non-treated control and 2.82×10^7 for bacteria treated with $0.9 \text{ mg}\cdot\text{mL}^{-1}$ of BioMIL-5, evidencing a bacteriostatic effect. In addition, a bactericidal effect was observed at 24 h when treating the bacteria with $4.3 \text{ mg}\cdot\text{mL}^{-1}$ (MBC), effect that was maintained until the end of the study. Considering the BioMOF degradation, one can estimate a delivery of $0.2 \text{ mg}\cdot\text{mL}^{-1}$ of each Zn^{2+} and AzA from BioMIL-5 ($4.3 \text{ mg}\cdot\text{mL}^{-1}$) to

the MHCA broth after 1 day. A bactericidal effect was achieved at much lower concentrations of BioMIL-5 (Fig. 5, page 178) than the MIC and MBC values established for the isolated Zn²⁺ and AzA components (Tab. 1, page 177), suggesting an additive effect between the Zn²⁺ and the azelate.

4. CONCLUSION

A new bioactive MOF material (BioMIL-5) was hydrothermally synthesised based on Zn²⁺ and AzA, and its structure was fully characterised. Both components exhibit interesting antibacterial and dermatological properties, and are currently being used for the treatment of several skin disorders and in cosmetic industry.

Remarkably, the progressive release of the active Zn²⁺ and AzA from BioMIL-5, in both water and bacterial culture media, led to interesting and time-maintained antibacterial properties when used for 7 days against *S. epidermidis*, a Gram-positive bacterium.

Finally, the incorporation of BioMIL-5 in more complex formulations (*i.e.* semisolid pharmaceutical dosage forms such as creams or gels) by controlling its particle size or its external surface functionalisation could improve its adhesion/penetration in various surfaces (*i.e.* skin, bacteria and other materials) and enhance its efficacy against a broader spectrum of bacteria.

ASSOCIATED CONTENT

Supporting Information

Crystallographic details, physicochemical characterisations (TGA, XRPD, XRTD, FTIR and SEM) and degradation studies are collected in this section. “This material is available free of charge via the Internet at <http://pubs.acs.org>.”

AUTHOR INFORMATION

Corresponding Author

*Patricia Horcajada, Institut Lavoisier, UMR CNRS 8180, Université de Versailles Saint-Quentin-en-Yvelines, 45 Avenue des Etats-Unis, 78035 Versailles Cedex, France. Tel: +33 (0)139254371. Fax: +33 (0)139254452. E-mail: patricia.horcajada-cortes@uvsq.fr

*María J. Blanco-Prieto, Department of Pharmacy and Pharmaceutical Technology, School of Pharmacy, University of Navarra, Irunlarrea 1, 31008 Pamplona, Spain. Tel: +34 948425600 Ext. 806519. Fax: +34 948425649. E-mail: mjblanco@unav.es

Present Addresses

†S.R.M.: UOP Research Center, UOP LLC, a Honeywell Company, 25 East Algonquin Road, Des Plaines, Illinois 60017 United States.

Author Contributions

The manuscript was written through contributions of all authors.

ACKNOWLEDGMENTS

Authors would like to acknowledge T. Devic, C. Thouvenot, T. Baati, L. Frizza and F. Bridoux for their help in XRD, AAS, HPLC and SEM characterisations. The authors thank Soleil for providing access to the beamline Cristal.

C.T.T. would like to thank Asociación de Amigos de la Universidad de Navarra for the predoctoral grant. This work was partially supported by FeUN (Fundación Empresa Universidad de Navarra). Authors acknowledge the CNRS funding, the French ANR 2010-MatePro VirMIL and the EU funding ERC-2007-209241-BioMOFs.

REFERENCES

1. See Special Issues: (a) Guest Editors J.R. Long and O.M. Yaghi, *Chem. Soc. Rev.* 2009, 38, 1201; (b) Guest Editors H.-C. Zhou, J.R. Long and O.M. Yaghi. *Chem. Rev.* 2012, 112, 613.
2. (a) P. Horcajada, R. Gref, T. Baati, P.K. Allan, G. Maurin, P. Couvreur, G. Férey, R.E. Morris and C. Serre, *Chem. Rev.*, 2012, 112, 1232; (b) F. Novio, J. Simmchen, N. Vázquez-Mera, L. Amorín-Ferré and D. Ruiz-Molina, *Coord. Chem. Rev.*, 2013, 257, 2839; (c) J. Della Rocca, D. Liu and W. Lin, *Acc. Chem. Res.*, 2011, 44, 957.
3. (a) P. Horcajada, C. Serre, M. Vallet-Regí, M. Sebban, F. Taulelle and G. Férey, *Angew. Chemie Int. Edit.*, 2006, 45, 5974; (b) P. Horcajada, T. Chalati, C. Serre, B. Gillet, C. Sebrie, T. Baati, J.F. Eubank, D. Heurtaux, P. Clayette, C. Kreuz, J.-S. Chang, Y.K. Hwang, V. Marsaud, P.-N. Bories, L. Cynober, S. Gil, G. Férey, P. Couvreur and R. Gref, *Nat. Mater.*, 2010, 9, 172.
4. D. Cunha, M. Ben Yahia, S. Hall, S.R. Miller, H. Chevreau, E. Elkaïm, G. Maurin, P. Horcajada and C. Serre, *Chem. Mater.*, 2013, 25, 2767.

5. (a) N.J. Hinks, A.C. McKinlay, B. Xiao, P.S. Wheatley and R.E. Morris, *Micropor. Mesopor. Mater.*, 2010, 129, 330; (b) B. Xiao, P.S. Wheatley, X. Zhao, A.J. Fletcher, S. Fox, A.G. Rossi, I. Megson, S. Bordiga, L. Regli, K.M. Thomas and R.E. Morris, *J. Am. Chem. Soc.*, 2007, 129, 1203.
6. (a) V. Lykourinou, Y. Chen, X.-S. Wang, L. Meng, T. Hoang, L.-J. Ming, R.L. Musselman and S. Ma, *J. Am. Chem. Soc.*, 2011, 133, 10382; (b) W.-L. Liu, S.-H. Lo, B. Singco, C.-C. Yang, H.-Y. Huang and C.-H. Lin, *J. Mater. Chem.*, B 2013, 1, 928.
7. (a) W.J. Rieter, K.M.L. Taylor, H. An, W Lin and W. Lin, *J. Am. Chem. Soc.*, 2006, 128, 9024; (b) Y. Wang, J. Yang, Y.-Y. Liu and J.-F. Ma, *Chem. Eur. J.*, 2013, 19, 14591.
8. (a) C. Wang, D. Liu and W. Lin, *J. Am. Chem. Soc.*, 2013, 135, 13222; (b) M.D. Rowe, D.H. Thamm, S.L. Kraft and S. Boyes, *Biomacromolecules*, 2009, 10, 983.
9. (a) S.R. Miller, D. Heurtaux, T. Baati, P. Horcajada, J.-M. Grenèche and C. Serre, *Chem. Commun.*, 2010, 46, 4526; (b) I. Imaz, M. Rubio-Martinez, J. An, I. Sole-Font, N.L. Rosi and D. Maspoch, *Chem. Commun.*, 2011, 47, 7287.
10. (a) T.V. Slenters, J.L. Sagué, P.S. Brunetto, S. Zuber, A. Fleury, L. Mirolo, A.Y. Robin, M. Meuwly, O. Gordon, R. Landmann, A.U. Daniels and K.M. Fromm, *Materials*, 2010, 3, 3407; (b) S.R. Miller, E. Alvarez, L. Fradcourt, T. Devic, S. Wuttke, P.S. Wheatley, N. Steunou, C. Bonhomme, C. Gervais, D. Laurencin, R.E. Morris, A. Vimont, M. Daturi, P. Horcajada and C. Serre, *Chem. Commun.*, 2013, 49, 7773; (c) E. Alvarez, A. García-Márquez, T. Devic, N. Steunou, C. Serre, C. Bonhomme, C. Gervais, I. Izquierdo-Barba, M. Vallet-Regí, D. Laurencin, F. Mauri and P. Horcajada, *CrystEngComm*, 2013, 15, 9899; (d) J. Della Rocca, D. Liu and W. Lin, *Nanomedicine*, 2012, 7, 303.
11. (a) D. Sharma, P. Kumar and B. Narasimhan, *Med. Chem. Res.*, 2012, 21, 796; (b) P. Mishra and K. Mishra, *J. Adv. Pharm. Educ. Res.*, 2012, 2, 110.
12. K. Wang, Y. Yin, C. Li, Z. Geng and Z. Wang, *CrystEngComm*, 2011, 13, 6231.
13. (a) T.V. Slenters, I. Hauser-Gerspach, A.U. Daniels and K.M. Fromm, *J. Mater. Chem.*, 2008, 18, 5359; (b) M. Berchel, T.L. Gall, C. Denis, S.L. Hir, F. Quentel, C. Elleouet, T. Montier, J.-M. Rueff, J.-Y. Salaun, J.-P. Haelters, G.B. Hix, P. Lehn and P.-A. Jaffes, *New J. Chem.*, 2011, 35, 1000; (c) A.M. Kirillov, S.W. Wiczorek, A. Lis, M.F. Guedes da Silva, M. Florek, J. Król, Z. Staroniewicz, P. Smolenski, A.J.L. Pompeiro, *Cryst. Growth Des.*, 2011, 11, 2711; (d) L. Xing, Y. Cao and S. Che, *Chem. Commun.* 2012, 48, 5995.
14. L.M. Plum, L. Rink and H. Haase, *Int. J. Environ. Res. Public Health*, 2010, 7, 1342.
15. J.R. Schwartz, R.G. Marsh and Z.D. Draelos, *Dermatol. Surg.*, 2005, 31, 837.
16. C. Charnock, B. Brudeli and J. Klaveness, *Eur. J. Pharm. Sci.*, 2004, 21, 589.
17. J.E. Wolf Jr., N. Kerrouche and S. Arsonnaud, *Cutis*, 2006, 77, 3.
18. (a) A. Katsambas and C. Dessinioti, *Dermatol. Ther.*, 2008, 21, 86; (b) S. Purdy and D. Deberker, *Clin. Evid.*, 2008, 5, 1714; (c) W.-I. Worret and J.W. Fluhr, *J. Dtsch. Dermatol. Ges.*, 2006, 4, 293.
19. D.M. Thiboutot, A.B. Fleischer Jr., J.Q. Del Rosso and K. Graupe, *J. Drugs Dermatol.*, 2008, 7, 541.

20. (a) K.U. Schallreuter and J.M. Wood, *Cancer Lett.*, 1987, 36, 297; (b) K. Addo-Boadu, J. Wojta, G. Christ, P. Hufnagl, H. Pehamberger and B.R. Binder, *Cancer Lett.*, 1996, 103, 125.
21. N.J. Lowe, D. Rizk, P. Grimes, M. Billips and S. Pincus, *Clin. Ther.*, 1998, 20, 945.
22. S. Farshi, *J. Cosmet. Dermatol.*, 2011, 10, 282.
23. R.A. Bojar, A.G. Cutcliffe, K. Graupe, W.J. Cunliffe and K.T. Holland, *Br. J. Dermatol.*, 1993, 129, 399.
24. A. Boultif and D. Louer, *J. Appl. Crystallogr.*, 2004, 37, 724.
25. Topas V4.2: General Profile and Structure Analysis Software for Powder Diffraction Data, Bruker AXS Ltd, 2008.
26. A. Altomare, M.C. Burla, M. Camalli, B. Carrozzini, G.L. Cascarano, C. Giacovazzo, A. Guagliardi, A.G.G. Moliterni, G. Polidori and R. Rizzi, *J. Appl. Crystallogr.*, 1999, 32, 339.
27. E. Capristo, G. Mingrone, A. De Gaetano, G. Addolorato, A.V. Greco and G. Gasbarrini, *Clin. Chim. Acta*, 1999, 289, 11.
28. CLSI, Clinical and Laboratory Standards Institute: Performance Standards for Antimicrobial Susceptibility Testin: Fifteenth Informational Supplement M100-S15. In Performance Standards for Antimicrobial Susceptibility Testing: Fifteenth Informational Supplement M100-S15. Wayne, PA, USA, 2005.
29. C. Livage, C. Egger, M. Noguez, G. Férey, *C.R. Acad. Sci. Paris Chimie*, 2001, 4, 221.
30. (a) J.-S. Kim, H. Kim and M. Ree, *Chem. Mater.*, 2004, 16, 2981; (b) P.J. Saines, P.T. Barton, P. Jain and A.K. Cheetham, *CrystEngComm*, 2012, 14, 2711.
31. BBLTM Mueller Hinton II Broth (Cation-Adjusted) (Assessed December 2013): [http://www.bd.com/ds/technicalCenter/inserts/LO07475\(12\)\(201102\).pdf](http://www.bd.com/ds/technicalCenter/inserts/LO07475(12)(201102).pdf).
32. Penn State Department of Chemistry (Assessed December 2013): http://research.chem.psu.edu/brpgroup/pKa_compilation.pdf
33. M.H. Kaye and W.T. Thompson; W.T., Uhlig's Corrosion Handbook; John Wiley & Sons: Hoboken, 2011.
34. K.M.L. Taylor-Pashow, J. Della Rocca, Z. Xie, S. Tran and W. Lin, *J. Am. Chem. Soc.*, 2009, 131, 14261.
35. (a) M. Huang, H.T. Wang, J.X. Chen, Z.B. Wang, J.Y. Sun, D.Y. Zhao, Y.S. Yan, *Micropor. Mesopor. Mater.*, 2003, 58, 105; (b) S.S. Kaye, A. Dailly, O.M. Yaghi and J.R. Long, *J. Am. Chem. Soc.*, 2007, 129, 14176; (c) S. Hausdorf, J. Wagler, R. Mossig and F. Mertens, *J. Phys. Chem. A*, 2008, 112, 7567.
36. (a) J. Yang, A. Grzech, F.M. Mulder and F.J. Dingemans, *Chem. Comm.*, 2011, 47, 5244; (b) J.G. Nguyen and S.M. Cohen, *J. Am. Chem. Soc.*, 2010, 13, 4560.

SUPPLEMENTARY INFORMATION

A ZINC AZELATE MOF: COMBINING
ANTIBACTERIAL EFFECT

SUPPLEMENTARY INFORMATION

A ZN AZELATE MOF: COMBINING ANTIBACTERIAL EFFECT

Cristina Tamames-Tabar,^{a,b} Edurne Imbuluzqueta,^a Nathalie Guillou,^b Christian Serre,^b
Stuart R. Miller,^{b†} Erik Elkaïm,^c Patricia Horcajada*^b and María J. Blanco-Prieto*^a

^a*Department of Pharmacy and Pharmaceutical Technology, School of Pharmacy, University of Navarra, Irunlarrea 1, 31008 Pamplona, Spain.*

^b*Institut Lavoisier, UMR CNRS 8180, Université de Versailles Saint-Quentin-en-Yvelines, 45 Avenue des Etats-Unis, 78035 Versailles Cedex, France.*

^c*Cristal beamline, Soleil Synchrotron, L'Orme des Merisiers Saint Aubin BP4891192 Gif-sur-Yvette Cedex, France.*

Accepted in CrystEngComm

1. CRYSTALLOGRAPHIC DATA

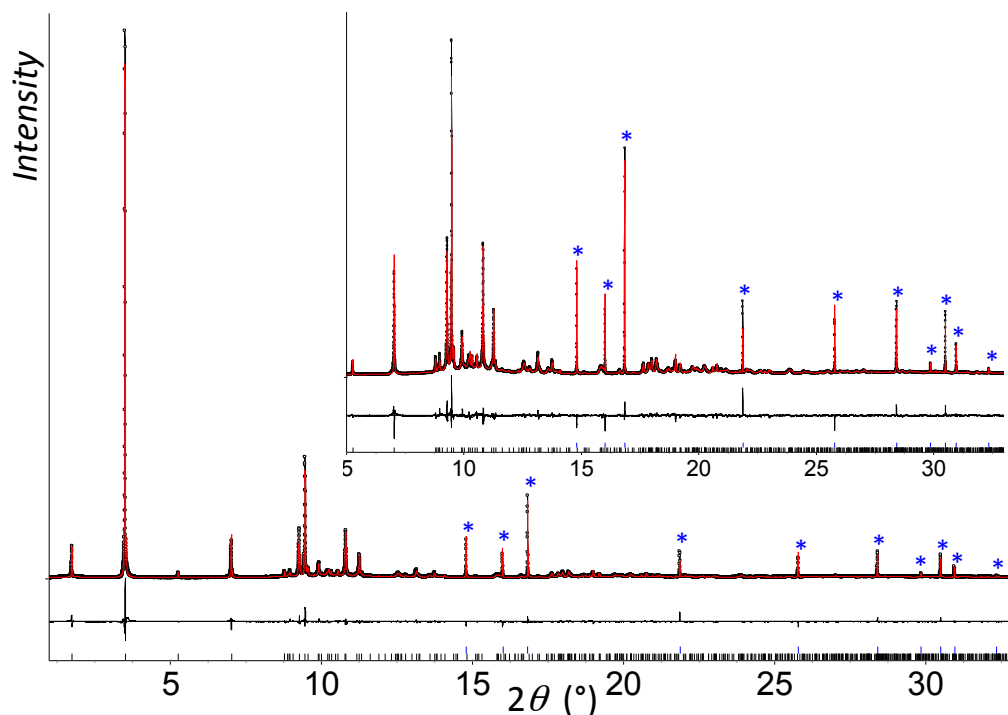


Fig. S1 Final Rietveld plot of BioMIL-5 showing observed (black circles), calculated (red line), and difference (black line) curves. A zoom at high angles is shown as inset. Blue marked lines and stars correspond to ZnO impurity ($\lambda=0.72528 \text{ \AA}$).

Tab. S1 Crystallographic data and Rietveld refinement parameter for BioMIL-5 or $\text{Zn}[\text{C}_9\text{O}_4\text{H}_{14}]$.

Empirical formula	$\text{C}_9\text{H}_{14}\text{O}_4\text{Zn}$
M_r	251.595
Crystal system	Orthorhombic
Space group	<i>Pcca</i>
a (\AA)	47.288(1)
b (\AA)	4.7297(2)
c (\AA)	9.3515(3)
V (\AA^3)	2091.5(1)
Z	8
λ (\AA)	0.72518
Number of reflections	555
No. of fitted structural parameters	47
Number of soft restraints	31
R_p, R_{wp}	0.076, 0.104
R_{Bragg}, GoF	0.029, 2.94

2. THERMOGRAVIMETRIC ANALYSIS (TGA)

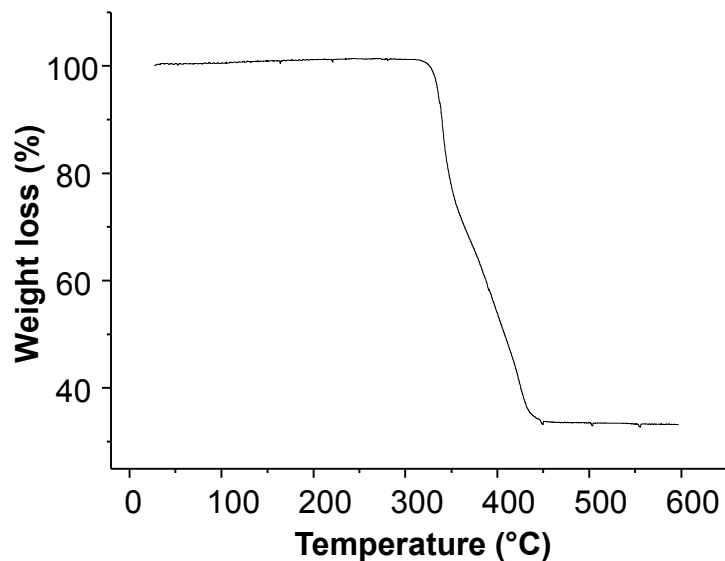


Fig. S2 Thermogravimetric analysis of BioMIL-5.

3. THERMAL STABILITY

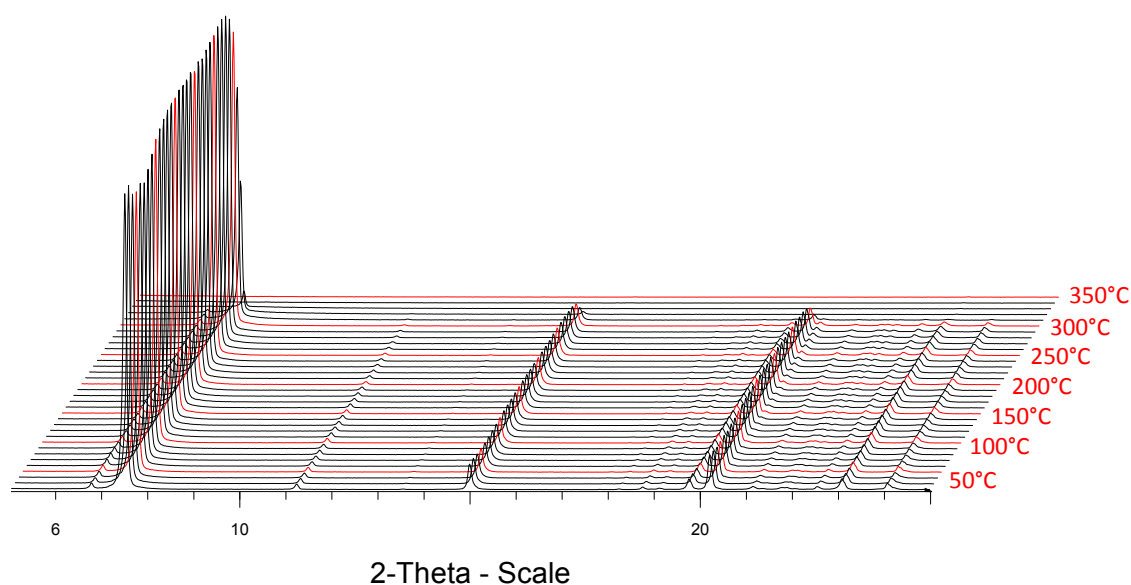


Fig. S3 X ray thermodiffraction patterns ($\lambda_{\text{Cu}}=1.5405 \text{ \AA}$) under air atmosphere of the BioMIL-5. Each red pattern corresponds to a multiple of 50 °C. X-ray powder thermodiffraction (XRTD) was performed using a Bruker D8 Advance diffractometer ($\theta - \theta$ mode, Cu radiation) equipped with a LYNXEYE XE detector. Data were collected in the 2θ range 5-25° with a 0.02° step width, in the temperature range of 20-400 °C at 10 °C intervals.

4. STABILITY IN SOLUTION

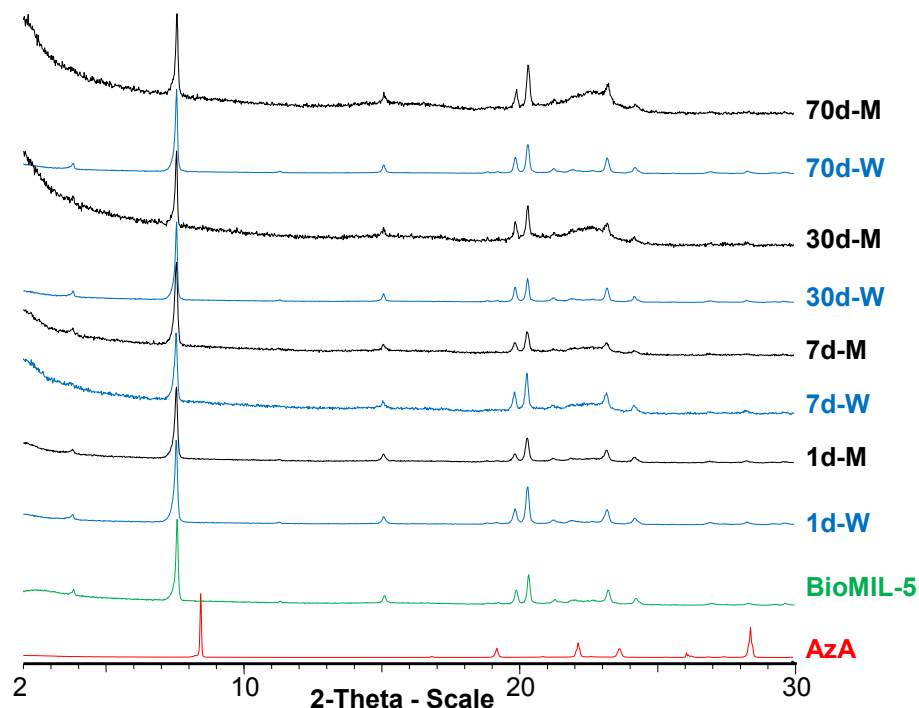


Fig. S4 XRPD patterns of azelaic acid (AzA; red), BioMIL-5 (green) and degradation samples after 1, 7, 30 and 70 days in water (W; blue) and in Mueller Hinton Cation Adjusted Broth medium or MHCA (M; black). X-ray powder diffraction (XRPD) patterns obtained during sample degradation were measured using a high-throughput Bruker D8 Advance diffractometer working on transmission mode and equipped with a focusing Göbel mirror producing $\text{CuK}\alpha$ radiation ($\lambda=1.5418 \text{ \AA}$) and a LYNXEYE detector. Data were collected at room temperature (RT), in the 2θ range $3\text{--}30^\circ$, with a 0.02° step width.

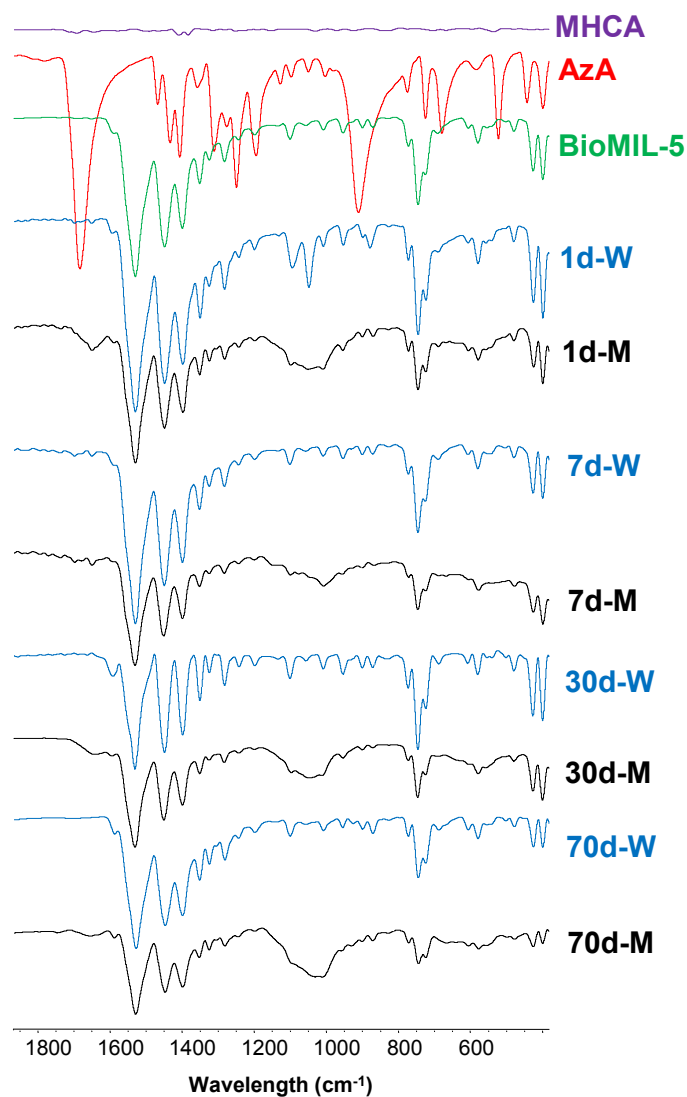


Fig. S5 FTIR spectra of azelaic acid (AzA; red), BioMIL-5 (green), degradation samples after 1, 7, 30 and 70 days in water (W; blue) and in MHCA (M; black).

FTIR spectrum showed the absence of the $\nu(\text{C}=\text{O})$ band at 1700 cm^{-1} confirmed the absence of free-remaining azelaic ligand. For the degradation samples, the presence of phosphates $\nu(\text{P}-\text{O})$ was observed at 1000 cm^{-1} .

GENERAL DISCUSSION

General Discussion

As previously described in the **Introduction** (pages 19-58), since the birth of medicine and pharmacy in the times of Hippocrates (460-370 B.C.) and Galen (130-200 A.D.), the perception of illness and its treatment have evolved over the years [Sonnedecker, 1986]. Pharmaceutical science has made outstanding progress over the centuries and we are now coming ever closer to the specific and individual treatment utopian idea, initially proposed in the 1980s, when the first pioneering works using microparticles (MPs)[Baillie *et al.*, 1987] and nanoparticles (NPs)[Harmia, Speiser and Kreuter, 1986] was carried out. These studies were based on targeting a drug towards a specific part of the body, in order to decrease the treatment's toxicity, enhance the drug's efficacy and most importantly, ameliorate the patient's quality of life to ensure that the treatment is completed [Adair *et al.*, 2010].

These characteristics are the principal objective of today's pharmaceutical technology, which, together with other disciplines, such as pharmacology and material chemistry, is focusing on the design of "new bullets" for treating a broad range of illnesses. A wide prism of diverse particulated systems, diverging in composition and in morphology, has been synthesized and used for this specific purpose, yielding very good results in cancer [Banerjee and Sengupta, 2011], as well as other therapeutic groups.

Within the world of particulated systems, we present Metal-Organic Frameworks (MOFs), which are biodegradable crystalline coordination polymer particles, built-up from inorganic units (cations) and organic polycomplexant linkers (carboxylates, phosphonates, etc), that have been previously proposed as promising solid for their used in diverse industrial applications, such as catalysis and separation [Special Issue Chem. Rev., 2012]. More recently, MOFs have been introduced in biomedicine with outstanding results as drug delivery systems (DDS) [Agostoni *et al.*, 2013a; Cunha *et al.*, 2013a; Cunha *et al.*, 2013b; Novio *et al.*, 2013; Horcajada *et al.*, 2011] and theranostics agents [Wang *et al.*, 2013; Wang, Liu and Lin, 2013 Della Rocca, Liu and Lin, 2011], among other areas.

The novelty of encapsulating drugs in MOFs not only concerns the advantages of encapsulating a drug inside a "traditional" DDS (to increase the drug efficacy and decrease toxicity), but would also permit us to use them in diagnosis and in therapeutic (theranostics), bringing us closer to tailored treatment for each individual.

By taking into account all these ideas, the main objective of this PhD Thesis was to use MOFs as novel DDS by encapsulating drugs within the MOF porosity (the case of "traditional" porous MOFs), and also by going one step further and inserting bioactive

molecules as a constitutive part of the MOF skeleton (the case of biologically active MOFs or BioMOFs), thus expanding the possibilities of this type of particle in bioapplications.

As the use of MOFs in drug delivery has not been exhaustively explored owing to their recent use as DDS (the first study on this subject was published by Horcajada and coworkers in 2006 [Horcajada *et al.*, 2008; Horcajada *et al.*, 2006]), no data regarding their cytotoxicity and cellular uptake was available. Hence, the relevant studies had to be carried out, which was the first objective of this PhD Thesis, encompassed in **Chapter 1** (pages 63-102).

Nonetheless, before any experiment was started, several considerations need to be made. The ultimate step was to reach preclinical studies, the optimization of the particle size and the synthetic conditions had to be performed. First, the particle size needs to be adapted to the administration route and targeted application, influencing the patient's lifestyle. Therefore, as our particular aim was to use MOFs as DDS for oral (p.o.) and intravenous (i.v.) administration, small and monodispersed NPs around 200 nm were required [Adair *et al.*, 2010]. Second, the use of toxic solvents, such as dimethylformamide (typically used for a large number of MOFs), may be avoided.

Once these starting points had been determined, we selected a series of MOFs to work with. As previously described in the **Introduction** (pages 19-58), MOFs are a very versatile type of hybrid materials due to having a broad range of metals and linkers to choose from. Hence, focusing on future bioapplications, and taking into account previous works using MOFs as DDS, different MOFs were chosen. First of all, a series of porous iron(III) carboxylates MOFs was selected due to the encouraging preliminary *in vivo* toxicity experiments in rats, as well as regarding the exceptional drug payloads achieved in these particular MOFs [Baati *et al.*, 2013; Horcajada *et al.*, 2010]. Secondly, the microporous zirconium(IV) terephthalate UiO-66 was chosen as a representative of Zr-based MOFs, which had been shown interesting encapsulation payloads [Cunha *et al.*, 2013a; Gaudin *et al.*, 2012], and has great potential in this field. Finally, the microporous zinc imidazolate ZIF-8 was selected also for its important drug capacities and *a priori* low toxicity based on an endogenous metal [Liédana *et al.*, 2012; Sun *et al.*, 2012]. In addition, ZIF-8 is commercialized by Sigma-Aldrich and produced by BASF as Basolite Z1200® [Park *et al.*, 2006], which highlights its importance in industrial processes, indicating that it could also be translated to biomedical applications.

Furthermore, once the considerations in regard of the particle size and the solvents had been accomplished and the MOFs for this study had been selected, they were reproducibly obtained as MOF NPs without notable changes in their crystalline structure, composition

and porosity, as determined in their complete physicochemical characterization (**Chapter 1, SI**; pages 91-102). In all of the cases, except for MIL-127(Fe)_NPs ($\varnothing \sim 400$ nm), the particle sizes ranged between 75-130 nm, being optimal for both p.o. and i.v. administration routes (**Chapter 1, Table 1**; page 76). Also, all the solvents were changed, when possible, to water and EtOH (*i.e.* MIL-100(Fe)_NPs was synthesized using water as solvent (**Chapter 1, SI**; pages 63-102).

Once all MOFs were correctly synthesized at the nanoscale, their cytotoxicity was evaluated in J774 mouse macrophage (for being the cell line of reference for cellular uptake studies due to its high phagocytic activity) and in HeLa human epithelial cervical carcinoma cell lines (because these are very similar in morphology to epithelial cells and due to the fact that MOFs have interesting potential dermal applications) by the MTT assay [Mosmann, 1983]. Apart from evaluating the MOFs cytotoxicity, their organic constitutive linkers were likewise studied, with the aim of determining the influence of the ligand on the MOF cytotoxicity. In general, the MOFs based on more hydrophobic-linkers MOFs being more toxic than those based on hydrophilic- ones (**Chapter 1, Figure 3**; page 82). Moreover, the fact of studying MOFs containing diverse metal cores (Fe, Zn and Zr), demonstrated that there was a “metal effect” regarding MOF cytotoxicity, as Fe-based MOFs were the least toxic, followed by Zr and Zn. The higher toxic effect of Zn-MOF could be related with the release of Zn^{2+} upon the MOF degradation, which can compete with Fe^{2+} and Ca^{2+} through ion channels and/or can induce DNA damage. In addition, all the results were very similar to other already commercialized metallic particles or to other reported systems [Soma *et al.*, 2000].

Remarkably, a clear difference in cell toxicity was seen regarding the IC_{50} values during 24 h for each cell line: they were in general more toxic in the mouse macrophage J774 cell line than in the HeLa cell line, which is most probably related to their different phagocytic activity. Although our results may sound discouraging since higher IC_{50} values were observed in the case of J774, the fact of studying the behavior of several MOFs in a cell line specialized in phagocytosis, permitted us to reach an intracellular target [Paulo, Pires das Neves and Ferreira, 2011], which will be further discussed alongside the internalization kinetic tests.

Coming back to the IC_{50} values displayed in **Chapter 1, Table 1** (page 76), the mesoporous iron(III) trimesate MIL-100(Fe) was determined to be a safe material and an excellent candidate for future bioapplications ($IC_{50}=0.7$ mg·mL⁻¹ in J774 cell line after 24 h), a fact that was in total agreement with initial *in vivo* studies previously carried out by our research group [Baati *et al.*, 2013; Horcajada *et al.*, 2010]. Hence, cellular penetration studies were carried out with this MOF, as it was necessary to understand the cell-MOF

interactions to plan future outer surface-engineering in order to modulate its *in vivo* biodistribution, as well as to determine its cellular uptake for interesting intracellular targeting.

Before these cellular uptake tests, we engrafted MIL-100(Fe) with a green fluorophore with the final goal of localizing this MOF inside the cells by confocal fluorescence microscopy. Briefly, a simple *ex situ* impregnation [Horcajada *et al.*, 2006] (by suspending the dry MOF into a solution containing the adsorbate, in this case the fluorophore) with a hydrophilic fluorophore called furazan, was accomplished. With this, we could observe by confocal microscopy an immediate cell penetration in the case of J774 when compared to the results in HeLa cells (**Chapter 1, Figure 4**; page 84), a fact which is in total concordance with the previous cytotoxicity observations. These results are very encouraging for various reasons. First, the fast internalization observed with J774 demonstrated the enormous potential that MOF NPs have regarding intracellular targeting, expanding the bioapplication field of these particles. Consequently, this expansion could be accompanied by interesting complementary research that would evaluate the main parameters governing the rapid cell uptake in a detailed way (*i.e.* engineered-surface MOF, particle size and morphology, among others). Secondly, although the kinetics in HeLa were slower, a very important internalization was observed after 8h (**Chapter 1, Figure 4**; page 84), demonstrating that a cell line that is not specialized in phagocytosis could intercept MOF NPs in its interior. This meant that if our final goal were to reach an intracellular target [Paulo, Pires das Neves and Ferreira, 2011], MOFs would act as a drug shelter and preserve an important amount of drug load that would be released in a determined intracellular target (due to rapid cell penetration). Thirdly, after the analysis of the z-axis stack internalization images, we proved that MIL-100(Fe) was homogeneously scattered in both cell lines (**Chapter 1, Figure 5**; page 86), being able to reach diverse cytoplasmic organelles. Nonetheless, this is a simple hypothesis based on our observations in these cellular internalization experiments. In order to determine the internal cytoplasmic penetration of MOFs and the involved cell uptake mechanisms, additional experiments should be carried out.

In conclusion, our first objective from this PhD Thesis was accomplished as displayed in **Chapter 1** (pages 63-102) by the synthesis and characterization of MOF NPs, depicting the parameters that take place in MOF cytotoxicity, in total agreement with the cellular uptake tests.

The natural step after **Chapter 1** was to use MOFs as DDS, which was done in **Chapter 2** (pages 103-157). Previous studies, some of which were carried out by our research group, have shown exceptional results [Agostoni *et al.*, 2013a; Cunha *et al.*, 2013a; Cunha *et al.*, 2013b; Chalati *et al.*, 2011; Horcajada *et al.*, 2008]. The first experiments were performed in 2006 by Horcajada *et al.*, in which the main concern was to study the encapsulation of a model drug (ibuprofen), as a proof of concept in a series of mesoporous metal carboxylates, achieving unprecedented drug payloads (1.4 g ibuprofen·g MOF⁻¹) [Horcajada *et al.*, 2006]. This molecule was further studied in other metal-based MOFs or other inorganic porous materials, achieving important drug loads (20.0-44.5% wt.), depending on the structure and composition of the solid [Cunha *et al.*, 2013; Rodrigues *et al.*, 2012; Babarao and Jiang, 2009; Horcajada *et al.*, 2008; Vallet-Regi *et al.*, 2001]. Among the different drugs encapsulated in porous MOFs, one of the most important groups is represented by antitumor agents, due to the high impact that cancer has in society [WHO Statistics, 2014]. Enthralling results have been obtained by encapsulating doxorubicin (load ~9-21% wt.) [Horcajada *et al.*, 2010; Imaz *et al.*, 2010], busulfan (load ~25% wt.) [Horcajada *et al.*, 2010], camptothecin and daunomycin (load ~21% wt.) [Imaz *et al.*, 2010], 5-fluorouracil (load ~24-50% wt.) [Lucena *et al.*, 2013; Wang *et al.*, 2013; Sun *et al.*, 2012; Sun *et al.*, 2011; Wang *et al.*, 2011] and cisplatin prodrug (load ~13%) [Taylor-Pashow *et al.*, 2009] in iron(III) carboxylates or zirconium(IV) terephthalates MOFs [He *et al.*, 2014].

Continuing along these lines, we chose the antitumor genistein (GEN), a non-toxic bioflavonoid from the family of isoflavones, which is found in many fruits, vegetables, legumes and plant leaves [Bennett *et al.*, 2004] and was first isolated in 1899 from *Genista tinctoria* [Perkin and Newbury, 1899]. This bioflavonoid has a wide array of compelling applications in therapeutics, due to its numerous beneficial effects, among which we find antitumor and antioxidant properties [Polkowski and Mazurek, 2000]. However, due to the scarce data regarding GEN encapsulation in DDS, as well as in *in vivo* pharmacokinetic/biodistribution studies, the second objective of this PhD Thesis proved very challenging.

As recently stated, the encapsulation payload by *ex situ* impregnation [Horcajada *et al.*, 2006] is the conjunction of several parameters [Cunha *et al.*, 2013b]. However, our goal was not to study the different parameters that govern encapsulations, but optimize the GEN loading by playing with some of them, and therefore obtain formulations with high drug loads.

After considering all the reported data, we selected a series of MOFs based on either iron or zirconium that *a priori* could encapsulate GEN for structural reasons. The best results

were obtained with a series of nanoparticulated iron(III) (MIL-100(Fe)_NPs) and (MIL-88C(Fe)_NPs) and microparticulated zirconium(IV)-based MOFs (UiO-66(Zr)_X_MPs, where X=-2CF₃, -NH₂, -BPDC and -NDC; MIL-140C(Zr)_MPs), whose drug cargo oscillated between 160 and 340 µg GEN·mg formulation⁻¹ (**Chapter 2, Table 1**; page 118), staying in the loading interval of other MIL-100(Fe) and UiO-66(Zr) reported formulations (9-37% wt.) [He *et al.*, 2014; Agostoni *et al.*, 2013a; Cunha *et al.*, 2013b; Gaudin *et al.*, 2012; Chalati *et al.*, 2011; Horcajada *et al.*, 2011; Horcajada *et al.*, 2008; Horcajada *et al.*, 2006]. Moreover, our loads were superior to other DDS containing GEN (up to 11.3 % wt.) [Pham, Brownlow and Elbayoumi, 2013; Zhang, Gao and Xu, 2013; Tang *et al.*, 2011; Shin *et al.*, 2010; Cohen *et al.*, 2008; Motlekar, Khan and Youan, 2006] and in some cases, in a similar range to other bioflavonoid encapsulations [Scalia *et al.*, 2013; Ghosh *et al.*, 2011; Tzeng *et al.*, 2011; Ge *et al.*, 2007].

To accomplish the GEN encapsulation, we selected some solvents exhibiting low-toxicity and -boiling points (b.p.), as well as important GEN solubilities. Therefore, after considering previous works in this field, we selected dichloromethane (DCM; S=1.3 mg·mL⁻¹; b.p.=39.6 °C) and ethanol (EtOH; S=2.0 mg·mL⁻¹; b.p.=78.4 °C) [Cunha *et al.*, 2013a; Chalati *et al.*, 2011] (**Chapter 2, Table S1**; page 140). These two solvents were tested, observing that DCM was optimal in all the Zr-based MOFs (~160-340 µg GEN·mg formulation⁻¹), whereas EtOH was suitable for MIL-88C(Fe)_NPs (~201.7±51.7 µg GEN·mg formulation⁻¹), to achieve the highest drug payloads without GEN recrystallization (**Chapter 2, Figure S1**; page 142). In fact, EtOH was used in the flexible MIL-88C(Fe)_NPs, as its fully opened pores in this solvent allowed the GEN diffusion/adsorption within the flexible porosity of this solid [Serre *et al.*, 2007]. Nonetheless, MIL-100(Fe)_NPs did not show good encapsulation results in these two solvents, so we developed a new strategy by synthesizing a GEN dicalcium salt (denoted GCa), which allowed to dramatically improve its water solubility (0.9 µg·mL⁻¹ to 1.4 mg·mL⁻¹; 37 °C) and then use GEN aqueous solutions for its encapsulation (**Chapter 2, SI**; pages 139-141). Additionally, different temperatures were tested, obtaining the best results at 37 °C (~174.0±24.9 µg GEN·mg formulation⁻¹) (**Chapter 2, Table 1**; page 118), probably due to an increase of the drug diffusion rate throughout the MOFs' pores. Interestingly, this plan permitted us to work with water, a non-toxic solvent, as well as other solvents with low toxicity such as DCM and EtOH (rat oral LD₅₀=2100 and 7060 mg·Kg⁻¹ for DCM and EtOH, respectively [MSDS, 2014; US Environmental Protection Agency, 1994]).

Interestingly, we found a clear relation between the drug load and the MOF porosity (**Chapter 2, Tables S4-S5 and Figures S3-S4**; pages 144, 146, 145 and 146,

respectively). MIL-88C(Fe)_NPs was the exception, as despite having the most elevated capacity when totally open, it did not reach the topmost GEN cargo, explained by its partially open porosity in presence of GEN.

Alongside analyzing the drug cargo, several qualitative determinations were made, observing the preservation of the crystalline structure after encapsulation (**Chapter 2, Figure S1**; page 142) and almost no residual porosity after GEN entrapping, consistent with the location of the drug inside the MOF porosity. Moreover, no differences in particle size were observed before and after the GEN encapsulation, although the ζ -potential varied, showing a general tendency towards becoming more negative post-encapsulation (**Chapter 2, Table S3**; page 143). Moreover, the different host-guest interactions were studied by computing simulation GCMC (Grand Canonical Monte Carlo) (**Chapter 2, Figure 3**; page 122), FTIR (**Chapter 2, Figure S5**; pages 147-148) and ^{13}C -NMR (**Chapter 2, Figure S6**; page 149).

One of the reasons for testing different MOF functionalizations (the amine and diperfluoromethyl analogues of the UiO-66_(Zr)), concerned recent works reporting a relationship between the drug load and the MOF functionalization [Cunha *et al.*, 2013a; Cunha *et al.*, 2013b; Gaudin *et al.*, 2012]. Interestingly, after a second impregnation of UiO-66(Zr)_NH₂, a dramatic increase in GEN load was observed, suggesting that this drug raise, might be owing to a partial filling of the pores, which still remained available after the first impregnation, being able to house more GEN (**Chapter 2, Table 1**; page 118). This fact was not observed by Cunha *et al.*, in which after testing several impregnations in a caffeine solution, no improvements in the drug cargo were depicted [Cunha *et al.*, 2013b]. Nevertheless, owing to the high versatility of MOFs, it would be interesting to further study a broader number of MOFs to determine if the GEN encapsulation tendencies can be applied to others. This would open up an exciting array of new possibilities for encapsulating GEN, and even other bioflavonoids, MOFs being an alternative for these non-toxic natural compounds.

Nonetheless, before that, further studies had to be carried out, as there is no sense in obtaining high drug payloads and then not being able to deliver them or to control this process. Therefore, once we had accomplished reproducible GEN formulations, the next step was to study their *in vitro* release under SINK conditions, with the aim of evaluating their release to obtain some idea of what could happen in a living organism. We should bear in mind that the presence of several macromolecules present in the different body fluids would influence the degradation of the DDS differently. However, this assay (*in vitro* release) is widely used for evaluating the suitability of a formulation.

As displayed in **Chapter 2, Figure 2** (page 120), diverse release profiles were observed, depending on the MOF biodegradation, host-guest interactions and drug diffusion (architectures). For example, recent studies evaluating the *in vitro* release of a drug (caffeine) from divergent MOFs and preserving the same release conditions, led to completely diverse release profiles [Cunha *et al.*, 2013a; Liédana *et al.*, 2012].

Briefly, GEN exhibited long release profiles within MOFs (weeks), with the exception of MIL-88C(Fe)_NPs, in which the total load was delivered (in 2 days). This particular MOF, had the greatest surface area, which would suggest that it had the highest capacity to internalize GEN, but in this case it did not have the highest load (**Chapter 2, Table 1**; page 118). As previously reported, the general long release profiles could be due to the hydrophobic character of the drug, impeding its solubilisation in PBS.

Interestingly, if we grouped the formulations regarding their particle size, NPs seemed to release GEN faster than MPs, fact that could be connected to the shorter diffusions that take place in NPs. Also, GEN was slower delivered from those solids bearing a higher hydrophobic character. Moreover, one parameter, which *a priori* was thought to be one of the most important in drug release (pore size), resulted to not being that essential. This could be owing to the diffusion of PBS through the MOF pores, decreasing the drug exchange, fact connected to the high hydrophobic character of GEN. Furthermore, and as it will be further discussed in **Chapter 3** (pages 159-190), the MOF degradation is together with the formation of specific host-guest interaction the other important parameter in drug release [Horcajada *et al.*, 2012].

By comparing our *in vitro* release results with other MOF formulations, in the case of MIL-100(Fe)_NPs, higher release profiles were reported [Agostoni *et al.*, 2013a; Agostoni *et al.*, 2013b; Horcajada *et al.*, 2012]. They were in any case lower than those observed with MIL-88C(Fe)_NPs, as what happened when contrasting our UiO-66(Zr) formulations with others using the same material [He *et al.*, 2014; Cunha *et al.*, 2013a].

At the same time, our release profiles were likewise compared to other published GEN and flavonoid formulations, which depicted similar release profiles to our results when the GEN formulations were immersed in PBS. This outline was dramatically changed by the addition of various chemicals, such as surfactants (improving the drug solubility, scaffold degradation, hence releasing its content) [Pham, Brownlow and Elbayoumi, 2013; Tang *et al.*, 2011; Motlekar, Khan and Youan, 2006], similarly to what happened to the MIL-100(Fe)_NPs formulation after its immersion in a solution containing DMSO/PEG 400/NaCl (10:25:65, v/v) (**Chapter 2, Figure S9**; page 156).

Furthermore, and after we had observed interesting long release GEN profiles from MOFs from a clinical point of view, MIL-100(Fe)_NPs formulation was selected for performing

the pharmacokinetic and biodistribution assays in mice (p.o.). It was chosen because (i) it had an ideal size for p.o. administration (likewise MIL-88C(Fe)_NPs; See **Chapter 2, Table S3**; page 143) and (ii) it exhibited a long *in vitro* release profile (unlike MIL-88C(Fe)_NPs; See **Chapter 2, Figures 2 and S7-S8**; pages 120 and 152-154). Moreover, free GEN was also administered.

By taking a look at **Figure 4 (Chapter 2; page 124)**, we can observe important pharmacokinetic differences between the two treatments. The drug's plasmatic levels were 12-fold higher in the case of the encapsulated GEN, and the mean residence time increased 4-fold (MRT; 3.82 *vs.* 16.23 h for free and encapsulated GEN, respectively). Moreover, its bioavailability increased 62-fold (relative) and ~25% (absolute; F), after its encapsulation in MIL-100(Fe)_NPs, when compared to the p.o. and i.v. administration of free GEN [Tamames-Tabar *et al.*, 2013]. The absolute bioavailability (F) was very similar to that reported by Yang *et al.*, which increased ~24% after the administration of 20 mg·Kg⁻¹ (i.v. and v.o.) to the same animal model [Yang *et al.*, 2010]. At the same time, the release of GEN from MIL-100(Fe)_NPs was determined in an *in vivo* model, being faster when correlated to the *in vitro* SINK conditions (**Chapter 2, Figure 2**; page 120).

Adjacently, the amount of GEN accumulated in several mouse organs was evaluated by a biodistribution study. In it, free GEN was found in liver 4h post-administration (0.58±0.47 µg GEN·g tissue⁻¹). This low value together with a high deviation (a repeated pattern in all analyzed organs), suggested that this was due to working with independent individuals (mice). Concurrently, these high interindividual differences along with the drug's low $t_{1/2}$, could indicate that the amount of free drug distributed to other organs could be under the LOQ (Limit of Quantification) of the technique [Tamames-Tabar *et al.*, 2013].

Rationally, due to the metabolic pathways GEN suffers in liver and in intestine [Steensma, 2006], we expected higher drug levels coming from the encapsulated group at 4 h (0.17±0.07 µg GEN·g tissue⁻¹). However, owing to the fact that mice were sacrificed after 4h, no encapsulated GEN tissue distribution was achieved, which is why these levels were so low. Additionally, the fact of observing a higher encapsulated GEN accumulation in spleen after 24 h (1.28±0.28 µg GEN·g tissue⁻¹), could suggest MOF macrophage removal, with a posterior MOF accumulation in this organ, from which the released GEN would be eliminated via the kidneys (48 h: 0.16±0.02 µg GEN·g tissue⁻¹).

All the previous data suggest, that the fact of encapsulating GEN inside a MOF enhances its plasmatic levels for an extended period of time, and protects it from its metabolization, which is one of the objectives of drug encapsulation in a DDS, fulfilling the second objective of this PhD Thesis. Belatedly, some changes in the experimental plan, such as

sacrifice of the animals 6-8 h post-administration, GEN metabolite monitoring and the evaluation of more organs, will be done in the near future in order to have a general view of this isoflavone in a living organism.

The third and last objective of this PhD Thesis described in **Chapter 3** (pages 159-190) returns to the incorporation of antibacterial agents into a MOF, being the treatment of infectious diseases the second basis for this PhD Thesis, owing to their importance in global terms [WHO Statistics, 2014].

However, this process is slightly different to that presented in **Chapter 2** (pages 103-157). As formerly illustrated in the **Introduction** (pages 19-58), there are two ways of employing MOFs as drug carriers: (i) by the encapsulation of a drug inside a porous MOF by *ex situ* impregnation (in our case the GEN encapsulation displayed in **Chapter 2**) [Horcajada *et al.*, 2006] or (ii) by incorporating a bioactive molecule during the synthetic process in a biologically active MOF called a BioMOF, as the MOF scaffold is built by the bioactive molecule (in our case a novel BioMOF, as displayed in **Chapter 3**) [Alvarez *et al.*, 2013; Miller *et al.*, 2013; Novio *et al.*, 2013; Imaz *et al.*, 2010; Miller *et al.*, 2010].

Infections encompass a wide variety of diseases in terms of the nature of the illness, symptoms and treatment. Prior to deciding what kind of antibacterial spectra we were going to work with, a detailed review of the literature was carried out in order to choose the optimal agents for the synthesis of this novel BioMOF. Hence, we selected azelaic acid (AZA), which had the role of the organic linker due to its dicarboxylic nature, and zinc as the metal core of the BioMOF. Moreover, both AZA and Zn have interesting antibacterial and dermatological properties [Farshi, 2011; Schwarz *et al.*, 2005]. In addition, AZA is poorly absorbed through the skin and requires several applications to maintain active levels for an extended period of time [Bojar *et al.*, 1993]. Hence, the final aim of this BioMOF denoted as BioMIL-5, was to build a new DDS, which enhanced the properties of both chemicals, to finally use it for the treatment of dermatological infections and skin care, pursuing the same aim as any other DDS.

The first goal in **Chapter 3** (pages 159-190) was to synthesize BioMIL-5 in biologically-friendly conditions, a general ambition pursued throughout the PhD Thesis, as seen in **Chapter 1** (pages 63-102), with the replacement of harmful solvents for MOF synthesis and in **Chapter 2** (pages 103-157), with the encapsulation of GEN in non-toxic solvents. BioMIL-5 was synthesized by a green and biocompatible hydrothermal method (**Chapter 3, SI**; pages 183-190). As observed in **Chapter 3, Figure 1** (page 173), we obtained a new hybrid material that crystallized in the orthorhombic group (cell unit: $a=47.288\text{\AA}(1)$; $b=4.7297\text{\AA}(2)$; $c=9.3515\text{\AA}(3)$; $V=2091.5\text{\AA}^3(1)$). In addition, its high thermal stability was

very interesting because of the attainable storage conditions, which is an issue people often do not consider.

Contrary to what is depicted in **Chapters 1** and **2**, where NPs were required due to the targeted future oral (p.o.) and intravenous (i.v.) administration routes, in **Chapter 3**, regarding the intention of using BioMIL-5 for a dermal application, particle size was not a major issue. Therefore, no synthetic modifications were made in order to decrease the particle size, and its micrometric scale size was maintained.

Once we had attained the synthesis and characterization of microparticulated BioMIL-5, the second goal was to study its degradation, which was done with a double purpose: (i) to determine the resistance of the material (keeping in mind the viable possibilities for its conservation) and (ii) to monitor the release of both active molecules (Zn and AzA), as the biological activity of the BioMOF will take place alongside the degradation and release of its components [Alvarez *et al.*, 2013; Miller *et al.*, 2013; Della Rocca, Liu and Lin, 2012; Slenters *et al.*, 2010]. Hence, and with the perspective of testing the efficacy of BioMIL-5 in bacteria, its degradation was accomplished in water and in MHCA bacterial broth, this last medium being more similar to real conditions. Moreover, BioMIL-5 water stability was tested with the scope of determining the differences between the two suspensions as well as possible uses as antibiotic surface-coatings.

These degradation studies done by BioMIL-5 immersion in both media for a total of 70 days, showed an unexpectedly high stability in solution. Moreover, important differences between the two media were observed by comparing both degradation profiles: the degradation was almost complete in MHCA bacterial broth (**Chapter 3, Figure 4**; page 175), as a result of its specific components, which are not present in water.

Subsequently, the efficacy of BioMIL-5 was tested in two common Gram-positive skin bacteria (*Staphylococcus aureus* and *Staphylococcus epidermidis*), as the final bioapplication of BioMIL-5 would be for the treatment of skin infections. First, MIC/MBC studies exhibited large values (at the mg·mL⁻¹ range), contrary to what we expected (µg·mL⁻¹) (**Chapter 3, Table 1**; page 177). In addition, as the free components of the BioMOF were also studied, we could conclude that Zn and AzA had an additive and not a synergic effect, as we first hypothesized. This initial theory was proposed owing to previous work in other application areas (catalysis), which showed a synergistic effect among the different components of the MOF [Wang *et al.*, 2012; Gu *et al.*, 2011; Jiang *et al.*, 2011].

Once we had obtained these MIC/MBC data, we faced our last assay, which consisted of monitoring a *S. epidermidis* suspension for 7 days after the addition of 3 different BioMIL-5 concentrations, with the purpose of determining whether BioMIL-5 had a time-

or concentration-dependent profile. Remarkably, 4.3 mg·mL⁻¹ of BioMIL-5 were bactericidal after 24h. The other two concentrations (0.9 and 1.7 mg·mL⁻¹) were bacteriostatic, an effect that was maintained for 7 days, when compared to the control group (**Chapter 3, Figure 5**; page 178), showing a concentration-dependent behavior that was maintained for at least 7 days. Although it would be useful if the BioMOFs' antibacterial effects were sustained for a more extended period of time, the current duration treatment of a *Staphylococcus* infection is of 7 days, a time span that is in correlation with the patients' clinical response [Stevens *et al.*, 2005].

Although our results with BioMIL-5 were positive, the fact of obtaining bactericidal and bacteriostatic effects at the mg·mL⁻¹ but not the µg·mL⁻¹ scale, made this result somewhat unappealing. Nonetheless, due to the earlier degradation tests performed in water and in MHCA bacterial broth (**Chapter 3, Figure 4**; page 175), we were able to know the exact amount of both Zn and Aza which was released to the solution over a total of 70 days. By looking at the release results after 7 days in MHCA (with the aim of understanding its efficacy in *S. epidermidis*), we observed that the amount of both chemicals was very low, suggesting that the real effect of BioMIL-5 was substantially higher than what was initially spotted (**Chapter 3, Table 1**; page 177). This could be explained, as the BioMIL-5 was only active when its components underwent sustained release from the BioMOF scaffold, so that although the efficacy studies were carried up to 7 days in *S. epidermidis*, it was likely that its effect would be maintained for a longer period. This would seem to indicate that BioMIL-5 has an interesting future perspective in therapeutics, where it is well placed to compete with other existing dermal treatments against this bacterium. Nonetheless, forthcoming evaluations of this BioMOF in a broader spectrum of bacteria would portray a wider scope of bioapplications for this novel material. Similarly, its formulation as composite creams or patches could also help to improve their skin performances.

All the previous results collected in **Chapters 1 to 3**, show significant technological progress in the field of MOF bioapplications, and provide a starting point for future works in this domain, making MOFs one of the most versatile and challenging particles that has come to the fore in recent years. Furthermore, by amalgamating MOFs in different semisolid or solid pharmaceutical dosage forms, as well as by functionalizing the outer particle surface, we could not only expand their intrinsic versatility, but also ameliorate the patient's lifestyle, and come closer to the utopian idea of a tailored treatment for each individual.

REFERENCES

- Adair, J.H.; Parette, M.P.; Altinoğlu, E.İ.; Kester, M., **2010**. Nanoparticulate alternatives for drug delivery. *ACS Nano*, 4(9): 4967-4970.
- Agostoni, V.; Chalati, T.; Horcajada, P.; Willaime, H.; Anand, R.; Semiramoth, N.; Baati, T.; Hall, S.; Maurin, G.; Chacun, H.; Bouchemal, K.; Martineau, C.; Taulelle, F.; Couvreur, P.; Rogez-Kreuz, C.; Clayette, P.; Monti, S.; Serre, C.; Gref, R., **2013**. Towards an improved anti-HIV activity of NRTI via metal-organic frameworks nanoparticles. *Adv. Healthc. Mater.*, 2(12): 1630-1637.
- Agostoni, V.; Anand, R.; Monti, S.; Hall, S.; Maurin, G.; Horcajada, P.; Serre, C.; Bouchemal, K.; Gref, R., **2013**. Impact of phosphorylation on the encapsulation of nucleoside analogues within porous iron(III) metal-organic framework MIL-100(Fe) nanoparticles. *J. Mater. Chem. B*, 1(34): 4231-4242.
- Alvarez, E.; Garcia-Marquez, A.; Devic, T.; Steunou, N.; Serre, C.; Bonhomme, C.; Gervais, C.; Izquierdo-Barba, I.; Vallet-Regí, M.; Laurencin, D.; Mauri, F.; Horcajada, P., **2013**. A biocompatible calcium bisphosphonate coordination polymer: towards a metal-linker synergistic therapeutic effect? *CrystEngComm*, 15: 9899-9905.
- Babarao, R.; Jiang, J., **2009**. Unravelling the energetics and dynamics of ibuprofen in mesoporous metal-organic frameworks. *J. Phys. Chem. C*, 113(42): 18287-18291.
- Baillie, A.J.; Coombs, G.H.; Dolan, T.F.; Hunter, C.A.; Laakso, T.; Sjöholm, I.; Stjärnkvist, P., **1987**. Biodegradable microspheres: polyacryl starch microparticles as a delivery system for the antileishmanial drug, sodium stibogluconate. *J. Pharm. Pharmacol.*, 39(10): 832-835.
- Banerjee, D.; Sengupta, S., **2011**. Nanoparticles in cancer chemotherapy. *Prog. Mol. Biol. Transl. Sci.*, 104: 489-507.
- Bennett, J.O.; Yu, O.; Heatherly, L.G.; Krishnan, H.B., **2004**. Accumulation of genistein and daidzein, soybean isoflavones implicated in promoting human health, is significantly elevated by irrigation. *J. Agric. Food Chem.*, 52(25): 7574-7579.
- Bojar, R.A.; Cutcliffe, A.G.; Graupe, K.; Cunliffe, W.J.; Holland, K.T., **1993**. Follicular concentrations of azelaic acid after a single topical application. *Br. J. Dermatol.*, 129(4): 399-402.
- Chalati, T.; Horcajada, P.; Couvreur, P.; Serre, C.; Ben Yahia, M.; Maurin, G.; Gref, R., **2011**. Porous metal organic framework nanoparticles to address the challenges related to busulfan encapsulation. *Nanomedicine*, 6(10): 1683-1695.
- Cohen, R.; Orlova, Y.; Kovalev, M.; Ungar, Y.; Shimoni, E., **2008**. Structural and functional properties of amylose complexes with genistein. *J. Agric. Food Chem.*, 56(11): 4212-4218.
- Cunha, D.; Ben Yahia, M.; Hall, S.; Miller, S.R.; Chevreau, H.; Elkaïm, E.; Maurin, G.; Horcajada, P.; Serre, C., **2013**. Rationale of drug encapsulation and release from biocompatible porous metal-organic frameworks. *Chem. Mater.*, 25(14): 2767-2776.
- Cunha, D.; Gaudin, C.; Collinet, I.; Horcajada, P.; Maurin, G.; Serre, C., **2013**. Rationalization of the entrapping of bioactive molecules into a series of functionalized porous zirconium terephthalate MOFs. *J. Mater. Chem. B*, 1: 1101-1108.

Della Rocca, J.; Liu, D.; Lin, W., **2012**. Are high drug loading nanoparticles the next step forward for chemotherapy? *Nanomedicine*, 7(3): 303-305.

Della Rocca, J.; Liu, D.; Lin, W., **2011**. Nanoscale metal–organic frameworks for biomedical imaging and drug delivery. *Accounts Chem. Res.*, 44(10): 957-968.

Farshi, S., **2011**. Comparative study of therapeutic effects of 20% azelaic acid and hydroquinone 4% cream in the treatment of melasma. *Cosmet. Dermatol.*, 10(4): 282-287.

Gaudin, C.; Cunha, D.; Ivanoff, E.; Horcajada, P.; Chevé, G.; Yasri, A.; Loget, O.; Serre, C.; Maurin, G., **2012**. A quantitative structure activity relationship approach to probe the influence of the functionalization on the drug encapsulation of porous metal-organic frameworks. *Micropor. Mesopor. Mater.*, 157: 124-130.

Gu, X.; Lu, Z-H.; Jiang, H-L.; Akita, T.; Xu, Q., **2011**. Synergistic catalysis of metalorganic framework-immobilized AuPd nanoparticles in dehydrogenation of formic acid for chemical hydrogen storage. *J. Am. Chem. Soc.*, 133(31): 11822-11825.

Harmia, T.; Speiser, P.; Kreuter, J., **1986**. A solid colloidal drug delivery system for the eye: encapsulation of pilocarpin in nanoparticles. *J. Microencapsul.*, 3(1): 3-12.

He, C.; Lu, K.; Liu, D.; Lin, W., **2014**. Nanoscale metal-organic frameworks for the co-delivery of cisplatin and pooled siRNAs to enhance therapeutic efficacy in drug-resistant ovarian cancer cells. *J. Am. Chem. Soc.* 136(14): 5181-5184.

Horcajada, P.; Gref, R.; Baati, T.; Allan, P.K.; Maurin, G.; Couvreur, P.; Férey, G.; Morris, R.E.; Serre, C., **2012**. Metal–organic frameworks in biomedicine. *Chem. Rev.*, 112(2): 1232-1268.

Horcajada, P.; Serre, C.; McKinlay, A.C.; Morris, R.E., **2011**. “Biomedical applications of metal–organic frameworks” in *Metal-Organic Frameworks: Applications from Catalysis to Gas Storage*, ed. D. Farrusseng, Wiley-VCH Verlag GmbH & Co. KGaA, Weinheim, pp. 213-250.

Horcajada, P.; Chalati, T.; Serre, C.; Gillet, B.; Sebrie, C.; Baati, T.; Eubank, J.F.; Heurtaux, D.; Clayette, P.; Kreuz, C.; Chang, J.-S.; Hwang, Y.K.; Marsaud, V.; Bories, P.-N.; Cynober, L.; Gil, S.; Férey, G.; Couvreur, P.; Gref, R., **2010**. Porous metal-organic-framework nanoscale carriers as a potential platform for drug delivery and imaging. *Nat. Mater.*, 9(2): 172-178.

Horcajada, P.; Serre, C.; Maurin, G.; Ramsahye, N.A.; Balas, F.; Vallet-Regí, M.; Sebban, M.; Taudelle, F.; Férey, G., **2008**. Flexible porous metal-organic frameworks for a controlled drug delivery. *J. Am. Chem. Soc.*, 130(21): 6774-6780.

Horcajada, P.; Serre, C.; Vallet-Regí, M.; Sebban, M.; Taulelle, F.; Férey, G., **2006**. Metal–organic frameworks as efficient materials for drug delivery. *Angew. Chem. Int. Edit.*, 45(36): 6120-6124.

Imaz, I.; Rubio-Martínez, M.; García-Fernández, L.; García, F.; Ruiz-Molina, D.; Hernando, J.; Puentes, V.; MasPOCH, D., **2010**. Coordination polymer particles as potential drug delivery systems. *Chem. Commun.*, 46(26): 4737-4739.

Jiang, H-L.; Akita, T.; Ishida, T.; Haruta, M.; Xu, Q., **2011**. Synergistic catalysis of Au@Ag core-shell nanoparticles stabilized on metal-organic framework. *J. Am. Chem. Soc.*, 133: 1304-1306.

Liédana, N.; Galve, A.; Rubio, C.; Téllez, C.; Coronas, J., **2012**. Caf@ZIF-8: One-step encapsulation of caffeine in MOF. *ACS Appl. Mater. Interfaces*, 4(9): 5016-5021.

- Lucena, F.R.S.; de Araújo, L.C.C.; Rodrigues, M.d.D.; Silva, T.G.; Pereira, V.R.A.; Militão, G.C.G.; Fontes, D.A.F.; Neto, P.J.R.; da Silva, F.F.; Nascimento, S.C., **2013**. Induction of cancer cell death by apoptosis and slow release of 5-fluorouracil from metal-organic frameworks Cu-btc. *Biomed. Pharmacother.*, 67(8): 707-713.
- Miller, S.R.; Alvarez, E.; Fradcourt, L.; Devic, T.; Wuttke, S.; Wheatley, P.S.; Steunou, N.; Bonhomme, C.; Gervais, C.; Laurencin, D.; Morris, R.E.; Vimont, A.; Daturi, M.; Horcajada, P.; Serre, C., **2013**. A rare example of a porous Ca-MOF for the controlled release of biologically active NO. *Chem. Commun.*, 49: 7773-7775.
- Miller, S.R.; Heurtaux, D.; Baati, T.; Horcajada, P.; Greneche, J.-M.; Serre, C., **2010**. Biodegradable therapeutic MOFs for the delivery of bioactive molecules. *Chem. Commun.*, 46(25):4526-4528.
- Mosmann, T., **1983**. Rapid colorimetric assay for cellular growth and survival: application to proliferation and cytotoxicity assays. *J. Immunol. Methods*, 65(1-2): 55-63.
- Motlekar, N.; Khan, M.A.; Youan, B.-B.C., **2006**. Preparation and characterization of genistein containing poly(ethylene glycol) microparticles. *J. Appl. Pol. Sci.*, 101(3): 2070-2078.
- MSDS Data Sheet. **2014**. http://www.spectrex.com/html_files2/pdf/MSDSXDRedSolution.pdf (Accessed April 2014).
- Novio, F.; Simmchen, J.; Vázquez-Mera, N.; Amorín-Ferré, L.; Ruiz-Molina, D., **2013**. Coordination polymer nanoparticles in medicine. *Coord. Chem. Rev.*, 257(19-20): 2839-2847.
- Park, K.S.; Ni, Z.; Côté, A.P.; Choi, J.Y.; Huang, R.; Uribe-Romo, F.J.; Chae, H.K.; O'Keeffe, M.; Yaghi, O.M., **2006**. Exceptional chemical and thermal stability of zeolitic imidazolate frameworks. *Proc. Natl. Acad. Sci. USA*, 130(27): 10186-10191.
- Paulo, C.S.; Pires das Neves, R.; Ferreira, L.S., **2011**. Nanoparticles for intracellular-targeted drug delivery. *Nanotechnology*, 22(49): 494002-494012.
- Perkin, A.G.; Newbury, F.G., **1899**. LXXIX.—The colouring matters contained in dyer's broom (*Genista tinctoria*) and heather (*Calluna vulgaris*). *J. Chem. Soc. Trans.*, 75: 830-839.
- Pham, J.; Brownlow, B.; Elbayoumi, T., **2013**. Mitochondria-specific pro-apoptotic activity of genistein lipidic nanocarriers. *Mol. Pharm.*, 10(10): 3789-3800.
- Polkowski, K.; Mazurek, A.P., **2000**. Biological properties of genistein. A review of *in vitro* and *in vivo* data. *Acta Pol. Pharm.*, 57(2): 135-155.
- Rodrigues, M.O.; de Paula, M.V.; Wanderley, K.A.; Vasconcelos, I.B.; Alves, S.; Soares, T.A., **2012**. Metal-organic frameworks for drug delivery and environmental remediation: a molecular docking approach. *Int. J. Quant. Chem.*, 112(20): 3346-3355.
- Schwartz, J.R.; Marsh, R.R.; Draelos, Z.D., **2005**. Zinc and skin health: overview of physiology and pharmacology. *Dermatol. Surg.*, 31: 837-847.
- Serre, C.; Mellot-Draznieks, C.; Surblé, S.; Audebrand, N.; Filinchuk, Y.; Férey, G., **2007**. Role of solvent-host interactions that lead to very large swelling of hybrid frameworks. *Science*, 315(5820): 1828-1831.
- Shin, J.; Shin, K.; Lee, H.; Nam, J.-B.; Jung, J.-E.; Ryu, J.-H.; Han, J.-H.; Suh, K.-D.; Kim, Y.-J.; Shim, J.; Kim, J.; Han, S.-H.; Char, K.; Kim, Y.M.; Chung, J.H.; Lee, M.J.; Kang, B.C.; Kim, J.-W.,

2010. Non-invasive transdermal delivery route using electrostatically interactive biocompatible nanocapsules. *Adv. Mater.*, 22(6): 739-743.

Slenters, T.V.; Sagué, J.L.; Brunetto, P.S.; Zuber, S.; Fleury, A.; Mirolo, L.; Robin, A.Y.; Meuwly, M.; Gordon, O.; Landmann, R.; Daniels, A.U.; Fromm, K.M., **2010.** Of chains and rings: synthetic strategies and theoretical investigations for tuning the structure of silver coordination compounds and their applications. *Materials*, 3(5): 3407-3429.

Soma, C.E.; Dubernet, C.; Barratt, G.; Benita, S.; Couvreur, P., **2000.** Investigation of the role of macrophages on the cytotoxicity of doxorubicin and doxorubicin-loaded nanoparticles on M5076 cells *in vitro*. *J. Control. Release*, 68(2): 283-289.

Sonnedecker, G., **1986.** *Kremers and Urdang's History of Pharmacy*. 4th edn. The American Institute of the History of Pharmacy, Madison (WI).

Special Issue **2012.** Guest Editors H.-C. Zhou, J.R. Long and O.M. Yaghi. *Chem. Rev.*, 112: 673-1268.

Steensma, A., **2006.** Bioavailability of genistein and its glycoside genistin. PhD Thesis (Wageningen University, The Netherlands).

Stevens, D.L.; Bisno, A.L.; Chambers, H.F.; Dale Everett, E.; Dellinger, P.; Goldstein, E.J.C.; Gorbach, S.L.; Hirschmann, J.V.; Kaplan, E.J.; Montoya, J.G.; Wade, J.C., **2005.** Practice guidelines for the diagnosis and management of skin and soft-tissue infections. *Clin. Infect. Dis.*, 41(10): 1373-1406.

Sun, C.-Y.; Qin, C.; Wang, X.-L.; Yang, G.-S.; Shao, K.-Z.; Lan, Y.-Q.; Su, Z.-M.; Huang, P.; Wang, C.-G.; Wang, E.-B., **2012.** Zeolitic imidazolate framework-8 as efficient pH- sensitive drug delivery vehicle. *Dalton Trans.*, 41(23): 6906-6909.

Sun, C.-Y.; Qin, C.; Wang, C.-G.; Su, Z.-M.; Wang, S.; Wang, X.-L.; Yang, G.-S.; Shao, K.-Z.; Lan, Y.-Q.; Wang, E.-B., **2011.** Chiral nanoporous metal-organic frameworks with high porosity as materials for drug delivery., *Adv. Mater.*, 23(47) : 5629-5632.

Tamames-Tabar; C., Imbuluzqueta, E.; Campanero, M.A.; Horcajada, P.; Blanco-Prieto, M.J., **2013.** A simple and robust high-performance liquid chromatography coupled to a diode-array detector method for the analysis of genistein in mouse tissues. *J. Chrom. B.*, 935(0): 47-53.

Tang, J.; Xu, N.; Ji, H.; Liu, H.; Wang, Z.; Wu, L., **2011.** Eudragit nanoparticles containing genistein: formulation, development, and bioavailability assessment. *Int. J. Nanomedicine*, 6: 2429-2435.

Taylor-Pashow, K.M.L.; Della Rocca, J.; Xie, Z.; Tran, S.; Lin, W., **2009.** Postsynthetic modifications of iron-carboxylate nanoscale metal-organic frameworks for imaging and drug delivery. *J. Am. Chem. Soc.*, 131(40): 14261-14263.

U.S. Environmental Protection Agency **1994.** (http://www.epa.gov/chemfact/s_dcm.txt) (Assessed April 2014).

Vallet-Regí, M.; Rámila, A.; Del Real, R.P.; Pérez-Pariente, J., **2001.** A new property for MCM-41: drug delivery system. *Chem. Mater.*, 13(2): 308-311.

Wang, C.; Liu, D.; Lin, W., **2013.** Metal-organic frameworks as a tunable platform for designing functional molecular materials. *J. Am. Chem. Soc.*, 135(36): 13222-13234.

Wang, Y.; Yang, J.; Liu, Y.-Y.; Ma, J.-F., **2013**. Controllable syntheses of porous metal–organic frameworks: encapsulation of LnIII cations for tunable luminescence and small drug molecules for efficient delivery. *Chem. Eur. J.*, 19(43): 14591-14599.

Wang, C.; deKrafft, K.E.; Lin, W., **2012**. Pt nanoparticles@photoactive metal–organic frameworks: efficient hydrogen evolution via synergistic photoexcitation and electron injection. *J. Am. Chem. Soc.*, 134: 7211-7214.

WHO (World Health Organization), **2012**. International Agency for Research on Cancer. Globocan 2012: Incidence, Mortality and Prevalence Worldwide in 2012. http://globocan.iarc.fr/Pages/fact_sheets_cancer.aspx (Accessed April 2014).

Yang, Z.; Zhu, W.; Gao, S.; Xu, H.; Wu, B.; Kulkarni, K., **2010**. Simultaneous determination of genistein and its four phase II metabolites in blood by a sensitive and robust UPLC-MS/MS method: Application to an oral bioavailability study of genistein in mice. *J. Pharm. Biomed. Anal.*, 53(1): 81-89.

Zhang, Y.; Gao, B.; Xu, Z., **2013**. Adsorption properties of polyvinyl-alcohol-grafted particles toward genistein driven by hydrogen-bond interaction. *J. Phys. Chem. B*, 117(18): 5730-5736

GENERAL CONCLUSIONS
CONCLUSIONES GENERALES
CONCLUSIONS GÉNÉRALES

GENERAL CONCLUSIONS

The studies included in this work allow us to conclude that:

- 1) A series of 14 nanoMOFs were successfully synthesized and fully characterized at the nanoscale, exhibiting a crystalline structure and textural properties comparable with their respective bulk materials.
- 2) The cytotoxicity of these MOF NPs was evaluated by the MTT assay on two cell lines (J774 and HeLa), exhibiting low toxicity values similar to those of other currently commercialized nanometric systems. Cytotoxicity strongly depended on the MOF composition such as: (i) the nature of the metal (being less toxic the Fe-based MOFs, compared with the Zr- or Zn-MOF NPs) and (ii) the constitutive organic linker (the hydrophobic–hydrophilic balance being an important parameter).
- 3) The higher cytotoxicity observed in J774 cells when compared to HeLa cells was mainly attributed to the faster internalization of the NPs in the macrophage line. Moreover, the stable fluorophore grafting within MIL-100(Fe)_NPs permitted the evaluation of the cell uptake by confocal fluorescence microscopy, indicating an immediate cell internalization in J774 cells, faster than in HeLa cells, in complete agreement with their different phagocytic activities. This fact showed interesting future intracellular targeting of MOF NPs.
- 4) Important GEN payloads were achieved, ranging from 160 to 340 $\mu\text{g GEN}\cdot\text{mg formulation}^{-1}$, using Zr and Fe based MOFs. These formulations were within the scope of other MOF formulations and higher than other GEN formulations. The encapsulation rate strongly depended on: (i) the MOF (architecture and composition), (ii) the solvent and (iii) the temperature.
- 5) Furthermore, GEN was slowly and sustainably released from the MOF-GEN formulations under *in vitro* SINK release studies. These long release profiles were important due to the significance they will have in future preclinical studies.
- 6) The *in vivo* evaluation of MIL-100(Fe)_NPs in a mouse model showed that after the administration of the encapsulated GEN p.o., longer-time and higher plasmatic levels were observed, as well as an increase in pharmacokinetic parameters such as drug oral bioavailability, among others. Moreover, the MOF worked as a shelter for GEN, impeding its metabolization. Hence, GEN levels were detected in organs up to 48h post-administration.
- 7) Alternatively to the drug encapsulation within the MOF porosity, we synthesized under biocompatible conditions and fully characterized a novel bioactive MOF, BioMIL-5, built

up from Zn and AzA, both exhibiting interesting antibacterial and dermatological properties.

8) The progressive release of the active Zn and AzA from BioMIL-5 in both water and bacterial broth, as a consequence of its outstanding stability, led to interesting and time-maintained antibacterial properties for 7 days against *S. epidermidis*, a Gram-positive bacterium. Moreover, thermal and chemical stability of BioMIL-5 might allow its easy and long storage.

9) The incorporation of BioMIL-5 in more complex formulations by controlling its particle size or its external surface functionalization could ameliorate its adhesion/penetration on several surfaces and enhance its efficacy in a broader spectrum of bacteria.

CONCLUSIONES GENERALES

Los resultados de estos estudios permiten concluir:

- 1) Tras sintetizar y caracterizar una nueva serie de nanoMOFs se encontró que presentaban una estructura cristalina y propiedades texturales comparables a las de sus respectivos materiales en escala micrométrica.
- 2) Se evaluó la citotoxicidad de estos nanoMOFs en dos líneas celulares (J774 y HeLa) y se encontraron valores bajos de toxicidad, similares a otros sistemas nanoparticulados comercializados. La citotoxicidad depende de la naturaleza del metal, los menos tóxicos son aquellos MOFs a base de Fe. Se observó que el balance hidrofóbico/hidrofílico es un parámetro importante.
- 3) La elevada citotoxicidad observada en células J774 comparada con las células HeLa, se atribuye principalmente a una internalización más rápida de las nanopartículas en la línea de macrófagos. Por otro lado, un marcaje de MIL-100(Fe)_NPs con un fluoróforo permitió evaluar su penetración celular mediante microscopía confocal de fluorescencia. Los resultados muestran una internalización celular inmediata en las células J774, más rápida que en las células HeLa en concordancia con sus diferentes actividades fagocíticas. Este resultado tiene gran interés para el “*targeting*” intracelular de los nanoMOFs.
- 4) En los MOFs a base de Fe y de Zr, se obtuvieron cargas elevadas de genisteína, comprendidas entre 160 y 340 mg por mg de formulación, valores superiores a los obtenidos con otros sistemas de liberación de genisteína. La encapsulación depende de la arquitectura y composición del MOF así como de las condiciones de impregnación (principalmente del solvente y la temperatura).
- 5) En los estudios de liberación *in vitro*, la genisteína se liberó de forma sostenida. Los perfiles de liberación son importantes a la hora de considerar futuros estudios preclínicos.
- 6) Tras la administración oral de MIL-100(Fe)_NPs a ratones, la genisteína presentó una mejor biodisponibilidad que cuando se administraba en forma libre. Se observaron niveles plasmáticos más elevados y más sostenidos (48 horas), debido a que el MOF protege al fármaco de su biotransformación.
- 7) Los MOFs preparados con los agentes antibacterianos Zn y azelato de Zn, resultaron ser dermatológicamente activos.
- 8) La liberación progresiva en agua y en medio de cultivo bacteriano de las formas activas de Zn y azelato de Zn desde el BioMIL-5 se prolongó a lo largo de siete días mostrándose efectivos frente a la bacteria Gram-positiva *S. epidermis*. La estabilidad térmica y química del BioMIL-5 puede permitir su almacenaje a temperatura ambiente.

9) La incorporación de BioMIL-5 en formulaciones controlando su tamaño de partícula y/o la funcionalización de la superficie externa puede mejorar su adhesión/penetración sobre diferentes superficies y aumentar su eficacia en una amplia variedad de bacterias.

CONCLUSIONS GÉNÉRALES

Les études issues de ce travail de thèse permettent de conclure que:

1) Une série de 14 nanoMOFs a été synthétisée et complètement caractérisée à l'échelle nanométrique, tout en conservant une structure cristalline et des propriétés texturales comparables à celles des matériaux micrométriques.

2) La cytotoxicité de ces nanoMOFs a été évaluée par le test MTT sur deux lignées cellulaires (J774 et HeLa), révélant une faible toxicité, similaire à celle d'autres nanoparticules commercialisées. Leur cytotoxicité dépendait de: (i) la nature du métal (étant les moins toxiques les MOFs à base du Fe, en comparaison avec ceux à base de Zr et Zn) et (ii) le ligand organique constitutif (étant le balance hydrophobe-hydrophile un paramètre crucial).

3) La cytotoxicité plus élevée des cellules J774 en comparaison avec les cellules HeLa, était attribuée à une internalisation plus rapide des NPs dans les macrophages. En outre, le marquage stable des MIL-100(Fe)_NPs avec un fluorophore, a permis d'évaluer leur pénétration cellulaire par microscopie confocale de fluorescence. L'internalisation cellulaire, immédiate dans la lignée J774, est plus rapide que dans les HeLa, en accord avec la différente activité phagocytaire des deux lignées. Ainsi, les nanoMOFs ont dévoilé un futur prometteur dans le ciblage intracellulaire.

4) Les capacités importantes de GEN, d'entre 160 à 340 $\mu\text{g GEN}\cdot\text{mg formulation}^{-1}$, obtenues dans les MOFs à base de Fe et Zr sont comparables à d'autres formulations à base de MOFs, voire plus élevées que d'autres formulations encapsulant la GEN. L'encapsulation dépendait principalement: (i) du MOF (architecture et composition), (ii) du solvant et (iii) de la température.

5) En plus, la GEN a été libérée progressivement depuis les formulations sous de conditions SINK *in vitro*. Ces cinétiques de libération contrôlée se révèlent très intéressantes en vue des futures études précliniques.

6) L'évaluation *in vivo* du MIL-100(Fe)_NPs sur un modèle murin a montré que l'administration de la formulation par voie orale permet d'obtenir des niveaux plasmatiques plus élevés et durables, ainsi qu'une augmentation des paramètres pharmacocinétiques tels que la biodisponibilité orale du médicament, entre autres. Au même temps, le MOF a permis de protéger la GEN, en évitant sa métabolisation. Or, des niveaux significatifs de GEN ont pu être détectés dans les organes même après 48 h de l'administration.

7) Alternativement à l'encapsulation des médicaments dans la porosité du MOF, nous avons synthétisé (sous des conditions biocompatibles) et caractérisé complètement un nouveau MOF bioactif, le BioMIL-5, construit à partir des agents antibactériens et dermatologiques actifs, le Zn et l'AzA.

8) La libération progressive des formes actives du Zn et de l'AzA depuis le BioMIL-5 dans l'eau et dans le milieu de culture bactérien, fut la conséquence d'une stabilité remarquable, ce qui a conduit à des propriétés antibactériennes intéressantes et temps-dépendantes pendant 7 jours contre la bactérie Gram-positive *S. epidermidis*. En outre, la stabilité thermique et chimique exceptionnelle du BioMIL-5 permettra son stockage simple et durable.

9) L'incorporation du BioMIL-5 dans des formulations plus complexes, en maîtrisant la taille de particule et/ou la fonctionnalisation de sa surface externe, pourra améliorer l'adhésion/pénétration du BioMIL-5 sur des diverses surfaces, voire augmenter son efficacité sur un range plus large de bactéries.

ANNEX I
RESUME GENERALE

Introduction

Depuis la naissance de la pharmacie et de la médecine avec Hippocrate (460-370 avant J.C.) et Galène (130-200 après J.C.), la perception de la maladie et de son traitement a changée pendant les années selon les besoins de la société [Sonnedecker, 1986]. Afin d'accomplir un traitement fait «sur mesure» pour chaque individu, la pharmacie a beaucoup évoluée jusqu'à présent pour y arriver aux traitements à base de micro et nanoparticules.

Le traitement du cancer et des maladies infectieuses, avec une relevance socioéconomique major est très varié. Ainsi, des nombreux médicaments sont actuellement disponibles avec une efficacité *in vitro* remarquable. Cependant, ces molécules présentent aussi des nombreux inconvénients, limitant son utilisation clinique (*i.e.* faible spécificité, toxicité élevée, entre autres).

En conséquence, un des objectifs actuels de la technologie pharmaceutique est de trouver des formulations adaptées pour véhiculer les médicaments afin de leur rendre plus sûres (en regardant la toxicité) et efficaces, avec en prime une amélioration de la qualité de vie du patient [Adair *et al.*, 2010]. Dans ce sens, l'encapsulation et la libération des médicaments depuis des systèmes de particules biodegradables a montrée des résultats très prometteurs.

D'entre les nombreux types de systèmes particuliers de vectorisation des médicaments (polymères, liposomes, silice, etc), nous nous sommes concentrés dans les solides hybrides cristallins du type MOF ou *Metal-Organic Frameworks*. Ce solides sont de matériaux hybrides tridimensionnels construits à partir d'un cation (métaux de transition, alcalin, lanthanides, etc) connecté par des liaisons fortes du type ionocovalent avec un ligand organique portant plusieurs fonctions complexantes (carboxylate, phosphonate, imidazolate, polyols, etc) [Meek, Greathouse and Allendorf, 2011]. Sa grande versatilité chimique et sa porosité élevée font de ces solides des candidats potentiels pour diverses applications industrielles, telles que la catalyse ou la séparation [Special Issue, 2012]. Plus récemment, ces solides se sont révélés de candidats très prometteurs pour la biomédecine, notamment comme systèmes de libération contrôlée de molécules thérapeutiques (médicaments, cosmétiques, gazes, etc). [Novio *et al.*, 2013; Horcajada *et al.*, 2012; Della Rocca, Liu and Lin, 2011]. En effet, certains MOFs poreux biocompatibles (les carboxylates de fer(III)) sont capables d'encapsuler des quantités exceptionnelles de médicaments dans sa porosité ainsi que libérer progressivement dans les milieux biologiques comme conséquence de la diffusion du médicament à travers des pores, de la

dégradation de la matrice hybride et de la création d'interactions spécifiques médicament-réseau [Agostoni *et al.*, 2013a; Horcajada *et al.*, 2012]. Egalement, le MOF puisse être construit à partir de composants (cation et/ou ligand organique) portant une activité biologique eux-mêmes, conduisant à la libération contrôlée des espèces actives par dégradation du MOF [Miller *et al.*, 2010].

En plus, quelques d'eux possèdent agents de contraste que bien directes d'entre son structure (inorganique ou organique), ou a travers d'un marquage avec molécules actives par leur surface (porosité externe ou interne), font de ce type de systèmes des candidats très intéressants pour theranostique.

Ensuite, les MOFs peuvent être produits en nanoparticules avec modifications en surface, en films, en parches, ou pellets, nécessaires pour développer différentes formulations adéquates pour diverses voies d'administration.

Finalement, malgré quelques structures sont biodegradables, elles peuvent être aussi toxiques, étant ce point étudié en détail dans futures évaluations *in vitro* et *in vivo*, incluant évaluations ADME et études d'efficacité. En ce sens, la formulation peut être spécifiquement adapté pour chaque voie d'administration.

Objectifs

En tenant en compte les idées précédentes, l'**Objectif Général** de ce projet de Thèse est le design, la synthèse et l'évaluation biomédicale des polymères de coordination poreux ou *Metal-Organic Frameworks* (MOFs). Ainsi, nous avons sélectionné deux molécules thérapeutiques: (i) l'antitumoral génistéine, d'origine naturelle, que sera encapsulé dans la porosité des MOFs et (ii) les agents antibiotiques (acide azélaïque et le zinc) que seront associés par liaisons fortes pour former un MOF (ou BioMOF) dont ces composants sont déjà bioactifs.

A ce propos, le travail a été organisé en trois volets principaux, décrits ici-bas:

- 1) La synthèse et la caractérisation d'une série de MOFs nanométriques à base de métaux non toxiques (Fe, Zr, Zn) ainsi que l'évaluation de leur cytotoxicité et pénétration cellulaire afin de sélectionner les particules les mieux adaptées pour l'encapsulation des médicaments (**Chapitre 1**).
- 2) L'encapsulation et la libération *in vitro* de l'isoflavone génistéine depuis une série des MOFs à base du fer(III) et du zirconium(IV), et l'étude de son profil pharmacocinétique et de biodistribution dans un modèle *in vivo* (**Chapitre 2**).

La synthèse et la caractérisation complète d'un nouveau azelate de zinc, ainsi que l'évaluation de ses propriétés antibactériennes pour le traitement des différentes pathologies cutanées (**Chapitre 3**).

Chapitre 1: C. Tamames-Tabar, D. Cunha, E. Imbuluzqueta, F. Ragon, C. Serre, M. J. Blanco-Prieto and P. Horcajada, **2014**. Cytotoxicity of Nanoscaled Metal-Organic Frameworks, *J. Mater. Chem. B.*, **2**, 262-271.

Bien que certains MOFs ont déjà montré des résultats très prometteurs en biomédecine, avec non seulement des capacités d'encapsulation exceptionnelles et des libérations progressives de la forme active du médicament, mais aussi avec de propriétés très intéressantes en imagerie médicale [Horcajada *et al.*, 2010], l'évaluation de leur toxicité se révèle impératif pour son application future en clinique. Malgré l'absence de toxicité sévère *in vivo* après l'administration intraveineuse de doses élevées (220 mg.kg^{-1}) des trois carboxylates de fer(III) microporeux nanométriques [Baati *et al.*, 2013; Horcajada *et al.*, 2010], la toxicité *in vitro* et *in vivo*, ainsi que l'étude des possibles interactions avec le vivant semblent indispensable pour chaque un des structures et compositions des MOFs. En conséquence, le **Chapitre 1** est focalisé sur l'évaluation de la toxicité *in vitro* d'une série de MOFs, *a priori* les plus prometteurs pour la libération contrôlée de médicaments, a été évaluée sur deux lignées cellulaires afin de déterminer les paramètres influençant leur toxicité.

Ainsi, nous avons synthétisé par voie hydro ou solvothermale une série de 14 MOFs à l'échelle nanométrique (nanoMOFs) avec différent structure et/ou composition (carboxylates ou imidazolates de Fe, Zr ou Zn). On a sélectionné les MOFs les plus intéressants en termes de son potentiel pour la libération de médicaments: (i) 12 carboxylates de fer(III) micro o mésoporeux à base de différents ligands organiques (fumarate, trimesate, 3,3',5,5'-azobenzene tetracarboxylate et divers téréphthalates portant différentes groupes fonctionnels tels que amine, méthyl ou perfluorométhyl) avec des topologies différentes (cubique, hexagonale...); (ii) un téréphthalate de zirconium(IV) microporeux cubique (UiO-66) et (iii) un imidazolate de zinc(II).

Ces nanoparticules ont été caractérisées par diverses techniques (diffraction de rayons X (XRPD), spectroscopie infra-rouge (FTIR), diffusion de lumière (DLS), ζ -potentiel, microscopie électronique à transmission (TEM), analyse thermogravimétrique (TGA), analyse chimique (EA), porosimétrie d'adsorption de N_2 , etc) (**SI**). De façon remarquable, des nanoparticules de taille petite ($\sim 100 \text{ nm}$) et monodisperse (polydispersité < 0.3 ; **Figure 1**), compatibles avec une administration intraveineuse [Adair *et al.*, 2010], avec

des charges superficielles négatives et des porosités très importantes (comparables à celles des matériaux en «bulk») ont pu être préparées avec des rendements élevés (<70%). Bien que la synthèse de plusieurs nanoMOFs nécessite l'utilisation de solvants toxiques du type diméthylformamide ou méthanol, nous avons pu synthétiser plusieurs nanoMOFs par une voie biocompatible en utilisant l'eau ou l'éthanol. Du même, les solvants toxiques ont pu aussi être compléments enlevés par différents traitements post-synthèse.

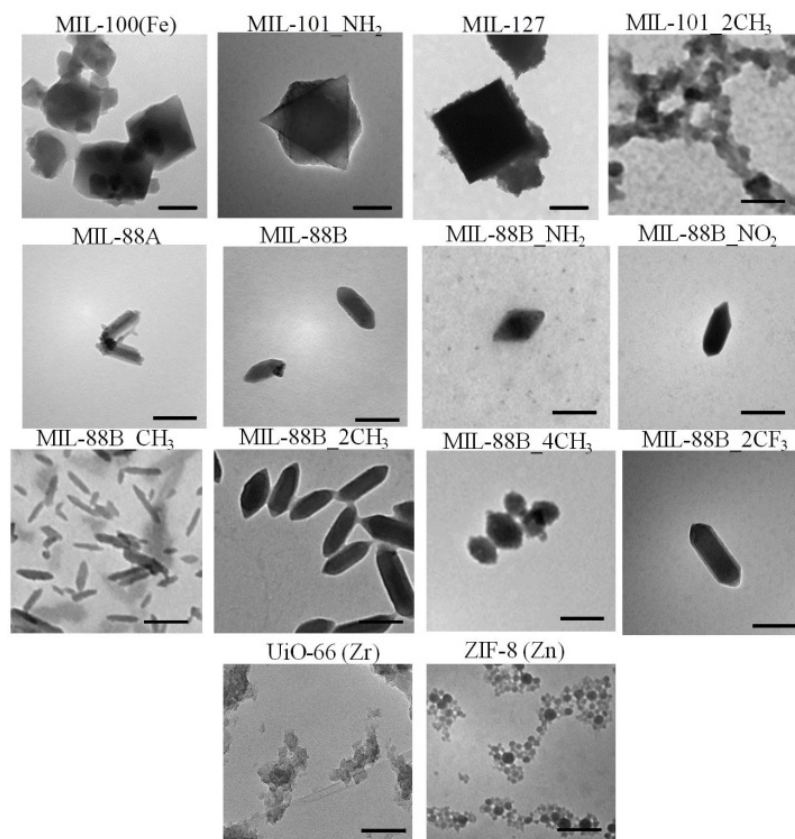
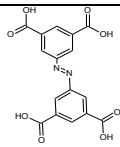
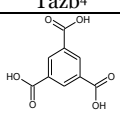
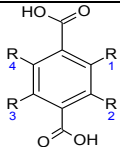
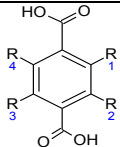
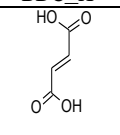
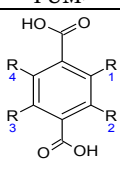
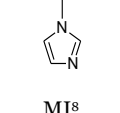


Figure 1. Microscopie électronique à transmission des nanoMOFs. Bar d'échelle=100 nm.

Une fois sa caractérisation complétée, sa cytotoxicité a été évaluée par le test MTT [Mosmann, 1983] sur deux lignes cellulaires. En vue de l'administration des nanoMOFs par voie intraveineuse, orale et topique, une ligne de macrophages murins (J774), couramment utilisée pour des tests de pénétration cellulaire, et une autre humaine dérivée du cancer cervicale (HeLa), largement utilisée pour des tests cutanées, ont été choisies. Du même, la cytotoxicité du ligand constitutif du MOF isolé a aussi été étudiée afin de comparer sa toxicité et celle des nanoMOFs.

Table 1. Caractérisation physicochimique des nanoMOFs ainsi que les valeurs IC_{50} après 24 h de contact avec les lignées cellulaires J774 et HeLa.

MOF NPs	M ¹	L ²	R _n ³	Size (nm)	ζ-pot (mV)	IC ₅₀ (mg·mL ⁻¹)				
						HeLa		J774		
						MOF NPs	L ²	MOF NPs	L ²	
MIL-127	Fe		-	476±82	-38.5±2.0	>2.00	0.80±0.02	0.44±0.02	0.82±0.17	
MIL-100			-	120±40	-18.3±0.6	1.10±0.15	2.00±0.06	0.70±0.02	>1.00	
MIL-101_2CH ₃			(CH ₃) _{1,3} (H) _{2,4}	120±15	-24.2±2.1	>2.50	>1.70	0.17±0.01	0.08±0.01	
MIL-101_NH ₂			(NH ₂) _{1,3} (H) _{2,4}	100±18	-27.4±1.5	>1.00	0.60±0.01	0.07±0.002	0.02±0.004	
MIL-88A			-	105±15	-25.0±4.3	0.015±0.005	0.03±0.003	0.05±0.002	0.40±0.01	
MIL-88B			(H) ₁₋₄	100±20	-23.5±1.8	1.26±0.08	0.80±0.02	0.37±0.08	0.43±0.03	
MIL-88B_CH ₃			(CH ₃) _{1,3} (H) _{2,4}	75±20	-22.8±2.2	>2.00	1.05±0.03	0.37±0.01	0.24±0.02	
MIL-88B_2CH ₃			(CH ₃) _{1,3} (H) _{2,4}	100±20	-26.0±0.4	2.10±0.08	>1.70	0.36±0.03	0.08±0.01	
MIL-88B_4CH ₃			(CH ₃) ₁₋₄	120±20	-41.3±0.6	0.69±0.02	>2.00	0.08±0.01	0.42±0.01	
MIL-88B_2CF ₃			(CF ₃) _{1,3} (H) _{2,4}	105±30	-53.2±7.3	>2.00	1.12±0.08	0.41±0.01	0.57±0.01	
MIL-88B_NH ₂			(NH ₂) _{1,3} (H) _{2,4}	115±20	-25.7±1.6	1.10±0.02	0.60±0.01	0.45±0.03	0.02±0.004	
MIL-88B_NO ₂			(NO ₂) _{1,3} (H) _{2,4}	130±15	-28.4±0.7	>2.00	>2.00	0.03±0.001	0.17±0.01	
UiO-66			Zr	BDC_X ⁶	(H) ₁₋₄	100±20	-26.3±1.5	0.40±0.01	0.80±0.02	0.06±0.001
ZIF-8		Zn		-	90±15	-11.0±0.6	0.10±0.01	1.40±0.02	0.025±0.001	>1.00

¹M: Metal; ²L: Linker; ³R_n: Functionalisations; ⁴Tabz: Azobenzenetetracarboxylic acid; ⁵BTC: 1,3,5-benzenetricarboxylic acid; ⁶BDC_X: 1,4-dicarboxylic acid or terephthalic acid; ⁷FUM: fumaric acid; ⁸MI: 2-methylimidazolate.

L'effet sur la cytotoxicité (par rapport à la concentration inhibitrice 50; IC₅₀) de plusieurs paramètres tels que la topologie et la composition (cation et ligand) du MOF, ainsi que le type cellulaire a été investiguée (**Table 1**). La cytotoxicité des MOFs est faible, tout à fait comparable à des systèmes nanométriques couramment commercialisés [Soma *et al.*, 2000]. En effet, la cytotoxicité semble être fortement dépendante de la composition du MOF et non pas de leur topologie. D'une part, la nature du métal, étant de forme général, les MOFs à base de Fe les moins toxiques, suivis par le MOFs au Zr (UiO-66) et finalement par le ZIF-8 à base du Zn. D'autre part, l'effet du ligand était remarquable, avec notamment une cytotoxicité dépendante du balance hydrophile/hydrophobe (**Figure 3**).

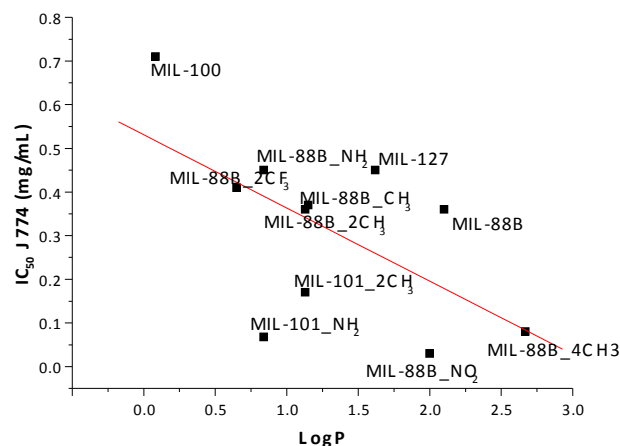


Figure 3. Cytotoxicité en fonction de la balance hydrophile/hydrophobe du MOF.

De façon remarquable, le fumarate de fer MIL-88A et le tetraméthyltéraphthalate de fer MIL-88B_4CH₃, semblent montrer une toxicité *in vitro* supérieure à celle observée *in vivo*. En effet, les nanoMOFs sont dégradés et ses composants (fer et ligands exogènes) éliminés par les urines et fèces, autant que le ligand endogène fumarate peut être réutilisé dans le cycle de Krebs en absence d'effets négatifs. [Baati *et al.*, 2013; Horcajada *et al.*, 2010].

En outre, les macrophages J774 sont plus sensibles aux concentrations des MOFs que la ligne cellulaire HeLa. La toxicité supérieure des macrophages puisse être expliquée par sa major activité phagocytaire.

Enfin, le trimesate de Fe(III) mésoporeux MIL-100(Fe) semble être le MOF le plus prometteur en termes pas seulement de ses performances en encapsulation et libération des médicaments [Horcajada *et al.*, 2010], mais aussi de par sa faible toxicité *in vitro* (IC₅₀ en J774 0,7 mg·mL⁻¹) et *in vivo* [Baati *et al.*, 2013] pour les futures bioapplications. Nous nous sommes focalisés sur cette structure pour étudier sa pénétration cellulaire dans les deux lignées cellulaires (J774 et HeLa). Afin de suivre la cinétique d'internalisation par microscopie confocale de fluorescence, un fluorophore vert (furazan) fut inséré *ex situ* et de forme stable dans la porosité du MIL-100(Fe).

Notamment, l'internalisation des nanoparticules du MIL-100(Fe) est immédiate dans les macrophages murines J774 et beaucoup plus rapide que dans les cellules épithéliales HeLa (**Figure 4**). Ce fait met en évidence la plus grande capacité phagocytaire des macrophages J774, en accord avec une toxicité supérieure.

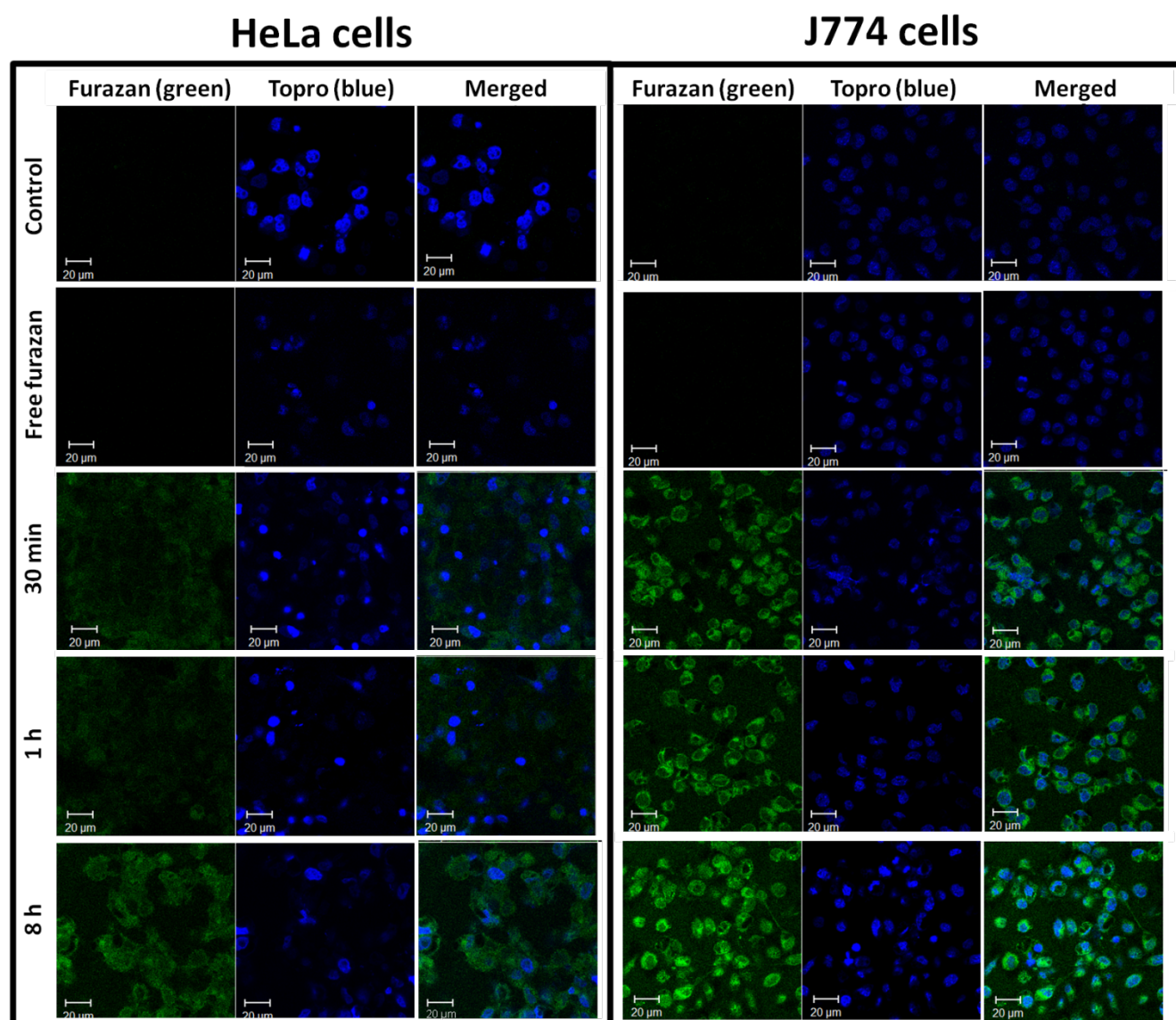


Figure 4. Suivi de la pénétration cellulaire de nanoparticules de MIL-100(Fe) dans les cellules HeLa (gauche) et HeLa (droite) par microscopie confocale de fluorescence. Bar d'échelle=20 µm.

En conclusion, la faible cytotoxicité des nanoparticules de MOFs, dépendante de sa composition, et son internalisation rapide en fonction du type cellulaire, révèlent les nanoMOFs comme des candidats très prometteurs pour la vectorisation de médicaments.

Chapitre 2: C. Tamames-Tabar, F. Salles, C. Martineau, G. Maurin, C. Serre, P. Horcajada and M.J. Blanco-Prieto. Metal-Organic Frameworks: New Delivery Systems for Genistein Administration.

La nutrition et la thérapeutique montrent actuellement une tendance générale à revenir vers les produits naturels. Citons par exemple les bioflavonoïdes ou phytoestrogènes. En particulier, l'isoflavone génistéine (GEN) présente un intérêt majeur, notamment du à son activité antitumorale et antioxydante [Sarkar and Li, 2006; Polkowski and Mazurek, 2000], récemment proposé comme alternative efficace et non-toxique pour le traitement de différents types du cancer [Azarova *et al.*, 2010; Li *et al.*, 2010; Sánchez *et al.*, 2009], [Banerjee *et al.*, 2008; Lamartiniere *et al.*, 2002; Lamartiniere, 2000] [Banerjee *et al.*, 2008; Lamartiniere *et al.*, 2002], [Pavese, Farmer and Bergan, 2010].

Malgré ses résultats, la faible solubilité et biodisponibilité de la GEN limitent fortement son utilisation clinique. L'encapsulation de la GEN dans les MOFs pourrait *a priori* aider à surmonter ces limitations.

Ainsi, nous avons proposé ici l'encapsulation et la libération de la GEN dans une série de nano ou microparticules de 7 MOFs poreux biocompatibles avec différentes structures et compositions. Une fois optimisées, nous nous sommes intéressés à l'étude de la pharmacocinétique (PK) et la biodisponibilité (BA) du MOF portant la GEN le plus prometteur après l'administration orale dans la souris.

L'encapsulation de la GEN a été menée à bien par simple imprégnation. Nous avons pu optimiser les conditions d'encapsulation en jouant avec différents paramètres tels que la température, le temps, le solvant, la nature et composition du MOF, le ratio ou le nombre des imprégnations), en observant une forte influence du solvant, la température et la nature et composition du MOF sur le taux d'encapsulation de la GEN. Ainsi, des capacités importantes oscillant entre 160-340 $\mu\text{g}\cdot\text{mg formulation}^{-1}$ (**Table 1**) ont été obtenues. Ces valeurs, dans le range des capacités obtenues dans les MOFs pour d'autres médicaments, sont largement supérieurs à ceux reportés pour d'autres vecteurs encapsulant la GEN (0.15 *vs.* 11.30% wt.) [Pham, Brownlow and Elbayoumi, 2013; Zhang, Gao and Xu, 2013; Tang *et al.*, 2011; Shin *et al.*, 2010; Cohen *et al.*, 2008; Motlekar, Khan and Youan, 2006].

Table 1. Valeurs d'encapsulation de GEN dans différents MOFs avec leur surface BET et le valeur de volume micropore.\$ μg of GEN *per* mg of formulation

MOF	GEN Loading		Raw MOF			Formulation	
	$^{\$}\mu\text{g}\cdot\text{mg form.}^{-1}$	$^{\text{£}}\text{Mol}\cdot\text{mol}^{-1}$	Windows size (Å)	Pore Volume ($\text{cm}^3\cdot\text{g}^{-1}$)*	BET Surface ($\text{m}^2\cdot\text{g}^{-1}$)	Pore Volume ($\text{cm}^3\cdot\text{g}^{-1}$)*	BET Surface ($\text{m}^2\cdot\text{g}^{-1}$)
MIL-100(Fe)_NPs	174.0 \pm 24.9	0.48	4.7*5.5 & 8.6	0.30	620	0.04	20
MIL-88C(Fe)_NPs [†]	201.7 \pm 51.7	0.79	13	1.6 [*]	4100 [*]	-	-
UiO-66_NH ₂ (Zr)_MPs	159.3 \pm 47.7 335.9 \pm 24.8*	1.23 3.28	5-7	0.34	680	** 0.06	** 110
UiO-66_2CF ₃ (Zr)_MPs	157.0 \pm 44.8	1.71	5-7	0.23	500	0.05	80
UiO-66_NDC(Zr)_MPs	329.3 \pm 45.7	3.57	8	0.72	1110	0.03	30
UiO-66_BPDC(Zr)_MPs	337.7 \pm 24.9	4.00	8	0.64	1240	0.02	30
MIL-140C(Zr)_MPs	225.6 \pm 88.2	0.37	7	0.80	1620	0.01	20

£ mol of GEN *per* mol of dry and empty MOF

*corresponding to a two successive impregnation processes.

**in progress

* theoretical values estimated by computing simulation (see SI).

Ensuite, la cinétique de libération de GEN depuis les MOFs a été suivie dans un milieu physiologique simulé (tampon phosphate pH 7.4, 37 °C sous des conditions SINK). La GEN est libérée lente et progressivement (de 2 jours à quelques semaines) dans le milieu (**Figure 2**). De façon remarquable, la libération semble ne pas être complète dans plusieurs matériaux. Ce fait, associé aux caractérisations expérimentales et numériques préliminaires, sont en accord avec (i) le fort caractère hydrophobe de la GEN et (ii) la formation des interactions fortes entre les groupes hydroxyles de la GEN et les MOFs.

Les profils de libération sont toutefois dépendants de la topologie et nature du MOF, en accord avec des études préalablement reportés en utilisant d'autres médicaments et les MOFs [Cunha *et al.*, 2013a; Liédana *et al.*, 2012]. Ses résultats, très prometteurs, sont en accord avec les cinétiques de libération reportées pour d'autres formulations contenant GEN ou autres flavonoïdes [Pham, Brownlow and Elbayoumi, 2013; Tang *et al.*, 2011; Motlekar, Khan and Youan, 2006].

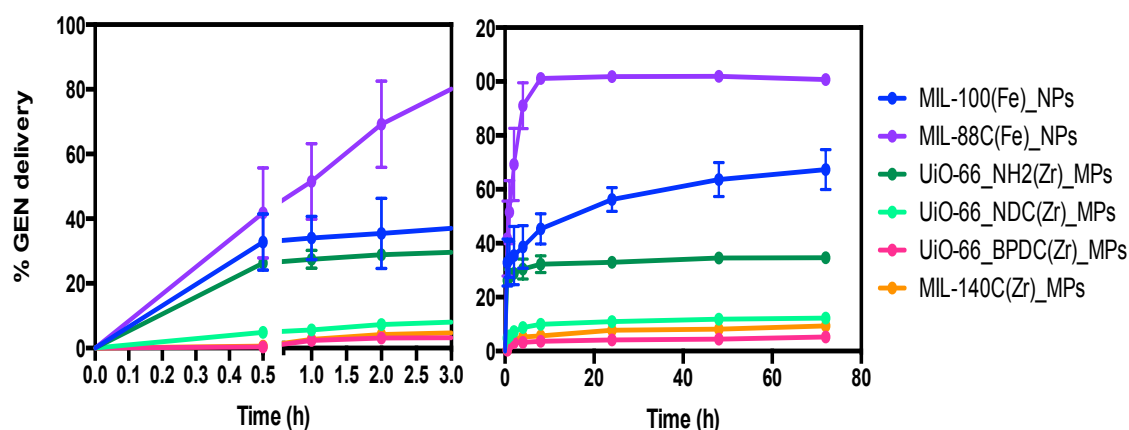


Figure 2. Profils de libération de GEN depuis différents MOFs à base de Fe (MIL-100 et MIL-88C) et à base de Zr (UiO-66_X (X=-NH₂, -NDC, -BPDC) et MIL-140C) pendant 3 jours après l'addition d'une solution NaOH 0.5 M aux supernatants de GEN en PBS. On a montré les résultats de libération jusqu'à 3 jours, car les résultats suivants sont dans un plateau.

Enfin, nous nous sommes focalisés sur l'étude préclinique de la PK et F du MOF le plus prometteur en termes de capacité d'encapsulation, cinétique de libération et toxicité. Ainsi, nous avons sélectionné les nanoparticules de MIL-100(Fe) (MIL-100(Fe)_NPs) contenant un 17% pds de GEN. Sa PK et sa F ont été évaluées après son administration orale unique ($D=30 \text{ mg}\cdot\text{Kg}^{-1}$) aux souris femelle BALB/C et comparées à celles du médicament libre (**Figure 4**). Ainsi nous avons validé une méthode HPLC-UV (voir **Annexe 2** afin de pouvoir quantifier la GEN dans le plasma et les organes (foies, reins et rates) du modèle animal.

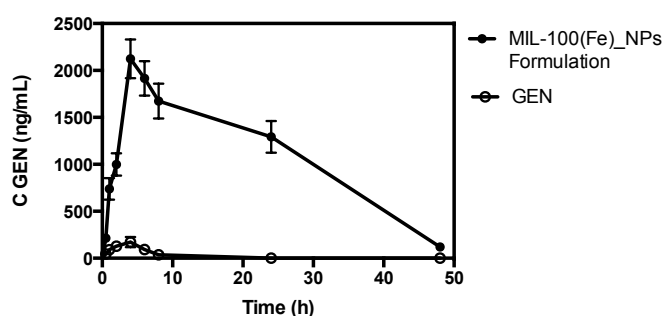


Figure 4. Curve de concentration de GEN libre (cercle vide) et de la formulation MIL-100(Fe)_NPs (cercle complet) après l'administration unique par voie orale de $30 \text{ mg}\cdot\text{Kg}^{-1}$ ($n=6$) pendant 48h.

De façon remarquable, la formulation GEN-MOF a permis d'améliorer les paramètres pharmacocinétiques de la GEN tels que le temps de vie moyenne $t_{1/2}$, le temps de

résidence moyen MRT et la biodisponibilité totale F de la GEN, obtenant des valeurs comparables auxquels reportés par Yang *et al.* [Tamames-Tabar *et al.*, 2013; Yang *et al.*, 2010]. En outre, l'administration de cette formulation permet de prolonger les niveaux de GEN dans les organes, ça que fait penser à un effet protecteur de la molécule contre sa métabolisation [Steensma, 2006].

Ces résultats, très encourageants, font des MOFs des candidats de choix pour la libération contrôlée (DDS) de GEN.

Chapitre 3: C. Tamames-Tabar, E. Imbuluzqueta, N. Guillou, C. Serre, S.R. Miller, E. Elkaïm, P. Horcajada and M.J. Blanco-Prieto, A Zinc Azelate MOF: Combining Antibacterial Effect. Accepted in CrystEngComm.

Une alternative intéressante à l'encapsulation de médicaments dans la porosité du MOF consiste à incorporer des substances thérapeutiques comme partie constitutive du réseau hybride (BioMOF). La molécule active se libère par la biodégradation du MOF et non pas par la désorption par échange avec le milieu. Cette méthode permet de s'affranchir de la toxicité dérivée du réseau et d'obtenir des encapsulations très importantes, indépendants de la porosité du MOF [Novio *et al.*, 2013; Imaz *et al.*, 2011; Miller *et al.*, 2010].

Nous nous sommes intéressés à la préparation d'un bioMOF à base d'un métal et un ligand organique portant une activité biologique complémentaire afin d'y obtenir un effet additif, voir synergique. Ainsi, un nouveau BioMOF biocompatible et bioactif (nommé BioMIL-5) a été préparé à base du Zn et de l'acide azélaïque (AZA), tous les deux portant des propriétés antibactériennes et dermatologiques remarquables et complémentaires utilisés actuellement isolés pour le soin de la peau, notamment dans le traitement de l'hyperpigmentation et l'acné [Farshi, 2011; Schwarz *et al.*, 2005]. En outre, l'AZA est faiblement absorbé à travers la peau, demandant de plusieurs applications [Bojar *et al.*, 1993]. Une libération contrôlée depuis le BioMIL-5 pourrait en effet libérer d'une façon soutenue les composants bioactifs.

L'azelate de zinc BioMIL-5 a été synthétisé par une voie verte hydrothermale. Sa structure cristalline a été résolue à l'aide de la diffraction de rayons X sur poudre en utilisant du rayonnement synchrotron (groupe de space *Pcca* (n. 54); paramètres de maille: ($a=47.288(1)$, $b=4.7297(2)$, $c=9.3515(3)$ Å; $V=2091.5(1)$ Å³).

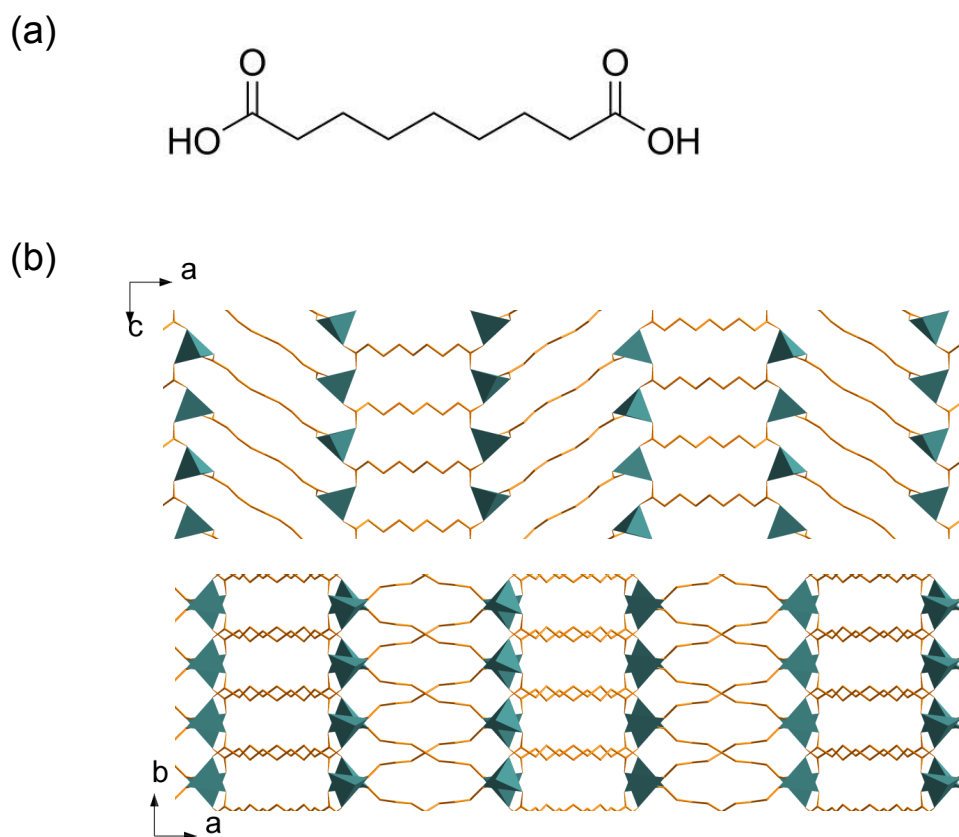


Figure 1. (a) Structure du ligand organique : acide azélaïque (AzA). (b) Projections de la structure cristalline du BioMIL-5 selon les directions $[010]$ et $[001]$. Les polyèdres du Zn et les atomes de carbone sont représentés en vert et en jaune, respectivement.

Une fois le solide BioMIL-5 complètement caractérisé (XRPD, FTIR, DLS, ζ -potentiel, TGA, EA et XRTD, **SI**), nous nous sommes intéressés à l'étude de son stabilité dans: (i) l'eau afin de viser des applications cutanées et (ii) le milieu de culture bactérien MHCA, utilisé ultérieurement pour l'évaluation de l'activité antibactérienne du BioMIL-5. Le BioMIL-5 se dégrade lentement (> 3 mois) et continuent dans les deux milieux, en libérant ses constituants actifs (**Figure 4**). Un pH plus élevé (7.4 vs. 6.0; $pK_a=4.55$ et 5.41) et la présence de groupements phosphates, entre autres, dans le milieu bactérien conduit cependant à une libération plus rapide que dans l'eau.

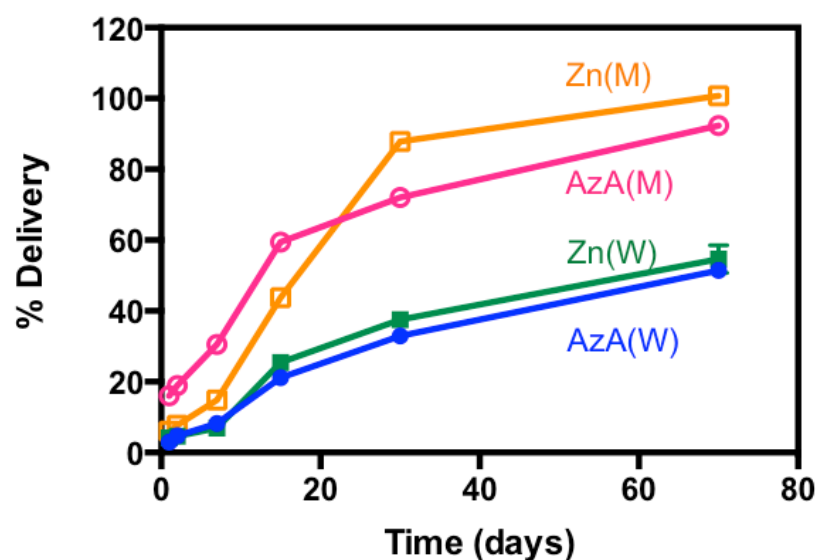


Figure 4. Cinétique de libération de l'AzA (●) et le Zn (■) dans l'eau et l'AzA (○) et le Zn (□) dans milieu bactérien depuis le BioMIL-5.

Enfin, l'activité antibactérienne du BioMIL-5 a été évaluée en contact avec deux souches bactériennes Gram-positives trouvées typiquement dans la peau: *Staphylococcus aureus* et *Staphylococcus epidermidis*. L'activité antibactérienne des composants du BioMIL-5 a été conservée après sa libération au milieu et la concentration minimale inhibitrice (MIC) et la concentration minimale bactéricide (MBC) calculées (**Table 1**). Malgré qu'aucun effet synergique n'a été observé, l'activité biologique de l'AzA et le Zn dans différents niveaux de la peau, permettra *a priori* de cibler simultanément différents effets pathologiques.

Table 1. Concentration minimale inhibitrice (MIC) et minimale bactéricide (MBC) en $\text{mg}\cdot\text{mL}^{-1}$ d'acide azélaïque (AzA), zinc et BioMIL-5 en *S. aureus* et en *S. epidermidis*.

Treatment	<i>S. aureus</i>		<i>S. epidermidis</i>	
	MIC	MBC	MIC	MBC
BioMIL-5	1.7	4.3	1.7	4.3
AzA	1.5	3.0	1.5	3.0
Zn²⁺	0.5	-	0.5	2.0

La libération progressive de l'AzA et le Zn permet en prime de prolonger la durée de l'effet pharmacologique. En effet, des concentrations de $0.5 \times \text{MIC}$ ($0.9 \mu\text{g}\cdot\text{mL}^{-1}$) permettent de diminuer significativement la croissance du *S. epidermidis* et de le stopper après 48 h

d'incubation. L'effet est dépendant de la concentration d'AzA et du Zn dans le milieu, donc de la dégradation du BioMIL-5. Considérant la dégradation du MOF et l'effet bactéricide, observé à des concentrations au-dessous des MIC et MBC des composés isolés, un effet aditif est donc mis en évidence (**Figure 5**).

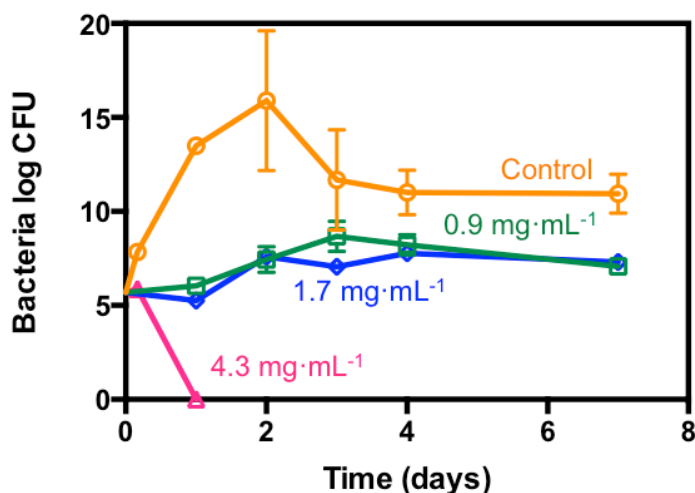


Figure 5. Curves de croissance bactérienne comparant le group control (○) avec BioMIL-5 en différentes concentrations ($\text{mg}\cdot\text{mL}^{-1}$): 0.9 (□), 1.7 (◇) and 4.3 $\text{mg}\cdot\text{mL}^{-1}$ (△) après une semaine en *S. epidermidis*.

Conclusions

La faible toxicité de MOFs ainsi que leur capacité d'encapsulation exceptionnelle font de MOFs des candidats très prometteurs dans le domaine de la libération contrôlée de médicaments. Cependant, la formulation des MOFs sous des formes pharmaceutiques solides et semi-solides bien adaptées aux applications, en passant sur la fonctionnalisation de leur surface externe, pourra dans une future proche modifier sa biodistribution pour améliorer ses performances précliniques et permettre dans une future plus lointain y arriver à l'idée utopique d'un traitement individualisé.

RÉFÉRENCES

- Adair, J.H.; Parette, M.P.; Altinoğlu, E.İ.; Kester, M., **2010**. Nanoparticulate alternatives for drug delivery. *ACS Nano*, 4(9): 4967-4970.
- Agostoni, V.; Chalati, T.; Horcajada, P.; Willaime, H.; Anand, R.; Semiramo, N.; Baati, T.; Hall, S.; Maurin, G.; Chacun, H.; Bouchemal, K.; Martineau, C.; Taulelle, F.; Couvreur, P.; Rogez-Kreuz,

- C.; Clayette, P.; Monti, S.; Serre, C.; Gref, R., **2013**. Towards an improved anti-HIV activity of NRTI via metal-organic frameworks nanoparticles. *Adv. Healthc. Mater.*, 2(12): 1630-1637.
- Agostoni, V.; Anand, R.; Monti, S.; Hall, S.; Maurin, G.; Horcajada, P.; Serre, C.; Bouchemal, K.; Gref, R., **2013**. Impact of phosphorylation on the encapsulation of nucleoside analogues within porous iron(III) metal-organic framework MIL-100(Fe) nanoparticles. *J. Mater. Chem. B*, 1(34): 4231-4242.
- Alvarez, E.; García-Márquez, A.; Devic, T.; Steunou, N.; Serre, C.; Bonhomme, C.; Gervais, C.; Izquierdo-Barba, I.; Vallet-Regí, M.; Laurencin, D.; Mauri, F.; Horcajada, P., **2013**. A biocompatible calcium bisphosphonate coordination polymer: towards a metal-linker synergistic therapeutic effect? *CrystEngComm.*, 15: 9899-9905.
- Baati, T.; Njim, L.; Neffati, F.; Kerkeni, A.; Bouttemi, M.; Gref, R.; Najjar, M.F.; Zakhama, A.; Couvreur, P.; Serre, C.; Horcajada, P., **2013**. In depth analysis of the *in vivo* toxicity of nanoparticles of porous iron(III) metal-organic frameworks. *Chem. Sci.*, 4: 1597-1607.
- Bennett, J.O.; Yu, O.; Heatherly, L.G.; Krishnan, H.B., **2004**. Accumulation of genistein and daidzein, soybean isoflavones implicated in promoting human health, is significantly elevated by irrigation. *J. Agric. Food Chem.*, 52(25): 7574-7579.
- Bojar, R.A.; Cutcliffe, A.G.; Graupe, K.; Cunliffe, W.J.; Holland, K.T., **1993**. Follicular concentrations of azelaic acid after a single topical application. *Br. J. Dermatol.*, 129(4): 399-402.
- Cohen, R.; Orlova, Y.; Kovalev, M.; Ungar, Y.; Shimoni, E., **2008**. Structural and functional properties of amylose complexes with genistein. *J. Agric. Food Chem.*, 56(11): 4212-4218.
- Cunha, D.; Ben Yahia, M.; Hall, S.; Miller, S.R.; Chevreau, H.; Elkaïm, E.; Maurin, G.; Horcajada, P.; Serre, C., **2013**. Rationale of drug encapsulation and release from biocompatible porous metal-organic frameworks. *Chem. Mater.*, 25(14): 2767-2776.
- Cunha, D.; Gaudin, C.; Collinet, I.; Horcajada, P.; Maurin, G.; Serre, C., **2013**. Rationalization of the entrapping of bioactive molecules into a series of functionalized porous zirconium terephthalate MOFs. *J. Mater. Chem. B*, 1: 1101-1108.
- Della Rocca, J.; Liu, D.; Lin, W., **2012**. Are high drug loading nanoparticles the next step forward for chemotherapy? *Nanomedicine*, 7(3): 303-305.
- Della Rocca, J.; Liu, D.; Lin, W., **2011**. Nanoscale metal-organic frameworks for biomedical imaging and drug delivery. *Accounts Chem. Res.*, 44(10): 957-968.
- Farshi, S., **2011**. Comparative study of therapeutic effects of 20% azelaic acid and hydroquinone 4% cream in the treatment of melasma. *Cosmet. Dermatol.*, 10(4): 282-287.
- Gaudin, C.; Cunha, D.; Ivanoff, E.; Horcajada, P.; Chev e, G.; Yasri, A.; Loget, O.; Serre, C.; Maurin, G., **2012**. A quantitative structure activity relationship approach to probe the influence of the functionalization on the drug encapsulation of porous metal-organic frameworks. *Micropor. Mesopor. Mater.*, 157: 124-130.
- He, C.; Lu, K.; Liu, D.; Lin, W., **2014**. Nanoscale metal-organic frameworks for the co-delivery of cisplatin and pooled siRNAs to enhance therapeutic efficacy in drug-resistant ovarian cancer cells. *J. Am. Chem. Soc.* 136(14): 5181-5184.

- Horcajada, P.; Gref, R.; Baati, T.; Allan, P.K.; Maurin, G.; Couvreur, P.; Férey, G.; Morris, R.E.; Serre, C., **2012**. Metal–organic frameworks in biomedicine. *Chem. Rev.*, 112(2): 1232-1268.
- Horcajada, P.; Serre, C.; McKinlay, A.C.; Morris, R.E., **2011**. “Biomedical applications of metal–organic frameworks” in *Metal-Organic Frameworks: Applications from Catalysis to Gas Storage*, ed. D. Farrusseng, Wiley-VCH Verlag GmbH & Co. KGaA, Weinheim, pp. 213-250.
- Horcajada, P.; Chalati, T.; Serre, C.; Gillet, B.; Sebrie, C.; Baati, T.; Eubank, J.F.; Heurtaux, D.; Clayette, P.; Kreuz, C.; Chang, J.-S.; Hwang, Y.K.; Marsaud, V.; Bories, P.-N.; Cynober, L.; Gil, S.; Férey, G.; Couvreur, P.; Gref, R., **2010**. Porous metal-organic-framework nanoscale carriers as a potential platform for drug delivery and imaging. *Nat. Mater.*, 9(2): 172-178.
- Horcajada, P.; Serre, C.; Maurin, G.; Ramsahye, N.A.; Balas, F.; Vallert-Regi, M.; Sebban, M.; Taudelle, F.; Férey, G., **2008**. Flexible porous metal-organic frameworks for a controlled drug delivery. *J. Am. Chem. Soc.*, 130(21): 6774-6780.
- Horcajada, P.; Serre, C.; Vallet-Regí, M.; Sebban, M.; Taulelle, F.; Férey, G., **2006**. Metal–organic frameworks as efficient materials for drug delivery. *Angew. Chem. Int. Edit.*, 45(36): 6120-6124.
- Imaz, I.; Rubio-Martínez, M.; García-Fernández, L.; García, F.; Ruiz-Molina, D.; Hernando, J.; Puentes, V.; MasPOCH, D., **2010**. Coordination polymer particles as potential drug delivery systems. *Chem. Commun.*, 46(26): 4737-4739.
- Liédana, N.; Galve, A.; Rubio, C.; Téllez, C.; Coronas, J., **2012**. Caf@ZIF-8: one-step encapsulation of caffeine in MOF. *ACS Appl. Mater. Interfaces*, 4(9): 5016-5021.
- Meek, S.T.; Greathouse, J.A.; Allendorf, M.D., **2011**. Metal-organic frameworks: a rapidly growing class of versatile mesoporous materials. *Adv. Mater.*, 23(3): 249-267.
- Miller, S.R.; Alvarez, E.; Fradcourt, L.; Devic, T.; Wuttke, S.; Wheatley, P.S.; Steunou, N.; Bonhomme, C.; Gervais, C.; Laurencin, D.; Morris, R.E.; Vimont, A.; Daturi, M.; Horcajada, P.; Serre, C., **2013**. A rare example of a porous Ca-MOF for the controlled release of biologically active NO. *Chem. Commun.*, 49: 7773-7775.
- Miller, S.R.; Heurtaux, D.; Baati, T.; Horcajada, P.; Greneche, J.-M.; Serre, C., **2010**. Biodegradable therapeutic MOFs for the delivery of bioactive molecules. *Chem. Commun.*, 46(25):4526-4528.
- Mosmann, T., **1983**. Rapid colorimetric assay for cellular growth and survival: application to proliferation and cytotoxicity assays. *J. Immunol. Methods*, 65(1-2): 55-63.
- Motlekar, N.; Khan, M.A.; Youan, B.-B.C., **2006**. Preparation and characterization of genistein containing poly(ethylene glycol) microparticles. *J. Appl. Pol. Sci.*, 101(3): 2070-2078.
- Novio, F.; Simmchen, J.; Vázquez-Mera, N.; Amorín-Ferré, L.; Ruiz-Molina, D., **2013**. Coordination polymer nanoparticles in medicine. *Coord. Chem. Rev.*, 257(19–20): 2839-2847.
- Perkin, A.G.; Newbury, F.G., **1899**. LXXIX.—The colouring matters contained in dyer's broom (*Genista tinctoria*) and heather (*Calluna vulgaris*). *J. Chem. Soc. Trans.*, 75, 830-839.
- Pham, J.; Brownlow, B.; Elbayoumi, T., **2013**. Mitochondria-specific pro-apoptotic activity of genistein lipidic nanocarriers. *Mol. Pharm.*, 10(10): 3789-3800.
- Polkowski, K.; Mazurek, A.P., **2000**. Biological properties of genistein. A review of *in vitro* and *in vivo* data. *Acta Pol. Pharm.*, 57(2): 135-155.

- Rowinsky, E.K.; Eisenhauer, E.A.; Chaudhry, V.; Arbuck, S.G.; Donehower, R.C., **1993**. Clinical toxicities encountered with paclitaxel (Taxol). *Semin. Oncol.*, 20(4 Suppl 3):1-15.
- Sarkar, F.H.; Li, Y., **2006**. Using chemopreventive agents to enhance the efficacy of cancer therapy. *Cancer Res.*, 66(7): 3347-3350.
- Schwartz, J.R.; Marsh, R.R.; Draelos, Z.D., **2005**. Zinc and skin health: overview of physiology and pharmacology. *Dermatol. Surg.*, 31: 837-847.
- Serre, C.; Mellot-Draznieks, C.; Surblé, S.; Audebrand, N.; Filinchuk, Y.; Férey, G., **2007**. Role of solvent-host interactions that lead to very large swelling of hybrid frameworks. *Science*, 315(5820): 1828-1831.
- Slengers, T.V.; Sagué, J.L.; Brunetto, P.S.; Zuber, S.; Fleury, A.; Miroló, L.; Robin, A.Y.; Meuwly, M.; Gordon, O.; Landmann, R.; Daniels, A.U.; Fromm, K.M., **2010**. Of chains and rings: synthetic strategies and theoretical investigations for tuning the structure of silver coordination compounds and their applications. *Materials*, 3(5): 3407-3429.
- Soma, C.E.; Dubernet, C.; Barratt, G.; Benita, S.; Couvreur, P., **2010**. Investigation of the role of macrophages on the cytotoxicity of doxorubicin and doxorubicin-loaded nanoparticles on M5076 cells *in vitro*. *J. Control. Release*, 68(2): 283-289.
- Sonnedecker, G., **1986**. *Kremers and Urdang's History of Pharmacy*. 4th edn. The American Institute of the History of Pharmacy, Madison (WI).
- Special Issue **2012**. Guest Editors H.-C. Zhou, J.R. Long and O.M. Yaghi. *Chem. Rev.*, 112: 673-1268.
- Steensma, A., **2006**. Bioavailability of genistein and its glycoside genistin. PhD Thesis (Wageningen University, The Netherlands).
- Sun, C.-Y.; Qin, C.; Wang, X.-L.; Yang, G.-S.; Shao, K.-Z.; Lan, Y.-Q.; Su, Z.-M.; Huang, P.; Wang, C.-G.; Wang, E.-B., **2012**. Zeolitic imidazolate framework-8 as efficient pH- sensitive drug delivery vehicle. *Dalton Trans.*, 41(23): 6906-6909.
- Tamames-Tabar, C.; Imbuluzqueta, E.; Campanero, M.A.; Horcajada, P.; Blanco-Prieto, M.J., **2013**. A simple and robust high-performance liquid chromatography coupled to a diode-array detector method for the analysis of genistein in mouse tissues. *J. Chrom. B.*, 935: 47-53.
- Tang, J.; Xu, N.; Ji, H.; Liu, H.; Wang, Z.; Wu, L., **2011**. Eudragit nanoparticles containing genistein: formulation, development, and bioavailability assessment. *Int. J. Nanomedicine*, 6: 2429-2435.
- Taylor-Pashow, K.M.L.; Della Rocca, J.; Xie, Z.; Tran, S.; Lin, W., **2009**. Postsynthetic modifications of iron-carboxylate nanoscale metal-organic frameworks for imaging and drug delivery. *J. Am. Chem. Soc.*, 131(40): 14261-14263.
- Wang, C.; Liu, D.; Lin, W., **2013**. Metal-organic frameworks as a tunable platform for designing functional molecular materials. *J. Am. Chem. Soc.*, 135(36): 13222-13234.
- Wang, Y.; Yang, J.; Liu, Y.-Y.; Ma, J.-F., **2013**. Controllable syntheses of porous metal-organic frameworks: encapsulation of LnIII cations for tunable luminescence and small drug molecules for efficient delivery. *Chem. Eur. J.*, 19(43): 14591-14599.

Wang, H.-N.; Meng, X.; Yang, G.-S.; Wang, X.-L.; Shao, K.-Z.; Su, Z.-M.; Wang, C.-G., **2011**. Stepwise assembly of metal-organic framework based on a metal-organic polyhedron precursor for drug delivery. *Chem. Commun.*, 47(25): 7128-7130.

WHO (World Health Organization), **2012**. International Agency for Research on Cancer. Globocan 2012: Incidence, Mortality and Prevalence Worldwide in 2012. http://globocan.iarc.fr/Pages/fact_sheets_cancer.aspx (Accessed April 2014).

Yang, Z.; Zhu, W.; Gao, S.; Xu, H.; Wu, B.; Kulkarni, K., **2010**. Simultaneous determination of genistein and its four phase II metabolites in blood by a sensitive and robust UPLC-MS/MS method: application to an oral bioavailability study of genistein in mice. *J. Pharm. Biomed. Anal.*, 53(1): 81-89.

Zhang, Y.; Gao, B.; Xu, Z., **2013**. Adsorption properties of polyvinyl-alcohol-grafted particles toward genistein driven by hydrogen-bond interaction. *J. Phys. Chem. B*, 117(18): 5730-5736

ANNEX II

**A SIMPLE AND ROBUST HIGH-PERFORMANCE
LIQUID CHROMATOGRAPHY COUPLED TO A DIODE-
ARRAY DETECTOR METHOD FOR THE ANALYSIS OF
GENISTEIN IN MOUSE TISSUES**

GENERAL OBJECTIVES AND AUTHOR CONTRIBUTIONS

C. Tamames-Tabar, E. Imbuluzqueta, M. A. Campanero, P. Horcajada and M. J. Blanco-Prieto, *Journal of Chromatography B*, 2013, 935, 47-53.

New investigation fields come along with the necessity of quantification set-up methods. In this sense, to evaluate the pharmacokinetics and biodistribution of drugs, it is necessary to develop fast and accurate methods for the quantification of the drug within biological matrices. In particular, due to the scarce reported methods for the antitumoral genistein (GEN; see Chapter 2), an HPLC method had to be validated for its quantification in mice biological matrices, making this work a priority.

Therefore, and with the aim of performing future *in vivo* experiments in mice (Chapter 2), the validation of an HPLC method coupled to a diode-array detector (DAD) was fulfilled on four different mice matrices, including plasma, liver, kidneys and spleen.

For an easier comprehension of the readers, the work has been divided into precise and clear subgroups, as several parameters have been studied: the GEN extraction process from the biological matrices and its quantification method.

All the authors have actively contributed in this article. C. Tamames-Tabar has worked in the whole HPLC method validation, as well as has contributed in the *in vivo* experiments for the method applicability. Dr. E. Imbuluzqueta has helped in all the data analysis obtained after each experiment during all the validation process, as well as has contributed in the *in vivo* experiments. Dr. M. A. Campanero has actively assessed during the complete work regarding the extraction method, the planning of each experiment, as well as in the article writing. Dr. P. Horcajada and Dr. M. J. Blanco-Prieto have actively contributed in this article by assessing the experimental work as well as the article writing.

Tamames-Tabar C, Imbuluzqueta E, Campanero MA, Horcajada P, Blanco-Prieto MJ. A simple and robust high-performance liquid chromatography coupled to a diode-array detector method for the analysis of genistein in mouse tissues. [J Chromatogr B](#) 2013 SEP 15;935:47-53